TESIS DE LA UNIVERSIDAD DE ZARAGOZA

2023

81

Christian Di Stasi

Developing biomass-derived carbons for catalytic syngas and methane production from renewable sources

Director/es

Manyà Cervelló, Joan José

González García, Belén

ISSN 2254-7606

Prensas de la Universidad Universidad Zaragoza

ISSN 2254-7606

Universidad Zaragoza
1542

Tesis Doctoral

DEVELOPING BIOMASS-DERIVED CARBONS FOR CATALYTIC SYNGAS AND METHANE PRODUCTION FROM RENEWABLE SOURCES

Autor

Christian Di Stasi

Director/es

Manyà Cervelló, Joan José
González García, Belén

UNIVERSIDAD DE ZARAGOZA
Escuela de Doctorado

Programa de Doctorado en Ingeniería Química y del Medio Ambiente

2022

Universidad Zaragoza

Department of Chemical Engineering and Environment Technologies

Developing biomass-derived carbons for catalytic syngas and methane production from renewable sources

A thesis submitted to the Department of Chemical Engineering and Environmental Technologies at the University of Zaragoza, Spain in partial fulfilment of the requirements for the degree of Doctor

Christian Di Stasi

Huesca, 2021

Departamento de Ingeniería Química y Tecnologías del Medio Ambiente
Universidad Zaragoza

Doctor Joan J. Manyà, associate Professor at the University of Zaragoza in the Department of Chemical Engineering and Environmental Technologies and member of the Thermochemical Research Group, and Doctor Belén González inform that:

The PhD thesis entitled:

"**Developing biomass-derived carbons for catalytic syngas and methane production from renewable sources**"

has been written by the PhD student Christian Di Stasi under our supervision in the Department of Chemical Engineering and Environmental Technologies and has not been submitted in support of an application for another degree at this or any other university and we authorize and approve the presentation of this dissertation.

Joan J. Manyà Belén González

The PhD thesis “Developing biomass-derived carbons for catalytic syngas and methane production from renewable sources” is presented by compendium of the following publications:

1) C. Di Stasi, D. Alvíra, G. Greco, B. González, J.J. Manyà. “Physically activated wheat straw-derived biochar for biomass pyrolysis vapors upgrading with high resistance against coke deactivation”. Fuel, 2019, 255: 115807.
   Impact Factor: 5.578; Q1: 18/143 (Chemical Engineering). Source: Journal Citation Reports (JCR) 2019.
2) C. Di Stasi, G. Greco, R. L. S. Canevesi, M. T. Izquierdo, V. Fierro, A. Celzard, B. González, J.J. Manyà. “Influence of activation conditions on textural properties and performance of activated biochars for pyrolysis vapors upgrading”. Fuel, 2021, 289: 119759.
   Impact Factor: 6.609; Q1: 20/143 (Chemical Engineering). Source: JCR 2020.
3) C. Di Stasi, M. Cortese, G. Greco, S. Renda, B. González, V. Palma, J.J. Manyà. “Optimization of the operating conditions for steam reforming of slow pyrolysis oil over an activated biochar-supported Ni-Co catalyst”. International Journal of Hydrogen Energy, 2021, 46: 26915.
   Impact Factor: 5.816; Q2: 45/133 (Energy & Fuels). Source: JCR 2020.
4) C. Di Stasi, S. Renda, G. Greco, B. González, V. Palma, J.J. Manyà. “Wheat-Straw-Derived Activated Biochar as a Renewable Support of Ni-CeO_2 Catalysts for CO_2 Methanation”. Sustainability, 2021, 13: 8939.
   Impact Factor: 3.251; Q2: 124/274 (Environmental Sciences). Source: JCR 2020.

To my family

He who sleeps doesn't catch fish

I. Acknowledgements

At the end of this experience, I think it is time for me to thank all the people that, one way or another, have contributed to this achievement…

First of all, I would like to express my deepest gratitude to Prof. Joan Manyà who guided me during these years. Thank you for your constant support and for your patience. Despite your tight schedule, you were always willing to roll up your sleeves and help me. I remember, struggling with tubes, valves, wrenches etc. and you patiently guided me through the assembly of the setups. If I have been able to finish my thesis and, more important, if today I know what a NPT fitting is, it is thanks to you.

I would also like to acknowledge Dr. Belén González for her guidance and constructive criticism. You helped me doing my first steps in this academic world. In particular I would like to thank you for your crucial help during my first months in Spain.

My sincere thanks to Prof. Vanessa Fierro and Prof. Vincenzo Palma for their guidance and their hospitality. During my secondments I felt like being at home.

Gracias a todos mis compañeros del laboratorio GPT. Este trabajo es el resultado de vuestra ayuda y de vuestro apoyo.

Gracias a mi primer y único estudiante de TFM. Gracias por tus dos (DOS!!) clases de guitarra y por tus postres de Sicilia, estaban buenísimos! Echaré de menos tu procrastinación y espero leer pronto tu review.

Gracias María por tu amistad, por las cervezas y por tus clases de español. Quiero que sepas que mi salud mental agradeció mucho nuestros vermú de los viernes en el huerto de la EPS. Espero que en los próximos años seremos capaces de darnos los regalos de cumpleaños con tiempo y no 5 meses después. Te aconsejo sacar una foto a esta página dado que es la primera y última vez que te dedico palabras bonitas.

Grazie a Gianluca, il mio compagno di ufficio e di laboratorio. Spero di riuscire a fare a meno dei tuoi “Hi chriscctian”. Credo sia inutile dire come il tuo arrivo mi abbia svoltato il dottorato, nel bene e nel male. Basti pensare che l’ultimo anno, durante il quale non abbiamo condiviso l’ufficio, é forse stato il piú produttivo di tutti. Peró, nonostante tutto, possiamo dire di aver percorso e concluso questo percorso spalla a spalla… ed é forse anche merito delle nostre 4 lauree.

Gracias a Dani, mi histórico compañero de piso, por su amistad y por sus imprescindibles aportaciones a esta tesis. Admiro tu forma de pensar y tu capacidad salir de tu comfort-zone, buscando siempre nuevos desafíos. Aunque no lo parece, he aprendido mucho de ti. A partir de la importancia de diversificar las inversiones, la inutilidad de Excel, a como negociar un aumento de sueldo. Espero que pronto podamos hacer un viaje juntos, quizás a América Latina dado que tú nunca lo visitaste. Un agradecimiento especial también a Conchita por nutrirnos durante la cuarentena.

Gracias a May, Miguel, Fer, Yana, Diego, Adrián y Melocotón. Más que grupo de amigos me gusta pensar a nosotros como una *familia*. Cuando pienso en vosotros solo me vienen a la mente momentos felices: openhuerto, las fiestas, las pizzas, las crepes, el Nowa, los viajes, las rutas (completadas fácilmente o a empujones)… La mayoría de nosotros se encontraba más o menos lejos de su casa y de su familia. En mi caso, gracias a vosotros, esa distancia pareció un poquito más pequeña.

Grazie a Federica che al mio arrivo in Spagna mi ha accolto a casa sua e mi ha insegnato le prime indispensabili parole in spagnolo: caña e tapas.

Grazie a Saponiero e Dente. Nonostante gli eventi ci abbiano portato a vivere cosí distanti, voi siete rimasti dei punti fermi nella mia vita, come sempre. Grazie per il vostro continuo sostegno. Vi siete meritati un paio di trecce a testa.

To my brother, Leandro, who is my lighthouse, the one who constantly guided me during this experience and the person who, despite the distance, was always supporting me wherever I was.

To my parents, Giovanna e Antonio, who through their sacrifices, allowed me to be where I am today and, more important, who I am today. Thank you for your support and for your unconditioned love (fatevela tradurre da qualcuno).

Among all the results obtained during this research about biochar and its applications, there is one which, even though it is not reported in this thesis, it is probably the most important founding of this PhD. To this person I would like to say::: Thank you.
“*Perché proprio in quell'istante? Non si sa. Fran.”*

II. Summary / Resumen

As result of the indiscriminate exploitation of fossil fuels, the level of anthropogenic gases, in particular CO_2, has drastically increased causing several environmental issues such as the greenhouse effect and the oceans acidification. In this context, several efforts are being made to reduce these emissions. The European Union, for example, through the European Green Deal (2019), set the objective to reach complete decarbonization through the promotion and diffusion of negative emission technologies (NETs).

Among all the NETs alternatives, biochar production represents one of the most promising strategies due to the versatile features of the material, and its relatively low production cost. Because of this, the interest of the scientific community for biochar has grown exponentially in the last years, and, in this sense, a particular interest has been paid to the production of activated biochars and to the employment of biochar-derived materials in catalytic applications

The present work was conducted within the framework of a European Training Network: The GreenCarbon project (Marie Skłodowska-Curie grant agreement No 721991), which main purpose was to develop advanced biomass-derived carbons to drive new technologies for biomass/biowaste upcycling. In this context, the main objective of this PhD Thesis was to study the activation and functionalization of pyrolysis chars to produce innovative biochar-supported catalysts to be employed as a more sustainable alternative to the commonly used ones.

The first part of the research dealt with the assessment of the suitability of biochars to be used as renewable and low-cost catalyst/support for pyrolysis vapors upgrading. After that the research was shifted to the identification of the most appropriate biochar activating conditions. Finally, the resulting activated biochar, produced through an optimized activating procedure, was used as support for the production of several catalysts which were then tested for two different processes: the pyrolysis oil steam reforming and the CO_2 methanation.

The most remarkable achievements obtained in this PhD project are: (i) the determination of the role that the activating pressure has on the textural properties of the resulting activated biochar and (ii) the production of a relatively stable activated biochar-based catalyst for the upgrading of pyrolysis vapors.

This document is conceptually divided in five main blocks:

I. The first block is composed of an introductory section and a chapter concerning the state of the art of the studied processes.

II. In the second block, a brief overview of the GreenCarbon project and the main objective of the PhD Thesis are reported.

III. The third block details the materials and methods employed in this work.

IV. The results of this work are resumed in the fourth block.

V. Finally, in the last section are drawn the overall conclusions reached in this work accompanied by the indications about the work which needs to be done in the future.

Como resultado de la explotación indiscriminada de los recursos fósiles, el nivel de gases antropogénicos – en particular, el CO_2 – ha aumentado drásticamente en los últimos años. Este incremento causaría problemas ambientales como el efecto invernadero y la acidificación de los océanos. En este contexto, diversos esfuerzos se están llevando a cabo para reducir estas emisiones. Por ejemplo, la Unión Europea, a través del Pacto Verde Europeo firmado en 2019, fijó el objetivo de alcanzar la descarbonización completa mediante la promoción y difusión de tecnologías de emisión negativa (NETs).

Entre todas las alternativas NETs, la producción de biochar representa una de las estrategias más prometedoras gracias a, entre otros, las características versátiles del material y su relativo bajo coste de producción. Por ello, el interés de la comunidad científica hacia el biochar ha aumentado exponencialmente en los últimos años y, en este sentido, se ha prestado un particular interés a la producción de biochares activados y el uso de materiales derivados de biochar en aplicaciones catalíticas.

Esta tesis doctoral se enmarca dentro del European Training Network: The GreenCarbon project (Marie Skłodowska-Curie grant agreement No 721991), cuyo propósito principal fue desarrollar carbonos procedentes de biomasa avanzados para nuevas tecnologías de reciclaje de biomasa/desechos. En este contexto, el objetivo principal de esta tesis doctoral fue estudiar la activación y funcionalización de carbonos producidos por pirolisis de biomasa para producir catalizadores novedosos soportados en biochar como alternativa sostenible a otros más comunes.

La primera parte de la investigación se enfocó en la evaluación de la idoneidad del uso de biochars como catalizadores renovables y de bajo coste para la mejora de vapores de pirólisis. A continuación, el trabajo se centró en la identificación de las condiciones más apropiadas de activación del biochar. La última parte de la investigación se dedicó a testar el uso del biochar activado derivado como soporte para la producción de varios catalizadores. Estos catalizadores fueron testados en dos procesos diferentes: el reformado húmedo de los aceites de pirólisis y la metanación del CO_2.

Los logros más notables obtenidos en esta tesis doctoral son: (i) la determinación del rol que tiene la presión de activación sobre las propiedades del biochar activado resultante y (ii) la producción de un catalizador basado en biochar activado relativamente estable para la mejora de los vapores de pirólisis.

El presente documento se divide conceptualmente en cinco bloques principales:

I. El primer bloque presenta la introducción y un capítulo relativo al estado del arte sobre los procesos estudiados.

II. El segundo bloque presenta una breve descripción del proyecto GreenCarbon y los principales objetivos del proyecto de tesis doctoral.

III. El tercer bloque detalla los materiales y métodos empleados en los experimentos realizados.

IV. El cuarto bloque presenta los resultados obtenidos.

V. El quinto bloque presenta las conclusiones de esta tesis doctoral y los pasos a seguir en el futuro.

III. List of Abbreviations and Acronyms

BET	Surface area evaluated through the Brunauer, Emmett, Teller model
CEC	Carbon Exchange Capacity
CCS	Carbon Capture and Storage
CCU	Carbon Capture and Utilization
CHN	Elemental analysis
DACCS	Direct Air Carbon Capture and Storage
DFT	Density functional theory
DR	Dubinin–Radushkevich model
FTIR	Fourier-Transform Infrared spectroscopy
GHSV	Gas hourly space velocity
IBI	International Biochar Initiative
LHSV	Liquid hourly space velocity
NETs	Negative Emission Technologies
NP	Nanoparticle
PSD	Pore size distribution
S/C	Steam to carbon molar ratio
SBA	Santa Barbara Amorphous
SCS	Soil Carbon Sequestration
SEM-EDX	Scanning Electron Microscopy - Energy Dispersive X-ray spectroscopy
TPD	Temperature programmed desorption
TPR	Temperature programmed reduction
UNFCCC	United Nations Framework Convention on Climate Change
WGS	Water gas shift
WP	Work Package
XPS	X-ray photoelectron spectroscopy
XRF	X-Ray Fluorescence
μ-GC	Micro gas chromatograph

Contents

1. Introduction

1.1. Towards a low-carbon future

Since the second industrial revolution, mankind started a continuous exploitation of fossil fuels. As result of this indiscriminate practice, the level of anthropogenic gases, in particular CO_2, has drastically increased causing several environmental issues such as the greenhouse effect and the oceans acidification. The first concerns about the catastrophic consequences related to the CO_2 emissions were raised by Arrhenius (1896). Since then, the scientific community has gradually recognized the carbon dioxide as an important threat to the environment.

Through the implementation of international agreements such as the Kyoto protocol (2005) and the Paris accords (2016), which encouraged the gradual transition from the fossil to renewable energy sources, it was possible to reduce the CO_2 emissions by 25% if compared with those of 1990. More recently, the European Green Deal in 2019 aimed even higher, pushing toward the ambitious achievement of 55% emissions reduction (using the value of 1990 as reference) by 2030 (European Commission, 2019). One of the main goals of the European Green Deal is to reach the complete decarbonization of the European Union through the promotion and diffusion of the negative emission technologies (NETs) (Yang *et al*., 2021). Each NET strategy essentially aims to remove CO_2 directly or indirectly from the atmosphere. Carbon capture and storage (CCS), soil carbon sequestration (SCS), and terrestrial carbon sequestration are some of the most famous NETs.

Through CCS techniques, for example, CO_2 is separated from flue gases and stored in underground sites. In this way, the anthropogenic emissions can be drastically reduced. However, CCS offers the illusion of a future in which the impact of fossil fuels exploitation could be mitigated. In this sense, Stephens (2014) analyzed the problematics related to the false promise of a “clean fossil fuel” and suggested that the governments should focus their investments on the transition to renewable energies instead.

Depending on the final product, carbon capture and utilization (CCU) processes could also be considered a NET strategy. CCU consists of the conversion of the anthropogenic CO_2 in chemicals and fuels which are generally produced from fossil sources. The main

drawback of these processes is that CO_2 has a very low energy level, which makes expensive, and therefore unattractive, its utilization (Bruhn *et al*., 2016).

Even though CCU and CCS share the first step (i.e., the capture of CO_2 from the atmosphere) their purposes are quite different. In fact, CCU aims at CO_2 upgrading to obtain valuable products such as methane or methanol, which can be employed as chemicals or fuels. The drawback of this application is that the amount of CO_2 which can be utilized in CCU processes is way smaller than that removed via CCS (Bruhn *et al*., 2016). Therefore, CCU technologies could only be considered useful to assure a certain independence from the fossil sources, contributing in an indirect way to CO_2 emission reduction.

Among all the NETs alternatives, biochar production represents one of the most promising strategies (Smith, 2016). The word *biochar* refers to a carbon-rich solid produced when a biomass such as wood, manure or leaves, is heated up to a moderate-low temperature (< 700 °C) in a closed container with little or unavailable air (Lehmann and Stephen, 2015; Sohi *et al*., 2009). The first signs of biochar employment could be traced back to 450 B.C. (Lehmann *et al*., 2004), when the pre-Colombian civilizations used this material as an amendment for the soil, with the aim to improve its fertility (Aller, 2016). The thermal degradation of the biomass to produce biochar "immobilizes" the CO_2 previously adsorbed by the plant for its own growth. Therefore, the employment of biochar into soils is considered a long-term stable carbon storage and could be considered as one of the NET strategies.

Despite the high potential of biochar in carbon sequestration applications, even higher than CCS technologies (Pratt and Moran, 2010), its considerable production cost (caused by the lack of production and the high demand) makes biochar employment unattractive for extensive applications (Vochozka *et al*., 2016).A possible solution could be the valorization of biochar beyond its usage in soil. Schmidt and Wilson (2014) proposed a cascade system to improve the overall profit obtained by the biochar production. Briefly, the produced biochar could be employed consecutively in several processes in which the residue of one process represents the input of the other until its disposal in soil, which would represent its last application. In this way, it may be possible to improve the economic value of the biochar, covering the costs related to its production and, finally, promoting the diffusion of this promising technology.

1.2. Biochar as a sustainable technology

1.2.1. The term biochar

In the literature, there is a common misconception about the word “biochar” which is sometimes confused with “charcoal” or “char”. Following the definition of the International Biochar Initiative (IBI), biochar is charcoal that can be employed in soils for agricultural and environmental purposes (Sohi *et al*., 2009). In some instances, the material properties of biochar and charcoal may overlap. However, many types of biochar do not easily burn and charcoals are typically not made to be used as soil amendment due to their non-adequate properties (Lehmann and Joseph, 2015).

For the sake of clarity, in this work the word *biochar* will be used to address the solid product of the thermal degradation of biomass material, without considering its final application.

1.2.2. Biomass as feedstock

Following the definition of the United Nations Framework Convention on Climate Change (UNFCCC), the word “biomass” should be referred to “non-fossilized and biodegradable organic material originated from plants, animals and micro-organisms. This shall also include products, by-products, residues and waste from agriculture, forestry and related industries as well as the non-fossilized and biodegradable organic fractions of industrial and municipal wastes” (UNFCCC, 2005). Nevertheless, in the case of renewable energy applications, the definition of *biomass* only includes agricultural and industrial plant-derived residues or crops exclusively cultivated for being used in energy production processes (Mielenz, 2009).

All the lignocellulosic biomasses are composed of a different distribution of the three main building blocks: cellulose, hemicelluloses, and lignin.

The cellulose is the most abundant organic polymer present in lignocellulosic biomass and mainly derives from the plant cell wall. Chemically speaking, it is a hexose sugar composed of glucose monomers bonded through β (1–4) glycose linkages. It has a non-homogeneous structure due to the presence of both crystalline and semi-crystalline forms. The covalent bonds that link the monomers and the hydrogen bonds among the cellulose chains provide chemical stability and mechanical strength (Dhyani and Bhaskar, 2018).

Hemicellulose is an amorphous heteropolymer of different polysaccharides composed of glucose, galactose, xylose, and mannose. In the biomass matrix, hemicelluloses act as structural glue between cellulose and lignin.

Lignin is mainly present in the external layer of the fiber and it is accounted for the structure stiffness (Dhyani and Bhaskar, 2018). The macromolecule is composed of phenylpropane polymers that render highly branched and phenolic structures with recalcitrant carbon-carbon bonds (Patra *et al*., 2021). The phenylpropane units are manly guaiacyl, syringyl and p-hydroxyphenol. The lignin content is strictly related to the biomass nature. The percentage of lignin in softwoods (in which the predominant component is the guaiacyl) usually ranges between 23–33 %, meanwhile, in hardwoods (where the sinapyl is the most present monomer), it varies between 16 and 25 % (Dhyani and Bhaskar, 2018).

In Addition, besides cellulose, hemicelluloses and lignin, biomass also contains a small percentage of other compounds: extractives and inorganics. Extractives are the small organic compounds such as oils, fats, proteins, etc. The inorganics, also known as ashes, mainly consist of calcium, potassium, magnesium, chlorine, and silicon. Their content depends on the nature of the biomass.

1.2.3. Biochar production via thermochemical processes

When the biomass is gradually heated under inert atmosphere, hemicelluloses is the first molecule that undergoes decomposition (200–260 °C), followed by the cellulose (240–350 °C), and lignin (280–500 °C) (Babu, 2008).

The yield of biochar obtained from the process strictly depends on the proportion among these three molecules in the feedstock. In particular, it was demonstrated that pyrolysis of biomasses with a high lignin content results in higher biochar yields (Antal and Grønli, 2003).

When the production of the biochar is aimed at sequestrating the atmospheric CO_2, the most relevant index to take into account is the fixed-carbon yield, the value of which can be associated with the stability of the biochar (Antal *et al*., 2000; Manyà *et al*., 2014a; Zimmerman, 2010). Higher fixed-carbon yields indicate higher carbon sequestration potentials or, in other words, higher capacity of the biochar to trap the CO_2 for longer times. On the other hand, Enders *et al*. (2012) also proposed to use a combination between

the volatile matter content and the elemental proportion between carbon and hydrogen/oxygen to evaluate the stability of biochars.

The processes through which is possible to obtain the thermal degradation of biomass are several and the employment of one or another depends on different factors such as the moisture content of the feedstock or the product of interest.

In recent years, hydrothermal carbonization (HTC) has attracted the interest of an increasing number of researchers worldwide. In this process, the raw feedstock is heated at moderate temperatures (150–250 °C) in presence of water and under autogenerated pressure. The solid resulting from this process is referred as hydrochar. The undiscussed advantage of HTC is that the presence of water in the process avoids the feedstock pre-drying step, permitting to employ biomasses with an elevated moisture content such as sewage sludge and digestate (Belete *et al*., 2021; X. Lu *et al*., 2021).

Gasification of biomass is a promising technology to produce renewable fuel and energy. It is carried out at high temperatures (usually 850–1000 °C) in presence of a gasifying agent such as oxygen, enriched air, steam or CO_2. Through this process it is produced a syngas rich in CO, CO_2, CH_4 and H_2 which could be burnt, converted into liquid through Fischer-Tropsch process, or used in other processes to produce chemicals. The main drawback related to the gasification is the production of tar, which clogs the reactor and reduces the hydrogen yield (Mishra and Kumar Upadhyay, 2021).

When the biomass is destined to be burnt for the generation of heat and power, torrefaction may be carried out to improve its properties as solid fuel. This process is performed under an inert atmosphere and mild temperature conditions (200–300 °C). After undergoing torrefaction, the biomass enhances its properties, increasing its value as fuel. In fact, the thermal treatment results in higher heating values, lower moisture content and O/C and H/C ratios, higher water-resistivity, and enhanced mechanical properties (Mishra and Kumar Upadhyay, 2021).

As for the torrefaction, pyrolysis of biomass is carried out in an inert or semi-inert atmosphere. The main difference between the two processes is the operating temperatures which, in the case of pyrolysis, are higher (> 350 °C) than those reached in torrefaction (< 300 °C).

Among all the above-mentioned processes for the production of biochar, pyrolysis of biomass represents the more versatile option and also the one with which it is possible to obtain the highest biochar yield (Manyà, 2012). During this process, besides biochar, it is also produced a permanent gas fraction and a condensable fraction which is commonly referred as pyrolysis oil. This liquid has a dark color, high viscosity and it is characterized by a pungent smell. It is a multicomponent mixture of hundreds of organic compounds (alcohols, ketones, carboxylic acids, etc.) deriving from depolymerization and fragmentation reactions involving the main constituents of the biomass. The elevated concentration of oxygen-containing compounds (deriving from the secondary pyrolysis reactions) is responsible for the high viscosity of the liquid. The sum of the condensable and permanent gaseous fractions is commonly referred as pyrolysis vapors.

The reactions taking place during biomass pyrolysis can be generally addressed as primary or secondary, depending on when they occur during the process. For what concerns primary reactions, Collard and Blin (2014) discerned them into three different categories. The first group of reactions leads to the formation of biochar, also called primary char, through intermolecular rearrangement, resulting in higher thermal stability and reticulation degree of the solid. The second group of reactions involves the depolymerization of the constituent bio-polymers which results in the formation of monomers that are condensable at ambient temperature and which are the main constituents of the liquid fraction (Mullen and Boateng, 2011; Scheirs *et al*., 2001). The production of permanent gases (e.g., CO_2, CO, CH_4 and H_2, and light hydrocarbons) occurs when the reactions of the third group take place. In this phase, the monomer units create several covalent bonds among them, releasing smaller molecules (Lu *et al*., 2011).

When the volatiles produced from the primary reactions are not stable under the pyrolysis conditions, they can undergo further decomposition or recombination. The reactions involving pyrolysis by-products are labeled as secondary reactions. The products of these reactions could condense on the biochar structure, resulting in the so-called secondary char and increasing the total yield of solid product.

By selecting the most appropriate set of pyrolysis operating conditions (i.e., peak temperature, heating rate, pressure, and inert gas used) it can be possible to drive the process toward the production of a different main product (biochar, pyrolysis oil, or gas).

In this sense, depending on the heating rate and the gas residence time of the process, pyrolysis can be distinguished between:

- **Slow pyrolysis.** It represents the preferred route to produce biochar and it is characterized by slow heating rates (< 10 °C min^{-1}) and long solid residence times (from minutes up to hours and even days). These conditions, in addition to relatively long residence times of the vapor phase, promote the volatiles decomposition and formation of secondary char, leading to an increase in the overall yield of solid product (Manyà, 2019).
- **Intermediate pyrolysis.** It includes aspects of both slow and fast pyrolysis with a heating rate of 30–100 °C min^{-1}, low temperatures (< 500 °C) and solid residence times in the range of 10–30 s.
- **Fast pyrolysis.** It is the process aimed at maximizing the production of pyrolysis oil (Liu *et al*., 2015). Using fast heating rates (>200 °C min^{-1}) and short solid residence times (around 2 s) result in a marked increase in the yield of organic condensable products.

Biomass pyrolysis involves numerous reactions in series and in parallel, whose extent depends on several factors. The complexity of the process makes it crucial to deeply understand the effects that the process conditions have on the biochar, pyrolysis oil and gas (in terms of products yield and quality).

Firstly, as mentioned in the previous section, the process heating rate discerns between fast, slow or intermediate pyrolysis. Slow pyrolysis is the one with the highest yield in biochar, meanwhile fast pyrolysis shows the highest yields of pyrolysis oil.

The reaction temperature is the most crucial parameter to consider. Several studies agree that the increase in pyrolysis temperature leads to an increase in the amount of gas produced, at the expense of the biochar yield (Demirbas, 2004; Di Blasi *et al*., 1999; Greco *et al*., 2020). The resulting biochar, however, is characterized by higher fixed carbon content (Greco *et al*., 2020). Pyrolysis temperature also affects the stability of the biochar. In fact, several studies have demonstrated that higher pyrolysis peak temperatures foster the polyaromatization reactions, resulting in an increase in the percentage of aromatic carbon in the biochar and, consequently, its stability and resistance against biotic and abiotic oxidation (Manyà *et al*., 2014b; Mcbeath *et al*., 2014).

Although pyrolysis is generally carried out under inert atmosphere, different studies have investigated the effects of using a different atmosphere (rather than pure inert gas such as nitrogen or argon) on pyrolysis behavior and product yields. Xu *et al*. (2020) found that mixtures of CH_4 and CO_2 can improve the pyrolysis oil production, if compared with the traditional N_2. On the other hand, Greco *et al*. (2018) observed an increase in gas production at the expense of pyrolysis oil when a mixture of CO_2 and N_2 was used instead of pure N_2. They ascribed this behavior to the promotion of the volatiles thermal cracking.

The effects of the pyrolysis absolute pressure on the process products are still unclear and the studies reported in the literature are inconsistent with each other (Manyà, 2019). However, in their recent study, Greco *et al*. (2020) analyzed the effect of several slow-pyrolysis conditions through a statistical approach, revealing that the increase in pyrolysis pressure resulted in an increase in the gas yield, without altering the biochar yield.

Pyrolysis conditions not only affect the biochar yield but also its physicochemical properties (Tomczyk *et al*., 2020). High pyrolysis temperatures cause the release of more volatile matter with consequent formation of micropores and, in particular, of ultra-micropores with a diameter smaller than 2 nm (Greco *et al*., 2020). Similar conclusions were drawn by Ronsse *et al*. (2013) but they also found that, depending on the biomass ash content, when the temperature was increased above 600 °C, the BET surface area started diminishing due to the onset of ash melting.

The increase in heating rate and residence time also results in the increase in BET surface area. The heating rate has also a positive effect on the micropores volume, while the residence time does not affect at all the pore size distribution (Zhao *et al*., 2018).

1.2.4. Biochar applications

Due to the heterogeneous composition of the starting material and depending on the production operating conditions, biochar could also be characterized by a certain concentration of surface functional groups, which could be useful for several applications (Greco *et al*., 2020; Xiong *et al*., 2021). **Figure 1** graphically summarizes all the different fields of applications of biochar.

The ability of biochar to enhance soil quality, due to its capacity to influence the biochemical and biological processes (Arif *et al*., 2017; Lehmann and Joseph, 2015; Paz-Ferreiro *et al*., 2015), has been extensively reported in the literature (Rathnayake *et al*., 2021a, 2021b; Y. Zhang *et al*., 2021). For example, application of biochar to soil is able to

increase the overall surface area, improving the retention of water (Lehmann and Joseph, 2015) and the soil aeration (Kolb *et al*., 2009). Furthermore, the high cation exchange capacity (CEC) of certain biochars increases the availability for plants of some essential nutrients (Ca^{2+}, Mg^{2+}, K^{+} and NH_4^{+}) (Videgain-Marco *et al*., 2020; Yuan *et al*., 2011). As a negative aspect, it should be mentioned that, depending on the nature of biomass and the process conditions selected during biomass pyrolysis, the resulting biochar can contain some amounts of heavy metals and polycyclic aromatic hydrocarbons (PAHs), which are considered as potentially toxic elements for soil (Freddo *et al*., 2012).

Biochar also finds application in the pollutant removal field, as a low-cost adsorbent for wastewater treatment (Inyang *et al*., 2016). Numerous studies have reported that biochar can be successfully employed in several contexts such as the removal of heavy metals (Georgieva *et al*., 2020; Junhong Liu *et al*., 2020; Ma *et al*., 2014) or organic compounds (Cheng *et al*., 2021; Escudero-Curiel *et al*., 2021). Another noteworthy application of biochar-based adsorbents is the adsorption of CO_2 under both pre- and post-combustion conditions (Durán *et al*., 2018; Inyang *et al*., 2016; Manyà *et al*., 2020, 2018b; Querejeta *et al*., 2019). Furthermore, a recent study showed the capacity of N-doped biochar of simultaneously remove H_2S and CO_2 from biomass-derived syngas (Ma *et al*., 2021).

Due to their adjustable chemical and physical properties, biomass-derived carbons are being considered as a valid alternative to other carbonaceous materials for the production of anodes for sodium-ion batteries (Zhao *et al*., 2021). Plant-derived hard carbons retain the plant tissue microstructure which facilitates the electrolyte penetration and Na^{+} diffusion. Moreover, HCs preserve part of the natural heteroatoms (N, S, K, B, etc.) providing more sodium storage sites and improving the sodium storage performance (Dou *et al*., 2019; Y. Li *et al*., 2020; Yu *et al*., 2020). In addition, biochar is also studied as a promising material for the production of electrodes for supercapacitors. Depending on the feedstock and on the pyrolysis conditions, biochar may have abundant oxygenated functional groups that can enhance the pseudocapacitance and increase the amount of energy stored in these biochar-based supercapacitors (Liu *et al*., 2015).

The employment of biochar as catalytic support or catalyst itself is gaining interest in the scientific community due to its relatively low production cost (thanks to the large availability of biomass (Chatterjee *et al*., 2018)) and to its easy functionalization. Biochar-based catalysts have been studied in different fields of application such as biodiesel

production (Yan *et al*., 2013), pyrolysis oil upgrading (Dong *et al*., 2018), and pyrolysis vapors upgrading (Fu *et al*., 2019). The main problem related to this type of catalysts is that, depending on the process involved, they are likely to undergo deactivation, due to the modification of the surface chemistry (Lee *et al*., 2017) or coke deposition (Chen *et al*., 2018).

Another interesting feature of biochar-based catalysts is that at their end-life stage, and depending on their composition, they could be employed as a soil amendment or gasified/burned to recover energy and active phases (Dufour *et al*., 2008; Shen, 2015). Lu and El Hanandeh (2019) investigated these two final utilizations of biochar concluding that the employment of biochar to displace coal in coal-fired power plants is the best choice in terms of economic and environmental performances.

However, despite the fact that biochar may possess a relatively developed porosity, it is usually not sufficient to guarantee satisfactory catalytic and adsorption performance (Shen *et al*., 2014). Because of this, a further treatment aimed at improving the original textural properties of the raw biochar is mandatory.

Figure 1 schematically shows all the possible applications of biochar, whereas Table 1 lists the advantages and disadvantages of the employment of biochar in the above-mentioned applications.

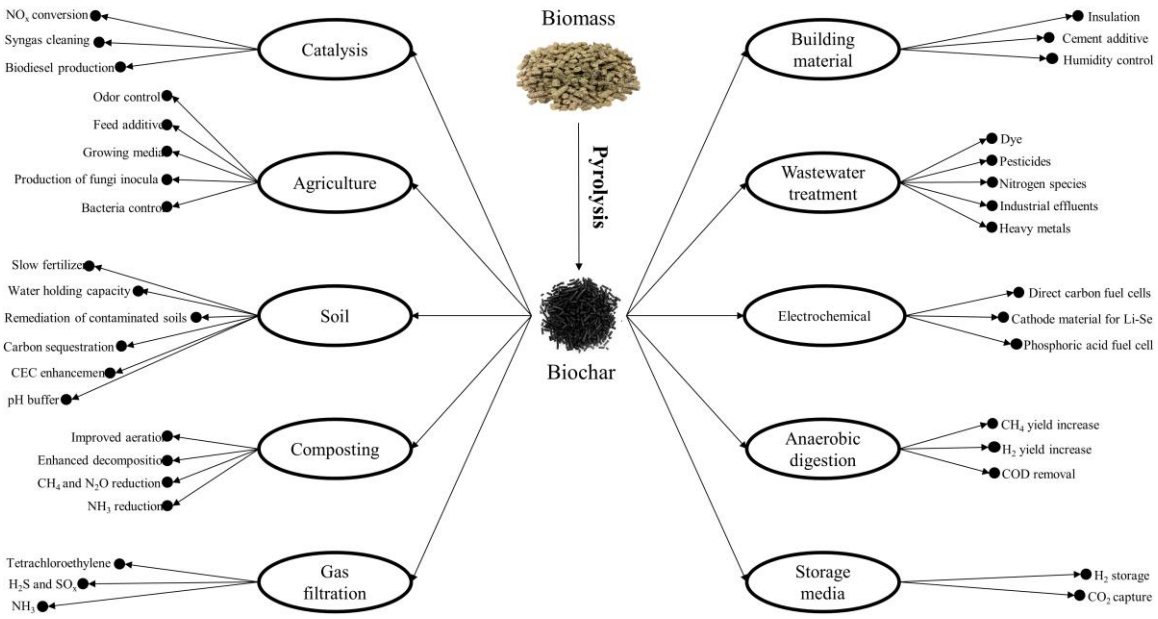

Figure 1. Biochar applications (Manyà, 2019).

Table 1. Advantages and disadvantages of biochar applications. Table adapted from Qian *et al*. (2015).

Application	Purpose	Advantages	Disadvantages
Catalysis	• Syngas cleaning/ upgrading • Bio-diesel production,	• Easy to recycle • Relatively cheap	• Low efficiency • Deactivation
Soil amendment	• Carbon sequestration • Soil quality improvement	• Relatively cheap • Nutrient retention	• PAH • Heavy metals
Sorbent of contaminants	• Contaminants adsorption	• Low cost • Abundant • Sustainable resource • Oxygenated groups on biochar surface facilitate adsorption	• Uncertain effectiveness • Heavy metals
Storage material	• CO_2 storage • H_2 storage	• Low cost, abundant and sustainable resource • Oxygenated groups on surface facilitate adsorption	• Uncertain efficiency
Activated carbon	• Activated carbon precursor	• Low cost • Abundant • Sustainable resource	• Requires surface improvement

1.2.5. The importance of tuning the properties of biochar

As mentioned in the previous section, depending on the production process and conditions, pristine biochar might not have the adequate textural properties or functional groups to be employed in different fields such as catalysis or adsorption, in which surface area and functionality play a crucial role (Manyà, 2019). Hence, an "activation process" is usually required to expand the biochar specific surface area and pore size distribution (PSD) or to provide some heterogenous atoms to the carbon matrix. Depending on the activation procedure and the activating agent employed, the activation methods can be categorized into physical or chemical ones (Cha *et al*., 2016; Guo and Lua, 1998).

Physical activation procedures (which are also referred as gaseous activation (Leng *et al*., 2021)) usually involve a gaseous agent, which reacts with biochar to partially gasify its

surface, leading to a certain increase in the specific surface area and an introduction of some oxygenated functional groups such as C=O and COOH.

During the activation process, the selective extraction of the carbon atoms by the gasifying agent produces a continuous recombination and reorganization of the remaining carbon layers. Therefore, the pore structure of the resulting activated biochar depends on the mechanism by which the activating agent reacts with the solid (Y. Liu *et al*., 2021a).

Even though the physical activation route requires high temperatures, it is considered an eco-friendly option because it does not involve potentially pollutant reactants (Lee *et al*., 2018).

In the case of chemical activations, the improvement of the specific surface area is obtained through the employment of a chemical agent, which decomposition products react with biochar, creating a porous structure. The starting material is mixed with a chemical agent (acid, base or salts), which promotes the gasification or the functionalization of the solid. Then, the blend undergoes thermal treatment (typically under inert atmosphere) to decompose the precursors. The procedure can involve the raw biomass before pyrolysis (one-step activation) or the pristine biochar (two-step activation).

Lower temperatures, higher carbon yield and finer tuning of the porous structure make this procedure more appealing than physical activation (Patra *et al*., 2021; Yorgun *et al*., 2009).

2. State of the art

Due to its relevance among the other NETs, its versatile features, and its relatively low cost, the interest of the scientific community for biochar has grown exponentially in the last years. In this sense, a particular interest has been paid to the production of activated biochars and to the employment of biochar-derived materials in catalytic applications (see Figure 2). Nevertheless, the related research is still at its early stage and presents a deep lack of knowledge to fill. Therefore, in this work, physically (with CO_2) and chemically (with K_2CO_3) activated biochars are proposed as catalysts and catalytic supports to be employed in two sustainable energy-related applications:

1. The improvement of the pyrolysis-syngas yield through the steam reforming of slow pyrolysis oil.
2. Methanation of CO_2 (Sabatier reaction) as CCU technology to produce methane to be directly injected into the distribution grid.

In this chapter, a comprehensive state of the art about the biochar activation techniques and its application in the two above-mentioned processes is given.

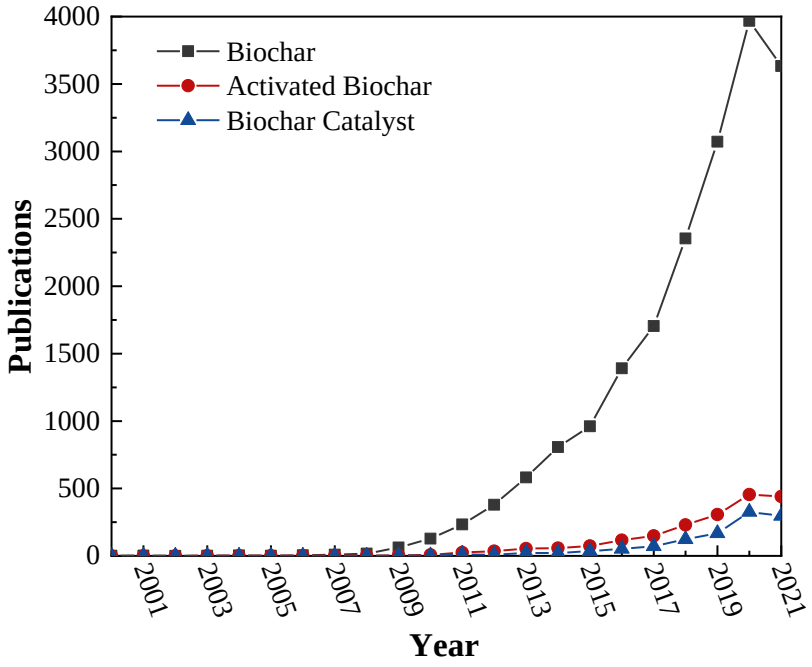

Figure 2. Number of publications per year whose abstract, keywords or title contains the words "biochar catalyst", “activated biochar” or “biochar” (Elsevier, 2021).

2.1. Activation and functionalization of biochar

2.1.1. Physical activation with CO_2

For this kind of activation process it is possible to employ any reactant with oxidizing properties being the most employed activating agents are O_2, H_2O, and CO_2. The choice of an activating agent rather than another also depends on the final application of the activated biochar. In fact, each agent involves different reaction mechanisms which lead to distinct results in terms of pore size distribution and activated carbon yield. For example, CO_2 activation tends to create a large fraction of micropores, meanwhile with steam it is possible to obtain a more heterogeneous pore size distribution (Lee *et al*., 2018; Lopes *et al*., 2021).

Air or O_2 activations are usually the most economical methods due to the high oxidizing potential of oxygen which results in a lower activating temperature (< 500 °C). The main drawback is represented by the high exothermicity of the involved reaction, which results in a not optimum control of the process and an excessive conversion of the solid, with the consequent decrease in the yield of activated carbon (Zhu *et al*., 2018).

On the other way, steam activation represents a very attractive alternative due to the huge availability of the reactant. The activation mechanism involves the formation of a carbon-oxygen complex and the production of hydrogen. Then, CO is released and could react with water in the reaction environment through water gas shift (WGS) to produce more H_2 and CO_2 (Sajjadi *et al*., 2019).

Nevertheless, the most used agent is probably CO_2 due to its extensive application in biomass and coal gasification processes (Habibollahzade *et al*., 2021; Midilli *et al*., 2021). Activation with CO_2 represents an appealing strategy in terms of energy efficiency and economic feasibility. In fact, CO_2-rich flue gas deriving from the pyrolysis step or biomass combustion could be recycled in the activation stage, reducing the overall cost of the activated biochar production (Azuara *et al*., 2017).

The main reaction involved in CO_2 activation is the reverse Boudouard reaction (Eq. 1) through which carbon dioxide reacts with the carbon surface of biochar, producing carbon monoxide and creating vacancies on the biochar surface. The reaction is endothermic; therefore the process must be carried out at medium-high temperatures (700–1300 °C) (Guizani *et al*., 2013; Lahijani *et al*., 2013; Senneca, 2007). The most widely accepted mechanism was firstly proposed by Ergun in 1956 (Lahijani *et al*., 2015):

$C + CO_2 \rightleftarrows 2\,CO$ ΔH_{298K}= 172 KJ mol^{-1} ΔH_{298K}=¬KJmol^{-1} (1)

$C_f + CO_2 \rightarrow C(O) + CO$ (2)

$C(O) + C \rightarrow CO + C_f$ (3)

where C_f represents a free carbon active site and C(O) a carbon-oxygen surface complex. Following this mechanism, CO_2 is firstly dissociated, and a free carbon is occupied by a C(O) complex with the production of one molecule of CO (Eq. 2). Afterward, the complex is released as CO and a new carbon site becomes available (Eq. 3).

Tancredi *et al*. (1996) associated the increase in the reactivity of the carbon toward gasification to its specific surface area, which gradually increased during the process. Nevertheless, the increase in reaction rate would eventually stop and starts to decline, as observed by Jing *et al*. (2013). They ascribed the initial increase in reaction rate to the enlargement of the clogged porous with the consequent increase in the specific surface area. This finding could also suggest that biochar with higher surface area (i.e., produced at higher pyrolysis temperatures) is more reactive toward physical activation. Nevertheless, Min *et al*. (2011) found a higher reactivity toward gasification in the case of biochars produced at lower temperatures. They attributed this result to the presence of very small pores on the biochar produced at higher temperatures, which hinder the diffusion of CO_2 inside the solid. With the proceeding of the reaction, the porous structure might collapse, reducing the available surface area with a consequent decrease in the gasification rate.

The reaction temperature is the most important parameter to consider for the biochar CO_2 activation. Tian *et al*. (2021) studied the effects of the pyrolysis conditions and gasification temperature on biochar gasification reactivity. They found that the reactivity of biochar toward CO_2 gasification was mainly affected by the gasification temperature. and also that the increase in the activation heating rate improved the reactivity of the biochar by 7.6 times.

X. Zhang *et al*. (2021) activated a soybean straw derived-biochar with CO_2 in a wide temperature range (500–900 °C). These authors identified 600 °C as threshold temperature below which no significant surface area development occurred.

It is well known that the observed conversion rate of a generic reaction is the result of the combination of several phenomena. In particular, the driven mechanism could be discerned between chemical and diffusion regimes. In the case of the gasification reaction,

it has been observed that the activation temperature plays a key role in determining the prevalent mechanism. Specifically, when the activation temperature is lower than 850 °C, the mechanism is dominated by the chemical reaction regime while at temperatures higher than 900 °C, the reaction rate is defined by the diffusion regime. Instead, in the range 875 < *T* < 900 °C there is a transition state in which chemical reaction and pore diffusion regimes coexist (Lahijani *et al*., 2013).

Previous studies focused on the influence of the activation temperature on the textural properties of the resulting activated biochars. Guo *et al*. (2009) characterized several biochars activated in the range of 750–950 °C, finding a correlation between the micropores volume and the specific surface area and the increase in temperature until 900 °C. Afterward, at T > 900 °C, the enlargement of the pores resulted in a decline of the area.

Even though at low temperatures the reaction rate is slow, through a wise selection of the activation time it is possible to obtain satisfactory results. Jedynak and Charmas (2021), for example, pyrolyzed Norway spruce cones to obtain the starting biomaterial and then, through a long activation step (6 h) at 850 °C, the resulting carbons exhibited a large surface area (1167 m^2 g^{-1}), which was mainly accounted by a large fraction of micropores. Despite long activation times lead to an important decrease in the final solid yield (Jung and Kim, 2014), a plateau value could eventually be reached, as demonstrated by Y. Liu *et al*. (2020).

Even though numerous works focused their attention on the influence of activation temperature and time on the textural properties of the resulting activated biochar, only a few of them investigated the effects of the activating pressure. In a single-step pyrolysis/activation scheme, it was found that the increase in pressure up to 1.0 MPa harmed the textural properties of the product, resulting in microporous area reduction not accompanied by an increase in the mesopore volume (Puig-Gamero *et al*., 2021). On the other hand, Schneider *et al*. (2021) demonstrated that the increase in activating pressure resulted in an increase in CO_2 gasification rate. Furthermore, they found a correlation between the pyrolysis temperature and the gasification reactivity. Specifically, a very high pyrolysis temperature (1600 °C) led to the formation of a thin layer of CaO, which catalyzed the gasification of the solid in the activation step.

Considering the non-homogeneous composition of biochar, the gasification reaction could be considered as the sum of two different mechanisms: non-catalytic gasification,

only depending on the gasification conditions and the biochar physicochemical properties; and a catalytic gasification, the extent of which depends on the ash content and composition (Lahijani *et al*., 2015). Kannan and Richards (1990) found a direct correlation between the K and Ca content in biochar and the rate of gasification. However, the presence of Si could hinder the catalytic process, reducing the K content to form silicate during the pyrolysis step.

2.1.2. Chemical activation with K_2CO_3

One of the most used chemical agents is H_3PO_4 with which it is possible to achieve high values of specific surface area (Z. Lu *et al*., 2021). Fotouhi Tehrani *et al*. (2015) investigated H_3PO_4 activation of coffee residue under different temperatures and acid concentrations, finding a maximum value of specific surface area at 600 °C using a 40 wt. % acid loading.

Numerous studies focused on chemical activation through $ZnCl_2$ demonstrated its effectiveness in the production of microporous activated carbons (Angin *et al*., 2013; Yorgun *et al*., 2009).

Other commonly used activating agents are H_2SO_4 (Jawad *et al*., 2021), KOH (Kaya and Uzun, 2021), H_2O_2 (Fu *et al*., 2017) and NaOH (Fu *et al*., 2013). Despite the proven capability of these chemicals, the main drawback related to their employment is that, due to the nature of the reactants involved, a large amount of wastewater is generated (Fu *et al*., 2013). Residual $ZnCl_2$ and H_3PO_4, for instance, are hardly separated from the activated biochar, hindering its applications in soils (Tsai *et al*., 2001). Furthermore, the employment of strong acids and bases can damage the equipment, and, consequently, increases the maintenance-related costs (Hayashi *et al*., 2002).

An appealing alternative, which could be employed in large-scale applications, is the usage of cheaper and non-hazardous carbonates such as K_2CO_3.

Although the use of K_2CO_3 as a catalyst in coal gasification processes has been widely reported in the literature (Mai *et al*., 2019; Sayğılı and Akkaya Sayğılı, 2019; L. Wang *et al*., 2020), the mechanism explaining its interaction with the carbon matrix is still unclear. The main reactions that probably occur during chemical activation of a carbonaceous material are the following (Dehkhoda *et al*., 2016):

$$K_2CO_3 \rightleftarrows K_2O + CO_2 \quad (4)$$

$$K_2CO_3 + 2C \rightleftarrows 2K + 3CO \quad (5)$$

$$K_2O + C \rightleftarrows 2K + CO \quad (6)$$

The increase in the specific surface area could be ascribed to the CO_2 released from carbonate decomposition (Eq. 4), which can diffuse into the solid structure and subsequently react with carbon, thereby stimulating the production of CO by the reverse Boudouard reaction (Eq. 1) and creating vacancies in the solid structure (Matos *et al*., 2005). Although the decomposition of K_2CO_3 mainly occurs at temperatures above 900 °C, its contact with the carbon matrix can promote its decomposition a relatively low temperature (Lozano-Castelló *et al*., 2007). The potassium oxide resulting from the decomposition of the carbonate, or the carbonate itself, can also react with the carbon-based material through Eqs. 5 and 6 towards CO and metallic potassium (Dehkhoda *et al*., 2016).

Chemical activation with K_2CO_3 has been reported to be effective to produce biomass-derived activated carbons, resulting in carbons with a high percentage of structural defects and high specific surface areas. In this sense, Kim *et al*. (2021) have compared the results obtained through the chemical activation with KOH and K_2CO_3. Their results show that, even though the carbonate is less effective than the hydroxide in the expansion of the BET area (2162 m^2g^{-1} and 3047 m^2g^{-1} obtained with K_2CO_3 and KOH, respectively), it remains a solid alternative to the commonly used agent.

When employed for the one-step activation (i.e., impregnation of the starting biomass) K_2CO_3 facilitates the decomposition of cellulose, allowing it to occur at 150 °C (100 °C lower than the non-catalyzed pyrolysis) (Chen *et al*., 2021). Another advantage of the employment of K_2CO_3 is that it could be effective even at temperatures lower than 500 °C (Hayashi *et al*., 2002).

Both chemical and physical activations could also be coupled. In this line, L. Wang *et al*. (2020) proposed a combined physical-chemical activation in which the carbon sample was previously impregnated with a small K_2CO_3 loading (< 2 wt. %) and subsequently physically activated with CO_2. In this case, the carbonate acted as a gasification catalyst, enhancing the textural properties of the produced carbon.

2.1.3. Doping with heteroatoms and metals

As already mentioned before, the employment of biochar as support for catalytic formulations is gaining interest due to its interesting and unique properties.

The production of biochar-based metallic catalysts is usually carried out through impregnation of the carbonaceous support with an aqueous solution of the desired metal precursor, followed by a calcination and a reduction step aimed to the decomposition of the precursor and to the reduction of the metal, respectively. The deposition of the metallic phase could also be carried out through precipitation methods. In this case, biochar is firstly soaked in an aqueous solution of the metal salt and then a precipitation of nanoparticles (NPs) is obtained through pH adjustments (Jiwei Liu *et al*., 2020).

An interesting alternative is the impregnation of the raw biomass instead of biochar. When biomass is mixed with some high-valent metal, the reducing properties of the resulting biochar and the presence of reducing agents in the pyrolysis vapors may lead to the formation of a biochar loaded with zerovalent metallic NPs. Through this procedure it is possible to avoid further calcination and reduction steps and, moreover, the metallic NPs could have catalytic effects during the process, improving the quality of the pyrolysis oil and/or the features of the biochar (Liu *et al*., 2015). The same method could also be used to integrate heteroatoms into the biochar structure. X. Wang *et al*., (2019), for example, successfully carried out the incorporation of N atoms into the biochar matrix to produce a Ru-based catalyst. They found that blending the biomass with urea before the pyrolysis was effective for introducing nitrogen atoms, which promoted the anchoring of the metallic active phase. However, the effects of the urea loading on the NPs distribution were not completely unveiled.

Both activation methods (one- and two-step) have advantages and disadvantages. Impregnation of raw biomass allows to avoid the energy-consuming reduction and calcination step and promotes the dispersion of metallic NPs. This route could be interesting when biomass-derived carbons are produced at small scale. However, when biomass is processed at industrial scale for biochar and bioenergy purposes, activating pristine biochar instead of its biomass precursor could be more interesting in order to promote its sequential use and strength the value chain, as mentioned in Section 1.1.

2.2. Activated carbons textural characterization

The assessment of the specific surface area and of the pore size distribution is a crucial analysis for an activated carbon because it allows to evaluate the effectiveness of the activation process and the influence of the different activating conditions.

The most popular method employed for this characterization is the physical adsorption of gases. Nitrogen, among all the other employed species, is the most commonly used one because, with this probe molecule, it is possible to cover a wide interval of relative pressures and, therefore, to characterize the sample in the entire range of micropores and mesopores. Nevertheless, the occurrence of diffusional issues in the narrowest pores leads to the necessity of moving toward very low relative pressures (Rodriguez-Reinoso *et al*., 1984). Taking into account that biochars and activated biochar are characterized by an important fraction of ultramicropores, N_2 is probably not the best option.

A possible solution to this problem is the usage of a different probe molecule. Given that the diffusion is strongly dependent on the operating temperature, a possible alternative to investigate solids with narrow porosity is the employment of CO_2 as adsorbate. In fact, N_2 physisorption is carried out at 77 K, meanwhile CO_2 adsorption is isothermally performed at 273 K and this higher temperature allows to overcome the diffusional problems.

Through the analysis of the adsorption isotherm using a mathematical model it is possible to extrapolate information about the porous volume and the specific surface area of the solid. Brunauer-Emmett-Teller (BET) and Dubinin–Radushkevich (DR) methos are probably the most popular of them. However, the results obtained through their application are not always reliable (Kwiatkowski *et al.*, 2019). More recently, the most common used method has been the non-local density functional theory (NLDFT) which also lack in reliability when the analyzed sample is characterized by a broad PSD.

In 2019, Jagiello *et al.* have successfully evaluated the PSD of two activated carbons through the employment of the two-dimensional version of the non-local density functional theory (2D-NLDFT) using the data collected by both N_2 and CO_2 isotherms. With this methodology they were able to accurately describe the whole PSD of the analyzed carbons.

2.3. Biomass pyrolysis oil

The yield and chemical composition of biomass pyrolysis oil depend on different factors such as composition and pyrolysis process conditions. In general, woody biomass produces pyrolysis oil with high content of phenols, meanwhile the pyrolysis liquid obtained via straw biomass pyrolysis is generally rich in ketones (Li *et al*., 2017). Pyrolysis of a feedstock with high content in ashes produces a lower yield of pyrolysis oil, which is characterized by a high content of water. This is due to the catalytic effect that potassium or other inorganic could have on the degradation of the pyrolysis vapors (Banks *et al*., 2016). Particle size also resulted to be influent on the total liquid yield. In fact, during the pyrolysis of larger pieces of biomass, the "actual heating rate" of the inner part of the particle is lower if compared with that of the reactor. This causes a decrease in pyrolysis oil yield due to the promotion of the recombination (charring) reactions over the simultaneous bond scission (formation of volatiles) (Shen *et al*., 2009).

Among the pyrolysis conditions, the process temperature is one of the most influential parameters that must be considered. In fact, high process temperatures can promote the formation of aromatic compounds, including polyaromatic structures (**Figure 3**) (Blanco *et al*., 2012).

Depending on its chemical composition, which is related to the pyrolysis conditions and starting biomass, the resulting pyrolysis oil could be employed as fuel or as a precursor to produce other chemicals (Czernik and Bridgwater, 2004). A comparison among the properties of pyrolysis oil, gasoline and diesel is reported in **Table 2**. These properties make pyrolysis oil a platform for the chemical industry and a valid alternative to the commonly used fossil sources. Furthermore, using biomass sources widely available in Europe for the production of bio-fuels could ensure a certain independence from crude oil and natural gas suppliers.

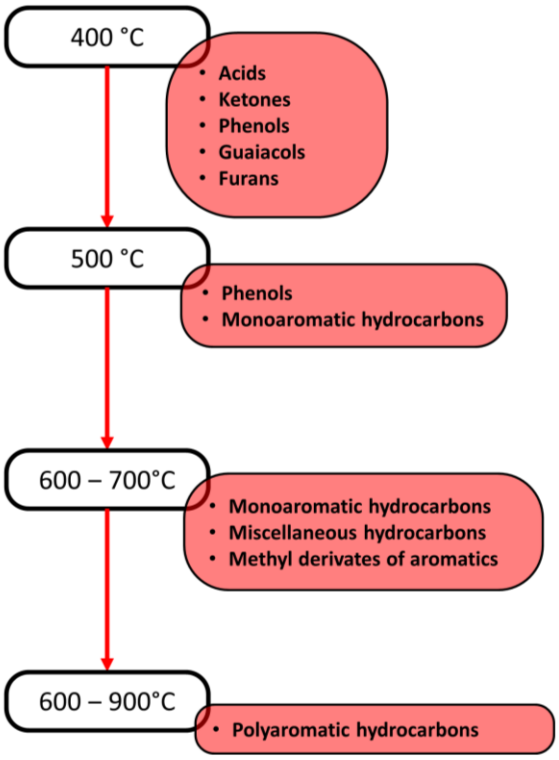

Figure 3. Pyrolysis oil composition as a function of pyrolysis temperature (Blanco *et al*., 2012).

Table 2. Comparison between the properties of pyrolysis oil, diesel and gasoline. Adapted from (Gupta *et al*., 2021).

	Pyrolysis oil	**Diesel**	**Gasoline**
Ultimate analysis (wt.%)			
C	54–58	86	87
H	5–8	11	13
O	34–40	0.02	Negligible
N	0–0.3	0.06	/
Physicochemical properties			
pH	2–3	7	7
Water content (wt. %)	20–40	Negligible	0–0.01
Viscosity (Cst) at 50 °C	26–1000	<2.30	0.77
Density (Kg m^{-3})	1200–1300	854	746
Pour point (ºC)	–10 to –20	–23	–40 to –50
Flash point (ºC)	60–80	85	–45
Heating value (MJ Kg^{-1})	16–20	44.5	46

However, several aspects hinder the pyrolysis oil exploitation. One of the main problems is related to the handling of such liquid, which is not chemically stable and, therefore, its composition is likely to change during the storage (Zhang *et al*., 2007). Another issue is linked to its content in water, deriving from dehydration reactions and from the biomass original moisture, which is recovered as a condensate product along with the pyrolysis oil. The presence of water in the pyrolysis oil (35–85 vol. %) has two big effects: it notably lowers the viscosity of the pyrolysis oil, which is convenient and on the other hand, the water lowers the mixture heating value and increase the ignition point of

the mixture, hindering its employment as a liquid fuel. Therefore, it is mandatory to perform further separation processes aimed at removing water. These processes cause a consequent increase in the overall costs related to the employment of pyrolysis oil as liquid fuel, which cannot compete with those of the oil market (de Miguel Mercader *et al*., 2010; Ning *et al*., 2013).

Kang *et al*. (2018) proposed an alternative use of pyrolysis oil. They studied the employment of the viscous liquid as a binder for the production of biomass fuel pellets with enhanced properties. Their results showed that the impregnated pellets were characterized by a higher energy density and higher hydrophobicity, with respect to the standard ones.

When pyrolysis is aimed at the production of biochar (i.e., slow pyrolysis), the condensable fraction (highly rich in water) is an undesired product because it reduces the yield of the solid and it could condense in the piping system, the reactors or the heat exchangers, causing clogs and system breakdowns. Therefore, the implementation of a strategy that involves upgrading processes aimed to remove or reduce the amount of this liquid is desirable. The upgrading process can be labeled as "primary" or "secondary", depending on where it takes place. If it is carried out using the water and the other products of the pyrolysis as reactants, it is called "primary process". Otherwise, if an external supply of reactants is needed, the process is referred as secondary.

2.4. Selected applications

2.4.1. Pyrolysis vapors upgrading

As mentioned before in Section 0, when the pyrolysis of the biomass is aimed at biochar production, the relatively low yield of pyrolysis oil represents an undesired product that should be removed. It is important to bear in mind that this pyrolysis product is a complex mixture that could contain more than 100 organic compounds (Merckel *et al*., 2021; Yang *et al*., 2016), which, depending on the storage conditions, are likely to undergo aging processes. Furthermore, the inherent composition of the biomass is related to numerous variables (species, soil, growth, storage, etc.) and this also affects the composition of the resulting pyrolysis oil (Kenney *et al*., 2013). Therefore, in order to guarantee the consistency of the studies, numerous research studies have been carried out using model compounds, such as benzene (Hervy *et al*., 2019; Park *et al*., 2010), acetic acid (Rioche *et*

al., 2005), eugenol (Ledesma *et al*., 2013), or a mixture of these to represent a likely pyrolysis oil composition (Hu and Lu, 2009).

One of the simplest upgrading routes is the thermal degradation (or thermal cracking) of the reactant. This process consists of feeding the pyrolysis oil in a secondary reactor at high temperatures (700–1000 °C) to decompose the organic condensable products into smaller molecules and permanent gases (Zhang *et al*., 2007). In order to improve the selectivity toward the desired product and/or to lower the operating temperature, it is a common practice to use a catalyst. The main drawback is that besides the above-cited products, coke is also produced to large extents. Carbon deposits could create a layer on the catalyst's surface, causing its deactivation. To address this problem, Iojoiu *et al*. (2007) proposed a two-step sequential process where the cracking phase is followed by a regeneration step of the catalyst with air to oxidize the coke and free its surface.

Steam reforming (SR) is considered the most promising strategy for pyrolysis vapors upgrading. Because of its high rate of reaction and high reliability (George W. Huber *et al*., 2006), SR represents a valid alternative for large-scale applications. The high amount of water generated during the pyrolysis step could be sufficient to guarantee high reactant conversion degrees and an elevated steam to carbon molar ratio (S/C), which is essential to limit coke formation. Furthermore, considering the endothermic nature of the reforming reaction, the hot gases generated during the pyrolysis can be directly fed to the upgrading reactor (reformer) without the implementation of any external heat supply.

Historically, steam reforming has largely been used to convert natural gas or hydrocarbons into syngas, a hydrogen and carbon monoxide mixture used as a platform for the synthesis of chemicals. Besides the main steam reforming, other reactions such as water gas shift (WGS), Boudouard, and thermal cracking are likely to occur.

In SR, the employment of a catalyst is essential to achieve high conversions and a adequate selectivity toward the desired products. The production of a highly performant catalyst involved formulations based on Rh, Ir (Vagia and Lemonidou, 2008), or Pt (Takanabe *et al*., 2004), the cost of which discourages their large-scale application. Transition metals such as Ni (Fu *et al*., 2019), Fe (Noichi *et al*., 2010), and Co (Phongprueksathat *et al*., 2019) represent a good trade-off between cost and catalytic performance (J. Li *et al*., 2020).

Considering that, during steam reforming of heavy compounds (such as that present in pyrolysis oil), metallic phase sintering and coke deposition are the two main deactivation mechanisms, it is important to employ a catalytic formulation that hinders such phenomena. In this context, X. Li *et al*. (2020) carried out a comprehensive study about the coking behavior of several pyrolysis oil model compounds during their steam reforming over a Co catalyst supported on Santa Barbara Amorphous (SBA), a mesoporous form of silica. Their findings showed that the formation of coke was the dominant reaction route in the steam reforming of sugars and furfuryl alcohol.

In the last years, a growing interest in using biochar as catalyst or catalyst support has arisen, due to its versatility, relatively low cost and tunable pore size distribution (Guo *et al*., 2020). In this way, it could be possible to create a circular economy approach around the biomass pyrolysis in which biochar is firstly produced through slow pyrolysis; activated and/or functionalized; employed to upgrade the pyrolysis vapors and, at their end-life stage, gasified/burned to recover energy and active phases (Dufour *et al*., 2008; Shen, 2015). Furthermore, depending on the added metals and on the contamination of the sample, spent biochar catalysts could also be used for soil amendment applications.

Despite the interesting opportunity offered by biochar-based catalyst employment, research related to its application in steam reforming of pyrolysis oil is still limited, as deduced from **Table 3**. Several authors studied the direct application of biochar as catalyst, without the addition of any external active phase. For example, Wang *et al*. (2017) found that, through a fixed bed of biochar, it was possible to completely convert all the C3s and C4s of the pyrolysis vapors, increasing the H_2 content of the resulting syngas. The catalytic activity of the biochar toward steam reforming is ascribed to its inherent ash composition. In particular, its high content of alkali and alkaline earth metal (AAEM) species plays a key role in these processes, especially in WGS (Ma *et al*., 2017). However, depending on the biomass source, the amount of AAEMs could not be sufficient to ensure an appropriate catalytic activity of biochar. Ducousso *et al*. (2019) *et al* found that biochar doped with Ca or K was able to notably increase the syngas production during CH_4 cracking. They ascribed this phenomenon to the capacity of AAEMs for trapping oxygen atoms and making them available to react with CH_4,

To better address the process needs, biochar can be activated prior to its employment in the catalytic process. Generally, CO_2 or steam activations are performed to increase the

specific surface area of the solid and to provide O-containing functional groups. Even though it was demonstrated that O-groups can improve the catalytic activity of biochar, they are likely to be removed during SR, causing a gradual deactivation of the catalyst (Yang *et al*., 2020). On the other hand, Y. Liu *et al*. (2021b) highlighted the stability of the morphology of H_2O-activated biochar, showing that SR of pyrolysis oil at 800 °C did not result in significant textural properties changes of the spent catalyst.

The porous structure also plays an important role, with macro and mesopores being more resilient toward deactivation and more reactive in pyrolysis oil steam reforming (Buentello-Montoya *et al*., 2020).

Due to its thermal stability, high surface area and functional groups, activated biochar is also being studied as support for metallic active phases, mainly Ni.

The biochar activation procedure could influence on the properties of the support producing positive or negative effects on the catalytic outcomes. It was demonstrated, for example, that HNO_3 pre-treatment can enhance the strength of the biochar acidic site but however, it weakens the Ni-biochar interactions causing sintering of the metallic particles. Furthermore, it could also change the hydrophobicity of the support, which was demonstrated to be able to modify the steam reaction mechanism (Y. Wang *et al*., 2020).

Du *et al*. (2019) produced nickel-functionalized biochar through a one-step process and then tested the catalyst in steam reforming of toluene and real pyrolysis oil. They found a close correlation between the size of the nickel nanoparticles and the catalytic outcomes, with the smallest particles performing better than the others. Chen *et al*. (2018) obtained astonishing results in terms of hydrogen yield (91%) during the steam reforming of acetic acid at 700 °C and using a chemically modified biochar loaded with 4 wt. % of Ni. However, neither of these authors reported any stability test results.

Table 3. Most recent studies about the employment of biochar as a catalyst or catalytic support for pyrolysis vapors upgrading through steam reforming.

Support modifications	Active phases, loading (wt.%)	Reactants	Temperature (°C)	H_2 yield	Ref.
$KOH+HNO_3$	Ni, 4	Acetic acid	700	91 %	(Chen *et al*., 2018)
KOH	/	Pyrolysis oil	600	/	(Yang *et al*., 2020)
/	/	Acetic acid, m-cresol, furfulal, acetone	900	89 %	(Ma *et al*., 2017)
CO_2	/	Pyrolysis oil	600	/	(S. Liu *et al*., 2021)
H_2O	/	Pyrolysis oil	800	/	(Y. Liu *et al*., 2021b)
HNO_3	Ni, 20	Acetic acid	700	80 %	(Y. Wang *et al*., 2020)
/	Ni,10	Ethanol	400	14 %	(Afolabi *et al*., 2021)
K_2CO_3	/	Pyrolysis oil	700	/	(Sueyasu *et al*., 2012)
CO_2	/	Benzene, toluene, naphthalene	850	/	(Buentello-Montoya *et al*., 2020)
H_2O	/	Pyrolysis oil	800	/	(Feng *et al*., 2020)
/	Ni, 5	Toluene, Pyrolysis oil	600		(Du *et al*., 2019)

2.4.2. CO_2 conversion to methane

Methanation of carbon dioxide is a newborn technology set in the framework of the CCU processes. Carbon Capture and Utilization coupled with Power-to-Gas (PtG) schemes could represent a very promising option to gradually move toward the employment of renewable energy sources (Baena-Moreno *et al*., 2019; Thema *et al*., 2019). The weather dependency of power generation leads to an oscillating production, characterized by surplus and deficit which does not have a good match with the electrical energy demand. Hence, the surplus energy needs to be stored. Among the possible technologies, the conversion of electrical in chemical energy is the most promising. Through this approach, the surplus energy produced from non-fossil sources (e.g., hydropower, solar or wind energy) is used to produce hydrogen via water electrolysis. The resulting hydrogen and the

CO_2 sequestered from power plants or industrial processes are then employed as reactants for the Sabatier reaction (Eq. 7) to produce methane, which, unlike hydrogen, could easily be injected into the national grid.

$$CO_2 + 4\,H_2 \rightleftarrows CH_4 + 2\,H_2O \qquad \Delta H_{298K} = -165\ \text{KJ mol}^{-1} \qquad (7)$$

The reaction is highly exothermic and generally carried out in the temperature range of 200−500 °C. However, CO_2 conversion toward CH_4 involves high activation energies, which make the reaction less favored at relatively low temperatures (Gonçalves *et al*., 2020). Furthermore, the competition with the reverse water-gas shift reaction, thermodynamically promoted within the same temperature range, lowers the selectivity of the process. Therefore, the use of an appropriate catalyst is mandatory.

Due to the high exothermicity of the process, a relatively high gas hourly space velocity, typically greater than 10000 h^{-1}, is required in order to avoid large temperature rises, which can negatively affect both conversion and selectivity and also cause a fast deactivation of the catalyst (i.e., metal phase sintering) (W. Wang *et al*., 2019).

Noble metals-based catalysts, such as Ru (Petersen *et al*., 2021), Rh (Younas *et al*., 2018) and Pt (Renda *et al*., 2021), were reported to be active and selective for methanation purposes. However, their high cost and limited availability encouraged research into cheaper alternatives, such as transition metal-based catalysts. Among the latter, Ni-based catalysts appear as a promising option due to their low cost and remarkable catalytic performance (Agnelli *et al*., 1998; Garbarino *et al*., 2021; Zhang *et al*., 2019). Since the main role of nickel is to dissociate H_2 molecules (Wolf *et al*., 2020), a catalyst support able to adsorb and activate a large amount of CO_2 is essential for a successful catalytic formulation. To this end, reducible metal oxides, such as ZrO_2 (Li *et al*., 2018) and CeO_2 (Hu *et al*., 2019), have been extensively used due to the presence of surface oxygen vacancies at the interface between the active metal and support. In the case of Ni/Ceria catalyst, Renda *et al*. (2021) obtained outstanding performances in terms of methane yield (75%) and CO_2 conversion (73%) at 0.1 MPa and 350 °C. Meanwhile, Alarcón *et al*. (2019) achieved, using a $Ni/CeO_2/\gamma\text{-}Al_2O_3$ catalyst, a stable CO_2 conversion of 90% for at least 120 h. The introduction of CeO_2 results in an increase in the number of basic sites, which promotes CO_2 adsorption, enhancing CH_4 production (Hu *et al*., 2019). It was also demonstrated that ceria is capable to stabilize and better disperse the nickel species,

leading to a stronger interaction between the catalytic active phase and its support (Le *et al*., 2017).

From a sustainability point of view, renewable carbon materials are, also in this process, excellent candidates to be used as catalyst supports. However, as displayed in **Table 4**, there are still very few studies in the literature describing the performance of biochar-based metal catalysts in CO_2 methanation.

Wang and co-workers produced and tested Ni- and Ru-based catalysts supported on ceria (X. Wang *et al*., 2020) and urea-doped biochar (X. Wang *et al*., 2019) obtaining very good results even at low temperatures. Nevertheless, ceria and urea-doped catalysts were produced through a one-step process, pyrolyzing the raw biomass blended with the doping agents. However, to strengthen the value chain of biochar systems, it seems more interesting to produce engineered biochar-derived materials as value-added products, in order to generate important benefits for large-scale biochar production systems.

Table 4. CO_2 conversion (X_{CO2}) and CH_4 selectivity (S_{CH4}) values reported in the literature for catalytic CO_2 methanation.

Catalyst	Loading (wt. %)	Support	X_{CO2} and S_{CH4} (%)	Ref.
Ni/γ- Al_2O_3	12 (Ni)	Alumina	80, 99.5	(Yang Lim *et al*., 2016)
35Ni5Fe_AX	35(Ni)/5(Fe)	Xerogel	63, 99.5	(Hwang *et al*., 2012)
Fe/N-CNT	9.5 (Fe)	CNT	25, 40	(Chew *et al*., 2014)
Ni/SiO_2	10 (Ni)	SiO_2	77, 100	(Ye *et al*., 2021)
Ni-15En/ZrO2-1.5	15 (Ni)	ZrO_2	94, 97	(Quan *et al*., 2021)
Co/ZrO_2	2 (Co)	ZrO_2	65, 99	(Li *et al*., 2019)
Ni/Ce-ABC	15 (Ni)/15 (CeO_2)	Activated biochar	87, 92	(X. Wang *et al*., 2020)
Ru/N-ABC	2 (Ru)	Activated biochar	94, 100	(X. Wang *et al*., 2019)

3. GreenCarbon Project

This work was carried out within the GreenCarbon[1] network, which purpose was to develop advanced biomass-derived carbons to be employed in several energy and environmental applications to drive new technologies for biomass/biowaste upcycling. The GreenCarbon project consortium was formed of eight beneficiaries and several partner organizations (see Table 5) from both academic and industrial sectors.

The research programme set different goals (graphically summarized in **Figure 4**):

- The development and optimization of thermochemical processes (HTC and pyrolysis) to produce tailor-made biomass-derived carbons.
- The production of novel cheap biochar-based materials by means of activation and functionalization procedures.
- The employment of the so-produced carbon material in several fields such as catalysis and pollutant adsorption.
- Feasibility study of the employment of biochars as soil enhancers.

Bearing in mind the above-mentioned objectives, the project was divided into 5 work packages (WPs), resumed and detailed in Table 6. Among them, the WPs 4, 5, 6, and 7 were designed to be interconnected. In particular, the biochar produced from the HTC and pyrolysis in WP 4 and WP 5 was used as starting material for the production of catalysts and adsorbents within the WP 6. The material spent in catalysis and adsorption, finally was used as input for the WP 7, which studied its application to soil.

[1] Project funded by the European Union's Horizon 2020 research and innovation programme under the Marie Skłodowska-Curie grant agreement No 721991 (2016–2021).

Table 5. Consortium of the GreenCarbon Project.

Academia	Industry	Country	Person in charge
• University of Zaragoza		Spain	Joan J. Manyà
• University of Ghent		Belgium	Frederik Ronsse
• Stockholm University	• Biokol Sverige AB	Sweden	Niklas Hedin
• University of Hohenheim	• PYREG GmbH • Fraunhofer Gesellschaft Zur Foerderun Der Angewandten Forschung E.V. • Deutsches Biomasseforschungszentrum Gemeinnutzige GmbH (DBFZ)	Germany	Andrea Kruse Moritz Leschinsky
• Aston University • University of Edinburgh • Queen Mary University of London	• Viridor Waste Management Limited • Surface Measurements Systems Limited • Freeland Horticulture Ltd.	United Kingdom	Magdalena Titirici Tony Bridgwater Ondřej Mašek

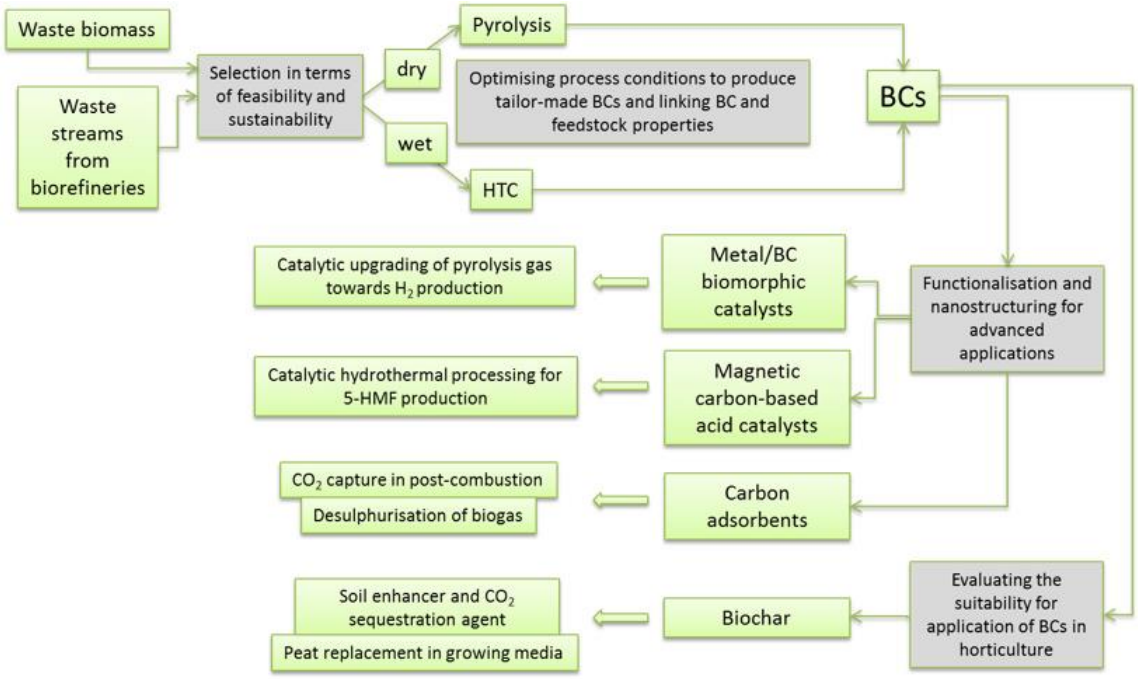

Figure 4. GreenCarbon Project objectives (reproduced under permission of the GreenCarbon project consortium).

Table 6. GreenCarbon's work packages organization

Work package and objectives	Beneficiary	Other partners involved
1. Network Management		
2. Early-stage researcher career development		
3. Transfer of technology and knowledge		
4. Pyrolysis routes for dry feedstocks • Selection of the dry waste biomass feedstock. • Setting the most appropriate slow pyrolysis process conditions. • Assessment of the effects of intermediate pyrolysis conditions on the resulting BC properties. • Fast pyrolysis conditions optimization to produce pyrolysis oil. • Development of a comprehensive pyrolysis/carbonization model	University of Ghent	University of Zaragoza Aston University Fraunhofer Organics DBFZ Pyreg
5. HTC conversion routes for wet feedstocks • Selection of wet waste biomass feedstocks. • Setting the most appropriate HTC process conditions to obtain high quality BC. • HTC and its integration with pyrolysis.	University of Hohenheim	University of Ghent Aston University Fraunhofer
6. Refining of BC • Development of low-cost BC-derived adsorbents for post-combustion CO_2 capture. • Development of low-cost BC-derived adsorbents for biogas desulphurization. • Development of novel metal/BC-supported catalysts for hydrogen production from pyrolysis gas. • Development of novel magnetic catalysts for 5-HMF synthesis through HTC.	Queen Mary University of London	SU, University of Zaragoza, University of Hohenheim, University of Ghent Pyreg, Surface Measurament Systems Viridor, Biokol
7. Sequential biochar systems • Characterization of BCs and BC-derived materials with the view of their final land use. • Identifying the opportunities for sequential uses of biochar.	Edinburgh University	University of Ghent, University of Hohenheim, Feeland

4. Objectives

Bearing in mind the current state of knowledge regarding the use of renewable biomass-derived carbons for catalytic pyrolysis vapors upgrading and CO_2 methanation, as well as the objectives within the WP 6 of the GreenCarbon network (described in the previous section), the main objective of this PhD Thesis is to study the activation and functionalization of biochars to produce an innovative biochar-supported catalyst to be employed as a more sustainable alternative to the commonly used ones.

The thesis is presented as a compendium of four published research articles, which have been published during the course of the PhD project as a result of the execution of four research studies. The topics covered by the four published papers reflect the progress of the work over time, starting from the preliminary screening of a number of biochar-based catalysts and ending with the optimization of the operating conditions of the catalytic processes.

Prior to the investigation on the production of biochar-based catalysts, particular attention was paid to the study of the biochar activation procedures and how the operating conditions affect the properties of the resulting material. Afterward, research was focused on developing mono and bimetallic catalysts supported on modified biochar to be employed in two different processes: i) steam reforming of slow pyrolysis oil; and ii) production of renewable CH_4 through CO_2 methanation. A schematic resume of the thesis goals is given in **Figure 5**.

The objectives of the four main sections (i.e., published research studies) are:

I. Assessment of the suitability and performance of biomass-derived activated biochars to be used as renewable and low-cost catalyst/support for pyrolysis vapors upgrading.

II. Assessment of the effects of several activation conditions on the textural properties of the resulting activated biochars and their performance as catalysts in pyrolysis vapors upgrading.

III. A comprehensive study on the suitability of activated biochar-derived metallic catalysts to be used in steam reforming of slow pyrolysis oil.

IV. Synthesis and performance evaluation of Ni-based catalysts supported on activated biochar in CO_2 methanation processes under different operating conditions.

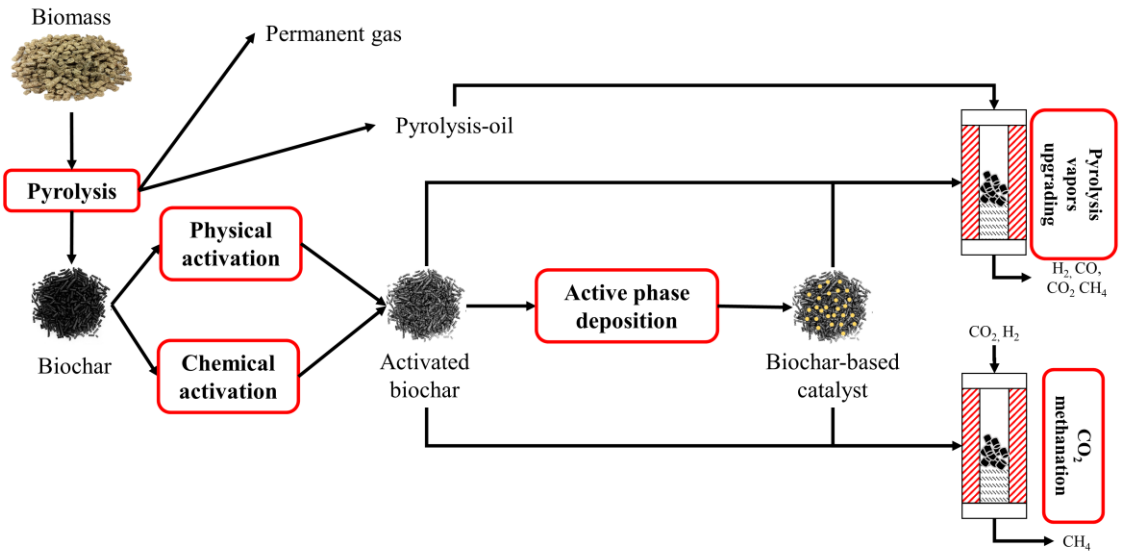

Figure 5. Schematic representation of the main objectives of this PhD Thesis.

.

5. Methodology

5.1. Biochar production

The biochar employed in this work was obtained from binder-free wheat straw pellets (9 mm OD and 10–13 mm long), which were provided by a Belgian company. Biochar was produced via slow pyrolysis (at an average heating rate of 5 °C min^{-1}) using a bench-scale fixed-bed reactor, at the highest temperature of 500 °C, a soaking time for the solid fraction of 60 min and a residence time of the carrier gas (N_2) within the reactor of 100 s. A detailed description of the pyrolysis experimental setup is available elsewhere (Manyà *et al*., 2018a). We chose these operating conditions considering the findings of a previous study (Greco *et al*., 2018), where these were found as the most appropriate conditions to reach a reasonable compromise between the yield of biochar and its properties in terms of potential stability. The resulting biochar (i.e., "pristine") was grounded and then thoroughly sieved to obtain particle sizes in the range from 0.212 to 1.41 mm.

5.2. Biochar activation

Once sieved, pristine biochar was activated via physical and chemical methods, with the aim to improve its textural properties. All the activations were carried out in a tubular fixed-bed reactor (made of nickel-chromium alloy UNS N06600, 28.1 mm ID and 600 mm long) placed in a vertical furnace (model EVA 12/300 from Carbolite Gero, UK). A schematic overview of the activation setup is given in **Figure 6**.

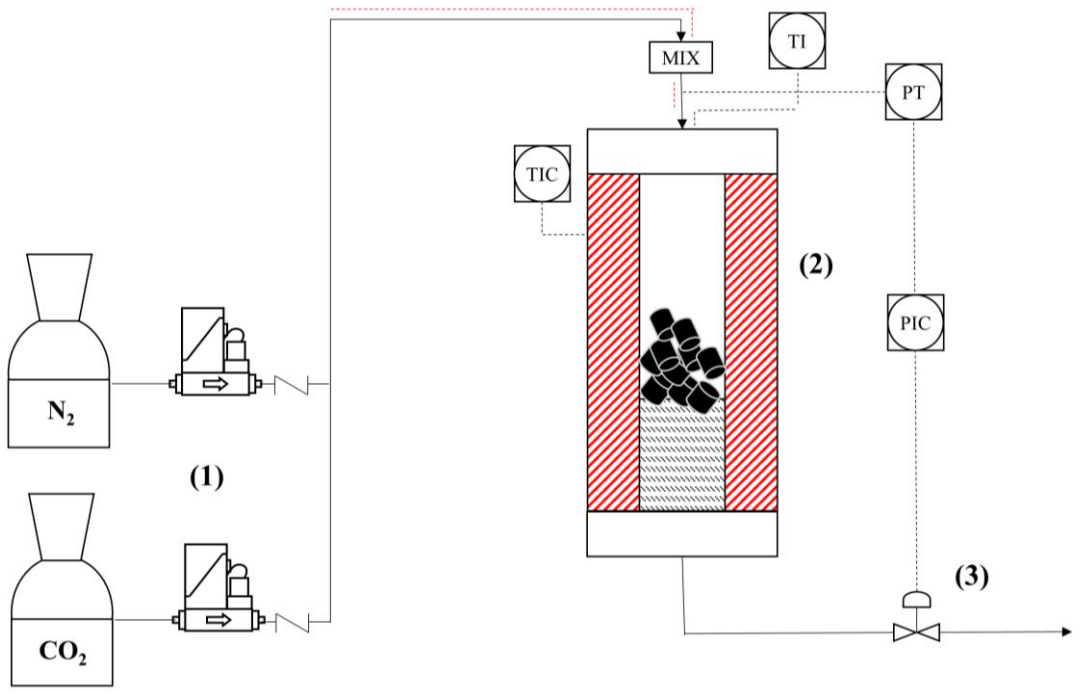

Figure 6. Activation setup. (1) Feeding system; (2) Fixed bed reactor; (3) Servo-valve.

5.2.1. Physical activation

Physically activated biochars were produced under an atmosphere of pure CO_2 at different temperatures (650–850 °C), and at three different absolute pressures (0.10, 0.55, and 1.00 MPa). The selected activation temperatures are within the range commonly reported in the literature, whereas the pressure values were established with the purpose to compare the properties of resulting activated carbons produced under atmospheric and moderate pressures. The pressure upper limit (1.00 MPa) was due to the limitation of the experimental setup.

Using the same device described in the previous section, 10 g of pristine biochar was heated under N_2 atmosphere, at a heating rate of 10 °C min^{-1}, until the target temperature was reached. The pressure within the reactor was adjusted using a downstream servo-controlled regulator valve. The gas hourly space velocity at the activation temperature was estimated to be 7000 h^{-1}, considering the pressure applied and a bed void factor of 0.5. Then, the gas supply was switched from N_2 to CO_2 at a constant GHSV of 7000 h^{-1}. These conditions were maintained during different activation times to study the influence of the degree of burnout (defined as the percentage of mass loss) on the resulting specific surface area and pore size distribution.

5.2.2. Chemical activation

For chemical activation, the pristine biochar was first impregnated with a 1 mol L^{-1} aqueous solution of K_2CO_3. Different K_2CO_3:biochar mass impregnation ratios were achieved by adjusting the volume of the solution. The heterogeneous mixture was then stirred for 2 h at 50 °C, filtered and dried overnight at 110 °C to remove the residual water. Afterward, 10 g of the impregnated samples were heated up to 700 °C in the setup reported in **Figure 6** at a heating rate of 10 °C min^{-1}, under an inert atmosphere (N_2), and at three different values of absolute pressure (0.10, 0.55 and 1.00 MPa). The relatively low activation temperature was chosen to avoid the evaporation of the metallic potassium derived from the decomposition of the activation agent and, also, to ensure low activation extent and clearly see the potential effects of the studied parameters. A soaking time at the highest temperature of 60 min was set.

Finally, the carbons were rinsed to remove the unreacted reagent and other impurities from their surface. To assess possible effects on the resulting surface area and the catalytic activity of the activated carbons produced, two different washing procedures were adopted: (i) rinse with hot deionized water (100 °C); and (ii) rinse with a 0.25 mol L^{-1} solution of HCl followed by hot water. Both washing procedures were carried out until neutral pH. The resulting activated biochars were then dried overnight at 110 °C.

5.3. Synthesis of activated biochar-based catalysts

After the identification of the optimal activating conditions, the biochars with the best pore size distribution and highest specific surface area were employed as supports for the synthesis of biomass-derived catalysts to be used in pyrolysis vapors upgrading and CO_2 methanation processes. Briefly, the activated biochar chosen as support was impregnated with an aqueous solution of a precursor salt of the desired active phase. The blend was stirred at 60–80 °C until complete water evaporation. Afterward, the sample was dried overnight at 110 °C. The dried sample was then loaded in a fixed-bed reactor and calcined in an inert atmosphere at the designed temperature. In the case of bimetallic catalysts, after the calcination, the sample was impregnated again with the second precursor salt solution, following the same procedure described above. **Table 7** shows all the metallic catalysts prepared during this work and their applications.

Table 7. Activated biochar-based metallic catalysts produced in this work. In this table: BC is the pristine biochar; BCP is the physically activated biochar (with CO_2); BCC is the chemically activated biochar (with K_2CO_3). All the metallic catalysts were prepared using a BCP as support.

	Sample	Active phase	Loading (wt. %)	Application
Support				
	BC	/	/	SR
	BCP			SR/Methanation
	BCC			SR
Monometallic				
	BCFe	Fe	7	SR
	BCCo	Co	7	SR
	BCCe	Ce	7	SR
	BCK	K	7	SR
	BCNi7	Ni	7	SR
	BCNi4	Ni	4	SR
	BCNi10	Ni	10	SR
	BCNi20	Ni	20	Methanation
	BCNi40	Ni	40	Methanation
Monometallic with doped support				
	BCCeNi	Ce/Ni	7/10	SR
	BCCe10Ni40	Ce/Ni	10/40	Methanation
	BCCe30Ni40	Ce/Ni	30/40	Methanation
	BCCe50Ni40	Ce/Ni	50/40	Methanation
	BCCe30Ni10	Ce/Ni	30/10	Methanation
	BCCe30Ni20	Ce/Ni	30/20	Methanation
	BCCe30Ni30	Ce/Ni	30/30	Methanation
	BCCe30Ni40	Ce/Ni	30/40	Methanation
	BCN50Ni20	N/Ni	50/20	Methanation
	BCN67Ni20	N/Ni	67/20	Methanation
	BCN75Ni20	N/Ni	75/20	Methanation
Bimetallic				
	BCFeNi	Fe/Ni	7/10	SR
	BCCoNi	Co/Ni	7/10	SR
	BCKNi	K/Ni	7/10	SR

5.4. Characterization techniques

All the samples produced in this work were characterized through several techniques which are detailed in this section and schematically resumed in **Figure 7**.

Due to the numerous characterization techniques employed in this work, some of them were carried out by third-party institutions. **Table 8** summarizes all the performed analyses and provides details on the partner institutions where the analyses were carried out.

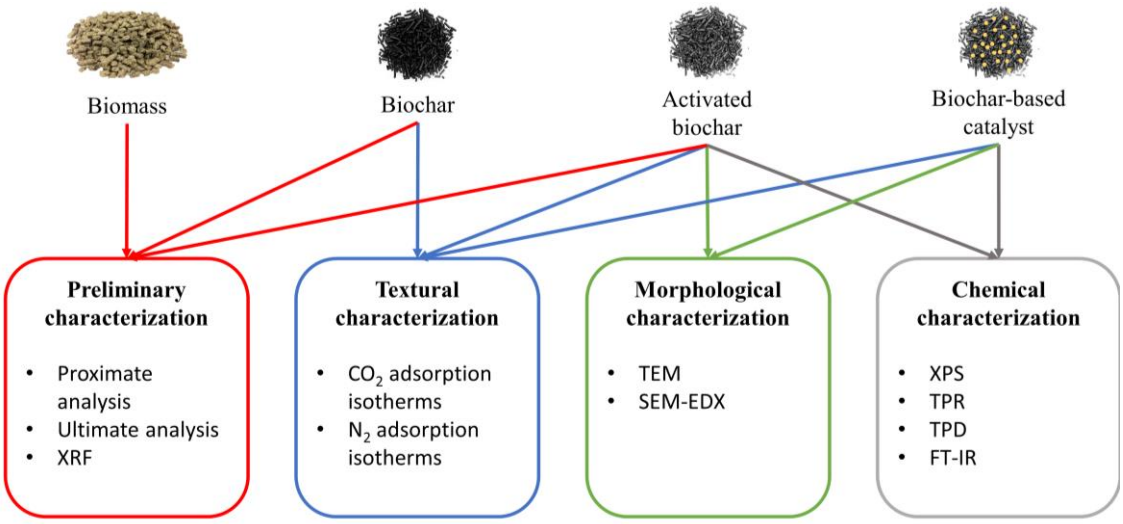

Figure 7. Characterization techniques employed in this work.

Table 8. Resume of all the characterization techniques and the institutions where they were carried out.

	UNIZAR[a]	UNISA[b]	UMA[c]	IJL[d]	ICC[e]	SAI[f]
CHN-S	X			X		
FTIR	X			X		
Isotherms			X	X		
Karl Fisher	X					
Proximate	X					
SEM				X		
TEM						X
TPD		X				
TPR		X				
XPS					X	X
XRF						X

[a] University of Zaragoza (Spain); [b] University of Salerno (Italy); [c] University of Málaga (Spain); [d] Institut Jean Lamour (France); [e] Instituto de Carboquímica (Spain); [f] Servicio de apoyo a la Investigación de UNIZAR (Spain).

5.4.1. Preliminary characterization

To determine the content of moisture, volatile matter, ashes and fixed carbon, proximate analysis was conducted in quadruplicate on raw biomass, biochar, and activated biochar following the ASTM standards (D3173 for moisture, D3174 for ash, and D3175 for volatile matter). For the determination of the elemental composition (C, H, N and S) of the samples, ultimate analysis was carried out with the elemental analyzer CHN628 from Leco Corporation (USA). The inorganic composition of ashes was evaluated through X-Ray Fluorescence (XRF) spectroscopy analysis (ADVANT'XP+XRF spectrometer from Thermo ARL, Switzerland).

For what concerns the characterization of the pyrolysis liquid, its moisture content was evaluated through Karl-Fischer titration, meanwhile its elemental analysis, including the sulfur content, was performed using the same elemental analyzer described above.

5.4.2. Textural characterization

The textural properties of pristine biochars, activated biochars and calcined catalysts were determined through N_2 and CO_2 adsorption isotherms performed at –196 °C and 0 °C, respectively. Around 120 mg of sample was degassed under vacuum at 150 ºC using for this purpose both ASAP 2020 and ASAP 2420 automatic adsorption analyzers (Micromeritics, USA). The results obtained from the isotherms were treated using the MicroActive software. The specific surface areas were quantified through the application of the BET, Langmuir and the enhanced 2D-NLDFT model (this last one was employed through the SAIEUS software available at www.nldft.com).

The pore size distribution (PSD), excluding narrow micropores, was estimated assuming a Non-Local Density Functional Theory (NLDFT) model and slit-pore geometry. Then, the volume of mesopores was determined by subtracting the volume of micropores from the cumulative pore volume up to 50 nm. To determine the volume of narrow micropores (i.e., ultra-micropores) and the corresponding PSD for the range comprised between 0.3 and 1.0 nm (Kim *et al*., 2016; Walton and Snurr, 2007) CO_2 adsorption isotherms were performed at 0 °C. The volume of ultra-micropores was then evaluated using conventional the Density Functional Theory (DFT) and assuming slit-pore geometry.

5.4.3. Morphological features

Scanning Electron Microscopy - Energy Dispersive X-ray spectroscopy **(**SEM-EDS) characterization was carried out with a FEI XL30 SFEG scanning electron microscope coupled with energy-dispersive X-ray spectroscopy (Oxford Instrument EDS SDD XMAX detector) on both fresh and spent catalysts. Secondary electron images were taken with an acceleration voltage of 3 or 5 kV to investigate the topology of the surface of the sample, while an acceleration tension of 10 kV was applied to carry out the chemical mapping of the materials by EDX analysis.

With the objective to observe the morphology of the samples and the dimension of the metallic nanoparticles, transmission electron microscopy (TEM) of produced catalysts was carried out using a Tecnai F30 microscope (FEI, USA) operating at 300 kV. Before each TEM measurement, samples were sonicated briefly (for 5 minutes) in an aqueous solution of ethanol, in order to improve the dispersion of the smaller particles without distorting their shape. The metal nanoparticle size distributions were evaluated from 200 data points using an image analysis software package (Sigmascan Pro).

5.4.4. Chemical characterization

The reducibility properties of the biochar-based catalysts were evaluated through temperature-programmed reduction (TPR) analysis. To this aim, each sample was heated under a reducing stream (5% H_2 in Ar, at a flow rate of 0.5 NL min^{-1}) at a heating rate of 15 °C min^{-1} from 50 to 600 °C. The hydrogen concentration at the outlet was continuously monitored by means of a Hiden QGA mass spectrometer (Hiden Analytical, UK).

CO_2 temperature-programmed desorption (CO_2-TPD) was also used to investigate the surface properties of the prepared catalysts. It is generally recognized that CO_2-TPD allows the determination of the basic sites on the catalyst surface (Song *et al.*, 2017; Wan *et al.*, 2007). The analysis was conducted as follows: CO_2 adsorption was firstly performed at 50 °C on 0.5 g of the reduced catalyst under a stream of CO_2 in Ar (40 vol. % CO_2) for 30 min; then, weakly adsorbed CO_2 was purged with a pure Ar stream at the same temperature for 1 h; finally, CO_2-TPD was performed in pure Ar raising the temperature from 50 to 700 °C at a heating rate of 5 °C min^{-1}. The desorbed CO_2 was measured by means of the above-mentioned mass spectrometer.

In the case of chemically activated samples, Fourier-transform Infrared Spectroscopy (FTIR) was employed to detect the presence of residual K_2CO_3 on the activated samples.

For the identification of the chemical species on the biochar and activated biochar surface, X-ray photoelectron spectroscopy (XPS) data were recorded using an ESCAPlus OMICROM system equipped with a hemispherical electron energy analyzer.

5.5. Pyrolysis vapors upgrading

Pyrolysis vapors upgrading tests were carried out in a tubular fixed-bed reactor (made of alloy UNS N10276, 300 mm long and 10 mm ID) placed in an electric tubular furnace. A K-type thermocouple placed in the middle of the catalytic bed was used to monitor the system temperature. In the case of the tests performed on biochar-based catalysts, before each experiment the system was heated up to 600 °C under a reducing atmosphere (N_2/H_2, 50/50 vol. %) to perform the activation. These conditions were kept for 2.5 h to assure complete reduction of the active metal oxides.

Since the pyrolysis oil is a very complex mixture of hundreds of organic compounds, the study was first carried out using representative model compounds. Therefore, an equimass mixture of acetone, acetic acid, ethanol, and eugenol was used to simulate the real composition of a pyrolytic oil. The first two compounds are usually released during

the thermal decomposition of cellulose and hemicelluloses compounds, whereas the last two are produced during the decomposition of lignin (Lozano *et al*., 2021; Paasikallio *et al*., 2015; Zhang *et al*., 2020). Finally, steam reforming of real pyrolysis oil was carried out using the liquid collected during the production of the pristine biochar.

The liquid blend was fed using an HPLC pump (model 521 from Analytical Scientific Instruments, USA) at different liquid hourly space velocities (LHSV) of the organic fraction. The liquid was forced to pass through a coil wrapped around a cartridge resistance, to reach complete vaporization of the blend, and mix with N_2 to be delivered to the reactor. The composition of the outlet gas was monitored using a dual-channel micro-gas chromatograph (μ-GC 490 from Agilent, USA) equipped with TCD detectors and two analytical columns (a Molsieve 5 A and a PoraPlot U). The known amount of N_2 fed was used as tracking compound to calculate the mass of produced gas. The evolution of the pressure drop along the reactor was measured employing a differential pressure sensor.
A schematic overview of the experimental device is given in **Figure 8**.

The performance of the different catalysts tested was evaluated through different variables depending on the reactant involved. In the case of the steam reforming of acetic acid, for example, the reactant conversion (X_{AcOH}) and the hydrogen yield (Y_{H2*}), defined as in Eqs. 7 and 8, were taken into account. When the study concerned about the steam reforming of a more complex reactant mixture such as real pyrolysis oil or a multicomponent model compound, the total carbon conversion (X_C) or the total gas yield (Y_g), defined in Eq. 9 and Eq. 10, respectively, were evaluated instead. In such equations, F_{AcOH}, F_{H2}, and F_C are the molar flow rates of acetic acid, hydrogen, and carbon (which was calculated considering all the species detected by the μ-GC: CO, CO_2, and CH_4) respectively; m_g was the cumulative mass of the gas produced during 60-min experiments, whereas m_L corresponded to the total mass of the liquid fed.

$$X_{AcOH} = \frac{F_{AcOH,in} - F_{AcOH,out}}{F_{AcOH,in}} 100 \quad (7)$$

$$Y_{H2*} = \frac{1}{4}\frac{F_{H2,out}}{F_{AcOH,in}} 100 \quad (8)$$

$$X_C = \frac{F_{C,out}}{F_{C,in}} 100 \quad (9)$$

$$Y_g = \frac{m_g}{m_L} 100 \quad (10)$$

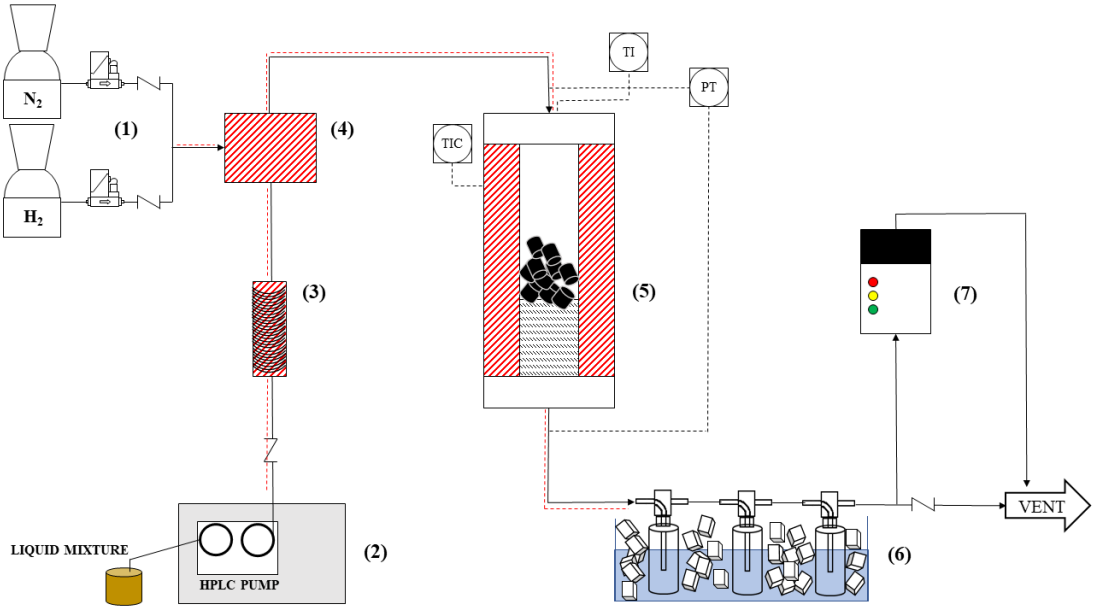

Figure 8. Schematic overview of the experimental device used in pyrolysis vapors upgrading experiments: feeding system (1); HPLC pump (2); evaporator (3); gas mixer (4); fixed-bed reactor and furnace (5); condensation train (6); and μ-GC analyzer (7).

5.6. CO_2 methanation

High-pressure CO_2 methanation experiments, using biochar-derived catalysts, were carried out using the experimental rig described in the previous section, but slightly modified for this purpose. The updated layout is schematically reported in **Figure 9**.

Once the preliminary reduction step (10 vol.% of H_2 in N_2 at 550 °C for 2.5 h) was concluded, the reactor was cooled down to 300 °C under an inert atmosphere and pressurized to the desired pressure value using a servo-controlled valve. Then, a mixture of $N_2/H_2/CO_2$ (50/40/10 vol. %) was fed to the reactor. Starting from 300 °C, the bed temperature was increased in steps of 50 °C and maintained constant the necessary time to obtain an almost constant product concentration. The composition of the outlet gaseous stream (CO, CO_2, CH_4, H_2, and light hydrocarbons such as C_2H_4, C_2H_6, and C_2H_2) was measured using the same μ-GC 490 described before.

The catalytic activity of the tested samples was evaluated in terms of CO_2 conversion (X_{CO2}) and selectivity toward CO and CH_4 (S_{CO}, S_{CH4}) as defined in Eqs. 11, 12 and 13. In these equations, F_i is the molar flow rate of the "*i*" specie.

$$X_{CO2} = \frac{F_{CO2,in} - F_{CO2,out}}{F_{CO2,in}} 100 \quad (11)$$

$$S_{CH4} = \frac{F_{CH4,out}}{F_{CO,out}+F_{CH4,out}+F_{C2H2,out}+F_{C2H6,out}+F_{C2H4,out}} 100 \quad (12)$$

$$S_{CO} = \frac{F_{CO,out}}{F_{CO,out}+F_{CH4,out}+F_{C2H2,out}+F_{C2H6,out}+F_{C2H4,out}} 100 \quad (13)$$

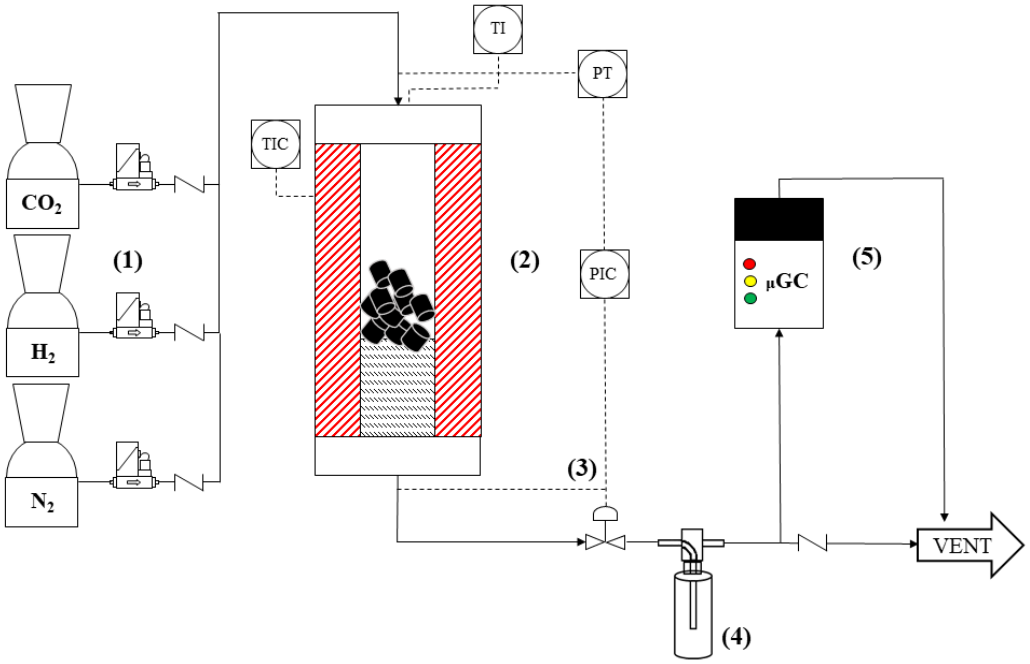

Figure 9. Schematic overview of the experimental device used in CO_2 methanation tests: feeding system (1); fixed-bed reactor and furnace (2); servo-controlled valve (3); water trap with $CaCl_2$ (4); and µ-GC analyzer (5).

6. Results

6.1. Assessment of the suitability of wheat straw-derived biochar as catalyst

This first part of the work was focused on the feasibility study of employing biochar and activated biochars as catalysts for the upgrading of pyrolysis vapors, in line with the objective I. Particular attention was paid to the identification of the main features of biochar, which favored the conversion of the reactants. To this aim, wheat straw-derived biochars (produced through slow pyrolysis at 500 °C and 0.1 MPa) were physically (with CO_2) and chemically (with K_2CO_3) activated to assess their performance. Preliminary cracking experiments, which were carried out at 700 °C using a mixture of four representative model compounds (acetone, acetic acid, ethanol, and eugenol), revealed a clear correlation between the volume of micropores of the catalyst and the total gas production, suggesting that physical activation, up to a degree of burn-off of 40%, was the most interesting activation route. Next, steam reforming experiments were conducted using the most microporous material to analyze the effect of both the bed temperature and gas hourly space velocity on the total gas production. The results showed a strong dependence between the bed temperature and the total gas production, obtaining the best results at the highest temperature (750 °C). On the other hand, the change in GHSV led to minor changes in the total gas yield, with a maximum achieved at 14500 h^{-1}. Under the best-operating conditions deduced in the previous stages, the addition of CO_2 into the feed gas stream (partial pressure of 20 kPa) resulted in a total gas production of 98% with a H_2/CO molar ratio of 2.16. This good result, which was also observed during the upgrading of the aqueous phase of a real biomass pyrolysis oil, was ascribed to the relatively high coke gasification rate, which was able to refresh the active surface area preventing deactivation by coke deposition.

Fuel 255 (2019) 115807

Contents lists available at ScienceDirect

Fuel

journal homepage: www.elsevier.com/locate/fuel

Full Length Article

Physically activated wheat straw-derived biochar for biomass pyrolysis vapors upgrading with high resistance against coke deactivation

Christian Di Stasi*, Darío Alvira, Gianluca Greco, Belén González, Joan J. Manyà

Aragón Institute of Engineering Research (I3A), Technological College of Huesca, University of Zaragoza, crta. Cuarte s/n, Huesca E-22071, Spain

GRAPHICAL ABSTRACT

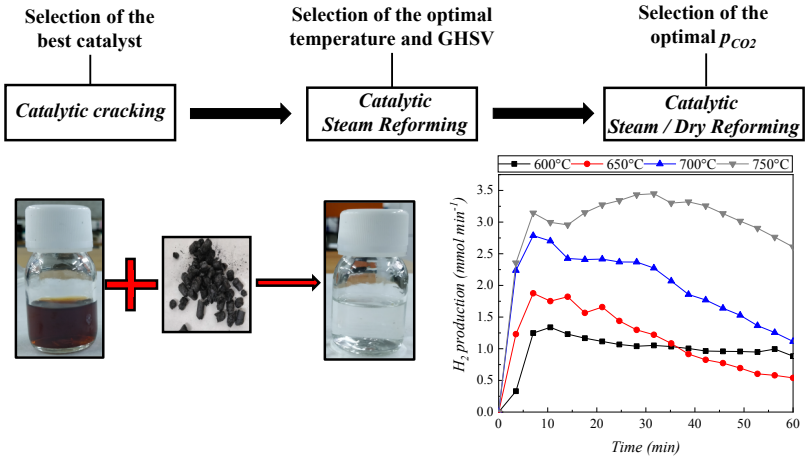

ARTICLE INFO

Keywords:
Activated biochar
Wheat straw
Pyrolysis vapor upgrading
Model compounds
Molar H_2/CO ratio

ABSTRACT

Wheat straw-derived biochars (produced through slow pyrolysis at 500 °C and 0.1 MPa) were physically (with CO_2) and chemically (with K_2CO_3) activated to assess their performance as renewable and low-cost catalysts for biomass pyrolysis vapors upgrading. Preliminary cracking experiments, which were carried out at 700 °C using a mixture of four representative model compounds, revealed a clear correlation between the volume of micropores of the catalyst and the total gas production, suggesting that physical activation up to a degree of burn-off of 40% was the most interesting activation route. Next, steam reforming experiments were conducted using the most microporous material to analyze the effect of both the bed temperature and gas hourly space velocity (GHSV) on the total gas production. The results showed a strong dependence between the bed temperature and the total gas production, with the best result obtained at the highest temperature (750 °C). On the other hand, the change in GHSV led to minor changes in the total gas yield, with a maximum achieved at 14500 h^{-1}. Under the best operating conditions deduced in the previous stages, the addition of CO_2 into the feed gas stream (partial pressure of 20 kPa) resulted in a total gas production of 98% with a H_2/CO molar ratio of 2.16. This good result, which was also observed during the upgrading of the aqueous phase of a real biomass pyrolysis oil, was ascribed to the relatively high coke gasification rate, which refresh the active surface area preventing deactivation by coke deposition.

* Corresponding author.
E-mail address: christiandistasi@unizar.es (C. Di Stasi).

https://doi.org/10.1016/j.fuel.2019.115807
Received 14 April 2019; Received in revised form 8 July 2019; Accepted 12 July 2019
Available online 18 July 2019

Nomenclature

BO	Degree of burn-off for the physically activated biochars (%)
m_0	Initial mass of biochar before activation (g)
m_g	Mass of produced gas during the upgrading process (g)
m_f	Final mass of biochar after activation (g)
m_L	Mass of liquid fed into the upgrading reactor (g)
n_i	Produced amount of a given gas specie (mmol)
S_{BET}	Brunauer-Emmett-Teller specific surface area ($m^2\ g^{-1}$)
V_{meso}	Volume of mesopores ($cm^3\ g^{-1}$)
V_{mic}	Volume of micropores ($cm^3\ g^{-1}$)
V_t	Total pores volume ($cm^3\ g^{-1}$)
V_{ultra}	Volume of ultra-micropores ($cm^3\ g^{-1}$)
Y_g	Total gas production (%)

Greek symbols

α	Fraction of mass loss of raw biochar after heating up to 800 °C under N_2 (–)
η_i	Yield of individual produced gas components (mmol g^{-1})

Acronyms

GHSV	Gas hourly space velocity
NLDFT	Non-local density functional theory
SDR	Steam and dry reforming
SR	Steam reforming
PSD	Pore size distribution
TCD	Thermal conductivity detector
μ-GC	Micro gas chromatograph
WGS	Water gas shift

1. Introduction

It is widely recognized that slow pyrolysis is the thermochemical process by which the yield of biochar is maximized (around 25–35 wt%, depending on the feedstock and operating conditions) [1]. The effluent stream from the pyrolysis process is composed of a fraction of permanent gases (CO_2, CO, CH_4, H_2, and light hydrocarbons), water and condensable organic compounds. After condensation, the resulting product, which is often referred to as "bio-oil"[2] or "pyrolysis oil" [3,4], consists of a mixture of water and oxygen-containing organic compounds (e.g., carboxylic acids, phenols, alcohols, aldehydes, ketones and furans [5–7]) derived from the thermal decomposition of major biomass components. Despite the fact that pyrolysis oil can be upgraded to liquid fuel by means of complex deoxygenation and hydrogenation processes [8], a practical approach to avoid undesirable condensation of volatiles (which causes operational issues in the downstream applications of the pyrolysis gas) is their conversion to permanent gases via cracking and steam/dry reforming, either thermally or catalytically.

Using a feasible catalyst in the pyrolysis vapor upgrading process is essential to reach high conversion levels with an appropriate selectivity to the desired products. So far, metal-based catalysts (mainly Ni [9,10], and, to a lesser extent, some transition metals such as Fe [11] and Co [12]) have been investigated for this purpose. In the last years, a growing interest in using biochar as catalyst or catalyst support has arisen [10,13–15]. The reason is that biochar is a versatile material that can further be upgraded by activation and/or functionalization processes [16–20]. Furthermore, using biochar as catalysts for pyrolysis vapors upgrading could offer practical advantages, such as higher resistance to deactivation by carbon deposition (due to the extent of both steam and CO_2 gasification reactions [12,21]) and the fact that spent biochar-based catalysts can be directly gasified or burnt to recover energy [22].

The performance of a catalyst generally depends on its textural properties. Indeed, an appropriate value of surface area guarantees a high level of interaction between the reactants and the active sites. In any case, pristine biochar has a relatively low specific surface area, which is generally dominated by narrow micropore contributions [23,24]. Therefore, an activation step is required to expand the initial porosity of biochar and thus, facilitating high mass transfer fluxes and high active loadings.

Activation processes are generally classified as either physical or chemical, depending on the activation procedure. Physical activation is the process in which the development of porosity is obtained through controlled gasification of carbon, using an oxidizing agent such as CO_2, H_2O or O_2 [25,26]. When the activation of biochar is obtained by means of a chemical agent that improves the gasification rate, the process is considered a chemical activation. The most used chemicals in literature are H_3PO_4, $ZnCl_2$, KOH, and NaOH, but all of them have drawbacks. For instance, H_3PO_4 [27] and $ZnCl_2$ [28] are hardly retrieved from the spent biochar, leading to eutrophication and heavy metal pollution [29]. On the other hand, KOH [30] and NaOH [31] are strong corrosive substances and their use in large-scale processes is not feasible. An interesting alternative is the use of K_2CO_3 since it has proven to be an effective chemical agent [32–34] and represents a more suitable material for scale-up purposes.

The specific aim of this study is to assess the suitability and performance (in terms of total gas yield, H_2/CO molar ratio, and resistance to deactivation) of wheat straw-derived activated biochars to be used as renewable and low-cost catalysts for pyrolysis vapors upgrading processes. Two biochar activation procedures (physical activation with CO_2 and chemical activation with K_2CO_3) were performed to identify which one was the most appropriate for the purpose of this work. Due to the complex composition of the real pyrolysis oil, a mixture of four biomass pyrolysis vapor model compounds (acetic acid, acetone, ethanol and eugenol) was used during the most part of the study in order to ensure reproducible results. The first two compounds are typically released during the pyrolysis of hemicelluloses and cellulose, whereas the last two are linked to the decomposition of lignin [7,35]. Similar model compounds were already employed in earlier studies [36–38]. Finally, for validation purposes, the last experimental stage was undertaken using the real bio-oil aqueous-phase produced during the slow pyrolysis of wheat straw pellets.

2. Experimental section

2.1. Production of biochar

The biochar employed in this work was obtained from binder-free wheat straw pellets (9 mm OD and 10–13 mm long), which were provided by a Belgian company. Biochar was produced via slow pyrolysis (at an average heating rate of 5 °C min^{-1}) using a bench-scale fixed-bed reactor (the description of which is available in previous studies [24,39]), at a highest temperature of 500 °C, a soaking time (at 500 °C) for the solid fraction of 60 min and a residence time of the carrier gas (N_2) within the reactor of 100 s. We chose these operating conditions in light of a previous study [24], where they were suggested as appropriate conditions to reach a reasonable compromise between the yield of biochar and its properties in terms of potential stability. The produced biochar (referred as "RW") was crushed and sieved to obtain particle sizes within the range of 0.212–1.41 mm.

Both the wheat straw pellets and the raw biochar were characterized by proximate and ultimate (CHN) analyses. Proximate analyses were conducted in quadruplicate according to ASTM standards. An

elemental analyzer, model CHN628 from Leco Corporation (USA), was used for ultimate analyses, which were performed in triplicate. Furthermore, X-Ray Fluorescence (XRF) spectroscopy analysis (ADVANT'XP + XRF spectrometer from Thermo ARL, Switzerland) were carried out to evaluate the inorganic content of the ashes present in the biomass and raw biochar.

2.2. Activation of biochar

Physical and chemical activations were conducted using a tubular quartz reactor (600 mm long and 17.5 mm ID), which was placed inside a vertical tubular furnace (model EVA 12/300 from Carbolite Gero, UK). The temperature inside the bed was monitored by means of a K-type thermocouple placed along the longitudinal axis of the reactor. A schematic diagram of the activation set-up is given in Fig. A.1 (Appendix 1: Supplementary Data).

The production of physically activated biochars was carried out under a pure CO_2 atmosphere at 800 °C. A sample of 10 g of raw biochar (RW) was heated under N_2 atmosphere (500 mL min^{-1} STP) at a heating rate of 10 °C min^{-1}. Once the target temperature (800 °C) was reached, the gas feed was switched from N_2 to CO_2. Under these conditions, the gas-hourly space velocity (GHSV) was estimated to be 6500 h^{-1}. The activation soaking time (under CO_2 atmosphere at 800 °C) was modified to obtain different degrees of burn-off (BO), which is defined in Eq. (1). In such equation, m_0 and m_f correspond to the initial mass of biochar and the final mass of activated biochar, respectively, whereas α is the devolatilization ratio (i.e., mass loss fraction of RW biochar after heating up to 800 °C under pure N_2), which in this work resulted to be equal to 0.12.

$$BO = \left[\frac{m_0(1-\alpha) - m_f}{m_0(1-\alpha)}\right] 100 \quad (1)$$

Regarding the chemical activation, the RW biochar was impregnated with an aqueous solution of K_2CO_3 (2 M) at a mass ratio K_2CO_3/biochar of 1/1. The heterogeneous mixture was stirred for 2 h at 60 °C to improve the diffusion of the agent into the solid. Then, the liquid phase was removed by filtration, and the biochar dried at 110 °C overnight. Afterward, the resulted impregnated biochar was heated up to 700 °C at a heating rate of 10 °C min^{-1} under inert atmosphere (N_2). The sample was kept at the final temperature for 1 h and cooled down to room temperature. The relatively low temperature (700 °C) used in chemical activation was chosen to avoid losses of metallic potassium due to its vaporization, which occurs at 760 °C [40]. Finally, the solid product was washed with hot deionized water followed by dilute HCl (0.5 M) to remove the excess of inorganic salts and dried at 110 °C overnight.

Besides its role as precursor, the catalytic activity of the non-activated biochar was also assessed in the catalytic cracking of a mixture of model compounds. In order to prevent any structural modification during the catalytic process, the RW biochar was heated at 10 °C min^{-1} under N_2 atmosphere up to 800 °C for 1 h (using the same device previously described). The resulting devolatilized biochar is referred as "BC".

Table 1 summarizes the nomenclature used to designate the activated and non-activated biochars.

2.3. Textural characterization

N_2 adsorption isotherms at −196 °C were performed to determine the specific surface area and pore size distribution (PSD) of both non-activated and activated biochars. A gas sorption analyzer, model ASAP2020 from Micromeritics (USA), was used for this purpose. Samples (120 mg) were previously degassed under dynamic vacuum conditions at 150 °C to remove water and other impurities. The specific surface area (S_{BET}) was obtained using the BET model, whereas the total pore volume (V_t) was determined from the amount of N_2 adsorbed at high relative pressure (p/p_0 = 0.98–0.99). The micropore volume (V_{mic}) was evaluated using the *t*-plot method. The PSD (excluding narrow micropores) was estimated assuming a Non-Local Density Functional Theory (NLDFT) model and slit-pore geometry. Then, the volume of mesopores (V_{meso}) was determined by subtracting the V_{mic} from the cumulative pore volume up to 50 nm. To determine the volume of narrow micropores (i.e., ultra-micropores) and the corresponding PSD for the range 0.3–1.0 nm [41,42], CO_2 adsorption isotherms at 0 °C were also performed. The volume of ultra-micropores (V_{ultra}) was then determined using conventional Density Functional Theory (DFT) and assuming slit-pore geometry.

2.4. Cracking and reforming experiments

The performance of the activated and non-activated biochars during cracking/reforming of pyrolysis vapors was tested in a bench-scale device. The core of the system was a fixed-bed reactor (10 mm ID and 300 mm long) made in Hastelloy C276 (EN 2.4819), in which 5 g of solid was loaded. The reactor was heated by a PID controlled electric furnace. A K-type thermocouple was placed within the packed bed. The pressure drop between the inlet and the outlet of the reactor was monitored with a differential pressure transmitter. The liquid reactant feed was introduced using an HPLC pump (model 521 from Analytical Scientific Instruments, USA) and then evaporated in a heater. For cracking experiments, an equal-mass mixture of the four model compounds (acetic acid, acetone, ethanol, and eugenol) was used as feed liquid and, for reforming tests, deionized water was added to the above-mentioned mixture, resulting in a feed liquid composed of 50 wt% of water. The resulting vapor stream was then mixed with the gas feed (N_2 or N_2/CO_2). The reactor outlet stream, which was composed of permanent gases and condensable compounds, was cooled down in a condensation train (composed of 3 Drechsel bottles placed in an ice bath). Permanent gases were analyzed using a dual channel micro-gas chromatograph (μ-GC 490 from Agilent, USA) equipped with TCD detectors and two analytical columns (a Molsieve 5 A and a PolarPlot U). The known amount of N_2 fed was used as tracking compound to calculate the mass of produced gas. Fig. 1 shows a schematic overview of the experimental device.

The total gas production (Y_g), as defined by Eq. (2), was chosen as a measure of the performance of the upgrading experiments. The selection of this parameter instead of the more common liquid conversion was due to the difficulties in recovering the total amount of condensable products from the reactor effluent. Since highly volatile compounds were present in the condensable fraction, a considerable amount of them could leave the system in the vapor phase. This was

Table 1
Summary of the nomenclature used in the present study for wheat straw-derived carbon materials.

Material	Further treatment
RW	Raw pyrolysis biochar
BC	Raw biochar devolatilized up to 800 °C under N_2
CAC	Chemically activated biochar through impregnation of a K_2CO_3 aqueous solution (2 M) and subsequent heating up to 700 °C under N_2
PAC15	Physically activated with CO_2 at 800 °C up to a degree of burn-off of 15%
PAC30	Physically activated with CO_2 at 800 °C up to a degree of burn-off of 30%
PAC40	Physically activated with CO_2 at 800 °C up to a degree of burn-off of 40%

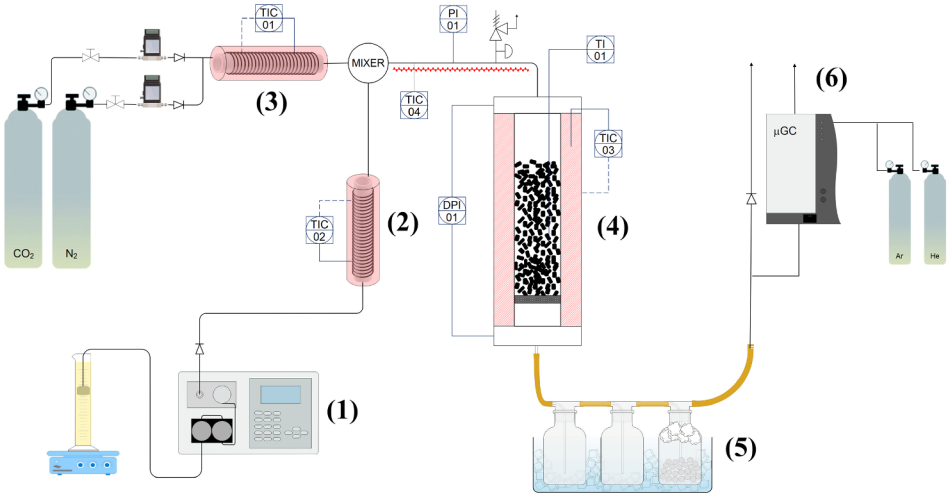

Fig. 1. Scheme of the experimental device used for cracking and reforming experiments: HPLC pump (1); evaporator (2); gas pre-heater (3); fixed-bed reactor and furnace (4); condensation train (5); and μ-GC analyzer (6).

confirmed by the results obtained from a simulation study using Aspen Plus (more details are available in Fig. A.2 and Table A.1). Besides the total gas production, the yields of individual gas species (η_i) were determined according to Eq. (3).

$$Y_g = \frac{m_g}{m_L} 100 \quad (2)$$

$$\eta_i = \frac{n_i}{m_L} \quad (3)$$

In Eqs. (2) and (3), m_g is the mass of produced gas (in grams), m_L the mass of liquid fed into the reactor (in g, dry basis) and n_i the amount produced of a given gas species (in mmol). It should be pointed out that values of Y_g greater than 100% can be obtained for reforming experiments, since the variable m_L does not include the mass of water fed.

To assess the catalytic activity of the wall of the reactor and/or the extent of thermal cracking of the liquid fed, two types of blank tests were firstly carried out: one using an empty reactor and the other one using a bed of silica sand. Catalytic cracking experiments were then conducted to choose the best activated biochar (in terms of Y_g) keeping constant the operating conditions (i.e., bed temperature and GHSV). In a second stage, steam reforming (SR) tests were performed using the best catalyst under different bed temperatures and GHSV values. Next, steam and dry reforming (SDR) tests were carried out (for the best catalyst and the best operating conditions deduced from SR tests) using a mixture of N_2 and CO_2 (at different CO_2 partial pressures) as feed gas stream. Since CO_2 was both a reactant and product in the reactions involved in the process, the Y_g and η_{CO2} values were calculated considering the net mass of CO_2 (i.e., the amount at the outlet minus the amount fed). The final stage of the experimental study consisted on the steam and dry reforming of the aqueous fraction of a real pyrolysis oil. To this end, we used the bio-oil aqueous-phase produced during the slow pyrolysis of wheat straw pellets at 500 °C and 0.1 MPa. The water content of the liquid fed was measured by Karl Fischer titration. A summary of the experimental tests and their operating conditions is given in Table 2.

3. Results and discussion

To guarantee a reasonable degree of reliability of the experimental results obtained from the used set-up, the repeatability of measurements was assessed by comparing three replicates of a given steam and dry reforming experiment (not reported in Table 2). The results from these repeated tests, which are summarized in Table A.2, showed an acceptable degree of repeatability.

3.1. Properties of the produced biochars

The results of the proximate, ultimate and XRF analyses of wheat straw biomass and pristine biochar (RW) are reported in Table A.3. For physically activated biochars at 800 °C, the desired degrees of burn-off (15%, 30%, and 40%) were reached by adjusting the soaking times at 30, 45 and 60 min, respectively.

The main results from the textural characterization of activated and non-activated biochars are reported in Table 3. For the non-activated biochar (BC), the extremely low (near zero) S_{BET} value and non-detectable pore volumes deduced from the N_2 adsorption isotherm at −196 °C can be explained by the fact that porosity is dominated by narrow micropores (i.e., ultra-micropores; pore sizes below 0.7 nm). At cryogenic temperatures, the diffusion rate of N_2 into ultra-micropores becomes extremely slow [42].

For the chemically activated biochar (CAC), the specific surface area (89.0 $m^2\ g^{-1}$, from N_2 isotherm) was significantly lower than the values found in the literature [29]. Since most of the previous studies impregnated biomass instead of biochar, a possible explanation of this low surface area could be due the hydrophobicity of the precursor used here (low atomic O:C ratio, as reported in Table A3 [43]), which hindered the diffusion of the aqueous solution into the solid bulk. Furthermore, the relatively low final activation temperature (700 °C) could not be

Table 2
Summary of the operating conditions used for the conducted experiments.

	Cracking	Steam Reforming	Steam and dry reforming	
Liquid fed	Model mixture	Model mixture + H_2O	Model mixture + H_2O	Pyrolysis oil (aqueous fraction)
Gas fed	N_2	N_2	Mixture of N_2 and CO_2 (p_{CO2} of 10, 20 and 30 kPa)	Mixture of N_2 and CO_2 (p_{CO2} of 20 kPa)
Catalyst	All	PAC40	PAC40	PAC40
Temperature (°C)	700	600, 650, 700, 750	750	750
GHSV (h^{-1})	19,500	12000, 14500, 19500, 35,000	14,500	14,500

Table 3
Specific surface areas and pore volumes of the carbon materials involved in the present study.

Material	Apparent specific surface area ($m^2\ g^{-1}$)		Specific pore volume ($cm^3\ g^{-1}$)			
	S_{BET} [a]	S_{BET} [b]	V_t	V_{mic}	V_{mes}	V_{ultra}
BC	1.68	72.4	ND	ND	ND	0.023
CAC	89.0	291	0.045	0.031	0.009	0.119
PAC15	455	351	0.196	0.145	0.010	0.141
PAC30	637	414	0.283	0.234	0.018	0.140
PAC40	815	440	0.366	0.306	0.024	0.151

[a] Determined from N_2 adsorption data a −196 °C.
[b] Determined from CO_2 adsorption data a 0 °C.

high enough to obtain an appropriate extent of reaction.

On the other hand, physically activated biochars exhibited appropriate specific surface areas and pore volumes (see Table 3). In addition, an increase in the degree of burn-off from 15% to 30% and 40% led to a progressive and marked increase in the specific surface area, which was mainly attributed to the development of new micropores. This is in good agreement with earlier studies available in the literature [44,45].

3.2. Catalytic cracking experiments

The cracking process mainly involves the decomposition of volatile organic compounds through successive reactions (the main of which are listed in Table 4), leading to the production of lighter compounds and permanent gases. In addition, coke can be formed through polymerization reactions of free radicals released during cracking. The deposition of coke on the catalyst surface can result in a fast deactivation of the catalyst by pore plugging [46,47].

The performance of all the catalysts tested during the cracking experiments (which were conducted at 700 °C and at a GHSV of 19500 h^{-1}) is shown in Fig. 2. For the two blank experiments (not displayed in Fig. 2), the total gas production (Y_g) was very low (6.1% and 7.4% using an empty reactor and a bed of silica sand, respectively), suggesting that both the catalytic effect of the reactor wall and the model mixture degradation (due to thermal cracking) were negligible under the operating conditions used here.

As can be seen in Fig. 2a, the total gas production obtained using the non-activated biochar (BC) was around 22%. Despite the fact that the value of Y_g was relatively low, it was considerably higher than that obtained using a bed of silica sand. This can indicate that, given the extremely low porosity of the non-activated biochar, the presence of inherent inorganic species available on their surface, especially K and Ca (see Table A.3), could lead to a certain catalytic activity [48,49]. On the other hand, slightly better results were obtained for physically activated biochar at mild conditions (BO = 15%).

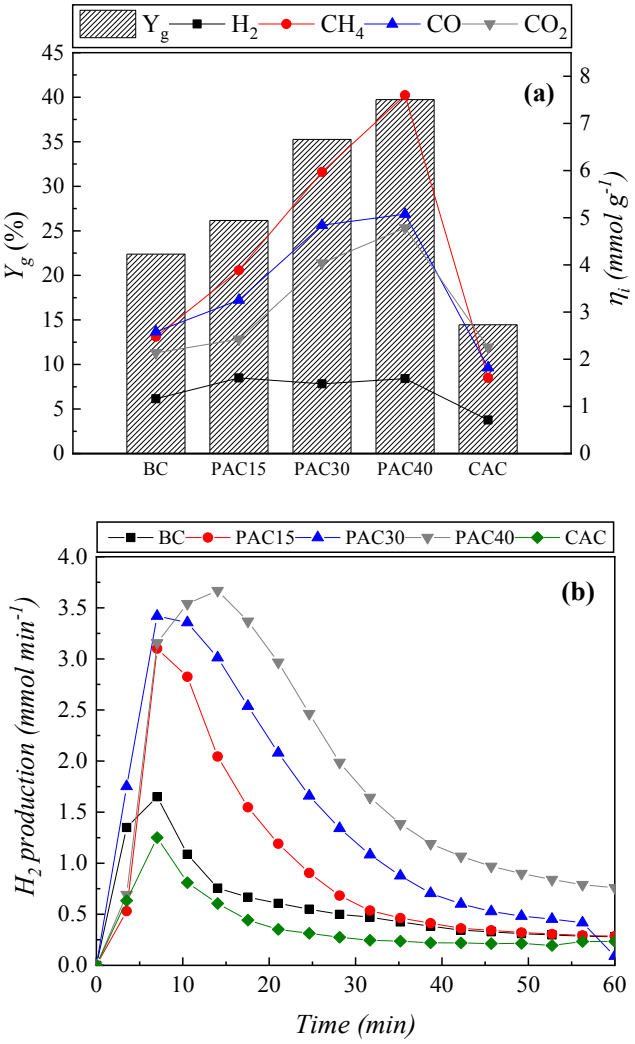

Fig. 2. Results obtained from the catalytic cracking experiments (700 °C and GHSV of 19500 h^{-1}): total gas production (Y_g) and yields of gaseous species (a), and time evolution of the H_2 production rate (b).

As expected, in accordance with the textural properties reported in Table 3, an increase in the degree of burn-off led to a progressive increase in the total gas production, which reached a maximum of 40% for the PAC40 catalyst (which had the highest V_{mic}). As it is also shown in Fig. 2a, the yields of produced CH_4, CO_2 and CO significantly increased with the degree of burn-off; however, the yield of H_2 was

Table 4
Main reactions occurring during the upgrading of pyrolysis vapors.

No.	Reaction	ΔH^0 (kJ mol^{-1})
1	$C_nH_mO_k \rightarrow C_xH_yO_z + gases(H_2, H_2O, CO_2, CO, CH_4, C_2H_x, C_3H_y, ...) + coke$	> 0
2	$C_nH_mO_k + (2n-k)H_2O \rightleftarrows nCO_2 + \left(2n + \frac{m}{2} - k\right)H_2$	173.6[c]
3	$C_nH_mO_k + (n-k)H_2O \rightleftarrows nCO + \left(n + \frac{m}{2} - k\right)H_2$	255.9[c]
4	$CO + H_2O \rightleftarrows CO_2 + H_2$	–41.2
5	$C_nH_mO_k + (n-k)CO_2 \rightleftarrows (2n-k)CO + \left(\frac{m}{2}\right)H_2$	297.0[c]
6	$C + H_2O \rightleftarrows CO + H_2$	131.3
7	$C + CO_2 \rightleftarrows 2CO$	172.5
8	$CO + 3H_2 \rightleftarrows CH_4 + H_2O$	–205.8
9	$CO_2 + 4H_2 \rightleftarrows CH_4 + H_2O$	77.2
10	$C + 2H_2 \rightleftarrows CH_4$	–74.5

[c] Referred to ethanol (C_2H_6O).

relatively low and almost constant for all experiments.

With regard to the chemically activated biochar (CAC), its catalytic activity was much lower than that observed for physically activated biochars. A total gas production of only 14% was obtained when a bed of this material was used. This poor performance (which was even lower than that measured for non-activated biochar) could be explained by the lack of microporous and the fact that the washing step with dilute HCl (performed at the end of the chemical activation process) led to a certain removal of the inorganic species from the biochar [50] and, consequently, an inhibition of the above-mentioned inherent catalytic activity. Indeed, such hypothesis was confirmed by XRF analysis of CAC ashes, which revealed that potassium content drastically decreased from 12.29 wt% of the RW ashes to 3.69 wt% of the acid-washed chemically activated biochar (CAC).

Fig. 2b compares the time evolution of the H_2 production rates for the cracking experiments conducted using activated biochars. From this figure, it can be deduced a relatively fast deactivation (occurring during the first 10 min of operation) of BC, CAC and, PAC15 catalysts. However, a slightly higher resistance to deactivation by coke deposition was observed for physically activated biochars at high degrees of burn-off (30% and 40% for PAC30 and PAC40, respectively), probably due to their higher initial microporosity [51].

In summary, one can conclude that physical activation up to a relatively high degree of burn-off (i.e., PAC40) was the most appropriate way to produce a biochar-derived catalyst, since cracking reactions were enhanced due to the relatively higher specific surface area and micropores content. Thus, the PAC40 catalyst was selected for the next experimental steps.

3.3. Catalytic steam reforming

In this experimental stage, a preliminary blank test was performed to measure the effect of the presence of water in the feed stream on the thermal stability of the mixture of model compounds. This test, which was conducted using a bed of silica sand at 700 °C and a GHSV of 19500 h^{-1}, resulted in a total gas production of only 6.0%. Therefore, the extent of uncatalyzed cracking and/or reforming reactions was negligible, even in the presence of water.

As expected, the addition of water led to an increase in the total gas production and sharp differences in the yields of gaseous species. As shown in Fig. 3a, the steam reforming (SR) test conducted using the PAC40 catalyst under the same conditions than those used for the catalytic cracking test (700 °C and a GHSV of 19500 h^{-1}) revealed a marked increase in the production of H_2 (and, to a lesser extent, CO_2) at the expense of CO and CH_4. A possible explanation for this finding is the fact that the water fed into the reactor was not only involved in reforming reactions (reactions (2) and (3) in Table 4), but also helped to keep the catalyst active through steam gasification of both the catalyst and formed coke (reaction 6 in Table 4) [12,48]. In addition, and as pointed out by Feng et al. [49], the oxidative nature of steam can lead to the formation of O-containing functional groups and related crystal lattice defects, which could provide further active sites for gasification. Because of the simultaneous deposition and gasification of coke, larger fluctuations in the pressure drop across the bed (in comparison with cracking experiments) were observed, as shown in Fig. A.3. On the other hand, the relatively low production of CO could be related to a promotion of the water-gas-shift reaction (reaction 4 in Table 4), which also leads to an additional production of CO_2 [50].

Concerning the effect of the gas-hourly space velocity, four SR tests at different values of GHSV were performed. From the results shown in Fig. 3a, it can be seen that the highest yield of H_2 (as well as Y_g) was obtained at 14500 h^{-1}. Earlier studies (see, for instance, the study by Hu et al. [52]) have reported a progressive increase in the total gas production as the gas residence time increased. However, a slight decrease in the total gas production (and yield of H_2) was observed at the lowest GHSV tested (12000 h^{-1}). This apparently contradictory result might be related to a higher extent of polymerization reactions at longer contact times, leading to excessive coke deposition. This is consistent with the slightly faster deactivation shown in Fig. 3b for the SR test conducted at the lowest GHSV. In view of these results, a GHSV of 14500 h^{-1} was chosen as the most appropriate for subsequent experiments.

With regard to the influence of the bed temperature, four additional SR tests were performed at 600, 650, 700 and 750 °C, keeping constant the GHSV at the best value deduced above. As can be observed in Fig. 4a, the total gas production was strongly dependent on the reforming temperature. As the temperature increased, it was observed a marked enhancement in the production of H_2 and, to a much lesser extent, CO_2, CO, and CH_4. Both the highest total gas production and yield of H_2 were maximized at the highest temperature tested (750 °C). Fig. 4b also shows that, at this temperature, the PAC40 exhibited a good resistance to deactivation. This finding seems to confirm that, at 750 °C, the rate of the steam gasification reaction was high enough to compensate for the deposition of coke on the surface of the catalyst. To gain additional insights on the porosity evolution, the catalysts used in SR tests conducted at 700 and 750 °C were analyzed in terms of S_{BET} and PSD. As expected, the spent catalysts exhibited differences in the specific surface area and PSD in comparison with the fresh ones, as illustrated in Fig. 5. The lower decrease in the S_{BET} observed for the spent catalyst at 750 °C (a 31% decrease instead of a 58% for the catalyst used

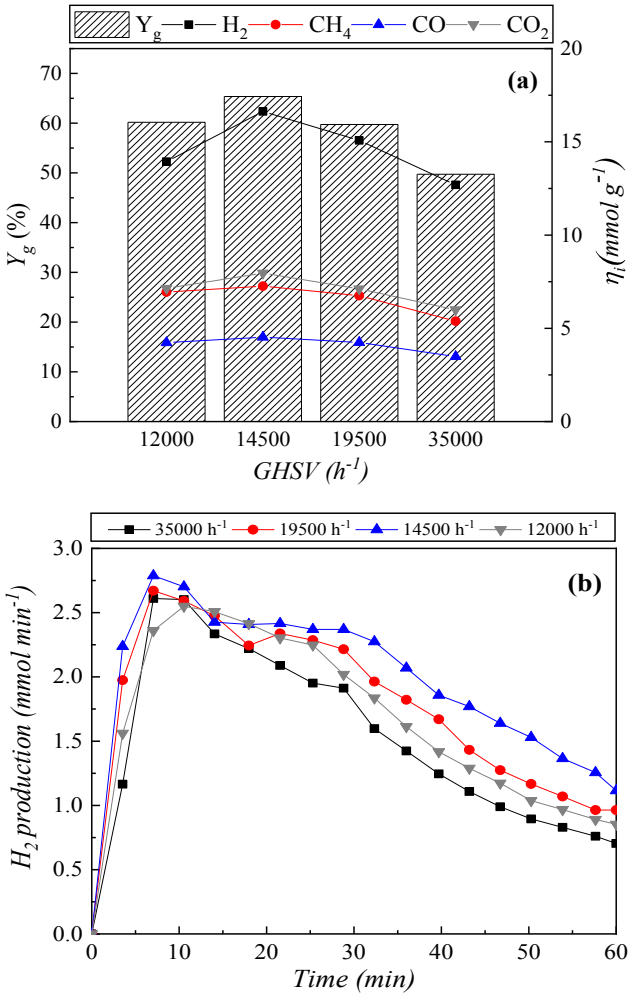

Fig. 3. Results obtained from the catalytic steam reforming experiments conducted at 700 °C, using the PAC40 material, and at different GHSV values: total gas production (Y_g) and yields of gaseous species (a), and time evolution of the H_2 production rate (b).

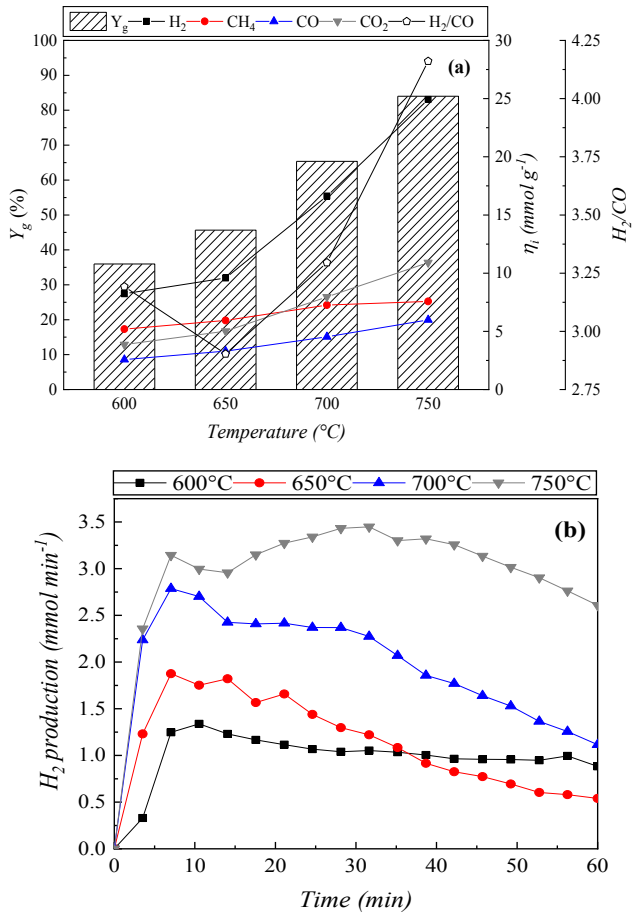

Fig. 4. Results obtained from the catalytic steam reforming experiments conducted at a GHSV of 14500 h^{-1}, using the PAC40 material, and at different bed temperatures: total gas production (Y_g) and yields of gaseous species (a), and time evolution of the H_2 production rate (b).

at 700 °C) could be related to the higher extent of the steam gasification reaction and subsequent further development of new pores. In addition, the spent biochars exhibited lower volumes of micropores (following the same trend observed for the S_{BET}); however, the volume of mesopores increased of 17% when the catalyst was tested at 750 °C.

3.4. Catalytic steam and dry reforming

Since the pyrolysis outlet stream always contains CO_2, more realistic steam and dry reforming (SDR) experiments are required. In addition, considerably lower H_2/CO ratios, in comparison with those obtained using steam reforming (which are too high for most applications [53]), can be obtained by feeding a certain amount of CO_2. The results obtained from SDR experiments performed at different partial pressures of CO_2 in the feed gas stream, under the best operating conditions deduced in the previous section and using the PAC40 catalyst are presented and discussed here.

As shown in Fig. 6a, the addition of CO_2 into the feed gas stream induced a progressive increase in the total gas production (Y_g). This was largely due to the promotion of dry reforming reactions as well as the reverse Boudouard reaction (reactions 5 and 7 in Table 4). Nevertheless, a certain decrease in the yield of H_2 was also observed when the highest amount of CO_2 (p_{CO2} = 30 kPa) was fed into the reactor. This finding could be explained by the fact that a higher CO_2 partial pressure can result in a higher extent of dry reforming at the expense of steam reforming, leading to a lower production of H_2. Similarly, the reverse Boudouard reaction could also be enhanced further, resulting in a lower steam gasification rate. In view of the results obtained from the SDR tests, we can conclude that a CO_2 partial pressure of 20 kPa in the feed gas stream can be considered as the best condition tested, since it provided the highest yield of H_2 (26.5 mmol g^{-1} with a composition in the produced gas of 46.5 vol%) and a molar H_2/CO ratio in the produced gas of 2.15, which was close to the optimal value for Fischer-Tropsch synthesis (2.00) [53,54].

A comparison of the resistance to deactivation of the PAC40 catalyst, working under the best reaction conditions for both SR and SDR processes, is given in Fig. 6b. As can be deduced from the time evolution of the instantaneous production of H_2, the addition of CO_2 into the gas feed resulted in an apparently improved resistance to coke formation. This finding was expected, since CO_2 can increase further the availability of defects in the biochar, which results in an enhanced reactivity towards steam and CO_2 gasification [49].

3.5. Real pyrolysis oil

The aqueous fraction of the bio-oil produced during the pyrolysis of wheat straw at the highest temperature of 500 °C and at 0.1 MPa was filtered and fed into the reformer. The best process operating conditions deduced from the SDR tests (for the mixture of model compounds) were selected for the catalytic upgrading of the real bio-oil sample. As can be seen in Fig. 7a, both the total gas production and yield of H_2 were improved when the real bio-oil sample was used instead of the mixture of model compounds. This finding could partly be explained by differences in composition between the two liquid feedstocks. In this sense, the real bio-oil sample could contain a higher fraction of light volatile compounds, which are more susceptible to thermal decomposition. Furthermore, the content of water in the bio-oil sample was considerably higher than that of the wet mixture of model compounds (75.6 vs. 50 wt%). The resulting increased amount of water could lead to a greater extent of the water-consuming reactions (e.g., WGS and steam reforming reactions), therefore resulting in increased yields of H_2 and CO_2 at the expense of CO and CH_4, as displayed in Fig. 7a.

Regarding the stability of the PAC40 catalysts during the upgrading of the real bio-oil sample, Fig. 7b reveals a good resistance to deactivation over the course of a 60-min experiment. In fact, the behavior observed was very similar to that seen previously for the upgrading of the mixture of model compounds.

In summary, the results reported here indicate that physically

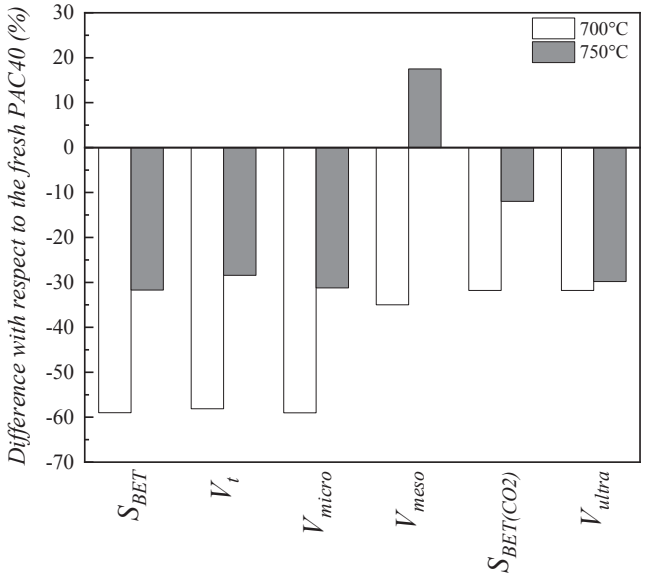

Fig. 5. Differences in textural properties between the fresh and spent PAC40 materials from the SR tests at 700 and 750 °C.

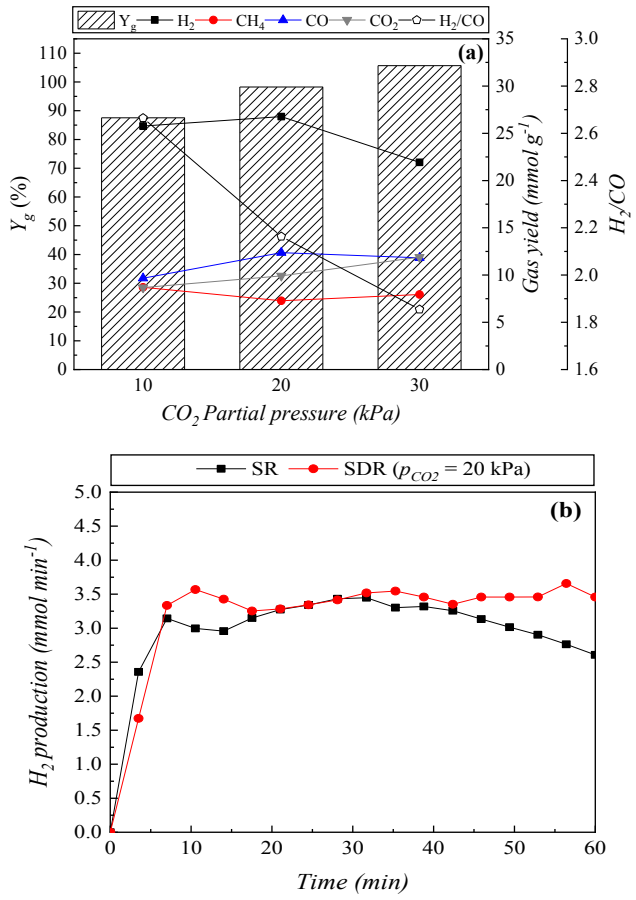

Fig. 6. Results obtained from the catalytic steam and dry reforming experiments conducted using the PAC40 material at 750 °C, a GHSV of 14500 h^{-1}, and at different partial pressures of CO_2 in the feed gas stream: total gas production (Y_g) and yields of gaseous species (a), and time evolution of the H_2 production rate for the best SR and SDR conditions (b).

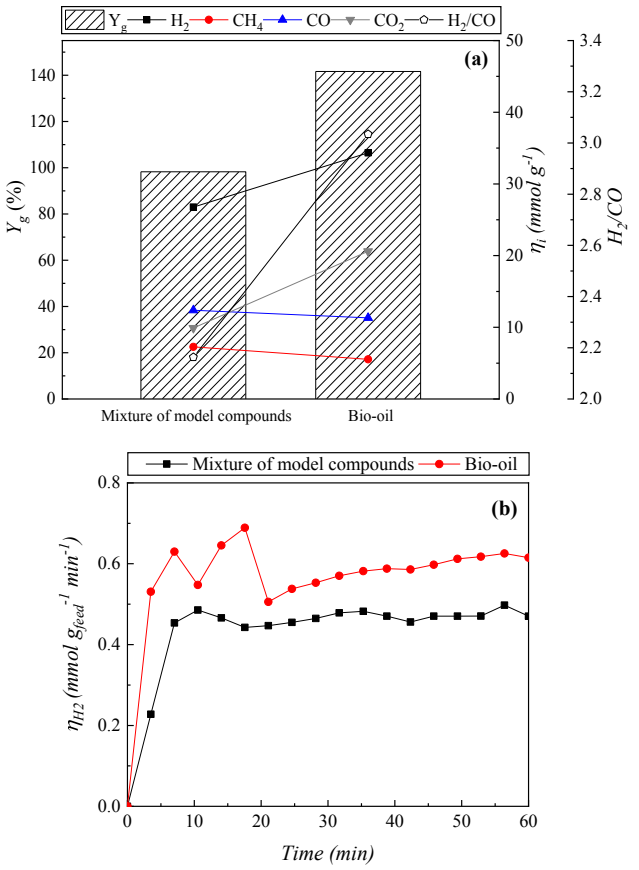

Fig. 7. Comparison of the results obtained from SDR tests of the mixture of model compounds and the real bio-oil sample: total gas production (Y_g) and yields of gaseous species (a), and time evolution of the instantaneous yield of H_2 (b). Both tests were conducted using the PAC40 material at 750 °C, a GHSV of 14500 h^{-1}, and a CO_2 partial pressure of 20 kPa.

activated wheat-straw derived biochars are appropriate for the upgrading of biomass pyrolysis vapors. It should be highlighted that the best performing activated biochar (PAC40) exhibited a good catalytic activity and resistance to deactivation by coke deposition at 750 °C (a moderate temperature for a non-metal-based catalyst) and with a low residence time within the catalyst bed (0.25 s). Further studies are needed to assess the long-term stability of biochars as well as the ability of such activated biochars to upgrade real pyrolysis vapors in a downstream fixed-bed reactor.

4. Conclusions

From the analysis of the results mentioned above, the following conclusions can be drawn:

(1) Wheat straw-derived biochars activated with CO_2 at 800 °C, up to a degree of burn-off of 40%, showed an appropriate specific surface area, which was mostly attributed to micropores.
(2) The good catalytic activity and stability observed for the best activated biochar (i.e., 40% BO) during the upgrading of a mixture of model compounds could be explained by three reasons: (*i*) the availability of alkali metals (e.g., K) on the surface of the char matrix, (*ii*) the high surface area and microporous volume obtained through biochar physical activation, and (*iii*) the oxidizing nature of steam and CO_2, which can result in the formation of crystal lattice defects. In all cases, the number of active sites on the surface of biochar can increase, leading to an enhancement of the biochar gasification reactivity. The higher extent of both steam gasification and reverse Boudouard reactions can help to refresh the active surface area and therefore prevent deactivation by coke deposition.
(3) The good results also obtained for an aqueous fraction of a real biomass pyrolysis oil seem to confirm the ability of the best activated biochar for upgrading purposes. Despite the fact that the process temperature used here was not so high (750 °C), further research should focus on lowering it. To this end, developing K-loaded activated biochars appears to be an interesting option.

Acknowledgments

This project received funding from the European Union's Horizon 2020 research and innovation programme under the Marie Skłodowska-Curie grant agreement No 721991. The authors also acknowledge the funding from the Aragón Government (Ref. T22_17R), co-funded by FEDER 2014-2020 "Construyendo Europa desde Aragón".

Appendix A. Supplementary data

Supplementary data to this article can be found online at https://doi.org/10.1016/j.fuel.2019.115807.

References

[1] Manyà JJ. Pyrolysis for biochar purposes: a review to establish current knowledge gaps and research needs. Environ Sci Technol 2012;46:7939–54. https://doi.org/10.1021/es301029g.

[2] Mourant D, Hasan MDM, Song Y, Li C-Z, Hu X, Gunawan R, et al. Upgrading of bio-oil via acid-catalyzed reactions in alcohols — A mini review. Fuel Process Technol 2016;155:2–19. https://doi.org/10.1016/j.fuproc.2016.08.020.

[3] Mahyoub SAA, Liao W, Ma P, Zhao H, Guo M, Li H, et al. Effect of pyrolysis temperature on characteristics and aromatic contaminants adsorption behavior of magnetic biochar derived from pyrolysis oil distillation residue. Bioresour Technol 2016;223:20–6. https://doi.org/10.1016/j.biortech.2016.10.033.

[4] Oasmaa A, Fonts I, Pelaez-Samaniego MR, Garcia-Perez ME, Garcia-Perez M. Pyrolysis oil multiphase behavior and phase stability: a review. Energy Fuels 2016;30:6179–200. https://doi.org/10.1021/acs.energyfuels.6b01287.

[5] Oasmaa A, Kuoppala E, Solantausta Y. Fast pyrolysis of forestry residue. 2. Physicochemical composition of product liquid. Energy Fuels 2003;17:433–43. https://doi.org/10.1021/ef020206g.

[6] Fraga AR, Gaines AF, Kandiyoti R. Characterization of biomass pyrolysis tars produced in the relative absence of extraparticle secondary reactions. Fuel 1991;70:803–9. https://doi.org/10.1016/0016-2361(91)90186-E.

[7] Yang Z, Kumar A, Huhnke RL, Buser M, Capareda S. Pyrolysis of eastern redcedar: distribution and characteristics of fast and slow pyrolysis products. Fuel 2016;166:157–65. https://doi.org/10.1016/j.fuel.2015.10.101.

[8] Lu Q, Li WZ, Zhu XF. Overview of fuel properties of biomass fast pyrolysis oils. Energy Convers Manag 2009;50:1376–83. https://doi.org/10.1016/j.enconman.2009.01.001.

[9] Hornung U, Schneider D, Hornung A, Tumiatti V, Seifert H. Sequential pyrolysis and catalytic low temperature reforming of wheat straw. J Anal Appl Pyrolysis 2009;85:145–50. https://doi.org/10.1016/j.jaap.2008.11.006.

[10] Shen Y, Zhao P, Shao Q, Ma D, Takahashi F, Yoshikawa K. In-situ catalytic conversion of tar using rice husk char-supported nickel-iron catalysts for biomass pyrolysis/gasification. Appl Catal B Environ 2014;152–153:140–51. https://doi.org/10.1016/j.apcatb.2014.01.032.

[11] Xiang J, Liu Q, Deng Z, Wang Y, Su S, Hu S, et al. Effect of the pre-reforming by Fe/bio-char catalyst on a two-stage catalytic steam reforming of bio-oil. Fuel 2018;239:282–9. https://doi.org/10.1016/j.fuel.2018.11.029.

[12] Hosokai S, Norinaga K, Kimura T, Nakano M, Li C-Z, Hayashi J. Reforming of volatiles from the biomass pyrolysis over charcoal in a sequence of coke deposition and steam gasification of coke. Energy Fuels 2011;25:5387–93. https://doi.org/10.1021/ef2003766.

[13] Shen Y, Chen M, Sun T, Jia J. Catalytic reforming of pyrolysis tar over metallic nickel nanoparticles embedded in pyrochar. Fuel 2015;159:570–9. https://doi.org/10.1016/j.fuel.2015.07.007.

[14] Wang Y, Jiang L, Hu S, Su S, Zhou Y, Xiang J, et al. Evolution of structure and activity of char-supported iron catalysts prepared for steam reforming of bio-oil. Fuel Process Technol 2017;158:180–90. https://doi.org/10.1016/j.fuproc.2017.01.002.

[15] Mani S, Kastner JR, Juneja A. Catalytic decomposition of toluene using a biomass derived catalyst. Fuel Process Technol 2013;114:118–25. https://doi.org/10.1016/j.fuproc.2013.03.015.

[16] Xue Y, Gao B, Yao Y, Inyang M, Zhang M, Zimmerman AR, et al. Hydrogen peroxide modification enhances the ability of biochar (hydrochar) produced from hydrothermal carbonization of peanut hull to remove aqueous heavy metals: Batch and column tests. Chem Eng J 2012;200–202:673–80. https://doi.org/10.1016/J.CEJ.2012.06.116.

[17] Jimenez-Cordero D, Heras F, Alonso-Morales N, Gilarranz MA, Rodriguez JJ. Ozone as oxidation agent in cyclic activation of biochar. Fuel Process Technol 2015;139:42–8. https://doi.org/10.1016/j.fuproc.2015.08.016.

[18] Feng W, Kwon S, Borguet E, Vidic R. Adsorption of hydrogen sulfide onto activated carbon fibers: Effect of pore structure and surface chemistry. Environ Sci Technol 2005;39:9744–9. https://doi.org/10.1021/es0507158.

[19] Titirici MM, Thomas A, Antonietti M. Aminated hydrophilic ordered mesoporous carbons. J Mater Chem 2007;17:3412–8. https://doi.org/10.1039/b703569a.

[20] Pérez-Cadenas AF, Maldonado-Hódar FJ, Moreno-Castilla C. On the nature of surface acid sites of chlorinated activated carbons. Carbon 2003;41:473–8. https://doi.org/10.1016/S0008-6223(02)00353-6.

[21] Abu El-Rub Z, Bramer EA, Brem G. Experimental comparison of biomass chars with other catalysts for tar reduction. Fuel 2008;87:2243–52. https://doi.org/10.1016/j.fuel.2008.01.004.

[22] Shen Y. Chars as carbonaceous adsorbents/catalysts for tar elimination during biomass pyrolysis or gasification. Renewable Sustainable Energy Rev 2015;43:281–95. https://doi.org/10.1016/j.rser.2014.11.061.

[23] Manyà JJ, González B, Azuara M, Arner G. Ultra-microporous adsorbents prepared from vine shoots-derived biochar with high CO2 uptake and CO2/N2 selectivity. Chem Eng J 2018;345:631–9. https://doi.org/10.1016/j.cej.2018.01.092.

[24] Greco G, Videgain M, Di Stasi C, González B, Manyà JJ. Evolution of the mass-loss rate during atmospheric and pressurized slow pyrolysis of wheat straw in a bench-scale reactor. J Anal Appl Pyrolysis 2018;136:18–26. https://doi.org/10.1016/j.jaap.2018.11.007.

[25] Molina-Sabio M, González MT, Rodriguez-Reinoso F, Sepúlveda-Escribano A. Effect of steam and carbon dioxide activation in the micropore size distribution of activated carbon. Carbon 1996;34:505–9. https://doi.org/10.1016/0008-6223(96)00006-1.

[26] Plaza MG, González AS, Pis JJ, Rubiera F, Pevida C. Production of microporous biochars by single-step oxidation: Effect of activation conditions on CO_2 capture. Appl Energy 2014;114:551–62. https://doi.org/10.1016/j.apenergy.2013.09.058.

[27] Lillo-Rodenas MA, Fletcher AJ, Thomas KM, Cazorla-Amoros D, Linares-Solano A. Competitive adsorption of a benzene-toluene mixture on activated carbons at low concentration. Carbon 2006;44:1455–63. https://doi.org/10.1016/j.carbon.2005.12.001.

[28] Sun K, Huang Q, Chi Y, Yan J. Effect of ZnCl2-activated biochar on catalytic pyrolysis of mixed waste plastics for producing aromatic-enriched oil. Waste Manage 2018;81:128–37. https://doi.org/10.1016/j.wasman.2018.09.054.

[29] Tsai WT, Chang CY, Wang SY, Chang CF, Chien SF, Sun HF. Preparation of activated carbons from corn cob catalyzed by potassium salts and subsequent gasification with CO_2. Bioresour Technol 2001;78:203–8. https://doi.org/10.1016/S0960-8524(00)00111-5.

[30] Dehkhoda AM, Gyenge E, Ellis N. A novel method to tailor the porous structure of KOH-activated biochar and its application in capacitive deionization and energy storage. Biomass Bioenergy 2016;87:107–21. https://doi.org/10.1016/j.biombioe.2016.02.023.

[31] Tseng RL. Physical and chemical properties and adsorption type of activated carbon prepared from plum kernels by NaOH activation. J Hazard Mater 2007;147(3):1020–7. https://doi.org/10.1016/j.jhazmat.2007.01.140.

[32] Adinata D, Wan Daud WMA, Aroua MK. Preparation and characterization of activated carbon from palm shell by chemical activation with K_2CO_3. Bioresour Technol 2007;98:145–9. https://doi.org/10.1016/j.biortech.2005.11.006.

[33] Foo KY, Hameed BH. Utilization of rice husks as a feedstock for preparation of activated carbon by microwave induced KOH and K_2CO_3 activation. Bioresour Technol 2011;102:9814–7. https://doi.org/10.1016/j.biortech.2011.07.102.

[34] Hayashi J, Horikawa T, Takeda I, Muroyama K, Nasir Ani F. Preparing activated carbon from various nutshells by chemical activation with K_2CO_3. Carbon 2002;40:2381–6. https://doi.org/10.1016/S0008-6223(02)00118-5.

[35] Mohan D, Pittman CU, Steele PH. Pyrolysis of wood/biomass for bio-oil: a critical review. Energy Fuels 2006;20:848–89. https://doi.org/10.1021/ef0502397.

[36] Rioche C, Kulkarni S, Meunier FC, Breen JP, Burch R. Steam reforming of model compounds and fast pyrolysis bio-oil on supported noble metal catalysts. Appl Catal B Environ 2005;61:130–9. https://doi.org/10.1016/j.apcatb.2005.04.015.

[37] Fu M, Qi W, Xu Q, Zhang S, Yan Y. Hydrogen production from bio-oil model compounds dry (CO2) reforming over Ni/Al2O3catalyst. Int J Hydrogen Energy 2016;41:1494–501. https://doi.org/10.1016/j.ijhydene.2015.11.104.

[38] Ledesma EB, Campos C, Cranmer DJ, Foytik BL, Ton MN, Dixon EA, et al. Vapor-phase cracking of eugenol: Distribution of tar products as functions of temperature and residence time. Energy Fuels 2013;27:868–78. https://doi.org/10.1021/ef3018332.

[39] Manyà JJ, Azuara M, Manso JA. Biochar production through slow pyrolysis of different biomass materials: seeking the best operating conditions. Biomass Bioenergy 2018;117:115–23. https://doi.org/10.1016/j.biombioe.2018.07.019.

[40] Robau-Sánchez A, Aguilar-Elguézabal A, Aguilar-Pliego J. Chemical activation of quercus agrifolia char using KOH: evidence of cyanide presence. Microporous Mesoporous Mater 2005;85:331–9. https://doi.org/10.1016/j.micromeso.2005.07.003.

[41] Walton KS, Snurr RQ. Applicability of the BET method for determining surface areas of microporous metal-organic frameworks. J Am Chem Soc 2007;129:8552–6. https://doi.org/10.1021/ja071174k.

[42] Kim KC, Yoon TU, Bae YS. Applicability of using CO_2 adsorption isotherms to determine BET surface areas of microporous materials. Microporous Mesoporous Mat 2016;224:294–301. https://doi.org/10.1016/j.micromeso.2016.01.003.

[43] Fang Q, Chen B, Lin Y, Guan Y. Aromatic and hydrophobic surfaces of wood-derived biochar enhance perchlorate adsorption via hydrogen bonding to oxygen-containing organic groups. Environ Sci Technol 2013;48:279–88. https://doi.org/10.1021/es403711y.

[44] Plaza MG, Pevida C, Arias B, Fermoso J, Casal MD, Martín CF, et al. Development of low-cost biomass-based adsorbents for postcombustion CO_2 capture. Fuel 2009;88:2442–7. https://doi.org/10.1016/j.fuel.2009.02.025.

[45] Jung SH, Kim JS. Production of biochars by intermediate pyrolysis and activated carbons from oak by three activation methods using CO_2. J Anal Appl Pyrolysis 2014;107:116–22. https://doi.org/10.1016/j.jaap.2014.02.011.

[46] Remiro A, Valle B, Aguayo AT, Bilbao J, Gayubo AG. Operating conditions for attenuating Ni/La2O3- αAl2O3 catalyst deactivation in the steam reforming of bio-oil aqueous fraction. Fuel Process Technol 2013;115:222–32. https://doi.org/10.1016/j.fuproc.2013.06.003.

[47] Arregi A, Lopez G, Amutio M, Artetxe M, Barbarias I, Bilbao J, et al. Role of operating conditions in the catalyst deactivation in the in-line steam reforming of volatiles from biomass fast pyrolysis. Fuel 2018;216:233–44. https://doi.org/10.1016/j.fuel.2017.12.002.

[48] Sueyasu T, Oike T, Mori A, Kudo S, Norinaga K, Hayashi JI. Simultaneous steam reforming of tar and steam gasification of char from the pyrolysis of potassium-loaded woody biomass. Energy Fuels 2012;26:199–208. https://doi.org/10.1021/ef201166a.

[49] Feng D, Zhao Y, Zhang Y, Sun S, Meng S, Guo Y, et al. Effects of K and Ca on reforming of model tar compounds with pyrolysis biochars under H_2O or CO_2. Chem Eng J 2016;306:422–32. https://doi.org/10.1016/j.cej.2016.07.065.

[50] Xu M, Sheng C. Influences of the heat-treatment temperature and inorganic matter

on combustion characteristics of cornstalk biochars. Energy Fuels 2012;26:209–18. https://doi.org/10.1021/ef2011657.
[51] Hosokai S, Kumabe K, Ohshita M, Norinaga K, Li CZ, Hayashi J. ichiro. Mechanism of decomposition of aromatics over charcoal and necessary condition for maintaining its activity. Fuel 2008;87:2914–22. https://doi.org/10.1016/j.fuel.2008.04.019.
[52] Hu M, Laghari M, Cui B, Xiao B, Zhang B, Guo D. Catalytic cracking of biomass tar over char supported nickel catalyst. Energy 2018;145:228–37. https://doi.org/10.1016/j.energy.2017.12.096.
[53] Cao Y, Gao Z, Jin J, Zhou H, Cohron M, Zhao H, et al. Synthesis gas production with an adjustable H2/CO ratio through the coal gasification process: effects of coal ranks and methane addition. Energy Fuels 2008;22:1720–30. https://doi.org/10.1021/ef7005707.
[54] Yuan H, Wu S, Yin X, Huang Y, Guo D, Wu C. Adjustment of biomass product gas to raise H_2/CO ratio and remove tar over sodium titanate catalysts. Renew Energy 2018;115:288–98. https://doi.org/10.1016/j.renene.2017.08.025.

Supplementary materials:

Physically activated wheat straw-derived biochar for biomass pyrolysis vapors upgrading with high resistance against coke deactivation

Christian Di Stasi*, Darío Alvira, Gianluca Greco, Belén González, Joan J. Manyà

Aragón Institute of Engineering Research (I3A), Technological College of Huesca, University of Zaragoza, crta. Cuarte s/n, Huesca E-22071, Spain

* Corresponding author at: *Aragón Institute of Engineering Research (I3A), Technological College of Huesca, University of Zaragoza, crta. Cuarte s/n, Huesca E-22071, Spain.*

E-mail address: christiandistasi@unizar.es.

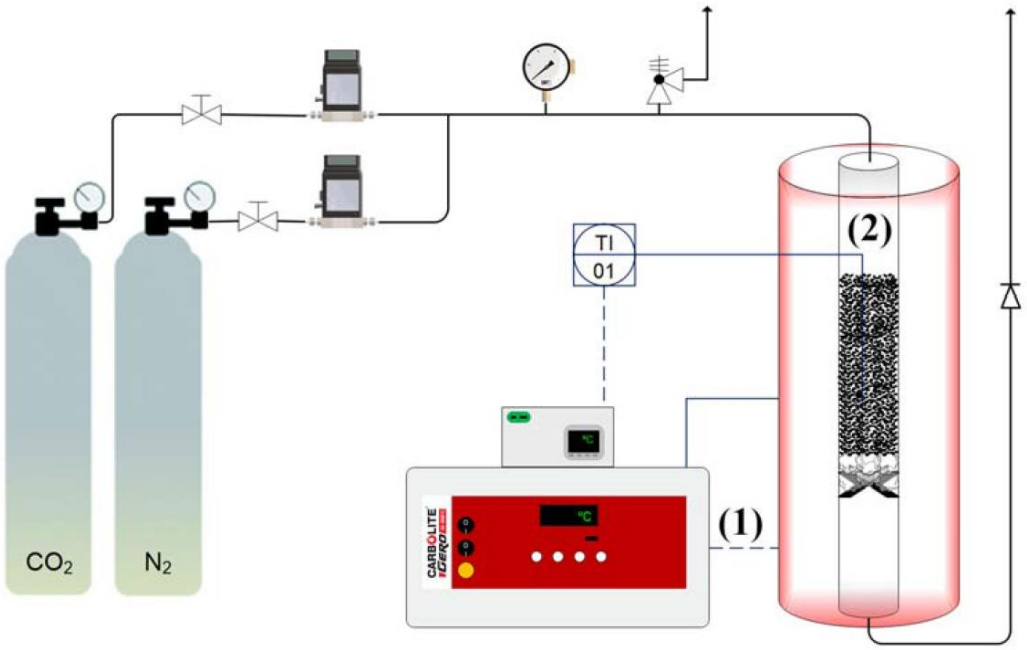

Fig. A.1. Schematic representation of the activation set-up used for the production of physically and chemically activated biochars: furnace (1) and quartz reactor (2).

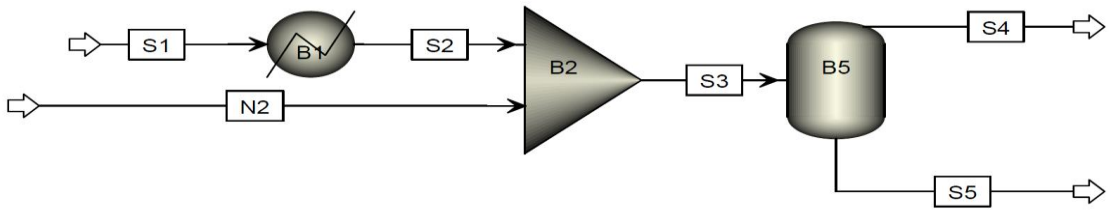

Fig A.2. Flowsheet of the simulation case conducted using Aspen Plus.

The simulation was carried out using the "NRTL" fluid package. The blocks B1, B2 and B3 in Fig. A.2 correspond to a heater, a mixer, and a flash separator; respectively. The results showed that non-negligible mass flow rates of acetic acid, ethanol and acetone are lost in the stream S4 (see Table A.1).

Table A.1

Summary of the simulation results.

	Stream					
	N2	*S1*	*S2*	*S3*	*S4*	*S5*
Phase	Vapor	Liquid	Vapor	Vapor	Vapor	Liquid
Temperature (°C)	300	20	183	255	25	25
Pressure (kPa)	101.3	101.3	101.3	101.3	101.3	101.3
Mass flow rate (g h^{-1})	37.52	13.58	13.58	51.10	42.82	8.276
Acetic acid (g h^{-1})	0.000	3.395	3.395	3.395	0.710	2.685
Ethanol (g h^{-1})	0.000	3.395	3.395	3.395	1.764	1.631
Acetone (g h^{-1})	0.000	3.395	3.395	3.395	2.832	0.563
Eugenol (g h^{-1})	0.000	3.395	3.395	3.395	0.001	3.394
N_2 (g h^{-1})	37.52	0.000	0.000	37.52	37.51	0.003

	Distribution of model compounds in streams S4 and S5	
	S4 (Vapors) wt. %	*S5 (Liquids) wt. %*
Acetic acid	20.90	79.10
Ethanol	51.95	48.05
Acetone	83.43	16.57
Eugenol	0.030	99.97

Table A.2

Results from the repeatability tests for the used experimental set-up. The repeated experiment (steam and dry reforming of the mixture of model compounds) was conducted using the PAC40 catalyst, at 700 °C, at a GHSV of 14500 h^{-1}, and a N_2/CO_2 feed gas ratio of 1:1 (v/v).

	Y_g	η_{H2}	η_{CH4}	η_{CO}
Replicate 1	38.0	12.4	6.55	8.19
Replicate 2	35.0	11.7	5.88	7.52
Replicate 3	37.8	11.8	6.47	8.26
Mean	36.9	12.0	6.30	7.99
Standard deviation	1.68	0.38	0.36	0.41
Coefficient of variation (%)	4.54	3.16	5.81	5.11

Table A.3

Proximate and elemental analyses of wheat straw pellets and non-activated biochars.

	Wheat straw	*BC*
Proximate analysis (wt. %)		
Moisture	7.60 ± 0.11	1.47 ± 0.06
Volatiles	74.8 ± 0.87	16.2 ± 0.71
Ashes	4.23 ± 0.28	13.5 ± 0.11
Fixed carbon	13.3 ± 1.17	68.8 ± 0.54
Elemental Analysis (wt. % in dry-ash-free basis)		
C	44.1 ± 0.10	93.2 ± 0.03
H	6.30 ± 0.02	4.13 ± 0.05
N	0.62 ± 0.02	1.98 ± 0.02
O[a]	48.97	0.71
Atomic H:C ratio	1.71	0.53

[a] Calculated by difference.

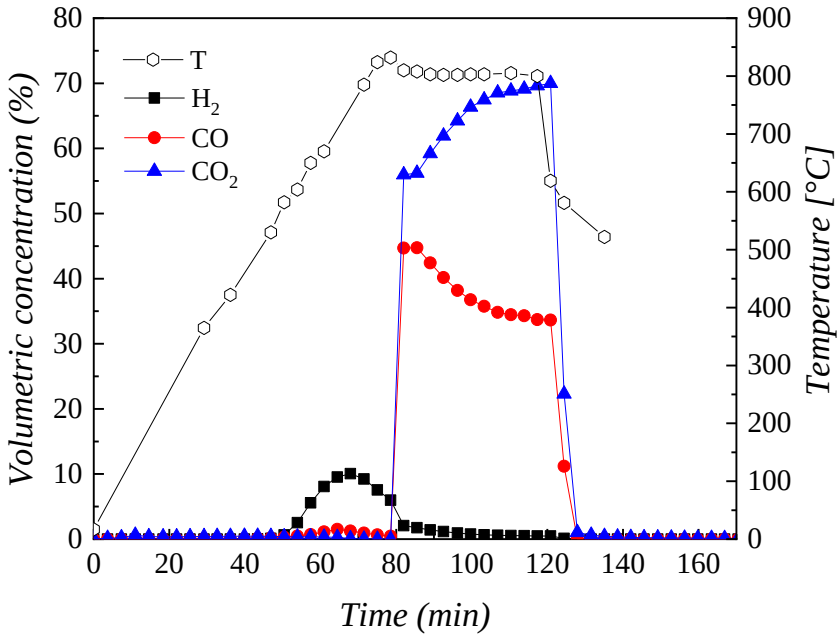

Fig. A.3. Evolution of the bed temperature and composition of the outlet gas stream during the production of a physically activated biochar (soaking time at 800 °C = 45 min).

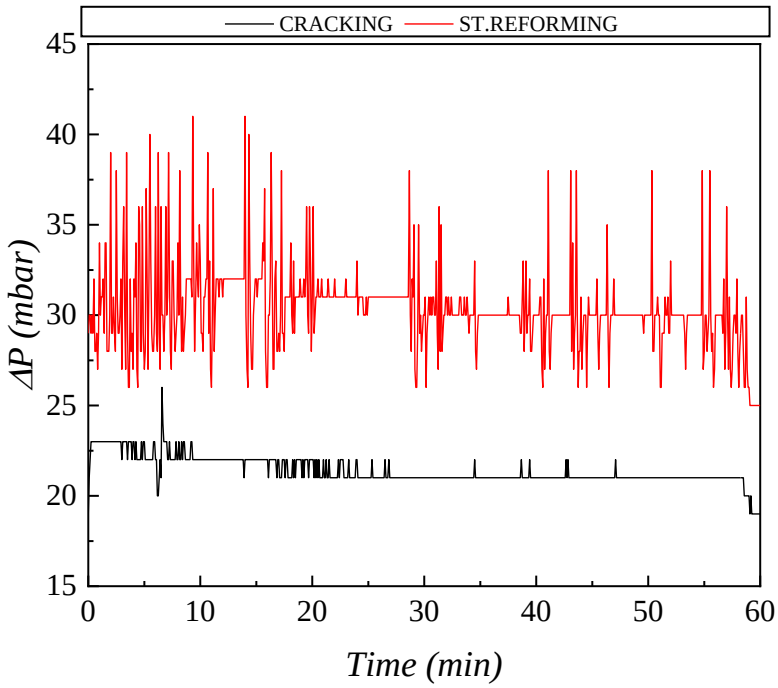

Fig. A.4. Comparison of the pressure drop (*ΔP*) evolution during the catalytic cracking and steam reforming tests for the PAC40 catalysts at 700 °C and at a GHSV of 19500 h^{-1}.

6.2. Influence of activation conditions on textural properties of activated biochar

Once the suitability of using wheat straw-derived biochar for catalytic pyrolysis vapors upgrading was verified (objective I), research was shifted to the identification of the most appropriate biochar activating conditions (objective II). In this context, a comprehensive assessment of the effects of chemical (with K_2CO_3) and physical (with CO_2) activations was carried out. Special attention was paid to the relationships among activation process conditions and the textural properties of the resulting carbons. Furthermore, the materials with the highest specific surface area and most hierarchical pore size distribution were then tested as catalysts for steam and dry reforming of the aqueous phase of pyrolysis oil.

Besides the employment of biochar in pyrolysis vapors upgrading, the main novelty of this research was the investigation of the effects of the operating pressure on the textural properties of activated carbons (for both chemical and physical pathways). To the best of my knowledge, this was never reported in the literature.

In the case of chemically activated biochars, it was found that specific surface area and pore size distribution were both only positively affected by increasing the carbonate loading. However, physically activated biochars produced at the highest pressure and lowest temperature (1.0 MPa and 700 °C) had the highest surface areas and widest pore size distributions. These features made the biochar activated under such conditions more suitable to be employed as catalytic support.

Additionally, it was also demonstrated that through the employment of relatively high activating pressure (1.0 MPa) it was possible to obtain an activated biochar with an acceptable specific surface area even at low activating temperature (650 °C).

Concerning the upgrade of pyrolysis vapors, the best catalytic performance (a total gas yield of 74% and a selectivity toward H_2 of almost 40%) was observed for a biochar firstly activated with CO_2 (activated at 1.0 MPa and 700 °C), and then impregnated with K_2CO_3 (mass ratio carbonate to support 3:1). This good performance was attributed to the high availability of K^0 on the catalyst surface (revealed by SEM-EDX analysis), which could promote the reactions involved in the upgrading process.

Fuel 289 (2021) 119759

Contents lists available at ScienceDirect

Fuel

journal homepage: www.elsevier.com/locate/fuel

Full Length Article

Influence of activation conditions on textural properties and performance of activated biochars for pyrolysis vapors upgrading

Christian Di Stasi [a,*], Gianluca Greco [a], Rafael L.S. Canevesi [b], M. Teresa Izquierdo [c], Vanessa Fierro [b], Alain Celzard [b], Belén González [a], Joan J. Manyà [a]

[a] Aragón Institute of Engineering Research (I3A), Thermochemical Processes Group, University of Zaragoza, Escuela Politécnica Superior, Crta. Cuarte s/n, 22071 Huesca, Spain
[b] Université de Lorraine, CNRS, IJL, Épinal F-88000, France
[c] Instituto de Carboquímica (ICB-CSIC), Miguel Luesma Castán 4, Zaragoza E-50018, Spain

ARTICLE INFO

Keywords:
Biochar
Chemical activation
K_2CO_3
Physical activation
Pressure
Steam and dry reforming of pyrolysis oil

ABSTRACT

The main aim of the present study is to provide a comprehensive assessment of the effects of process activation conditions on the textural properties of the resulting activated carbons, which were produced from wheat straw-derived biochar through chemical activation (with K_2CO_3 at different pressures and mass impregnation ratios) and physical activation (with CO_2 at different temperatures and pressures). For chemically activated biochars, it was found that specific surface area and pore size distribution were both only positively affected by increasing the carbonate loading. However, physically activated biochars produced at the highest pressure and lowest temperature (1.0 MPa and 700 °C) had the highest surface areas and widest pore size distributions. The materials with the most appropriate textural properties were then tested as catalysts for steam and dry reforming of the aqueous phase of pyrolysis oil. The best catalytic performance (a total gas yield of 74% and a selectivity toward H_2 of almost 40%) was observed for a physically activated biochar. This good performance was ascribed to the high availability of K^0 on the catalyst surface, which could effectively promote the reactions involved in the upgrading process.

1. Introduction

In recent years, the demand for activated carbons has increased due to their usefulness in a wide range of different applications such as gas and liquid purification [1], electrochemistry [2], soil remediation [3] and catalysis [4]. Thanks to their versatility to be adapted to specific applications, these materials are considered promising candidates to address environmental issues related to global warming and pollution [5]. Nevertheless, the current main drawback is that the production of activated carbons is still partly based on fossil fuels, which do not meet sustainability criteria [6,7]. Hence, much more efforts should be made to produce much more carbons from biomass. However, the direct conversion of biomass feedstock into the final product has a low yield. Thus, the production of activated carbons from biochar produced by slow pyrolysis seems to be more appropriate in terms of scalability, while at the same time these value-added materials can strengthen the value chain of existing biochar production systems.

In general, pristine biochar has neither a well-developed surface area nor a hierarchical pore size distribution, which is mainly dominated by narrow pores with a diameter (d_p) lower than 0.7 nm (ultra-micropores). Hence, a subsequent activation step is required to improve the textural properties of the carbon material. The activation process involves the development and opening of the porosity of a char using an activation agent. Depending on the agent used, the procedure can be called chemical or physical activation. Chemical activation usually involves two steps. First, the biochar is impregnated with an aqueous solution of the chemical activation agent, or mixed with it in the dry state, and, in a second step, the blend is heated up to a given temperature at which oxidation, dehydration, aromatization and crosslinking reactions, among others, occur. Although the most widely used chemical reagents are KOH [8] and H_3PO_4 [9], non-hazardous and relatively cheap alternative compounds such as K_2CO_3 [10,11] have recently attracted considerable attention. Mai *et al.* [12] have recently reported that activation with potassium carbonate can result in carbons with a high percentage of structural defects and a well-balanced porosity between micro- and mesopores.

* Corresponding author at: Aragón Institute of Engineering Research (I3A), Thermochemical Processes Group, University of Zaragoza, Escuela Politécnica Superior, Crta. Cuarte s/n, 22071 Huesca, Spain.
E-mail address: christiandistasi@unizar.es (C. Di Stasi).

https://doi.org/10.1016/j.fuel.2020.119759
Received 13 July 2020; Received in revised form 29 September 2020; Accepted 11 November 2020
Available online 4 December 2020

Nomenclature

A_{BET}	Brunauer-Emmett-Teller area ($m^2\ g^{-1}$)
d_p	Pore diameter (nm)
F_{BO}	Molar flow rate of dry bio oil (mol min^{-1})
$F_{H2\ Av}$	Experimental average H_2 molar flow rate (mol min^{-1})
$F_{H2\ Stoi}$	H_2 stoichiometric molar flow rate (mol min^{-1})
m_0	Initial mass of biochar before activation (g)
m_c	Biochar mass before the washing step (g)
m_f	Final mass of biochar after activation (g)
m_g	Total mass of produced gas during the upgrading process (g)
m_l	Mass of liquid fed into the upgrading reactor (g)
m_w	Biochar mass after the washing step (g)
n_i	Produced amount of a given gaseous specie i (mol)
n_{tot}	Total amount of produced gas (mol)
$S_{2D\text{-}NLDFT}$	2D-NLDFT specific surface area ($m^2\ g^{-1}$)
S_i	Selectivity toward a given gaseous specie *i* (%)
$V_{0.97}$	Gurvitch pore volume ($cm^3\ g^{-1}$)
V_{meso}	Volume of mesopores ($cm^3\ g^{-1}$)
V_{micro}	Volume of micropores ($cm^3\ g^{-1}$)
V_t	Total pore volume ($cm^3\ g^{-1}$)
V_{ultra}	Volume of ultra-micropores ($cm^3\ g^{-1}$)
Y_g	Total gas yield (%)
Y_{H2}	Hydrogen yield (%)
Y_{wash}	Washing yield (%)
η	Degree of burnout (%)

Acronyms

FTIR	Fourier-Transform Infrared spectroscopy
GHSV	Gas hourly space velocity
LHSV	Liquid hourly space velocity
PSD	Pore size distribution
RSM	Response surface methodology
S:C	Steam to carbon molar ratio
STP	Standard temperature and pressure
TPD	Temperature-programmed desorption
XPS	X-ray photoelectron spectroscopy
μ-GC	Micro gas chromatograph

When activation is carried out by exposing the precursor to relatively high temperatures under an oxidizing atmosphere (e.g., CO_2 [13], H_2O [14] and O_2 [15]), the process is called physical activation. Through either physical or chemical activation, it is possible to tune the textural features of the starting biochar by properly adjusting the activation conditions, mainly temperature, type and/or concentration of activation agent, as well as pressure. To the best of our knowledge, although both activation procedures are widely reported in the literature, a thorough study on the effects that the activation parameters and their possible interactions have on the textural properties of the resulting activated biochar, has never been reported so far. Such information could be very helpful to properly establish the most appropriate operating conditions to produce engineered carbon materials from biomass.

One of the most interesting fields of application of activated carbons is the upgrading of raw pyrolysis vapors, which contain both permanent gases (e.g., CO_2, CO, CH_4, and H_2) and condensable compounds. The condensable fraction, which is generally called pyrolysis oil or bio-oil, is a mixture of hundreds of organic compounds (alcohols, ketones, acids, etc.) and water, and its composition strictly depends on the biomass composition and the pyrolysis operating conditions [16]. For biochar production systems based on slow pyrolysis, downstream processes aimed at upgrading pyrolysis vapors are required to avoid undesirable condensation of organic compounds and to increase simultaneously the quality of the gaseous product. For this purpose, combined steam and dry reforming of pyrolysis oil is a promising option [17,18], due to the presence of a relatively high amount of CO_2 and steam in the raw vapor phase. Heterogeneous catalysts based on transition metals such as Ni [19,20], Co [21], Pt and Rh [22] can be used to improve the overall conversion and the selectivity of the products. However, the main drawback of these catalysts is that the relatively expensive active phase can easily be poisoned and/or deactivated by deposition of coke [23]. One possible solution to reduce the overall cost of the upgrading process is to use activated biochar as catalyst. Its porous structure and inherent inorganic contents (especially K, Mg and Ca) could result in a relatively good catalytic activity [24–29]. Furthermore, due to the presence in the reaction system of H_2O and CO_2, the carbonaceous support, as well as coke deposits, could be continuously partly gasified, thus creating new pores to avoid deactivation. In addition, the spent biochar can be burned to recover energy [30] or, depending on the metal loaded on the support, employed as soil conditioner [31].

Keeping in mind all the above, the main objective of this study was to perform a preliminary investigation about the effects of several activation conditions on the textural properties and the catalytic activity of the resulting activated biochars. To this end, wheat straw-derived biochar was activated chemically and physically with K_2CO_3 and CO_2, respectively, under different operating conditions. To objectively assess the effect of the selected operation conditions (temperature and mass ratio K_2CO_3/precursor for chemical activation, and temperature and pressure for CO_2 activation), we implemented two factorial designs of experiments, with two factors and three replicates at the center point. The specific surface areas and pore size distributions of the resulting activated biochars were then evaluated. The most promising activated biochars were finally tested as catalysts for steam and dry reforming of pyrolysis oil. Their performance was evaluated in terms of conversion of liquid into gas, product selectivity and resistance to deactivation.

2. Experimental section

This study was divided into two main steps: in the first, we carried out physical and chemical activations under different process conditions in order to study their influence on the pore size distribution and specific surface area of the resulting activated biochars; in the second part, the most promising materials were then tested as catalysts in pyrolysis vapors upgrading experiments. The methodology used in this study is summarized graphically in Fig. A.1.

2.1. Biochar production

The biochar used in this study was produced by slow pyrolysis of binder-free wheat straw pellets (9 mm OD and 10–13 mm long). Pyrolysis was carried out at atmospheric pressure in a fixed bed reactor, which was placed inside a furnace and heated up to 500 °C at an average heating rate of 5 °C min^{-1} and using N_2 as carrier gas. More details on the pyrolysis device and the experimental procedure are available elsewhere [32]. The resulting biochar (i.e., "pristine") was ground and then thoroughly sieved to obtain particle sizes in the range of 0.212 to 1.41 mm. The pristine biochar was characterized by proximate analysis (performed in quadruplicate according to ASTM standards D3173 for moisture, D3174 for ash, and D3175 for volatile matter) and ultimate analysis by means of an elemental analyzer CHN628 from Leco Corporation (USA).

2.2. Activation of pristine biochar

2.2.1. Chemical activation

For chemical activation, the pristine biochar was first impregnated with a 1 mol L^{-1} aqueous solution of K_2CO_3. Three K_2CO_3: biochar mass impregnation ratios (1:1, 2:1 and 3:1) were achieved by adjusting the volume of solution. The heterogeneous mixture was then stirred for 2 h at 50 °C, filtered and dried overnight at 110 °C to remove the residual water. Afterwards, 10 g of the impregnated samples were heated up to 700 °C at a heating rate of 10 °C min^{-1}, under an inert atmosphere (N_2), and at three different values of absolute pressure (0.10, 0.55 and 1.00 MPa). For this purpose, a tubular fixed bed reactor (made of nickel-chromium alloy UNS N06600, 28.1 mm ID and 600 mm long) placed in a vertical furnace (model EVA 12/300 from Carbolite Gero, UK) was used. The relatively low activation temperature was chosen to avoid the evaporation of the metallic potassium derived from the decomposition of the activation agent and, also, to ensure low activation extensions and clearly see the potential effects of the studied parameters. On the other hand, the range of activating pressures was chosen in order to allow this experimental setup to be easily scaled up, since the involved pressures were not too high (up to 1.0 MPa). A soaking time at the highest temperature of 60 min was set. The pressure within the reactor was adjusted using a downstream servo-controlled regulator valve. The gas hourly space velocity (GHSV) at the activation temperature was estimated to be 7000 h^{-1}, considering the pressure applied and a bed void factor of 0.5. Thus, the mass flow rate of the inlet gas stream (N_2) was properly adjusted as a function of the selected pressure and the highest temperature to achieve the aforementioned GHSV value.

As a last step, the carbons were rinsed to remove the unreacted reagent and other impurities from their surface. In this work, two different washing procedures were adopted to assess possible effects on the resulting surface area and the catalytic activity of the activated carbons produced. For this purpose, among all the unwashed chemically activated biochars, four of them were just washed with hot deionized water (100 °C), while the seven chemically activated biochars adopted in the design of experiments were washed with a 0.25 mol L^{-1} solution of HCl followed by hot water. Both washing procedures were carried out until neutral pH. The resulting activated biochars were then dried overnight at 110 °C. The efficiency of the washing step was evaluated according to the washing yield, calculated from Eq. (1), in which m_c and m_w are the masses of activated carbon before and after the washing steps, respectively.

$$Y_{wash} = \left(1 - \frac{m_c - m_w}{m_c}\right)100 \quad (1)$$

2.2.2. Physical activation

Physically activated biochars were produced under an atmosphere of pure CO_2 at three different temperatures (700, 775 and 850 °C), and at three different absolute pressures (0.10, 0.55, and 1.00 MPa). The selected activation temperatures are within the range commonly reported in the literature, whereas the pressure values were established with the purpose to compare the properties of resulting activated carbons produced under atmospheric and moderate pressures. Using the same device described in the previous section, 10 g of pristine biochar were heated under N_2 atmosphere, at a heating rate of 10 °C min^{-1}, until the target temperature was reached. Then, the gas supply was switched from N_2 to CO_2 at a constant GHSV of 7000 h^{-1}. These conditions were maintained during the time required to reach a degree of burnout (η, defined as the percentage of mass loss) in the range of 30% to 60%.

2.2.3. Design of experiments

To objectively assess the effects of the activation conditions on the textural properties of activated biochars, an unreplicated two-level factorial design of experiments (with two factors and three replicates at the center point) was adopted for both chemical and physical activations. For chemical activation, the analyzed factors were the absolute pressure and the impregnation ratio of K_2CO_3 to raw biochar, whereas in the case of physical activation, the temperature and the absolute pressure were the studied factors. The structure of the regression model used in the statistical analysis was the following:

$$\text{Å}\cdot = \beta_0 + \beta_i A + \beta_j B + \beta_{ij} AB \quad (2)$$

where A and B corresponded to the assessed factors (normalized values in the range from –1 to 1), whereas β_0, β_i, and β_{ij} were the intercept, linear, and interaction coefficients, respectively. The results obtained for the selected response variables (y) were analyzed using the Minitab v17 statistical package. A significance level of 5% was assumed and the adjusted coefficient of determination (R^2_{adj}) was taken as an indicator of the quality of the fit. Table 1 summarizes the adopted designs of experiments and lists the names of the activated biochars produced. Briefly, activated biochar are referred as *X_Y_P*. *X* corresponds to the activation procedure (CB or PB for *chemically activated biochar* and *physically activated biochar*, respectively); *Y* is the activation temperature for PBs or the impregnation ratio for CBs; and *P* is the activation pressure.

Table 1
Matrix of the factorial designs adopted to assess the effects of the selected factors during both chemical and physical activations. For example, a physical activation carried out at A = –1 and B = 1 means that the process was performed at 700 °C and 1.0 MPa.

Chemical activation (thermal treatment under N_2 up to 700 °C and 1 h soaking time)			
	Factors		***Response Variables***
	A	*B*	$S_{2D\text{-}NLDFT}$, V_b, V_{ultra}, V_{micro}, V_{meso}
Level	Pressure (MPa)	Mass ratio (K_2CO_3: raw biochar)	
Low (−1)	0.10	1:1	
Middle (0)	0.55	2:1	
High (+1)	1.00	3:1	
Runs			**Activated biochar designation** (all washed with an acidic solution)
1	0	0	CB_2_0.55
2	−1	+1	CB_3_0.10
3	+1	+1	CB_3_1.00
4	0	0	CB_2_0.55
5	0	0	CB_2_0.55
6	−1	−1	CB_1_0.10
7	+1	−1	CB_1_1.00
Physical activation			
	Factors		***Response Variables***
	A	*B*	$S_{2D\text{-}NLDFT}$, V_b, V_{ultra}, V_{micro}, V_{meso}
Level	Temperature (°C)	Pressure (MPa)	
Low (−1)	700	0.10	
Middle (0)	775	0.55	
High (+1)	850	1.00	
Runs			**Activated biochar designation**
1	−1	−1	PB_700_0.10
2	−1	+1	PB_700_1.00
3	+1	+1	PB_850_1.00
4	0	0	PB_775_0.55
5	0	0	PB_775_0.55
6	+1	−1	PB_850_0.10
7	0	0	PB_775_0.55

2.3. Catalytic pyrolysis vapors upgrading

The liquid feed used here for pyrolysis vapors upgrading tests was the filtered aqueous phase of the pyrolysis oil formed during the production of pristine biochar derived from wheat straw. This resulting liquid product was characterized in terms of elemental composition, using the same CHN analyzer as mentioned in section 2.1, and water content, using a volumetric Karl-Fischer titrator Titrino plus 870 from Metrohm (Switzerland).

A schematic overview of the experimental device used for the reforming tests is shown in Fig. A.2 (Appendix A). The reactor and furnace elements were the same as those previously described in section 2.2. The reforming operating conditions were selected based on the findings of a previous study [33], which aimed to establish the best process conditions to minimize deactivation by coke deposition.

Briefly, activated biochar (2–5 g) was loaded into the reactor and heated under N_2 atmosphere at an absolute pressure slightly above 0.1 MPa. Once the bed temperature reached the target value of 750 °C, CO_2 was added to the inlet gas stream at a partial CO_2 pressure of 0.02 MPa. The liquid feed was then injected into the gas stream at the inlet of the reactor by means of a HPLC pump (model 521 from Analytical Scientific Instruments, USA). The liquid hourly space velocity (LHSV) was kept constant and equal to 2 h^{-1} for all the experiments conducted. The duration of the experiments was 60 min. The reactor outlet stream, consisting of permanent gases, unreacted pyrolysis oil, and condensable side products, was forced to pass through an ice-bath condensation train. The permanent gases were analyzed using a dual-channel micro gas chromatograph (μ-GC 490 from Agilent, USA) equipped with TCD detectors and two analytical columns (a Molsieve 5 A and a PolarPlot U). The known amount of N_2 fed was used as a tracking compound to calculate the yield of produced gas.

The performance of the activated biochars tested was measured in terms of total gas yield (Y_g) and hydrogen yield (Y_{H2}), as defined by Eqs. (3) and (4), respectively.

$$Y_g = \frac{m_g}{m_L} 100 \tag{3}$$

$$Y_{H2} = \frac{F_{H2\,av}}{F_{H2stoi}} 100 \tag{4}$$

$$F_{H2stoi} = \left(2n + \frac{m}{2} - k\right) F_{BO} \tag{5}$$

$$S_i = \frac{n_i}{n_{tot}} 100 \tag{6}$$

In Eq. (3), m_g was the cumulative mass of the gas produced during the 60-min experiments, whereas m_L corresponded to the total mass of the liquid fed. In Eq. (4), F_{H2av} was the experimental average molar flow rate of hydrogen from minute 20 to minute 40. F_{H2stoi}, which was calculated according to Eq. (5), corresponded to the stoichiometric molar flow rate of hydrogen considering the contribution from steam reforming reaction. F_{BO} was the molar flow rate of the dry pyrolysis oil fed. The selectivity towards specific gaseous products (S_i) was calculated according to Eq. (6), in which n_{tot} was the sum of the gaseous products in moles at the outlet stream.

2.4. Characterization of carbon materials

The textural properties of pristine and activated biochars were determined from both N_2 and CO_2 adsorption isotherms at –196 °C and 0 °C, respectively. Around 120 mg of sample were degassed under vacuum at 150 °C. ASAP 2020 and ASAP 2420 automatic adsorption analyzers (Micromeritics, USA) were used. The results obtained from the isotherms were treated using the MicroActive software. We determined the BET area (A_{BET}) by application of the BET model, as well as the Gurvitch volume ($V_{0.97}$). The enhanced 2D-NLDFT model [34] was employed using SAIEUS software (available at www.nldft.com) to evaluate the pore size distributions (PSDs) and other related parameters: surface area ($S_{2D\text{-}NLDFT}$), ultra-micropore volume (V_{ultra}, $d_p < 0.7$ nm), micropore volume (V_{micro}, $d_p < 2$ nm), total pore volume (V_t) and mesopore volume (V_{meso}, d_p in the range of 2 to 50 nm). The latter was calculated as the difference between V_t and V_{micro}.

To evaluate the availability of residual potassium carbonate on the surface of chemically activated biochars, Fourier-transform Infrared Spectroscopy (FTIR) analyses were conducted using a Frontier MIR/NIR Spectrometer from PerkinElmer (USA).

Qualitative temperature-programmed desorption (TPD) analyses of pristine biochar and fresh catalysts used in reforming tests were also performed to assess the thermal stability of these samples. TPD measurements were carried out using a thermogravimetric analyzer coupled with a mass spectrometer (STA 449 F3 and QMS 403 Aëolos Quadro from Netzsch, Germany), by heating the sample up to 750 °C at a heating rate of 5 °C min^{-1} under an Ar atmosphere.

A FEI XL30 SFEG scanning electron microscope coupled with energy-dispersive X-ray spectroscopy (Oxford Instrument EDS SDD XMAX detector) was used to characterize the surface of fresh and spent activated biochars. The secondary electron images were taken with an acceleration voltage of 3 or 5 kV to investigate the topology of the samples surface, while an acceleration tension of 10 kV was applied to carry out the chemical mapping of the materials by EDX analysis. Additionally, X-ray photoelectron spectroscopy (XPS) data of spent and fresh catalysts were recorded using an ESCAPlus OMICROM system equipped with a hemispherical electron energy analyzer, following the procedure detailed elsewhere [35].

Table 2
Results of textural characterization and washing efficiency of chemically activated biochars.

Material	Specific surface area		Pore volumes					Washing yield
	A_{BET}	$S_{2D\text{-}NLDFT}$	$V_{0.97}$	V_t	V_{ultra}	V_{micro}	V_{meso}	Y_{wash}
	$m^2\ g^{-1}$		$cm^3\ g^{-1}$					%
CB_1_0.10	170	712	0.078	0.181	0.143	0.175	0.006 (3.19%) [a]	77.0
CB_1_0.10_W [b]	142	700	0.068	0.180	0.135	0.169	0.011 (6.14%) [a]	77.1
CB_1_1.00	180	761	0.081	0.195	0.149	0.188	0.007 (3.82%) [a]	76.4
CB_1_1.00_W [b]	100	700	0.049	0.168	0.144	0.160	0.008 (5.01%) [a]	78.1
CB_3_0.10	413	933	0.181	0.259	0.197	0.246	0.013 (4.96%) [a]	54.3
CB_3_0.10_W [b]	368	893	0.158	0.242	0.193	0.229	0.013 (5.35%) [a]	56.0
CB_3_1.00	337	834	0.148	0.230	0.169	0.218	0.012 (5.23%) [a]	56.9
CB_3_1.00_W [b]	316	851	0.138	0.229	0.180	0.217	0.012 (5.40%) [a]	60.6
CB_2_0.55	316	900	0.137	0.238	0.180	0.228	0.009 (3.92%) [a]	58.1
CB_2_0.55	310	872	0.136	0.233	0.177	0.222	0.011 (4.63%) [a]	54.4
CB_2_0.55	307	864	0.137	0.233	0.171	0.221	0.011 (4.86%) [a]	55.5

[a] Calculated as $\frac{Vmeso}{Vt} 100$.
[b] Carbons just washed with water that were not included in the design of experiments.

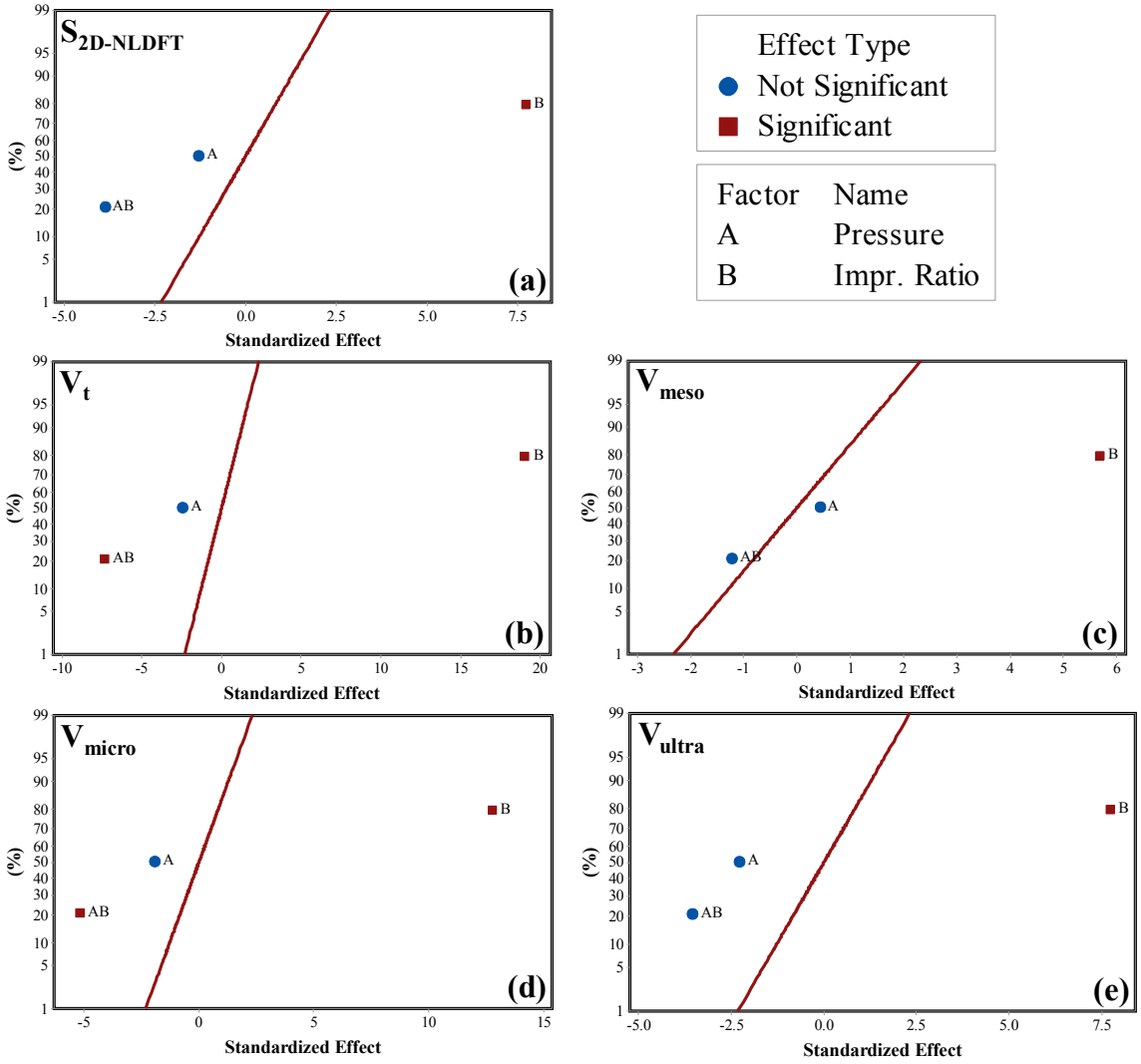

Fig. 1. Normal plots of standardized effects (α = 0.05) for chemically activated biochars: specific surface area (a); total pore volume (b); mesopore volume (c); micropore volume (d); ultra-micropore volume (e).

3. Results and discussion

The results of the textural characterization as well as the proximate and ultimate analyses of the pristine biochar are summarized in Table A.1. The reported values of A_{BET} and $S_{2D\text{-}NLDFT}$ confirm that the porosity of the pristine biochar, as previously stated, was characterized by a very high fraction of ultra-micropores.

3.1. Chemical activation

Although the use of K_2CO_3 as catalyst in coal gasification processes has been widely reported in the literature [10–12,33], the mechanism explaining its interaction with the carbon matrix still remains unclear. The main reactions that probably occur during chemical activation of a carbonaceous material are the following:

$$K_2CO_3 \rightleftarrows K_2O + CO_2 \quad (7)$$

$$CO_2 + C \rightleftarrows 2CO \quad (8)$$

$$K_2CO_3 + 2C \rightleftarrows 2K + 3CO \quad (9)$$

$$K_2O + C \rightleftarrows 2K + CO \quad (10)$$

The increase in specific surface area could be ascribed to the CO_2 released from carbonate decomposition (Reaction (7)), which can diffuse into the solid structure and subsequently react with carbon, thereby stimulating the production of CO by the reverse Boudouard reaction (Reaction (8)) and creating vacancies in the solid structure [36]. Despite the fact that the decomposition of K_2CO_3 mainly occurs at temperatures above 900 °C, its contact with the carbon matrix can promote its decomposition a relatively low temperatures [37,38]. The potassium oxide resulting from the decomposition of the carbonate, or the carbonate itself, can also react with the carbon-based material through Reaction (9) and (10) towards CO and metallic potassium [39].

The assessed textural properties of chemically activated biochars are listed in Table 2. Fig. 1 shows the normalized plots of the standardized effects for the response variables considered: $S_{2D\text{-}NLDFT}$, V_t, V_{ultra}, V_{micro}, and V_{meso}. The PSDs obtained for biochars activated with different impregnation ratios and the N_2 adsorption isotherms of such samples are shown in Figs. A.3a and A.4, respectively. More detailed statistical outcomes for the results reported in the present section can be found in Table A.2.

Regarding the results obtained in terms of specific surface area ($S_{2D\text{-}NLDFT}$), Fig. 1a clearly shows that a higher concentration of activation agent led to a significant increase in the porosity of the resulting activated biochars. In contrast, the absolute pressure proved to be irrelevant

Table 3
Degrees of burnout activation times and textural properties for physically activated biochars.

Material	Activation time	Burnout	Specific surface area		Pore volumes				
	t_{act}	η	A_{BET}	$S_{2D\text{-}NLDFT}$	$V_{0.97}$	V_t	V_{ultra}	V_{micro}	V_{meso}
	min	%	$m^2\ g^{-1}$		$cm^3\ g^{-1}$				
PB_700_0.10	180	30.1	552	833	0.237	0.243	0.184	0.227	0.016 (6.77%) [c]
PB_700_1.00	180	52.8	743	1008	0.333	0.333	0.226	0.301	0.032 (9.55%) [c]
PB_850_0.10	60	54.9	600	818	0.263	0.266	0.169	0.240	0.026 (9.64%) [c]
PB_850_1.00	30	56. 7	688	881	0.298	0.296	0.176	0.273	0.022 (7.57%) [c]
PB_775_0.50	60	43.7	719	931	0.314	0.312	0.176	0.285	0.027 (8.62%) [c]
PB_775_0.50	60	42.2	707	936	0.309	0.306	0.171	0.282	0.025 (8.02%) [c]
PB_775_0.50	60	42.4	707	949	0.308	0.306	0.174	0.282	0.023 (7.64%) [c]
PB_650_0.10 [d]	60	12.5	68.8	482	0.029	0.126	0.100	0.124	0.001 (1.07%) [c]
PB_650_1.00 [d]	180	25.0	447	750	0.191	0.214	0.154	0.200	0.014 (6.46%) [c]

[c] Calculated as $\frac{Vmeso}{Vt}100$.
[d] Additional carbons that were not included in the design of experiments.

for the values of final specific surface area. Our results regarding the development of porosity when higher impregnation ratios were used confirm the relevance of K_2CO_3 as a chemical reagent for the production of tailored activated carbons. All pore volumes analyzed in the present study were also found to be strongly dependent on the amount of activating agent (see Fig. 1). The chemical activation process was able to slightly broaden the original pore size distribution of the pristine biochar, leading to a more hierarchical porous structure with a large contribution of ultra-micropores and a slightly increased amount of mesopores. Almost all the carried out N_2 isotherms required more than 70 h to be completed, thus confirming the predominant narrow microporous structure of chemically activated biochars (see Fig. A.3a), which

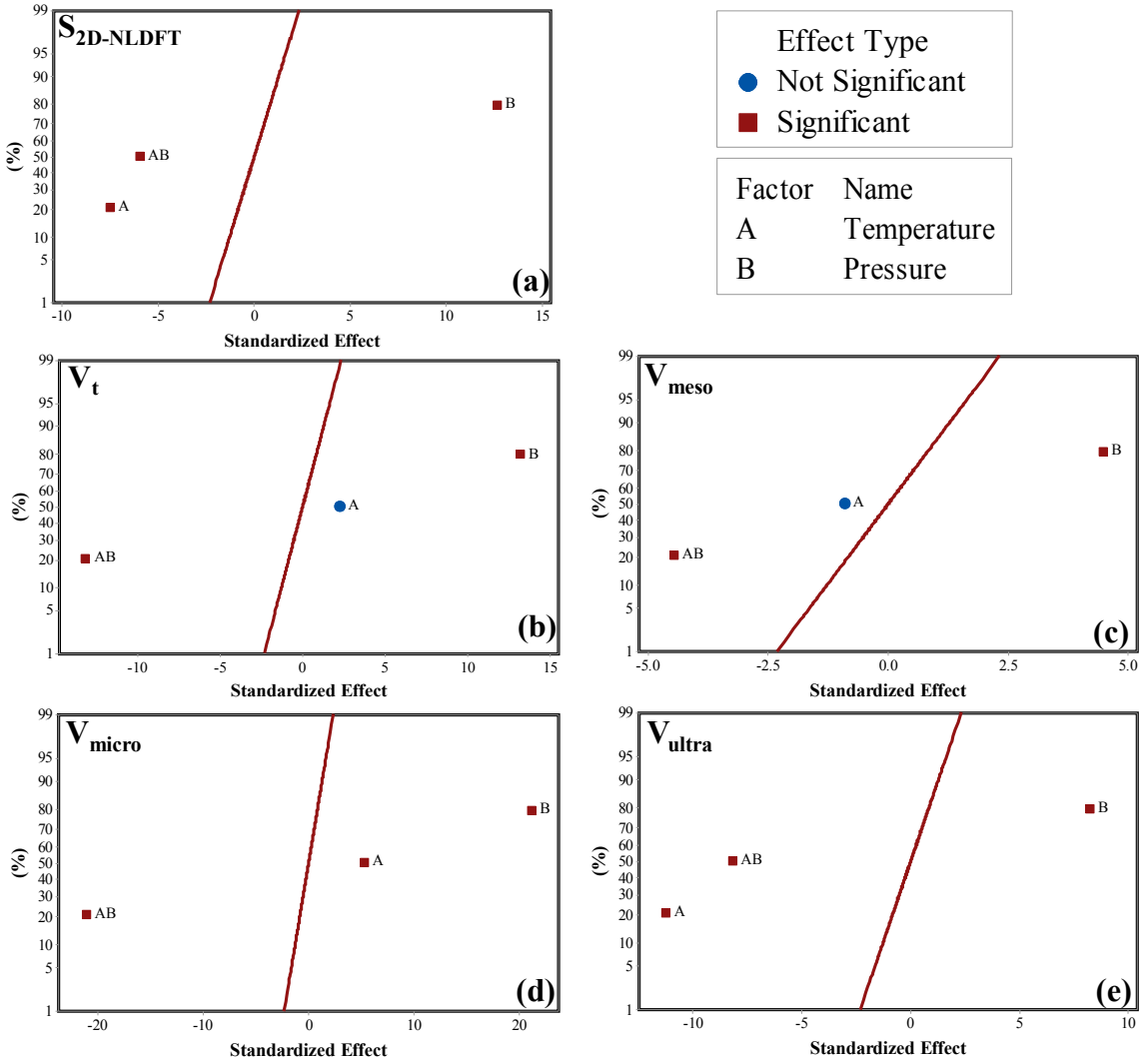

Fig. 2. Normal plots of standardized effects (α = 0.05) for physically activated biochars: specific surface area (a); total pore volume (b); mesopore volume (c); micropore volume (d); ultra-micropore volume (e).

hindered the diffusion of N_2 within the porosity. For both total and micropore volumes, a statistically significant combined effect of pressure and impregnation ratio (AB) was found. However, these effects were comparatively much weaker than that observed for the main effect of the impregnation ratio (B). From a thermodynamics point of view, an increased pressure shifts the equilibrium of the activation reactions to the left. The fact that the textural properties of the resulting activated carbons were practically independent of pressure could indicate that the chemical activation process was mainly kinetically controlled.

It should be pointed out that the overall curvature terms for $S_{2D\text{-}NLDFT}$, V_t and V_{micro} were statistically significant (p-values below 0.05, as reported in Table A.2). This indicates that, in further studies, our adopted factorial design should be expanded to a central composite design to be able to evaluate the pure quadratic regression coefficients and then apply Response Surface Methodology (RSM) for optimization purposes.

As shown in Table 2, after the carbons were washed only with hot water, there was a slight decrease in both the specific surface area and the micropore volume, compared to those measured for carbons washed with the acidic solution. This can be explained by the fact that water could not completely remove the remaining carbonate (and other chemical species) from the solid surface, thus causing blockage of some micropores. By focusing on the difference between the washing procedures of activated carbons at the same loadings of K_2CO_3, the results reported in Table 2 indicate that a higher activation pressure led to an increased amount of product not soluble in water, i.e., to higher Y_{wash} values. This finding agrees with results reported by Malekshahian *et al.* [40], who concluded that high gasification pressures can limit the volatilization of potassium.

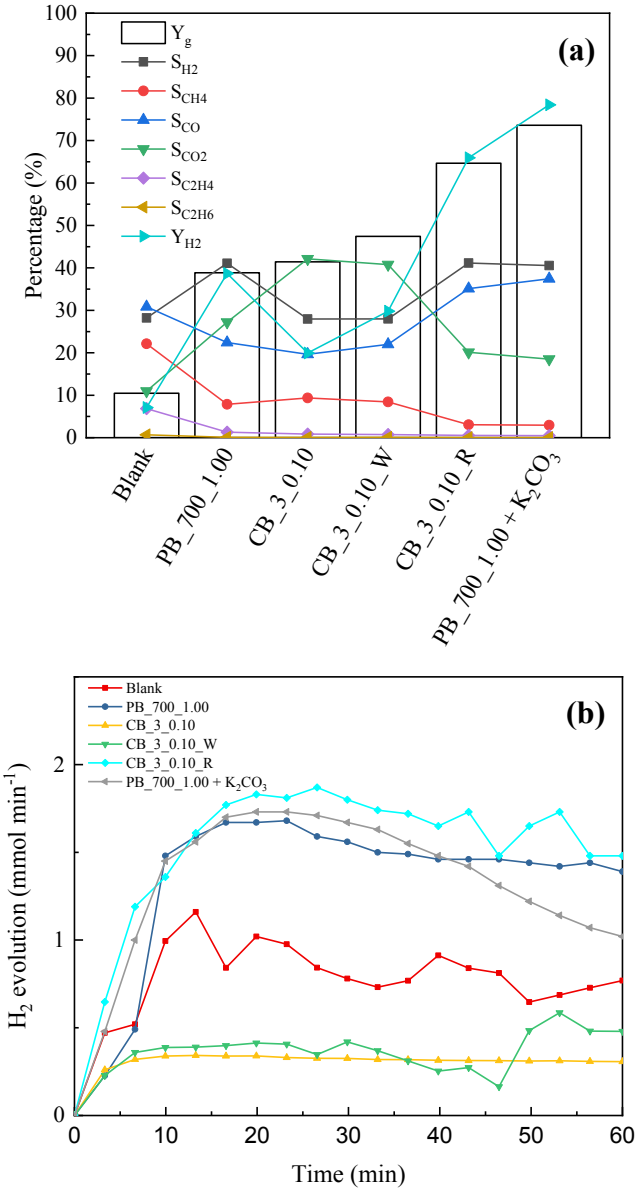

Fig. 3. Results obtained from combined steam and dry reforming of pyrolysis oil at 750 °C: total and H_2 yields (Y_g and Y_{H2}, respectively) as well as selectivities toward a given gaseous product, S_i (a); and evolution of the hydrogen production rate (b).

3.2. Physical activation

It must be pointed out that an increase in absolute pressure also implied an increase in the partial pressure of the reactant (CO_2). In the literature, the effects of absolute pressure and partial pressure of reactant are commonly assessed separately. Nevertheless, and as far as we know, no previous studies have addressed the question of whether activation under pressure can cause textural changes in the resulting physically activated biochars. Activation of biomass-derived carbon had only been studied using supercritical water at high pressure [41], but such conditions are too different from the present ones for allowing some comparison to be done.

Table 3 lists the textural properties of the activated carbons produced, whereas Fig. 2 shows the normal plots of the standardized effects obtained for each response variable. More detailed statistical outcomes are reported in Table A.3. The most relevant PSDs and N_2 adsorption isotherms are shown in Figs. A.3b and A.5, respectively. As previously mentioned in Section 2.2.2, the activation times (also shown in Table 3) were varied to obtain degrees of burnout in the range of 30% to 60%, since the gasification rate was strictly dependent on reaction temperature and reactant partial pressure. As expected, the reaction rate was minimal at the lowest temperature (700 °C). In fact, and whatever the pressure applied, an activation time of 180 min was required to reach the desired reaction extent. For activation temperatures of 775 and 850 °C, an activation time of 60 min was enough, except for the material PB_850_1.00, for which this reaction time led to an almost complete gasification of the sample ($\eta = 85\%$). Hence, the activation time at the highest levels of temperature and pressure was finally set at 30 min to obtain a degree of burnout of 57%.

It was clear that a high pressure accelerated carbon gasification, even at 700 °C. At this temperature, an increase in pressure from 0.1 to 1.0 MPa led to a marked increase in the burnout, from 30.1% to 52.8%, due to the higher reaction rate. In this sense, an increased CO_2 partial pressure resulted in a higher fraction of reactant adsorbed on the surface of the sample [42]. These outcomes are in agreement with the study conducted by Malekshahian *et al.* [42], but disagree with the results reported by Fermoso *et al.* [43], who observed that gasification of heartwood was enhanced using low partial pressures of CO_2.

The specific surface areas reported in Table 3 were in line with expectations, given the present activation conditions. Even at the lowest temperatures (700 °C) it was possible to obtain relatively high surface areas, even greater than those measured for activated biochars produced at higher temperatures. As can be seen in Fig. 2a, the specific surface area was positively influenced by the absolute pressure and negatively affected by the activation temperature. Especially at 1.0 MPa, relatively low temperatures and longer activation times allowed the biochar to be gasified more homogeneously, thus resulting in a more developed porous structure. Conversely, higher temperatures led to faster reaction rates, which can result in a more severe enlargement of micropores and the subsequent loss of surface area.

Fig. 2b shows that the total pore volume increased significantly when the pressure was raised from 0.1 to 1.0 MPa. In general, the total pore volumes for physically activated biochars, which were not significantly

affected by the activation temperature, were higher than those measured for chemically activated carbons. As can be seen when comparing the data reported in Tables 2 and 3, physical activation led to porous carbons with slightly higher ultra-micropore volumes. An inspection of Fig. 2d, e and A.3b reveals that high temperatures can lead to some widening of the narrowest micropores, since the activation temperature had a negative effect on the ultra-micropore volumes and a positive one on the micropore volumes. With regards to the volume of mesopores, which was mainly affected by pressure (see Fig. 2c), it should be noticed that physical activation under pressure resulted in more hierarchical porous structures with higher contributions of mesopores (see values of V_{meso} and relative percentages in Table 3). The statistically significant overall curvature terms reported in Table A.3 for $S_{2D\text{-}NLDFT}$, V_t, V_{meso}, and V_{micro} response variables also suggest that a central composite design could be required for optimization purposes.

Given the significant effects of pressure on the textural properties of carbons activated at 700–850 °C, we decided to perform two additional physical activations at 650 °C, leading to the materials called PB_650_0.10 and PB_650_1.00. The results obtained, which are also reported in Table 3, seem to confirm that activation with CO_2 under pressure is a very interesting way to produce biomass-derived porous carbons with high specific surface area and wide pore size distributions (including relatively high mesopore volumes), even at relatively low temperatures.

3.3. Catalytic activity

Due to their relatively high specific surface area, both PB_700_1.00 and CB_3_0.10 activated biochars (one for each activation procedure) were selected as catalysts and tested during the upgrading process of the aqueous phase of a real pyrolysis oil.

Elemental and moisture analyses of the aqueous phase of the pyrolysis oil revealed that the liquid sample had an average chemical formula of $C_5\ H_{6.7}\ O_2$ and a water content of 80 wt%. Since the liquid was fed to the reformer without providing additional water, the steam to carbon molar ratio, S:C, was 4:1.

It is generally assumed that deactivation and/or instability of the catalyst can be attributed to two different phenomena: (1) the deposition of carbonaceous material (coke) on the surface of the catalyst, which clogs part of the available active sites; and (2) the extent of gasification reactions (both with steam and CO_2) of the carbon-based catalyst, which leads to a loss of mass and a subsequent increase in LHSV (i.e., less contact time).

The results obtained in terms of total gas yield, selectivity towards specific gaseous species, hydrogen yield and hydrogen release over time are displayed in Fig. 3a. It should be noted that the poor results measured for the blank test (i.e., empty reactor) suggested that the reactor wall did not play a crucial catalytic role. The physically activated biochar (PB_700_1.00) exhibited performances comparable to those obtained in a previous study [33]. Using this material, which showed a good stability during the whole experiment (see Fig. 3b), a total gas yield of about 40% was obtained. Nevertheless, its relatively low hydrogen yield indicates that the extent of steam reforming was modest.

Regarding the performance of the chemically activated biochar (CB_3_0.10), a similar total gas yield was measured, compared to the physically activated one. However, selectivity to gaseous products were markedly different, leading to a decrease in the production of H_2 (the hydrogen yield was even lower than that of PB_700_1.00) and an increase in that of CO_2. This result could suggest that the decomposition of pyrolysis oil instead of steam and/or dry reforming, was the main process involved.

As can be deduced from Fig. 3a, similar results were also obtained for the chemically activated biochar that was washed with just water (CB_3_0.10_W). The differences in the performance between the physically and chemically activated biochars could be related to their textural properties. In this respect, the physically activated biochar exhibited a higher specific surface area and higher volumes of micro- and mesopores, thus providing more catalytic active sites of inherent alkali or alkaline earth metal species (AAEMs). The catalytic role of these species (especially K, Mg and Ca) in both steam reforming and gasification of carbon has been widely reported [25,44–46]. Furthermore, the more hierarchical pore size distribution of PB_700_1.00, with relatively high contributions of the mesopores, could shorten the diffusion path to reach the active sites.

Fig. 3b clearly shows that H_2 release rates fluctuated over time for most of biochars tested. There are at least two possible explanations for this: First, the coke deposits, which gradually covered the catalyst surface, could have ted to large fluctuations in the extent of the reactions involved. Second, the structural modification of the activated carbons (the process temperature was higher than the activation temperature) could also led to unsteady hydrogen flow rates at the outlet. It should be noted that the reaction system studied was certainly complex, due the numerous competitive reactions that can affect the yields of the different gaseous products. Nevertheless, it can be assumed that methane is mainly produced by the cracking of the heaviest fraction of the pyrolysis oil, and that its yield will be correlated to the amount of coke produced [47]. Similarly, Fig. 3a reveals that the selectivity towards methane was almost constant for PB_700_1.00, CB_3_0.10, and CB_3_0.10_W materials. Therefore, it can be concluded that the coke production in the process was quite similar for the above-mentioned carbons, suggesting that some structural modifications in the carbons could be accounted for the unsteady production of hydrogen. These modifications could be ascribed to the reverse Boudouard reaction [48,49], steam gasification and, in the case of the chemical activated biochars, potassium-catalyzed gasification. To support this argument, Fig. 4 shows the textural properties of fresh and spent activated biochars. Contrary to the loss of porosity observed for spent PB_700_1.00 and CB_3_0.10 catalysts, the spent CB_3_0.1_W material showed an increase in pore volumes, especially for micropores. In addition, the results from TPD measurements, which are summarized graphically in Figs. 5 and A.6, indicate that the water-washed chemically activated carbon exhibited a larger mass loss (with an increased release of CO_2 and CO, as shown in Fig. A.6) than that of the acid-washed carbon, thus confirming a greater extent of carbon gasification. This fact could be attributed to the residual amount of activation reagent available on the surface of the catalyst CB_3_0.10_W, which might promote further biochar gasification during the experiment, as recently reported by Wang *et al.* [11].

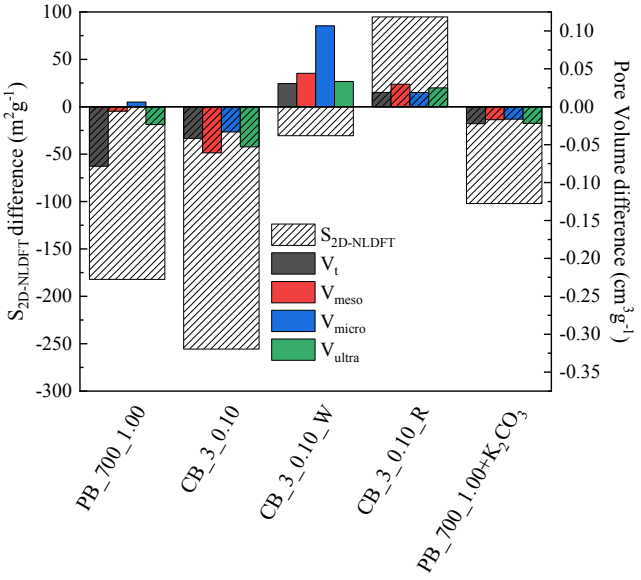

Fig. 4. Differences in textural properties between the fresh and spent activated biochars used as catalysts in steam and dry reforming tests.

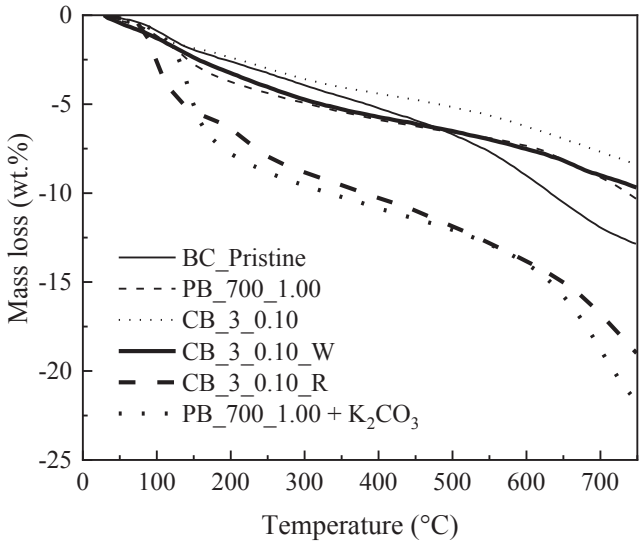

Fig. 5. Results from TPD characterization (percentage of mass loss vs. temperature) for pristine and activated biochars.

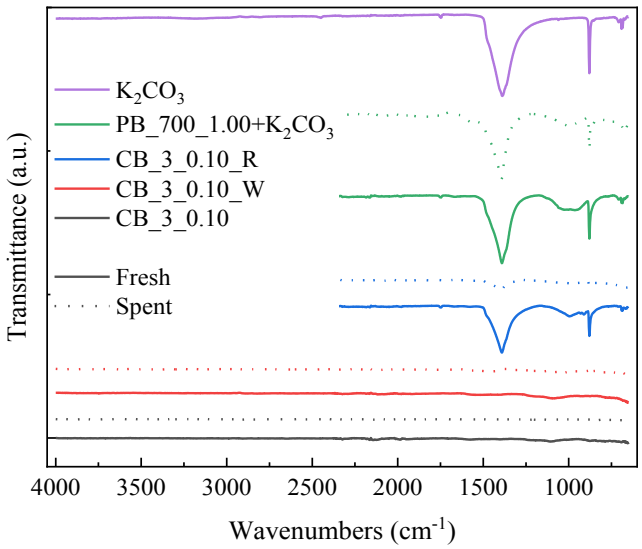

Fig. 6. Comparison of the FTIR spectra obtained for pure K_2CO_3 and some activated biochars tested in the present study.

To understand better the effect of the washing procedure on the performance of chemically activated biochars, an unwashed (raw) material (CB_3_0.10_R) was also tested as catalyst. In this case, the total gas yield was 65% with enhanced selectivity towards both H_2 and CO (see Fig. 3a), thus indicating a higher extent of the steam reforming reactions (leading to a Y_{H2} of 66%). Fig. 6 displays the FTIR spectra obtained for fresh and spent chemically activated biochars as well as for pure K_2CO_3. In the case of acid and water-washed samples, no evident K_2CO_3 content was detected on the surface, indicating the effectiveness of both washing procedures. On the other hand, most of the chemical activating agent available on the surface of the fresh CB_3_0.10_R catalyst disappeared after the catalytic test. The potassium carbonate (and other chemical species derived from its partial decomposition) available on the surface of the catalyst at the beginning of the reforming test (reductive environment) could progressively be reduced to metallic potassium (K^0), leading to a further promotion of reforming reactions. Furthermore, a process temperature relatively close to the volatilization point of potassium can enhance the mobility and reactivity of the metal [50]. Generally speaking, activated biochars have relatively abundant oxygen and nitrogen-containing functional groups, which are not present in the materials shown in Fig. 6. The reason behind this could be the relatively high activation temperatures, since the majority of functional groups decompose below 800 °C [51]. Furthermore, the relatively high amount of K_2CO_3 loaded on the analyzed samples resulted in a very large peak, which may hide other peaks of interest, such as those related to oxygenated functionalities.

The results from TPD measurements (see Fig. 5) showed that the mass loss under an inert atmosphere was much higher for the unwashed catalyst. In addition, the release of CO during TPD also increased for the material CB_3_0.10_R (see Fig. A.6c). The increase in both mass loss and CO production when heating in N_2 up to 750 °C could be due to the reaction of K_2CO_3 with carbon, which results in an additional release of CO, especially at temperatures near 700 °C and above, and the formation of catalytically active COK and CK complexes [52]. Hence, a certain gasification of carbon during the catalytic upgrading tests should be expected. In line with this, Fig. 4 shows that the spent CB_3_0.10_R exhibited more developed textural properties than the fresh one (for instance, the specific surface area increased from 29 $m^2\ g^{-1}$ to 124 $m^2\ g^{-1}$), thus confirming the extent of gasification reactions. Despite the loss of catalyst through carbon gasification, which results in a higher LHSV, the production rate of H_2 for this catalyst was relatively stable during the experiment. This could be explained by the fact that the carbon gasification catalyzed by K_2CO_3 contributes to creating new pores and then counterbalancing the deposition of coke, which induces micropore blockage and active sites coverage.

Based on the findings discussed above, it seems reasonable to assume

Table 4
Surface composition measured by XPS and peak contributions of C1s, O1s and K2p.

Sample	Surface concentration (at. %)			Binding energies (eV) and relative peak areas (%)[e]								
				C1s region					O1s region			K2p3/2 region
	C	O	K	CI	CII	CIII	CIV	Carbide	OI	OII	OIII	K-O
PB_700_1.00 (Fresh)	87.3	11.3	1.4	284.4 (68.5)	285.7 (23.8)	287.6 (6.3)	289.2 (1.3)		531.1 (30.7)	532.8 (55.4)	534.5 (13.9)	293.3 (100)
PB_700_1.00 (Spent)	82.8	15.1	2.1	284.5 (62.7)	285.5 (31.3)	287.6 (4.1)	289.4 (1.9)		531.3 (20.0)	532.9 (60.2)	534.5 (19.8)	293.7 (100)
PB_700_1.00 + K_2CO_3 (Fresh)	72.6	21.6	5.8	284.6 (47.3)	285.8 (40.6)	287.6 (11.0)	289.3 (1.1)		531.3 (12.0)	532.7 (50.5)	534.5 (37.5)	293.7 (100)
PB_700_1.00 + K_2CO_3 (Spent)	42.0	27.8	30.2	284.5 (64.2)			288.7 (22.5)	283.1 (22.5)	531.1 (57.9)			292.8 (100)

O1s binding energies in carbon materials: **OI**, C═O quinone type groups (around 531 eV); **OII**, C–OH phenol groups and/or C–O–C ether groups (532.5 eV), **OIII**, chemisorbed oxygen (COOH carboxylic groups) and/or water (535 eV).

[e] C1s binding energies in carbon materials: **CI**, hydrocarbons, aromatics, aliphatics (284.5 eV); **CII**, single bond C–O associated to alcohols, phenols, carboxyls (286 eV); **CIII**, double bond C═O in carbonyl, quinone (287.5 eV); **CIV**, carboxyl and carbonate groups (288.7 eV).

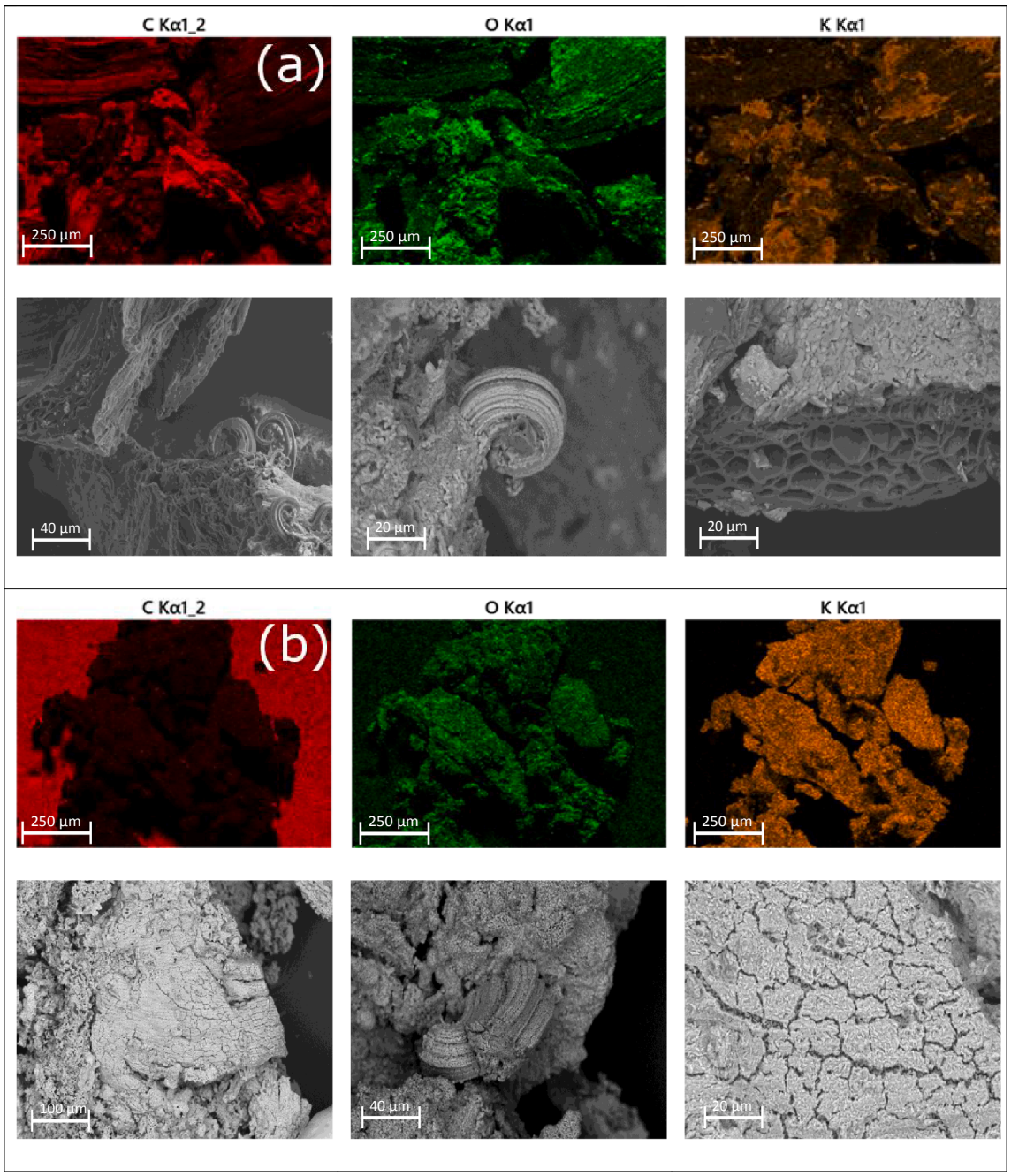

Fig. 7. SEM-EDX images of fresh (a) and spent (b) PB_700_1.00 + K_2CO_3 catalyst.

that an activated biochar having a wider hierarchical pore size distribution and some availability of K_2CO_3 on its surface appears as an excellent candidate for catalytic pyrolysis vapors upgrading. With this in mind, a new biochar-derived material, designated as PB_700_1.00 + K_2CO_3, was prepared by impregnating the material PB_700_1.00 with K_2CO_3 at a mass ratio of carbonate to precursor of 3:1. It should be expected that the better textural properties of the starting physically activated biochar could lead to a more homogeneous dispersion of the active phase on the carbon support, thus resulting in an improved performance of the catalyst.

The results obtained for the catalyst PB_700_1.00 + K_2CO_3 confirmed our expectation. The total gas yield reached a maximum value of 74%, whereas the hydrogen yield was the highest reported in the present study (78%). From the FTIR spectra given in Fig. 6, it can be seen that a fraction of K_2CO_3 was still present on the catalyst surface after running the test.

XPS analyses were carried out for both PB_700_1.00 and PB_700_1.00 + K_2CO_3 materials to get additional insight into the role of K_2CO_3 during the pyrolysis vapors upgrading process. From the summarized XPS results given in Table 4, it can be observed that the atomic composition of PB_700_1.00 remained relatively constant after the catalytic test, even though the simultaneous increase of the peaks related to CII and OII seemed to indicate the formation of phenolic groups on the catalysts. The comparison of the atomic compositions between the fresh and spent PB_700_1.00 + K_2CO_3 materials indicates that the extent of carbon gasification reactions was much higher than that of the PB_700_1.00 material. Furthermore, from the spectra displayed in Fig. A.7, an additional peak at 283 eV, which is attributed to KC_x carbides, was observed for the spent PB_700_1.00 + K_2CO_3. On the other hand, the K2p3/2 region presented only a contribution and suggested the presence of potassium on the surface as K_2O or K_2O_2, according to Li

et al.[53]. This fact was also confirmed by the shift to lower binding energies of the OII and OIII peaks (see Fig. A.7). The marked difference in the potassium content between fresh and spent PB_700_1.00 + K_2CO_3 was probably due to the migration of the potassium-based compounds from the internal pores to the external surface, which can lead to the formation of a coating layer composed of K_2O, as confirmed by SEM-EDX images reported in Fig. 7. The presence of potassium oxides on the surface of the catalyst can be ascribed to (*i*) the direct decomposition of the carbonate (Reaction (7)) and/or (*ii*) the formation of metallic potassium. The latter can migrate from the inner structure of the catalyst to its surface during the course of the pyrolysis vapors upgrading tests and finally be oxidized when the catalyst has been removed from the reactor. This fact can also justify the significant decrease in the specific surface area reported in Fig. 4 for the spent PB_700_1.00 + K_2CO_3 catalyst (from 130 to 27.7 $m^2\ g^{-1}$).

From the SEM-EDX analyses, it can also be deduced that a relatively homogeneous dispersion of K_2CO_3 was achieved for the fresh catalyst. Nevertheless, both fresh and spent catalysts exhibited some clusters and snail shell-like agglomerates, which could be attributed to the relatively high load of carbonate. However, no visible surface carbon layers was found on the superficial K_2O of the spent catalyst, thus suggesting that the extent of the carbon gasification was probably sufficient to prevent the deposition of coke on the surface.

4. Conclusions

From the results obtained in this study, the following conclusions can be drawn:

1. The chemical activation of the pristine biochar led to carbonaceous solids with a relatively high specific surface area and well-developed microporous structure. The most important activation parameter was found to be the amount of activation agent, which accounted for the development of the porous structure. Activation pressure, on the other hand, was not significant for the outcomes of the procedure. Regarding the washing efficiency, acid washing resulted to be effective in cleaning the surface of the samples, whereas washing with water was not sufficient to remove completely the residual reactants, partially clogging the porosity of the samples.
2. Physical activation was found to be more sensitive to the process parameters. It was possible to obtain acceptable values of specific surface area even at low temperature (650 °C) by increasing the activation pressure to 1.00 MPa. A negative effect of the activation temperature on the results was also observed. In fact, the surface area decreased with the increase in the activation temperature, probably due to the widening of the smaller pores by a too rapid (and thus less controlled) gasification.
3. The most promising material produced by physical or chemical activation (PB_700_1.00 and CB_3_0.10) were tested as catalysts in the upgrading of the aqueous fraction of a real pyrolysis oil. Both activated biochars, which were initially characterized by a well-developed porosity, did not exhibit good performance, showing a huge decrease in the specific surface area, probably due to coke deposition. Nevertheless, the addition of K_2CO_3 to the best physically activated biochar boosted the overall performance towards the production of more hydrogen, as a consequence of the enhanced reforming of pyrolysis oil. This finding can be related to the availability of K^0, which was formed from the decomposition of the K_2CO_3 previously deposited on the activated biochar.

CRediT authorship contribution statement

Christian Di Stasi: Conceptualization, Methodology, Validation, Formal analysis, Investigation, Data curation, Writing - original draft. **Gianluca Greco:** Data curation, Methodology, Investigation, Resources. **Rafael L.S. Canevesi:** Data curation, Investigation. **M. Teresa Izquierdo:** Data curation, Investigation. **Vanessa Fierro:** Data curation, Investigation, Writing - review & editing. **Alain Celzard:** Data curation, Investigation, Writing - review & editing. **Belén González:** Resources, Writing - review & editing, Project administration. **Joan J. Manyà:** Resources, Writing - review & editing, Visualization, Supervision, Project administration, Funding acquisition.

Declaration of Competing Interest

The authors declare that they have no known competing financial interests or personal relationships that could have appeared to influence the work reported in this paper.

Acknowledgments

This project received funding from the European Union's Horizon 2020 research and innovation programme under the Marie Skłodowska-Curie grant agreement No 721991. The authors also acknowledge the funding from the Aragón Government (Ref. T22_20R), co-funded by FEDER 2014-2020 "Construyendo Europa desde Aragón". This study was partly supported by the French PIA project "Lorraine Université d'Excellence", reference ANR-15-IDEX-04-LUE, PROMOTEE project and TALiSMAN project, funded by FEDER (2019-000214). The authors gratefully thank José Antonio Manso (UNIZAR) and Philippe Gadonneix (IJL) for their help in the preparation and characterization of the samples and Sandrine Mathieu (IJL) for the SEM characterization.

Appendix A. Supplementary data

Supplementary data to this article can be found online at https://doi.org/10.1016/j.fuel.2020.119759.

References

[1] Guedidi H, Lakehal I, Reinert L, Lévêque J-M, Bellakhal N, Duclaux L. Removal of ionic liquids and ibuprofen by adsorption on a microporous activated carbon: kinetics, isotherms, and pore sites. Arab J Chem 2020;13(1):258–70. https://doi.org/10.1016/j.arabjc.2017.04.006.
[2] Santoyo-Cisneros R, Rangel-Mendez JR, Nava JL, Larios-Durán ER, Chazaro-Ruiz LF. Influence of surface chemistry of activated carbon electrodes on electro-assisted adsorption of arsenate. J Hazard Mater 2020;392:122349. https://doi.org/10.1016/j.jhazmat.2020.122349.
[3] Acharya SP, Johnson J, Weidhaas J. Adsorption kinetics of the herbicide safeners, benoxacor and furilazole, to activated carbon and agricultural soils. J Environ Sci 2020;89:23–34. https://doi.org/10.1016/j.jes.2019.09.022.
[4] Palomo J, Rodríguez-Cano MA, Rodríguez-Mirasol J, Cordero T. On the kinetics of methanol dehydration to dimethyl ether on Zr-loaded P-containing mesoporous activated carbon catalyst. Chem Eng J 2019;378:122198. https://doi.org/10.1016/j.cej.2019.122198.
[5] Liu W-J, Jiang H, Yu H-Q. Development of biochar-based functional materials: toward a sustainable platform carbon material. Chem Rev 2015;115(22):12251–85. https://doi.org/10.1021/acs.chemrev.5b00195.
[6] Wang Y, Yang He, Jin L, Li Y, Hu H, Ding H, Bai X. Effect of mineral in coal on preparation of activated carbon for methane decomposition to hydrogen. Fuel 2019;258:116138. https://doi.org/10.1016/j.fuel.2019.116138.
[7] Li H, Zheng F, Wang J, Zhou J, Huang X, Chen L, Hu P, Gao J-M, Zhen Q, Bashir S, Liu JL. Facile preparation of zeolite-activated carbon composite from coal gangue with enhanced adsorption performance. Chem Eng J 2020;390:124513. https://doi.org/10.1016/j.cej.2020.124513.
[8] Ding S, Liu Y. Adsorption of CO2 from flue gas by novel seaweed-based KOH-activated porous biochars. Fuel 2020;260:116382. https://doi.org/10.1016/j.fuel.2019.116382.
[9] Iriarte-Velasco U, Sierra I, Zudaire L, Ayastuy JL. Preparation of a porous biochar from the acid activation of pork bones. Food Bioprod Process 2016;98:341–53. https://doi.org/10.1016/j.fbp.2016.03.003.
[10] Sayğılı H, Akkaya SG. Optimized preparation for bimodal porous carbon from lentil processing waste by microwave-assisted K2 CO3 activation: spectroscopic characterization and dye decolorization activity. J Clean Prod 2019;226:968–76. https://doi.org/10.1016/j.jclepro.2019.04.121.
[11] Wang L, Sun F, Hao F, Qu Z, Gao J, Liu M, Wang K, Zhao G, Qin Y. A green trace K2CO3 induced catalytic activation strategy for developing coal-converted activated carbon as advanced candidate for CO2 adsorption and supercapacitors. Chem Eng J 2020;383:123205. https://doi.org/10.1016/j.cej.2019.123205.
[12] Mai T-T, Vu D-L, Huynh D-C, Wu N-L, Le A-T. Cost-effective porous carbon materials synthesized by carbonizing rice husk and K2CO3 activation and their

application for lithium-sulfur batteries. J Sci: Adv Mater Devices 2019;4(2):223–9. https://doi.org/10.1016/j.jsamd.2019.04.009.
[13] Lahijani P, Zainal ZA, Mohammadi M, Mohamed AR. Conversion of the greenhouse gas CO2 to the fuel gas CO via the Boudouard reaction: a review. Renew Sustain Energy Rev 2015;41:615–32. https://doi.org/10.1016/j.rser.2014.08.034.
[14] Şahin Ö, Saka C. Preparation and characterization of activated carbon from acorn shell by physical activation with H2O–CO2 in two-step pretreatment. Bioresour Technol 2013;136:163–8. https://doi.org/10.1016/j.biortech.2013.02.074.
[15] Guo Y, Tan C, Sun J, Li W, Zhang J, Zhao C. Porous activated carbons derived from waste sugarcane bagasse for CO2 adsorption. Chem Eng J 2020;381:122736. https://doi.org/10.1016/j.cej.2019.122736.
[16] Bertero M, De PG, Sedran U. Fuels from bio-oils: bio-oil production from different residual sources, characterization and thermal conditioning. Fuel 2012;95:263–71. https://doi.org/10.1016/j.fuel.2011.08.041.
[17] Fu M, Qi W, Xu Q, Zhang S, Yan Y. Hydrogen production from bio-oil model compounds dry (CO2) reforming over Ni/Al2O3 catalyst. Int J Hydrogen Energy 2016;41(3):1494–501. https://doi.org/10.1016/j.ijhydene.2015.11.104.
[18] Santamaria L, Artetxe M, Lopez G, Cortazar M, Amutio M, Bilbao J, Olazar M. Effect of CeO2 and MgO promoters on the performance of a Ni/Al2O3 catalyst in the steam reforming of biomass pyrolysis volatiles. Fuel Process Technol 2020;198:106223. https://doi.org/10.1016/j.fuproc.2019.106223.
[19] Santamaria L, Lopez G, Arregi A, Amutio M, Artetxe M, Bilbao J, Olazar M. Stability of different Ni supported catalysts in the in-line steam reforming of biomass fast pyrolysis volatiles. Appl Catal B 2019;242:109–20. https://doi.org/10.1016/j.apcatb.2018.09.081.
[20] Bimbela F, Ábrego J, Puerta R, García L, Arauzo J. Catalytic steam reforming of the aqueous fraction of bio-oil using Ni-Ce/Mg-Al catalysts. Appl Catal B 2017;209:346–57. https://doi.org/10.1016/j.apcatb.2017.03.009.
[21] Phongprueksathat N, Meeyoo V, Rirksomboon T. Steam reforming of acetic acid for hydrogenproduction: catalytic performances of Ni and Co supported on Ce0·75Zr0·25O2 catalysts. Int J Hydrogen Energy 2019;44:9359–67. https://doi.org/10.1016/j.ijhydene.2019.02.085.
[22] Domine ME, Iojoiu EE, Davidian T, Guilhaume N, Mirodatos C. Hydrogen production from biomass-derived oil over monolithic Pt- and Rh-based catalysts using steam reforming and sequential cracking processes. Catal Today 2008;133-135:565–73. https://doi.org/10.1016/j.cattod.2007.12.062.
[23] Li X, Zhang Z, Zhang L, Fan H, Li X, Liu Q, Wang S, Hu X. Investigation of coking behaviors of model compounds in bio-oil during steam reforming. Fuel 2020;265:116961. https://doi.org/10.1016/j.fuel.2019.116961.
[24] Ma Z, Xiao R, Zhang H. Catalytic steam reforming of bio-oil model compounds for hydrogen-rich gas production using bio-char as catalyst. Int J Hydrogen Energy 2017;42(6):3579–85. https://doi.org/10.1016/j.ijhydene.2016.11.107.
[25] Feng D, Zhao Y, Zhang Yu, Sun S, Meng S, Guo Y, Huang Y. Effects of K and Ca on reforming of model tar compounds with pyrolysis biochars under H 2 O or CO 2. Chem Eng J 2016;306:422–32. https://doi.org/10.1016/j.cej.2016.07.065.
[26] Buentello-Montoya D, Zhang X, Li J, Ranade V, Marques S, Geron M. Performance of biochar as a catalyst for tar steam reforming: Effect of the porous structure. Appl Energy 2020;259:114176. https://doi.org/10.1016/j.apenergy.2019.114176.
[27] Feng D, Zhao Y, Zhang Yu, Zhang Z, Sun S. Roles and fates of K and Ca species on biochar structure during in-situ tar H2O reforming over nascent biochar. Int J Hydrogen Energy 2017;42(34):21686–96. https://doi.org/10.1016/j.ijhydene.2017.07.096.
[28] Zhang Z, Ou Z, Qin C, Ran J, Wu C. Roles of alkali/alkaline earth metals in steam reforming of biomass tar for hydrogen production over perovskite supported Ni catalysts. Fuel 2019;257:116032. https://doi.org/10.1016/j.fuel.2019.116032.
[29] Megaritis A, Zhuo Y, Messenböck R, Dugwell DR, Kandiyoti R. Pyrolysis and gasification in a bench-scale high-pressure fluidized-bed reactor. Energy Fuels 1998;12(1):144–51. https://doi.org/10.1021/ef970115x.
[30] Dufour A, Celzard A, Fierro V, Martin E, Broust F, Zoulalian A. Catalytic decomposition of methane over a wood char concurrently activated by a pyrolysis gas. Appl Catal A 2008;346(1-2):164–73. https://doi.org/10.1016/j.apcata.2008.05.023.
[31] Ranguin R, Jean-Marius C, Yacou C, Gaspard S, Feidt C, Rychen G, Delannoy M. Reduction of chlordecone environmental availability by soil amendment of biochars and activated carbons from lignocellulosic biomass. Environ Sci Pollut Res 2020;27(33):41093–104. https://doi.org/10.1007/s11356-019-07366-2.
[32] Greco G, Videgain M, Di Stasi C, González B, Manyà JJ. Evolution of the mass-loss rate during atmospheric and pressurized slow pyrolysis of wheat straw in a bench-scale reactor. J Anal Appl Pyrol 2018;136:18–26. https://doi.org/10.1016/j.jaap.2018.11.007.
[33] Di Stasi C, Alvira D, Greco G, González B, Manyà JJ. Physically activated wheat straw-derived biochar for biomass pyrolysis vapors upgrading with high resistance against coke deactivation. Fuel 2019;255:115807. https://doi.org/10.1016/j.fuel.2019.115807.
[34] Jagiello J, Kenvin J, Celzard A, Fierro V. Enhanced resolution of ultra micropore size determination of biochars and activated carbons by dual gas analysis using N2 and CO2 with 2D-NLDFT adsorption models. Carbon 2019;144:206–15. https://doi.org/10.1016/j.carbon.2018.12.028.
[35] Sanchez-Sanchez A, Izquierdo MT, Medjahdi G, Ghanbaja J, Celzard A, Fierro V. Ordered mesoporous carbons obtained by soft-templating of tannin in mild conditions. Microporous Mesoporous Mater 2018;270:127–39. https://doi.org/10.1016/j.micromeso.2018.05.017.
[36] Matos J, Labady M, Albornoz A, Laine J, Brito JL. Catalytic effect of KOH on textural changes of carbon macro-networks by physical activation. J Mol Catal A: Chem 2005;228(1-2):189–94. https://doi.org/10.1016/j.molcata.2004.09.039.
[37] Lozano-Castelló D, Calo JM, Cazorla-Amorós D, Linares-Solano A. Carbon activation with KOH as explored by temperature programmed techniques, and the effects of hydrogen. Carbon 2007;45(13):2529–36. https://doi.org/10.1016/j.carbon.2007.08.021.
[38] Ganga Devi T, Kannan MP. Calcium catalysis in air gasification of cellulosic chars. Fuel 1998;77(15):1825–30. https://doi.org/10.1016/S0016-2361(98)00038-6.
[39] Dehkhoda AM, Gyenge E, Ellis N. A novel method to tailor the porous structure of KOH-activated biochar and its application in capacitive deionization and energy storage. Biomass Bioenergy 2016;87:107–21. https://doi.org/10.1016/j.biombioe.2016.02.023.
[40] Malekshahian M, Hill JM. Effect of pyrolysis and CO 2 gasification pressure on the surface area and pore size distribution of petroleum coke. Energy Fuels 2011;25(11):5250–6. https://doi.org/10.1021/ef201231w.
[41] Montané D, Fierro V, Marèché J-F, Aranda L, Celzard A. Activation of biomass-derived charcoal with supercritical water. Microporous Mesoporous Mater 2009;119(1-3):53–9. https://doi.org/10.1016/j.micromeso.2008.09.040.
[42] Malekshahian M, Hill JM. Kinetic analysis of CO 2 gasification of petroleum coke at high pressures. Energy Fuels 2011;25(9):4043–8. https://doi.org/10.1021/ef2009259.
[43] Fermoso J, Stevanov C, Moghtaderi B, Arias B, Pevida C, Plaza MG, Rubiera F, Pis JJ. High-pressure gasification reactivity of biomass chars produced at different temperatures. J Anal Appl Pyrol 2009;85(1-2):287–93. https://doi.org/10.1016/j.jaap.2008.09.017.
[44] Yip K, Tian F, Hayashi J-I, Wu H. Effect of alkali and alkaline earth metallic species on biochar reactivity and syngas compositions during steam gasification. Energy Fuels 2010;24(1):173–81. https://doi.org/10.1021/ef900534n.
[45] Sueyasu T, Oike T, Mori A, Kudo S, Norinaga K, Hayashi J-I. Simultaneous steam reforming of tar and steam gasification of char from the pyrolysis of potassium-loaded woody biomass. Energy Fuels 2012;26(1):199–208. https://doi.org/10.1021/ef201166a.
[46] Jiang L, Hu S, Wang Yi, Su S, Sun L, Xu B, He L, Xiang J. Catalytic effects of inherent alkali and alkaline earth metallic species on steam gasification of biomass. Int J Hydrogen Energy 2015;40(45):15460–9. https://doi.org/10.1016/j.ijhydene.2015.08.111.
[47] Matos J, Laine J. Ethylene conversion on activated carbon-supported NiMo catalysts: effect of the support. Appl Catal A 2003;241(1-2):25–38. https://doi.org/10.1016/S0926-860X(02)00427-1.
[48] Díaz K, García V, Matos J. Activated carbon supported Ni–Ca: Influence of reaction parameters on activity and stability of catalyst on methane reformation. Fuel 2007;86(9):1337–44. https://doi.org/10.1016/j.fuel.2006.05.011.
[49] Matos J, Díaz K, García V, Cordero TC, Brito JL. Methane transformation in presence of carbon dioxide on activated carbon supported nickel–calcium catalysts. Catal Lett 2006;109(3-4):163–9. https://doi.org/10.1007/s10562-006-0073-3.
[50] Ducousso M, Weiss-Hortala E, Lyczko N, Nzihou A, Castaldi MJ. 110th Anniversary: syngas production enhancement using calcium- and potassium-impregnated chars. Ind Eng Chem Res 2019;58(33):15134–41. https://doi.org/10.1021/acs.iecr.9b02238.
[51] Figueiredo JL, Pereira MFR. The role of surface chemistry in catalysis with carbons. Catal Today 2010;150(1-2):2–7. https://doi.org/10.1016/j.cattod.2009.04.010.
[52] Kopyscinski J, Rahman M, Gupta R, Mims CA, Hill JM. K2CO3 catalyzed CO2 gasification of ash-free coal. Interactions of the catalyst with carbon in N2 and CO2 atmosphere. Fuel 2014;117:1181–9. https://doi.org/10.1016/j.fuel.2013.07.030.
[53] Li X-R, Liu J, Kong F-Y, Liu X-C, Xu J-J, Chen H-Y. Potassium-doped graphene for simultaneous determination of nitrite and sulfite in polluted water. Electrochem Commun 2012;20:109–12. https://doi.org/10.1016/j.elecom.2012.04.014.

Appendix A: supplementary material

Influence of activation conditions on textural properties and performance of activated biochars for pyrolysis vapors upgrading

Christian Di Stasi[1*], *Gianluca Greco*[1], *Rafael L. S. Canevesi*[2], *M. Teresa Izquierdo*[3], *Vanessa Fierro*[2], *Alain Celzard*[2], *Belén González*[1], *Joan J. Manyà*[1]

[1] Aragón Institute of Engineering Research (I3A), Thermochemical Processes Group, University of Zaragoza, Technological College of Huesca, Crta. Cuarte s/n, 22071 Huesca, Spain

[2] Université de Lorraine, CNRS, IJL, *Épinal*, F-88000, France

[3] Instituto de Carboquímica (ICB-CSIC), Miguel Luesma Castán 4, Zaragoza, E-50018, Spain

[*] Corresponding author at: Aragón Institute of Engineering Research (I3A), Thermochemical Processes Group, University of Zaragoza, Technological College of Huesca, Crta. Cuarte s/n, 22071 Huesca, Spain

E-mail address: christiandistasi@unizar.es.

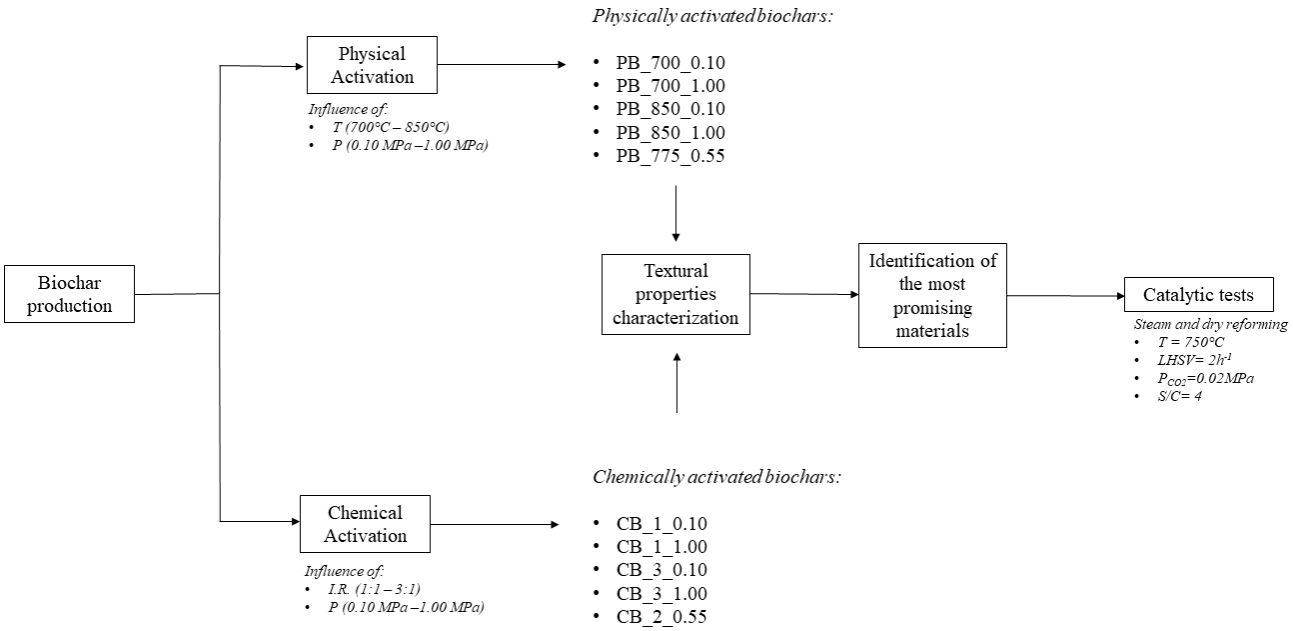

Fig. A.1. Schematic representation of the methodology followed in this study.

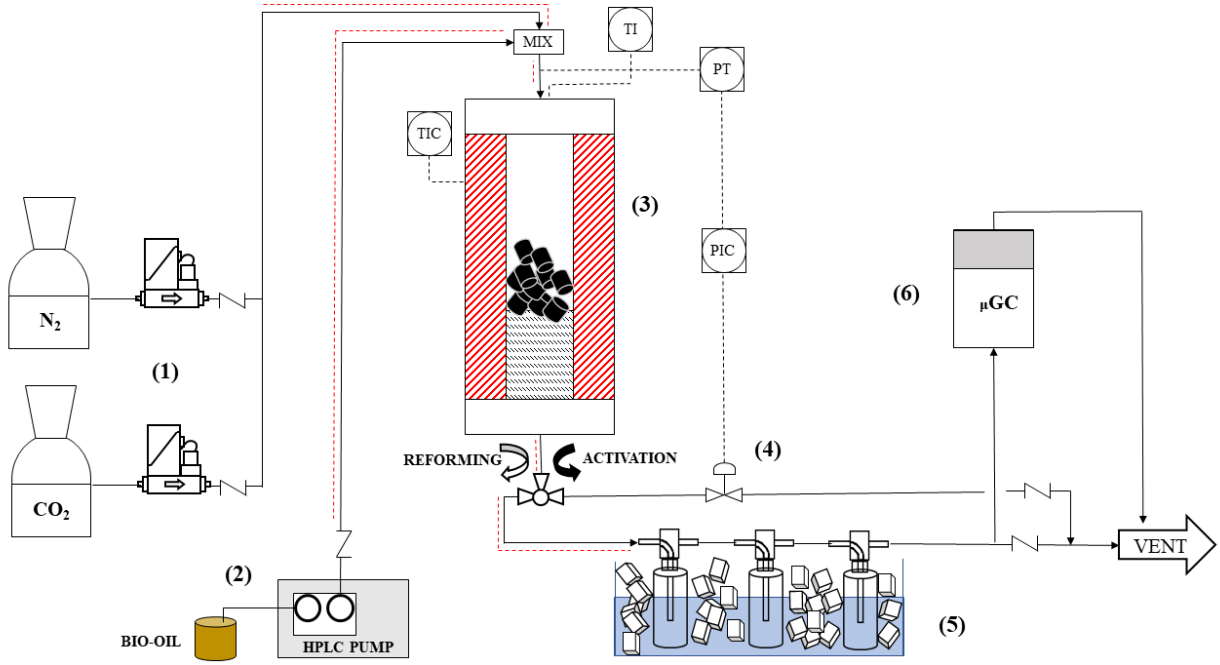

Fig. A.2. Overview of the experimental device used for activation and reforming tests: Feeding system (1); HPLC pump (2); fixed-bed reactor and furnace (3); Servo-controlled valve (4); condensation train (5); and µ-GC analyzer (6).

Table A.1. Results of textural characterization, proximate analysis and elemental analysis of pristine biochar derived from wheat straw

Proximate analysis (wt. %)	
Moisture	2.00 ± 0.08
Volatile matter	10.8 ± 0.63
Ashes	12.7 ± 0.21
Fixed carbon	74.5 ± 0.55
Ultimate (wt. % on a dry ash-free basis)	
C	92.6 ± 0.07
H	4.02 ± 0.05
N	2.01 ± 0.08
O	1.32
Molar H:C ratio	0.52
Textural characterization	
A_{BET} ($m^2\ g^{-1}$)	2.90
$S_{2D\text{-}NLDFT}$ ($m^2\ g^{-1}$)	341
$V_{0.97}$ ($cm^3\ g^{-1}$)	0.0026
V_{tot} ($cm^3\ g^{-1}$)	0.084
V_{ultra} ($cm^3\ g^{-1}$)	0.083
V_{micro} ($cm^3\ g^{-1}$)	0.083
V_{meso} ($cm^3\ g^{-1}$)	0.001 **(1.28 vol. %)**

Table A.2. Regression coefficients and quality-of-fit statistics for the design of experiments on chemical activation. The values in brackets correspond to the *p*-values resulting from the *t*-tests. The significant terms are marked in bold

	Response variable				
	$S_{2D\text{-}NLDFT}$	V_t	V_{meso}	V_{micro}	V_{ultra}
β_0	810.1	0.21605	0.009516	0.2065	0.16447
	(0.000)	(0.000)	(0.003)	(0.000)	(0.000)
β_A (Pressure)	–12.24	–0.00364	0.000215	–0.00385	–0.00553
	(0.326)	(0.132)	(0.715)	(0.190)	(0.150)
β_B (Mass ratio)	**73.32**	**0.02801**	**0.002904**	**0.02511**	**0.01871**
	(0.016)	**(0.003)**	**(0.030)**	**(0.006)**	**(0.016)**
β_{AB}	–36.90	**–0.1089**	–0.000625	–0.01026	–0.00865
	(0.060)	**(0.018)**	(0.346)	(0.035)	(0.070)
R^2_{adj} **(%)**	94.05	98.78	83.90	97.38	93.27
Curvature	**(0.042)**	**(0.015)**	(0.350)	**(0.029)**	(0.090)

Table A.3. Regression coefficients and quality-of-fit statistics for the design of experiments on physical activation. The values in brackets correspond to the *p*-values resulting from the *t*-tests. The significant terms are marked in bold

	Response variable				
	$S_{2D\text{-}NLDFT}$	V_t	V_{meso}	V_{micro}	V_{ultra}
β_0	884.9	0.29181	0.023189	0.268623	0.19055
	(0.000)	(0.000)	(0.001)	(0.000)	(0.000)
β_A (Temperature)	**–35.46**	0.00381	–0.000811	**0.004623**	**–0.01445**
	(0.017)	(0.155)	(0.461)	**(0.034)**	**(0.008)**
β_B (Pressure)	**59.54**	**0.02250**	**0.004000**	**0.018500**	**0.01050**
	(0.006)	**(0.006)**	**(0.047)**	**(0.002)**	**(0.015)**
β_{AB}	**–28.08**	**–0.02250**	**–0.004000**	**–0.018500**	**–0.01050**
	(0.027)	**(0.006)**	**(0.047)**	**(0.002)**	**(0.015)**
R^2_{adj} **(%)**	98.06	98.47	86.47	99.42	98.22
Curvature	**(0.018)**	**(0.025)**	(0.328)	**(0.008)**	**(0.013)**

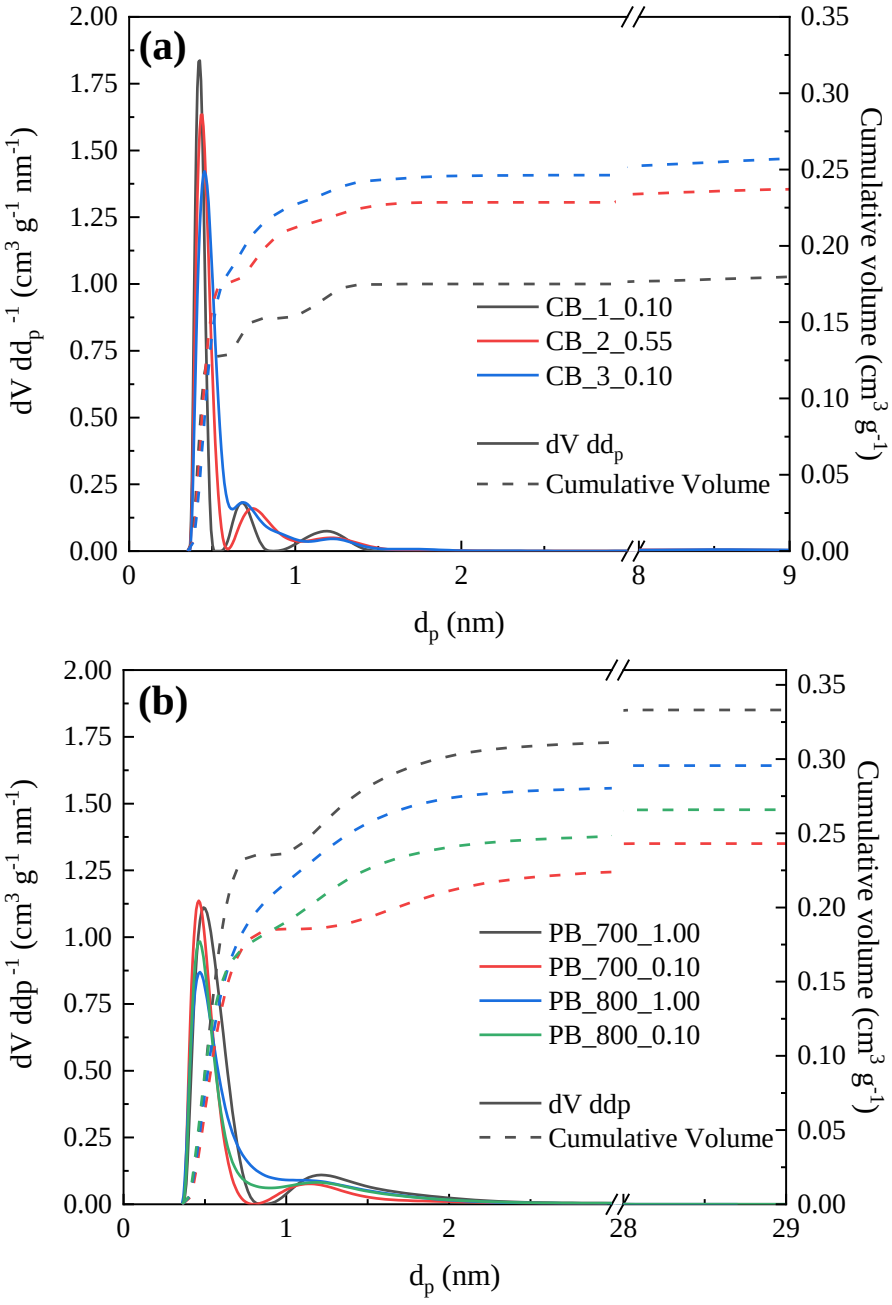

Fig. A.3. PSD and cumulative pore volume of chemical (a) and physical (b) activated biochars.

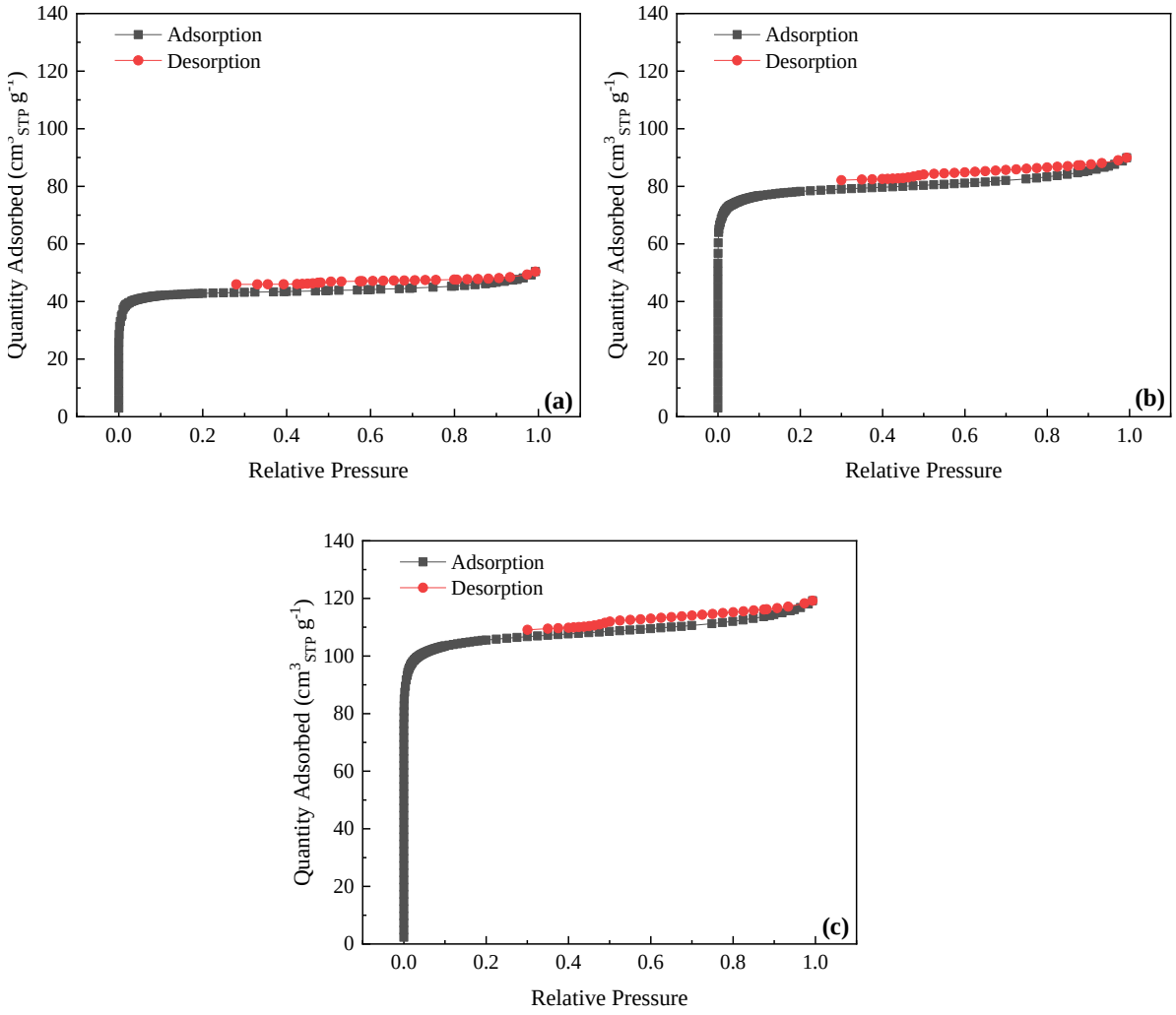

Fig. A.4. N_2 adsorption/desorption isotherms of the following chemically activated biochars: CB_3_0.10 (a); CB_2_0.55 (b); and CB_3_0.10 (c).

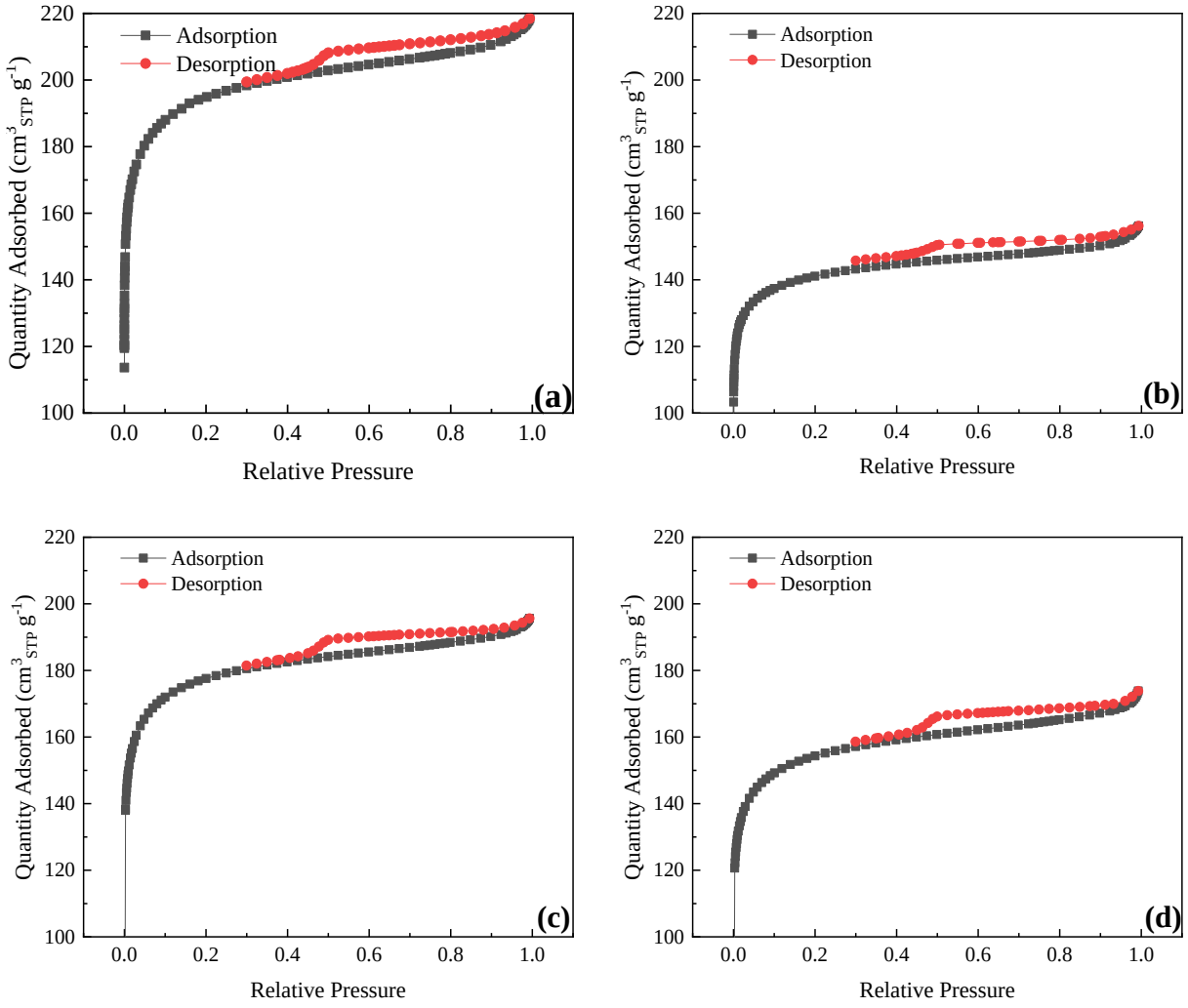

Fig. A.5. N_2 adsorption/desorption isotherms of the following physically activated biochars: PB_700_1.00 (a); PB_700_0.10 (b); PB_850_1.00 (c); and PB_850_0.10 (d).

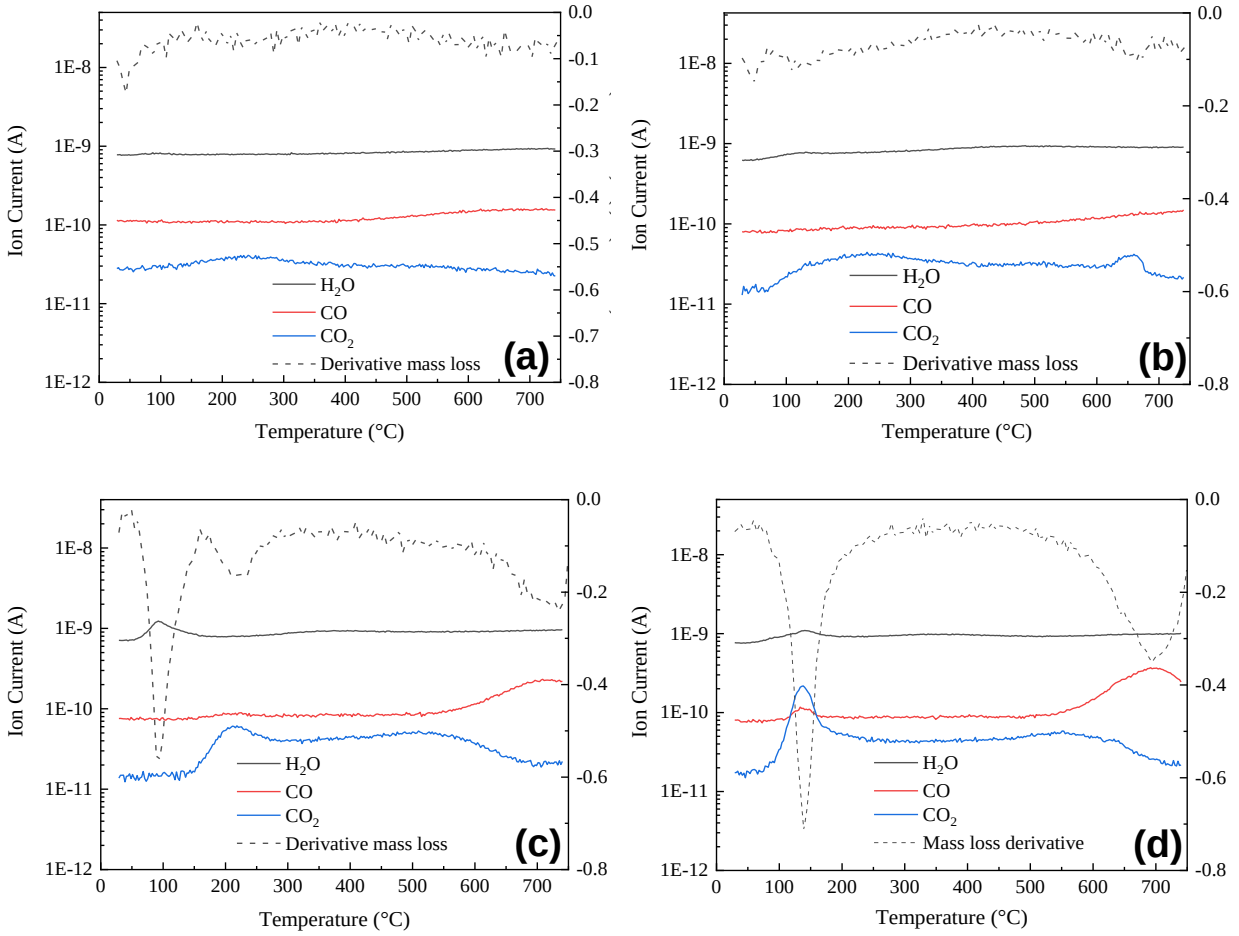

Fig. A.6. Differential thermogravimetric curves (in % of mass min^{-1}) and profiles of released species (H_2O, CO_2, and CO) from the TPD measurements conducted for the following materials: CB_3_0.10 (a); CB_3_0.10_W (b); CB_3_0.10_R (c); and PB_700_1.00+K_2CO_3 (d).

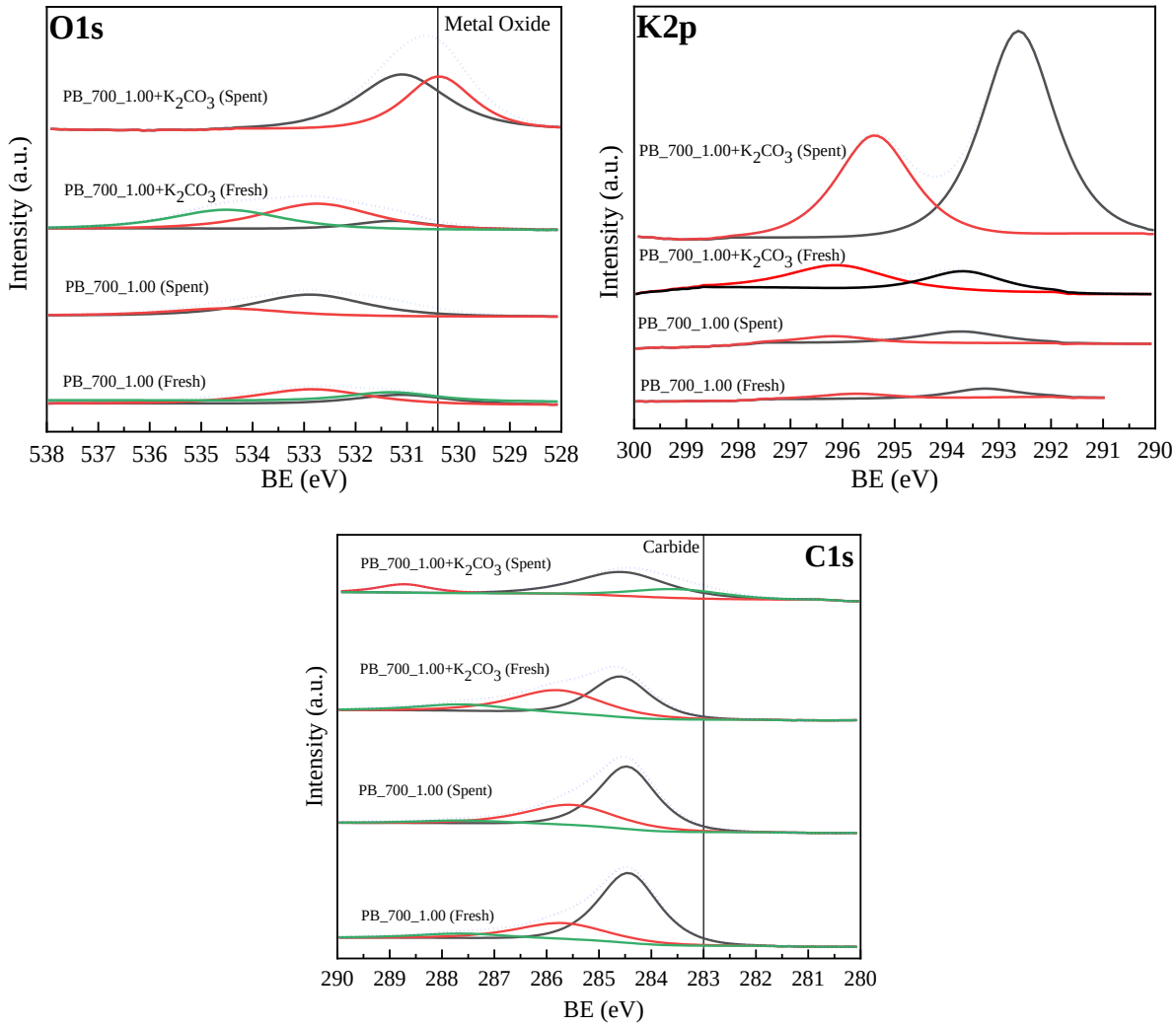

Fig. A.7. C1s, O1s and K2p spectra of fresh and spent PB_700_1.00 and PB_700_1.00+K_2CO_3.

6.3. Activated biochar as support for mono and bimetallic catalysts and their application in reforming of pyrolysis oil

Once the best activation process conditions were identified, the optimized activated biochar (physically activated with CO_2 at 700 °C and 1.0 MPa) was used as support for the preparation of different metallic catalysts (objective III). The produced Me/activated biochar catalysts were then tested in the steam reforming of slow pyrolysis oil with the aim at maximizing the hydrogen yield and catalytic stability.

Preliminary tests on steam reforming of acetic acid at 600 °C showed that using activated biochar-supported catalysts containing 10 wt. % Ni and 7 wt. % Co led to a conversion above 90% with a relatively slow deactivation rate. When a representative organic model compounds mixture was used as feed, relatively fast deactivation of the catalyst was observed, probably due to the adsorption of heavy organic compounds, which could subsequently react to form not easily desorbable reaction intermediates and compromising the catalytic activity. Then, the bimetallic Ni-Co catalysts were also tested for the steam reforming of raw slow pyrolysis oil and, also in this case, the catalyst exhibited low stability, showing fast deactivation after few minutes of run time. This behavior was ascribed to the presence of sugar-like compounds in the pyrolysis oil. These compounds are likely to go thermal decomposition and charring instead of vaporization. Additional tests, which were carried out feeding distilled pyrolysis oil, showed that, at 750 °C, the Ni-Co catalyst was stable during a 14 h test, showing a constant carbon conversion equal to 65% without any sign of deactivation.

Available online at www.sciencedirect.com

ScienceDirect

journal homepage: www.elsevier.com/locate/he

Optimization of the operating conditions for steam reforming of slow pyrolysis oil over an activated biochar-supported Ni–Co catalyst

Christian Di Stasi [a,*], *Marta Cortese* [b], *Gianluca Greco* [a], *Simona Renda* [b], *Belén González* [a], *Vincenzo Palma* [b], *Joan J. Manyà* [a]

[a] *Aragón Institute of Engineering Research (I3A), Thermochemical Processes Group, University of Zaragoza, Escuela Politécnica Superior, Crta. Cuarte s/n, 22071, Huesca, Spain*

[b] *University of Salerno, Department of Industrial Engineering, Via Giovanni Paolo II 132, 84084, Fisciano (SA), Italy*

HIGHLIGHTS

- Activated biochar is a suitable catalyst support for the upgrading of pyrolysis oil.
- Ni–Co catalyst showed the best performance in acetic acid steam reforming.
- Heavy organic compounds could poison the metallic active sites of the catalyst.
- Steam reforming of pyrolysis oil was achieved with a carbon conversion of 65%.
- No catalyst deactivation was observed during the first 850 min.

GRAPHICAL ABSTRACT

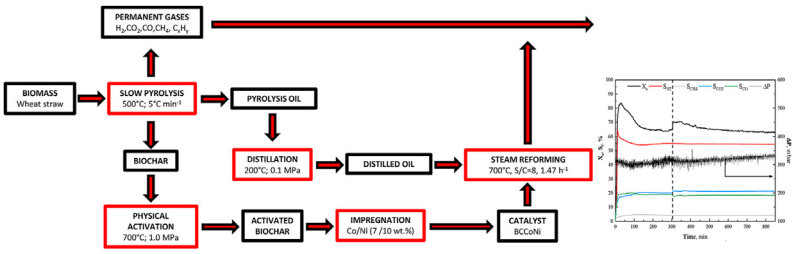

ARTICLE INFO

Article history:
Received 10 March 2021
Received in revised form
20 May 2021
Accepted 26 May 2021
Available online 17 June 2021

Keywords:
Bio-oil
Steam reforming
Pyrolysis

ABSTRACT

Highly performing activated biochar-based catalysts were produced for steam reforming of slow pyrolysis oil. The raw biochar obtained from the slow pyrolysis step was physically activated with CO_2 at 700 °C and 1.0 MPa and then employed as support. Preliminary tests on steam reforming of acetic acid at 600 °C showed that using activated biochar-supported catalysts containing 10 wt % Ni and 7 wt % Co led to a conversion above 90% with a relatively slow deactivation rate. When a representative organic model compounds mixture was used as feed, relatively fast deactivation of the catalyst was observed, probably due to the adsorption of heavy organic compounds, which could subsequently react to form not easily desorbable reaction intermediates. However, the dual Ni–Co catalysts exhibited a good performance during the steam reforming of a real slow pyrolysis oil at 750 °C, showing long stability and a constant carbon conversion of 65%.

* *Corresponding author.*
E-mail address: christiandistasi@unizar.es (C. Di Stasi).

https://doi.org/10.1016/j.ijhydene.2021.05.193

Catalyst
Model compound

Introduction

Pyrolysis oil is a side-product obtained from the pyrolysis or gasification of biomass. Despite its composition strictly depends on biomass nature and pyrolysis conditions, it is usually composed of a high fraction of water (especially for slow pyrolysis processes) and a complex mixture of oxygenated organic compounds (produced from the decomposition of the main biomass constituents) [1–3]. The high contents of water and the heterogeneity of its composition make slow pyrolysis-derived bio-oil not appropriate to be used as fuel [4]. Moreover, the main problem is that it could condensate in the reactor or pipes, causing plant breakdowns. Thus, upgrading pyrolysis vapors via steam reforming represents an interesting option to avoid the above-mentioned problems [5–7].

A very detailed list of all the reactions involved in bio-oil upgrading could be found in the work by Hu et al. [8]. The syngas generated by the pyrolysis oil steam reforming could be supplied to processes such as Fischer-Tropsch, hydrotreating, and ammonia or methanol synthesis [9]. Given that the main steam reforming reaction is endothermic, the pyrolysis outlet stream could be directly fed to the reformer without the need to cool down the gaseous stream. Furthermore, the high water content present in the pyrolysis oil could be sufficient to obtain a relatively high yield of hydrogen without the need to add water from external sources. However, in order to increase the reactants conversion and the desired products yield, the employment of a catalyst is mandatory. The production of highly efficient and selective catalysts requires the use of Rh, Pt, or Ir, which is discouraged due to their excessive cost [10]. A good trade-off between cost and efficiency is given by the employment of transition metals, mainly Ni [11], Fe [12], Co [13], alkaline metals such as K [7], and rare earth metals as Ce [14], which are widely used in catalytic formulations for steam reforming.

The most significant challenge in reforming processes, in particular when heavy compounds are involved as hydrocarbon source, is to achieve a good catalyst stability, which is quite difficult considering all the possible deactivation phenomena, mainly related to metal sintering or coke deposition, being the latter the most relevant pathway for catalyst deactivation [15–17]. Secondary and undesired reactions, which lead to the formation of undesired by-products, can be hindered through a reasonable choice of the support. Alumina, olivine, mixed Ce and Zn oxides, HZSM-5, and carbon nanotubes are the most used supports for steam reforming catalysts [18]. The main drawback, however, is the relatively high cost of these supports, since their synthesis involves energy-intense processes [12]. As an alternative, biochar-based catalysts are gaining interest year after year due to their relatively low price, easy functionalization, and versatility [19–21]. Furthermore, at their end-life stage, they could be gasified/burned to recover energy and active phases [22,23]. Biochar is generally produced by biomass slow pyrolysis, which guarantees relevant solid yield [24]. The resulting pristine biochar is usually characterized by poor textural properties (i.e., very low surface area and porosity) [25,26]. Relatively large surface areas and tailor-made pore size distributions are usually key features for catalyst supports. Fortunately, the porosity of pristine biochar can easily be engineered through activation post-treatments, leading to refined carbon materials with high potential to ensure a homogeneous loading of a given active phase [27,28]. In the last years, a growing number of research studies focused on using biochar-based catalysts for pyrolysis oil upgrading purposes [29–32]. However, catalytic steam reforming of a model compound, instead of real pyrolysis oil, is usually reported in the majority of previous works.

The specific aim of this work was to perform a comprehensive study on the suitability of activated biochar-derived catalysts to be used in the steam reforming of slow pyrolysis oil. For this purpose, several mono and bimetallic catalysts were produced using Ni, Co, K, Ce, and Fe as active phases. Due to the complex composition of the pyrolysis oil, model compounds were firstly used to test the performances of produced catalysts. Firstly, steam reforming of acetic acid was carried out to identify the best catalytic formulation. Then, a more complex model mixture (composed of acetone, acetic acid, eugenol, and ethanol) was employed to optimize the operating conditions and to study the deactivation mechanism. In the final experimental stage, steam reforming of a real pyrolysis oil was tested.

Experimental section

Catalysts production

The biochar used in this study was produced by slow pyrolysis (at 500 °C and 0.1 MPa) of binder-free wheat straw pellets (9 mm OD and 10–13 mm long). The pristine biochar was then physically activated with pure CO_2 at 700 °C and 1.00 MPa in order to increase its specific surface area and pore size distribution (PSD). The choice of the activation conditions was based on the results of a previous work, in which the beneficial effect of pressure on the mesoporosity development of the resulting activated biochars was observed. More details on the pyrolysis and activation procedure are available elsewhere [28,33,34].

The metallic active phases were deposited on the carbonaceous support via wet impregnation. $Fe(NO_3)_3 \cdot 9H_2O$, $Ni(NO_3)_2 \cdot 6H_2O$, $Co(NO_3)_2 \cdot 6H_2O$, $Ce(NO_3)_3 \cdot 6H_2O$ and KNO_3 were used as precursors of the catalyst active phase. The percentage of the

metal loading was relative to the mass of activated biochar used as support. Briefly, the activated biochar was impregnated with an aqueous solution of the precursor salt containing the desired loading of the active phase and then stirred at 60 °C until complete water evaporation. The impregnated sample was then dried overnight at 110 °C. After that, the catalysts were calcinated for 3 h at 600 °C under N_2 flow to decompose all the precursor salts and subsequently sieved in order to obtain a particle size distribution in the range of 0.125–0.250 mm. The bimetallic catalysts were prepared in four steps: (1) deposition of the first precursor; (2) calcination; (3) impregnation of the second precursor; and (4) final calcination. The employed nomenclature and a resume of the produced catalysts are reported in Table 1.

Table 1 – Resume of the mono and bimetallic catalysts prepared and tested in this work.

Support	Sample	Active phase	Loading (wt. %)
	BC	/	/
Monometallic			
	BCFe	Fe	7
	BCCo	Co	7
	BCCe	Ce	7
	BCK	K	7
	BCNi7	Ni	7
	BCNi4	Ni	4
	BCNi10	Ni	10
Bimetallic			
	BCFeNi	Fe/Ni	7/10
	BCCoNi	Co/Ni	7/10
	BCCeNi	Ce/Ni	7/10
	BCKNi	K/Ni	7/10

Characterization of carbon materials and liquids

The textural properties of the activated biochar support (BC) and calcinated catalysts were determined from the N_2 adsorption/desorption isotherms at −196 °C, which were obtained using an ASAP 2020 automatic adsorption analyzer (Micromeritics, USA). Around 120 mg of sample was degassed under vacuum at 150 °C. The specific surface area was evaluated using the Langmuir model (S_L); total pore volume (V_{tot}) was obtained from the N_2 adsorbed at high relative pressure (0.99); the specific volume of micropores (V_{micro}) was calculated using the t-plot method; the mesopore volume (V_{meso}) was evaluated from the pore size distribution (assuming a non-local density functional theory, NLDFT, and slit-pore geometry) by subtracting the cumulative volume of the smaller pores (d_p < 2 nm) from the total volume (d_p < 50 nm). The software MicroActive from Micromeritics was used for all the above-mentioned calculations.

The activated biochar support was also characterized by proximate analysis (in quadruplicate according to ASTM standards) and ultimate analysis (CHN), which was carried out using an elemental analyzer model CHN628 from Leco Corporation (USA). X-Ray Fluorescence (XRF) spectroscopy analysis (using an ADVANT'XP + XRF spectrometer from Thermo ARL, Switzerland) was also carried out to identify and quantify the inorganic species available in the biochar ash.

The moisture content of the pyrolysis oil was evaluated by Karl-Fischer titration. Ultimate analysis, including the sulfur content, was also performed for pyrolysis oil using the same elemental analyzer described above.

The reducibility properties of the prepared biochar-based catalysts were investigated by means of temperature-programmed reduction (TPR) analysis. To this aim, 0.5 g of each sample was loaded into the reactor and heated under a reducing stream (5% H_2 in Ar, at a flow rate of 0.5 NL min^{-1}) at a heating rate of 15 °C min^{-1} from 50 to 600 °C. The hydrogen concentration at the outlet was continuously monitored by means of a Hiden QGA mass spectrometer (Hiden Analytical, UK).

CO_2 temperature-programmed desorption (CO_2-TPD) was also used to investigate the surface properties of the prepared catalysts. It is generally recognized that CO_2-TPD allows the determination of weak, medium, and strong basic sites on the catalyst surface [35,36]. The analysis was conducted as follows: CO_2 adsorption was firstly performed at 50 °C on 0.5 g of the reduced catalyst under a stream of CO_2 in Ar (40 vol % CO_2) for 30 min; then, weakly adsorbed CO_2 was purged with a pure Ar stream at the same temperature for 1 h; finally, CO_2-TPD was performed in pure Ar raising the temperature from 50 to 700 °C at a heating rate of 5 °C min^{-1}. Desorbed CO_2 was measured by means of the above-mentioned mass spectrometer.

In order to observe the morphology of the coke deposition and the dimension of the metallic nanoparticles, transmission electron microscopy (TEM) of fresh and spent catalysts was carried out using a Tecnai F30 microscope (FEI, USA) operating at 300 kV. Samples were previously sonicated for 5 min in an aqueous solution of ethanol.

Catalytic tests

Catalytic tests were carried out in a tubular fixed-bed reactor (made of Hastelloy C276, 300 mm long and 10 mm ID) placed in an electric tubular furnace. Around 0.5 g of sample was located inside the reactor and packed with an inert filler (Kaowool™ fiber). A K-type thermocouple placed in the middle of the catalytic bed was used to monitor the system temperature. Prior to each steam reforming experiment, the catalyst was heated up to 600 °C under reducing atmosphere (N_2/H_2, 50/50 vol %). These conditions were kept for 2.5 h to assure complete reduction of the active metal oxides.

Since the pyrolysis oil is a very complex mixture of hundreds of organic compounds, the study was firstly carried out using representative model compounds. In a first stage, an aqueous solution of acetic acid (steam to carbon molar ratio, S/C, of 4) was used to study the performance of the different catalysts. The reason behind this choice lays in the high content of this carboxylic acid in slow pyrolysis oils (up to 20 wt %) [37–39] and in the availability of numerous studies in the literature, which can be useful for comparison purposes. In a second stage, an equimass mixture of acetone, acetic acid, ethanol, and eugenol was used for the best performing catalyst during acetic acid reforming. These compounds were

chosen as representative products from the thermal decomposition of lignin, cellulose, and hemicelluloses [37,40,41]. Finally, steam reforming of real pyrolysis oil was carried out using the liquid collected during the production of the pristine biochar.

Steam reforming experiments were carried out at different temperatures in the range of 400–750 °C. The liquid blend was fed using a HPLC pump, maintaining a liquid hourly space velocity (LHSV) of the organic fraction equal to 2.94 h^{-1} (considering a bed void fraction of 0.5). The liquid was forced to pass through a coil wrapped around a cartridge resistance, to reach complete evaporation of the blend, and mixed with N_2 to be delivered to the reactor. The composition of the outlet gas was monitored using the above-mentioned spectrometer, which was able to measure, in real-time, the concentrations of acetic acid, acetone, and permanent gases. For steam reforming of the model mixture and real pyrolysis oil, the gas composition was analyzed using a dual-channel micro-gas chromatograph (μ-GC 490 from Agilent, USA) equipped with TCD detectors and two analytical columns (a Molsieve 5 A and a PoraPlot U). The known amount of N_2 fed was used as tracking compound to calculate the mass of produced gas. The evolution of the pressure drop along the reactor was measured employing a differential pressure sensor. A schematic overview of the experimental device is given in Fig. 1.

The performance of the different catalysts tested was evaluated in terms of acetic acid conversion (X_{AcOH}), as well as hydrogen (Y_{H2*}), and acetone yield (Y_{Ac*}), as defined in Eq. (1)–(3). On the other hand, for the results obtained using the model mixture and real pyrolysis oil, the carbon conversion (X_C), product yield (Y_i), and selectivity (S_i) were calculated according to Eq. (4)–(6). In such equations, F_i is the molar flow rate of the "i" specie; F_c is the carbon molar flow rate (which was calculated considering all the species detected by the μ-GC: CO, CO_2, and CH_4); and F_{iEq} is the molar flow rate of the "i" specie at the thermodynamic equilibrium condition (which was calculated using the process simulation software Aspen Plus v. 10 from Gibbs free energies).

$$X_{AcOH} = \frac{F_{AcOH,in} - F_{AcOH,out}}{F_{AcOH,in}} 100 \quad (1)$$

$$Y_{H2*} = \frac{1}{4}\frac{F_{H2,out}}{F_{AcOH,in}} 100 \quad (2)$$

$$Y_{Ac*} = 2\frac{F_{Ac,out}}{F_{AcOH,in}} 100 \quad (3)$$

$$X_C = \frac{F_{C,out}}{F_{C,in}} 100 \quad (4)$$

$$Y_i = \frac{F_{i,out}}{F_{iEq,\ out}} 100 \quad (5)$$

$$S_i = \frac{F_{i,out}}{F_{H2,\ out} + F_{CO2,\ out} + F_{CO,\ out} + F_{CH4,\ out}} 100 \quad (6)$$

Results and discussion

Catalysts characterization

Results from proximate, ultimate, and inorganic matter analyses of the activated carbon (BC), which was used as support, are reported in Table 2. The most important textural properties for all the produced catalysts are shown in Fig. 2. The high ash percentage of BC was the result of the activation procedure, which created a high specific surface area through the gasification of the carbon structure, leading to an increase in the specific ash content. The inherent inorganic matter of biomass could promote the gasification of the coke produced during the course of the reforming experiments [12,26,42,43]. As shown in Fig. 2, the activated carbon (BC) had the highest

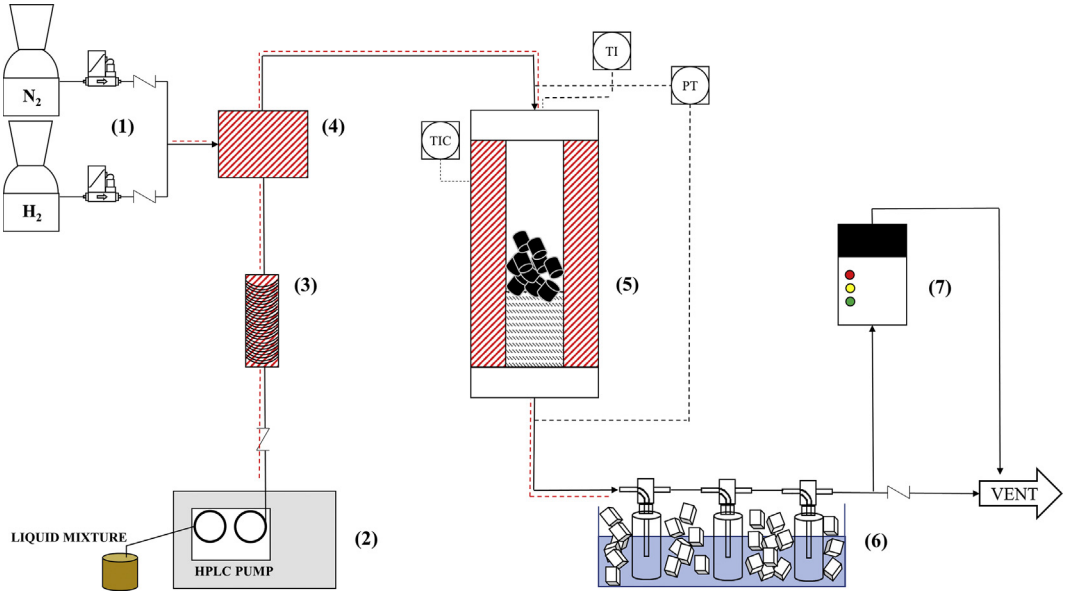

Fig. 1 – Schematic overview of the experimental device used in this work: feeding system (1); HPLC pump (2); evaporator (3); gas mixer (4); fixed-bed reactor and furnace (5); condensation train (6); and μ-GC analyzer/quadrupole mass spectrometer (7).

Table 2 – Proximate, ultimate, and inorganic matter (as oxides) analyses of the physically activated biochar employed as support of the produced catalysts.

Ultimate analysis (wt.%)	
Carbon	61.59
Hydrogen	1.16
Nitrogen	1.84
Oxygen[a]	35.40
Proximate analysis (wt.%)	
Moisture	N.D.
Volatiles	8.16
Ashes	41.98
Fixed Carbon[a]	50.75
Inorganic matter (wt.%)	
SiO_2	17.52
K_2O	16.68
CaO	7.40
P_2O_5	2.45
MgO	1.51
Al_2O_3	1.11
Fe_2O_3	1.05
S	0.716
Cl	0.702
Na_2O	0.216

[a] Values calculated by difference.

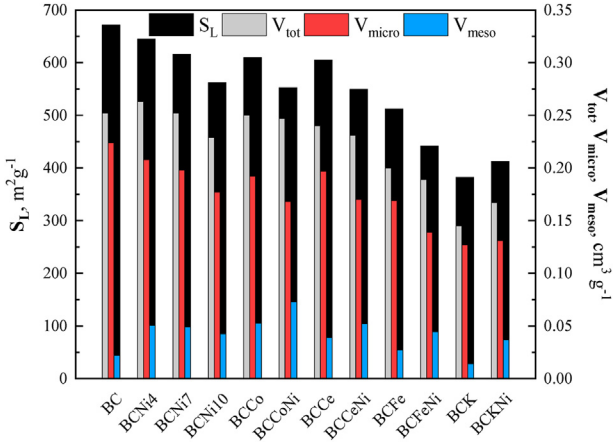

Fig. 2 – Specific surface area (Langmuir, S_L) and pore volumes (V_{tot}, V_{micro}, and V_{meso}) of the twelve catalysts produced in the present study.

specific surface area, which was mainly contributed by micropores. In general, the impregnation and subsequent calcination steps of the resulting BC-based catalysts led to a decrease in the surface area (see Fig. 2). The magnitude of this observed reduction depends on the nature and loading of the active metal phase, which could partly clog the pores of the support, leading to a decrease in the available surface area. Furthermore, an increase in the volume of mesopores at the expense of that of micropores was observed for BC-based catalysts. This could be attributed to interactions between the carbon matrix, which has reductive properties [31,44], and the metal oxides resulting from the decomposition of the precursor salts [45–47]. Recently, Li et al. [48] have reported an increase in the mesopore volume of Ni-laden chemically activated biochars. The authors ascribed this increase in mesoporosity to the role of Ni in promoting the decomposition of carbonates (inducing more production of metallic elements for creating new pores) and the erosion of carbon layer. Since Co and Fe have similar properties and chemical behaviors to those of Ni, a similar effect on the mesoporisty development can also be expected (as shown in Fig. 2).

The results obtained from temperature-programmed reductions are summarized in Fig. 3. In the case of BCNi catalysts, it is possible to observe that NiO reduction occurred between 500 and 600 °C. This observed behavior is in good agreement with earlier studies [32,49]. Furthermore, from the reduction profiles, it is evident that Ni loading had a marked influence on the reducibility properties, suggesting that the active metal dispersion had a non-negligible impact on Ni-biochar bond strength. Indeed, the α peak (low-temperature NiO reduction) appeared as a shoulder for the BCNi4 sample, while it was more evident for the BCNi7 sample and even more intense for the BCNi10 catalyst. For the latter, the intensity of the α peak was almost the same as that of the β reduction peak. This suggests that the higher the Ni loading, the higher the amount of low-interactive Ni sites on the biochar surface. Besides, the observed decrease in the reduction temperature at higher Ni loadings (which was previously reported by Nguyen et al. [50]) could be ascribed to NiO multilayers, which weakened the Ni-biochar interactions. Nevertheless, considering the low reduction temperature of unsupported NiO (325 °C [51]) it can be stated that all the Ni-based samples revealed a remarkable interaction between active metal and support.

Regarding the cobalt catalysts, it was observed that Co reduction occurred in series, describing two distinct reduction peaks corresponding to the consecutive reduction of Co_3O_4 to CoO and CoO to Co [52,53]. CeO_2 reduction occurred in two steps as well (the first one at ca 400 °C and the second one at ca 600 °C). The low temperature (i.e., below 500 °C) observed for the reduction of CeO_2 was somewhat unexpected. However, this finding could be related to the reducing activity of the BC support. Regarding the BCFe catalyst, it is well known that iron oxide commonly undergoes reduction in three steps,

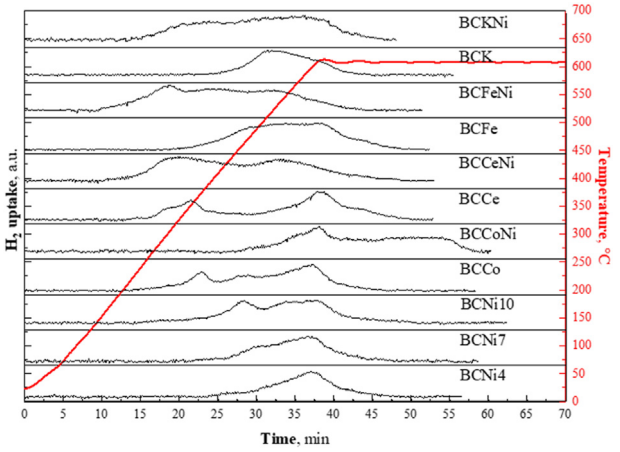

Fig. 3 – Temperature-programmed reduction results obtained for all the produced catalysts.

from Fe_2O_3 to Fe_3O_4, Fe_3O_4 to FeO, and FeO to Fe [36]. As can be seen in Fig. 3, the BCFe catalyst exhibited a broad reduction peak starting at approximately 300 °C. As mentioned above for the case of BCCe catalyst, iron oxides reduction was anticipated because of the interaction with the activated biochar support [54]. Finally, for the BCK catalyst, K_2O reduction was observed, as expected [55], at approximately 500 °C, suggesting that the BC support did not play any effect on the reduction of potassium oxide.

The bimetallic BCCeNi, BCFeNi, and BCKNi formulations demonstrated even more enhanced reducibility if compared to the respective monometallic samples. A possible explanation for this is that the higher amount of active species led to the formation of bulk oxides, which could be easily reduced. In addition, the increase in NiO reducibility in the presence of K_2O has previously been observed [56]. The bimetallic BCCoNi catalyst showed lower reducibility compared to that of the BCCo and BCNi10 samples. This might be due to the formation of a Co–Ni alloy, which has a higher bond strength than metals themselves [57]. This particular result would suggest that the active species in the BCCoNi dual catalyst have lower mobility; however, and despite its weaker reducibility, this could be beneficial for the reaction, especially in terms of catalyst stability.

Results from the CO_2-TPD measurements are detailed in Appendix A (Supplementary Material). The main outcomes showed that the addition of a metallic phase on the carbonaceous support resulted in the formation of new CO_2 chemisorption sites (see Fig. A1). Basic sites can be weak, medium or strong depending on the temperature at which CO_2 desorbed (100–150 °C, 150–250 °C, and above 250 °C; respectively). Since surface energies strongly depend on the metal specie, different metals can result in different basic sites [58]. In the present study, the introduction of Ni to the BCCo catalyst led to new medium and strong basic sites. This finding is in agreement with the previous studies by Nagban et al. [61] and Turap et al. [62], in which it was reported that the addition of Co to a Ni-based catalyst (supported on ZrO_2 and CeO_2) resulted in the formation of new strong basic sites. It is well known that catalysts having higher surface basicity are less prone to coke deposition and subsequent deactivation [63].

Steam reforming of acetic acid

Monometallic catalysts

Fig. 4a graphically summarizes the outcomes obtained from the steam reforming of acetic acid at 600 °C using the monometallic catalysts. The non-impregnated activated biochar (BC) showed a certain activity, but also a low stability, leading to a rapid decrease in the acetic acid conversion (X_{AcOH}). As mentioned above, BC was characterized by a high surface area and a high ash content. These two features, together with the carbon deposits produced via secondary reactions, could explain the certain catalytic activity of BC. Similar instability was also observed for the cobalt-, potassium- and cerium-based catalysts, which exhibited a pronounced deactivation after only a few minutes of run time. The BCFe catalyst showed a quite different performance. During the first 5 min, acetic acid was completely converted. After that, however, the

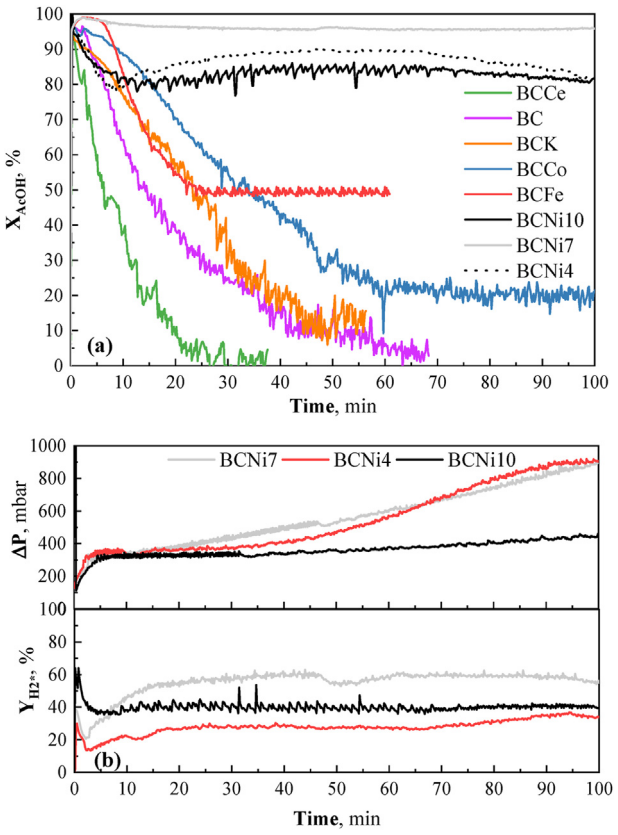

Fig. 4 – Results obtained from the steam reforming of acetic acid at 600 °C and 2.94 h^{-1}: Acetic acid conversion obtained with the monometallic catalysts (a); hydrogen yield and pressure drop evolution during the experiments involving the three nickel-based catalysts (b).

catalyst activity decreased to a conversion value of 50%, which remained stable for the rest of the experiment.

As can be seen in Fig. 4a, the nickel-based catalysts clearly exhibited the best performances in terms of acetic acid conversion and stability. The ability of nickel to break the C–O and C–H bonds is widely recognized in the literature [16,31,41,64], making this metal commonly employed in steam reforming processes. All the three Ni loadings showed high conversion values (80%–95%), which remained almost constant during the entire run time. In terms of conversion, it was clear that 7 wt % of nickel was the best formulation for our purpose. Nevertheless, from the pressure drop measurement across the bed (see Fig. 4b), it can be deduced a certain extent of coke deposition, which gradually clogged the catalytic bed. In particular, for BCNi4 and BCNi7 catalysts, which showed the highest conversion values, the highest coke deposition rates were observed. Therefore, these catalysts could be considered not suitable for long-time applications. For the catalyst having the highest nickel loading (BCNi10), an almost constant pressure drop value was observed, suggesting that the relatively high nickel content was able to hinder the deposition of coke on the catalyst. Moreover, from the evolutions of the hydrogen yield shown in Fig. 4b, it can be deduced that the BCNi10 catalysts exhibited a stable performance. Thus, it can be concluded that a 10 wt % of Ni loading

represents the most convenient alternative to simultaneously reach a good conversion towards hydrogen and good stability over time. This finding partly agrees with the results reported by Zhang et al. [65], who gave evidence that relatively low Ni loadings (i.e., below 10 wt %) in a Ni/Al_2O_3 catalyst led to relatively low catalytic activity and fast deactivation by coke deposition.

Bimetallic catalysts

This phase of the study was addressed to improve the overall performance of the BCNi10 catalyst. To this end, four bimetallic catalysts were produced by adding a 10 wt % of nickel to the BCK, BCCe, BCFe, and BCCo catalysts.

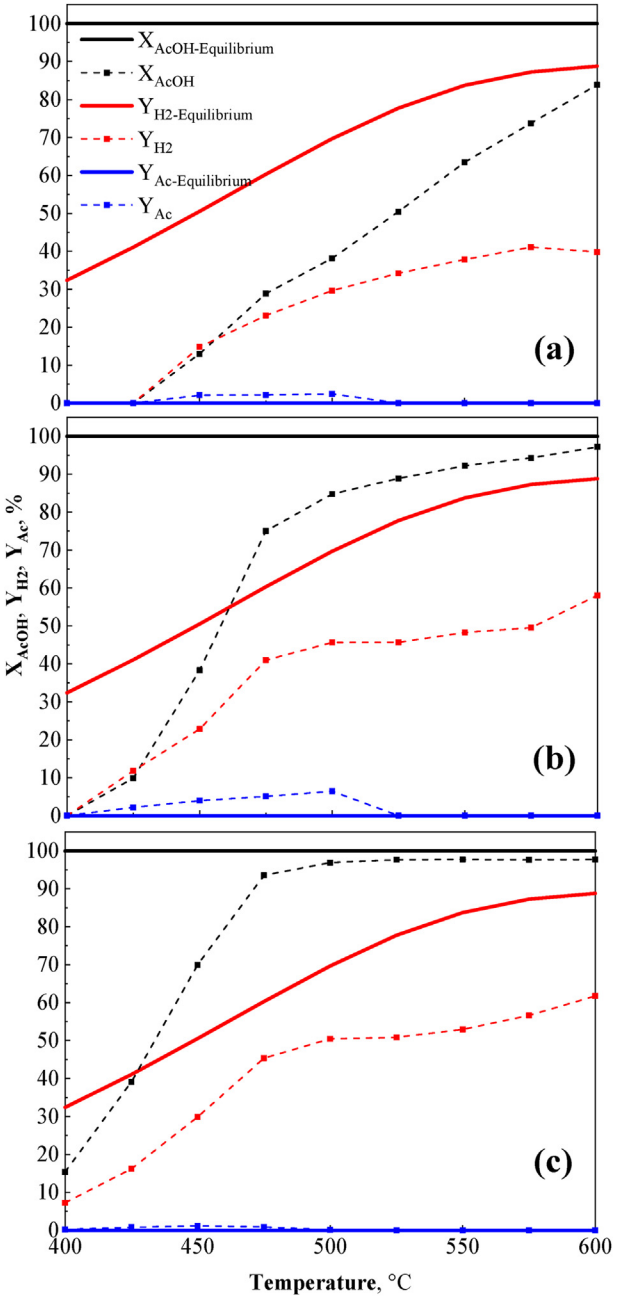

Fig. 5 – Experimental and theoretical equilibrium values of acetic acid conversion, H_2 yield, and acetone yield as a function of the bed temperature for different bimetallic catalysts: BCFeNi (a); BCCeNi (b); and BCCoNi (c).

Fig. 5 shows the results obtained for three of the four bimetallic catalysts during acetic acid steam reforming at different temperatures. Since the potassium-nickel catalyst (BCKNi) showed severe instability during the reforming test, which was comparable to that of BCK, the obtained outcomes for this catalyst are not reported herein. From the data shown in Fig. 5, it can be concluded that the addition of nickel to the tested monometallic catalysts was able to enhance their catalytic performance and stability. In the case of the iron-based catalysts (see Fig. 5a), for example, the acetic acid conversion at 600 °C increased by around 30% when the second metal phase (Ni) was added. Nevertheless, the results for the BCFeNi catalyst were similar to those obtained for the BCNi10 monometallic catalyst (Fig. 4a). For the BCCeNi catalyst (see Fig. 5b), however, the synergistic effect of cerium and nickel was more evident in view of the improved conversion and hydrogen yield (which increased by around 15% and 20%, respectively, compared to the monometallic BCNi10 catalyst). On the other hand, a decrease in the reactor temperature from 600 to 500 °C did not result in a substantial loss of catalytic activity of the BCCeNi catalyst. Nonetheless, at 500 °C and below, a higher production of acetone was observed, probably as a result of the ketonization of acetic acid [66].

Among the four bimetallic catalysts tested, the cobalt-nickel one (BCCoNi) resulted to be the most suitable for acetic acid steam reforming. In fact, as shown in Fig. 5c, the experimental conversion was close to the thermodynamic equilibrium value at 600 °C. The hydrogen yield decreased from 61% (at 600 °C) to 45% (at 475 °C). In any case, the decrease in the hydrogen yield at lower temperatures was not accompanied by an increase in the acetone yield, suggesting that the main reaction mechanisms were catalytic steam reforming and cracking for temperatures above 475 °C.

In light of the good results obtained for the BCCoNi catalyst, a long-time stability test (i.e., 750 min) was carried out at 600 °C. Results shown in Fig. 6a correspond to the sum of two consecutive runs. At the end of the first run (475 min), the pump was stopped and the reactor cooled down under N_2 to room temperature. The following experiment started when the reactor temperature reached again 600 °C. A conversion value above 90% was obtained during the first 250 min. After that, conversion decreased gradually. This deactivation could be ascribed to two different phenomena: (1) carbon deposition on the active sites and (2) formation of byproducts, which are strongly adsorbed on the catalytic sites. The latter assumption was confirmed by the results obtained during the second run. In fact, after the heating step under N_2, the catalyst was partially regenerated. Nevertheless, the conversion obtained with the fresh catalyst was not achieved again, probably due to a certain availability of coke on the surface.

An additional stability test was carried out changing the operating temperature. The run started at 600 °C until stabilization was reached; then, the system was cooled down to 500 °C (at 5 °C min^{-1}) and the conditions were kept for 15 min. After that, the system was cooled down to 400 °C, at the same cooling rate, and kept at this temperature for 15 min. Finally, the system was then heated up to 600 °C. As shown in Fig. 6b, both the conversion and hydrogen yield remained reasonably

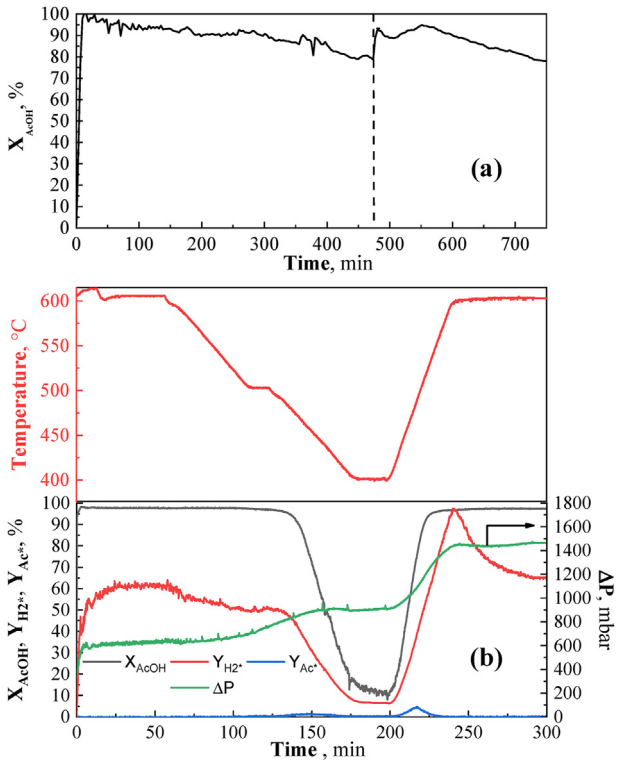

Fig. 6 – Stability test of BCCoNi catalyst for steam reforming of acetic acid: 2-step stability test performed at 600 °C (a); and cycling stability test carried out in the range of 400–600 °C (b).

stable in the range of 475–600 °C and were coherent to the outcomes displayed in Fig. 5c. The pressure drop across the bed remained almost constant during the first isothermal phase and started to increase when the temperature began to fall, due to the higher extent of coke formation. In addition, a certain production of acetone was also observed during the cooling down stage [8]. When the experimental device was heated up again to 600 °C, the conversion of acetic acid reached the same value as that of the first stage, indicating negligible catalyst deactivation. For its part, the hydrogen yield achieved a transient peak of 95% and then settled back to a stable plateau of 65%. Similar behavior was observed for the acetone yield. Since the observed increases in the production of both hydrogen and acetone were not accompanied by an increase in the reactant conversion, one can hypothesize that a considerable fraction of these compounds was previously adsorbed on the catalyst surface and then released with the increase in temperature, confirming the double nature of the deactivation mechanism.

Based on the above-explained results, one can conclude that the dual Ni–Co biochar-supported catalyst was suitable for acetic acid steam reforming applications. In particular, it was possible to obtain excellent performances comparable to those obtained for commonly used supports, such as Al_2O_3 and SBA [16,67–69].

Steam reforming of a mixture of acetic acid, acetone, ethanol, and eugenol

Once identified the most promising metal/BC catalyst (BCCoNi), research was focused on assessing the effect of the operating conditions on the overall performance of the steam reforming of a model mixture composed of acetone, acetic acid, ethanol, eugenol, and water (S/C = 4). Previous studies reported that acetone, ethanol, and acetic acid could easily be reformed over a Ni- or Co-based catalyst [8,67,70–72]. To the best of our knowledge, no studies concerning the steam reforming of eugenol (a phenolic compound) have been published so far.

From the results obtained for the steam reforming at 600 °C, which are shown in Fig. 7a, it can be observed that carbon conversion (X_c) rapidly decreased from an initial value of 50% to an almost constant value of ca. 30%. This behavior was similar to that observed for the BCFe catalyst for the acetic acid steam reforming. The similarity between the obtained hydrogen and carbon dioxide yields (see Fig. 7a) seems to suggest that the steam reforming was the main reaction involved. Despite the relatively low conversion attained at steady-state, the products selectivity remained relatively constant during the entire experiment (see Fig. 7b), indicating that the catalyst deactivation did not result in significant changes in the reforming mechanism. More in detail, the low yields of both CO and CH_4 (below 10%), could suggest a relatively low extent of both the reverse Boudouard and decomposition reactions, respectively [73–75]. As it can be deduced from a reference experiment, which was conducted using only activated biochar as catalytic bed (see Fig. A2), it seems clear that steam reforming reactions only took place at the surface of metal nanoparticles. On the other hand, Fig. A3 displays the product evolution measured for a catalytic test, which was conducted at a LHSV of 2.94 h^{-1}, 600 °C and using a relatively high flow (the double than that used previously) of the carrier gas (N_2). This experiment was aimed at assessing the influence of the partial pressure of the reactant. For this test, we expected a decrease in the overall performance of the catalyst but a better stability. Nevertheless, the results showed an even faster deactivation, which could be directly related to the water partial pressure. Probably, during the previous experiment (which corresponds to Fig. 7a), the higher water content was able to hinder the coke deposition or, at least, to gasify part of the carbon deposits on the catalyst surface, leading to a decrease in the deactivation rate.

To further improve the catalytic performances, a study on the influence of the operating temperature and liquid hourly space velocity was carried out. Fig. A4 shows the carbon conversions obtained at different temperatures in the range of 500–600 °C and the corresponding equilibrium values (at a constant LHSV of 2.94 h^{-1}). Even though the conversion of the reactant was thermodynamically promoted, our configuration only allowed us to reach a maximum carbon conversion of 30%.

When the liquid residence time was set at 5.88 h^{-1}, a drastic reduction of the carbon conversion was observed (see Fig. 8a). Conversely, when the lowest LHSV value (1.47 h^{-1}) was used, the performance of the catalyst was slightly improved with respect to the initial condition (i.e., 2.94 h^{-1}).

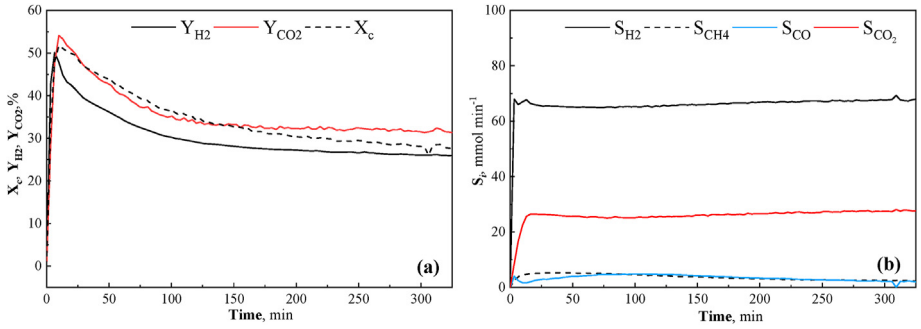

Fig. 7 – Test of BCCoNi catalyst for steam reforming of the model mixture at 600 °C and 2.94 h^{-1}: carbon conversion, hydrogen and carbon dioxide yields (a); and products selectivity (b).

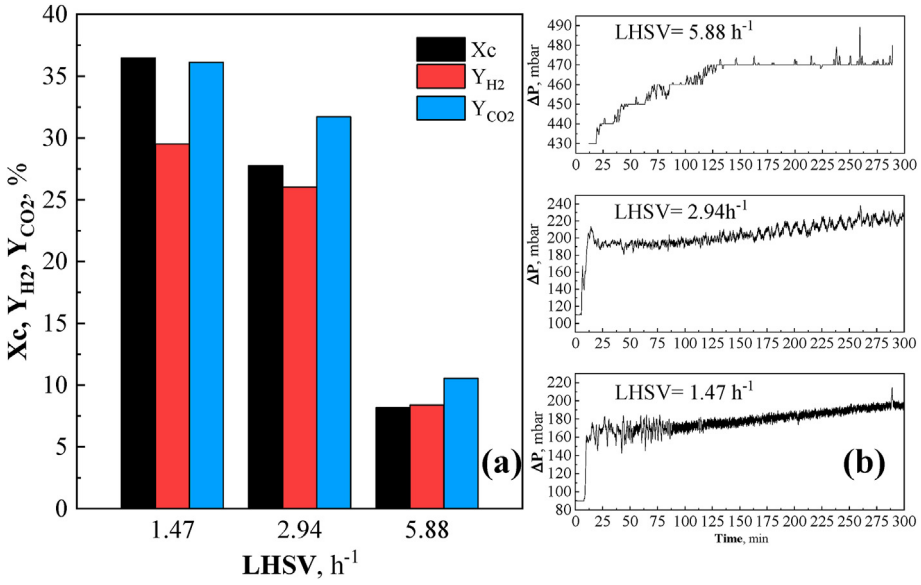

Fig. 8 – Outcomes in terms of X_c, Y_{H2}, and Y_{CO2} (a) and pressure drops evolution (b) obtained for the study of the influence of LHSV on the reforming of the model mixture at 600 °C using BCCoNi as catalyst.

The fast deactivation observed during the early stage of the experiment (see Fig. 7) could be ascribed to different mechanisms: (1) sintering of the metal phases [76], (2) oxidation of the metal active phase [10,77], (3) gasification of the support [78], (4) coke deposition [16,17]; and (5) catalyst poisoning [15,41]. Sintering of the active phases is strictly related to the operating temperature and to the reaction environment [79]. Since the experiments involving acetic acid (where fast deactivation was not deduced from Fig. 6) and the model mixture were conducted under similar conditions, we can hypothesize that sintering does not explain the observed deactivation. To verify if the deactivation was due to active phase oxidation, the spent catalyst was reduced and tested again under the same conditions. The results obtained did not show the activity peak detected when the fresh catalyst was firstly tested. Therefore, the oxidation of the metal phase could also be ruled out. Gasification of the carbon matrix caused by the water available in the liquid feed mixture could lead to a modification of the support structure with subsequent loss of active phase. However, a test employing only BC as catalytic bed was performed feeding only water along with N_2 at 600 °C and monitoring the gas outlet stream compositions. Results from this test revealed an almost negligible occurrence of the steam gasification reaction. In summary, it could be concluded that the deactivation was mainly caused by coke deposition or catalyst poisoning during the first minutes of the catalytic test.

The nature of coke could be distinguished between filamentous and amorphous, with the latter being responsible for the catalytic activity loss due to encapsulation of the metallic phase [80–82]. This kind of deactivation is particularly significant in the case of microporous materials since the smaller pores are the first ones to be filled by coke [83,84]. However, and in light of the similar pressure drops measured at the three LHSV values (see Fig. 8b), a relatively good dispersion of the metal phases (which could hinder carbon deposition [85]) can be assumed. Therefore, the observed fast deactivation should mainly be ascribed to the production of relatively heavy organic compounds, which could be adsorbed on the active sites, and

subsequently react to form more stable and not easily desorbable reaction intermediates. In line with this, Zhang et al. [15] reported that the strong adsorption of phenolic compounds on a Ni/Al_2O_3 catalyst could explain the observed low catalytic activity in steam reforming of guaiacol. In the present study, the poisoning of catalyst could eventually reach a quasi-steady-state after 100 min (see Fig. 7a), in which the fraction of available catalytic sites could remain constant.

Steam reforming of slow pyrolysis oil

Even though the BCCoNi catalyst showed a modest catalytic activity for the steam reforming of the model mixture, its stability at steady-state was encouraging. Therefore, the catalytic activity of this catalyst was also evaluated for the steam reforming of a real slow pyrolysis bio-oil, which had a mean empirical formula of $CH_{2.34}O_{0.88}$ and a water content of 71 wt % (S/C = 3.87). No sulfur, which could irreversibly poison the catalyst [86], was detected in the bio-oil.

The results obtained from the catalytic test using the above-mentioned pyrolysis oil were clearly unsatisfactory, as shown in Fig. A5. After a few minutes of run time, the catalytic activity drastically dropped to a value comparable to that obtained for the model mixture and using only the BC support as catalytic bed. Such behavior could probably be ascribed to the sugar-type compounds present in the pyrolysis oil. Paasikallio et al. [37] identified a 4.3 wt % of levoglucosan in a forest thinnings-derived oil. These compounds, which are non-volatile and undergo thermal decomposition rather than vaporization, can produce charring matter, which unavoidably covers the catalyst surface [87]. Furthermore, the presence of such compounds caused numerous clogs in the evaporation system of the experimental setup, even at low temperatures (150–250 °C). To avoid the above-mentioned issues, the raw pyrolysis oil was distilled at atmospheric pressure and 200 °C in order to obtain a lighter fraction, free of sugar-type compounds. The obtained distillate had an empirical formula of $CH_{2.42}O_{0.75}$ and a water content of 85 wt % (S/C = 8.32).

The effects of LHSV on the carbon conversion and products selectivity (using the distilled fraction of pyrolysis oil at a constant temperature of 600 °C) are summarized graphically in Fig. 9a. In contrast to the outcomes previously reported for the model mixture, an increase in reactants residence time led to a marked increase in the carbon conversion up to 45%. Regardless of the value of LHSV, hydrogen was always the most abundant product, followed by CO_2. CH_4 could be produced by methanation of CO and CO_2 or, more probably, by thermal decomposition of reactants.

Fig. 9b reports the conversion and selectivity values obtained at different operating temperatures (at a constant LHSV of 2.94 h^{-1}). An increase from 550 to 700 °C led to a marked increase in the carbon conversion, whereas a further increase from 700 to 750 °C resulted in a slight enhancement of the reactant conversion. In the range of 600–750 °C, the temperature did not significantly affect the distribution of products. This suggests that the operating temperature only influenced the process from a kinetic point of view, without affecting the main reaction mechanism.

A stability test was also performed for the steam reforming of the distilled pyrolysis oil under the previously-identified optimal conditions (700 °C and 1.47 h^{-1}). The evolution of the conversion, products selectivity, and pressure drop across the bed are shown in Fig. 10. The stability test was divided into two separate runs. At the end of the first one (vertical dashed line in Fig. 10) the pump was stopped. The reactor was then cooled down to 20 °C and heated up again to 700 °C under N_2.

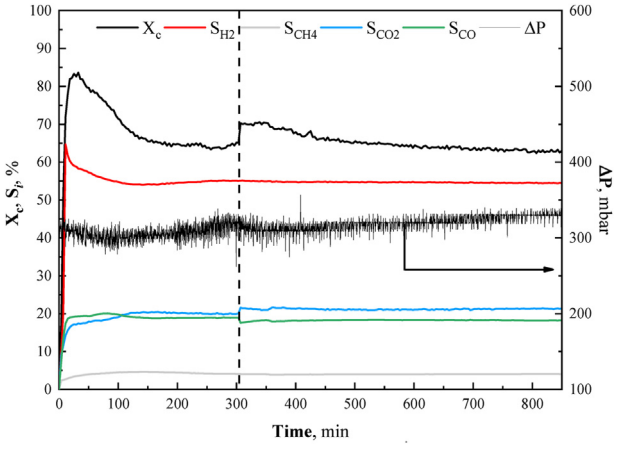

Fig. 10 – 2-Step long-term stability test for the BCCoNi catalyst during the steam reforming of distilled pyrolysis oil at 700 °C and 1.47 h^{-1}.

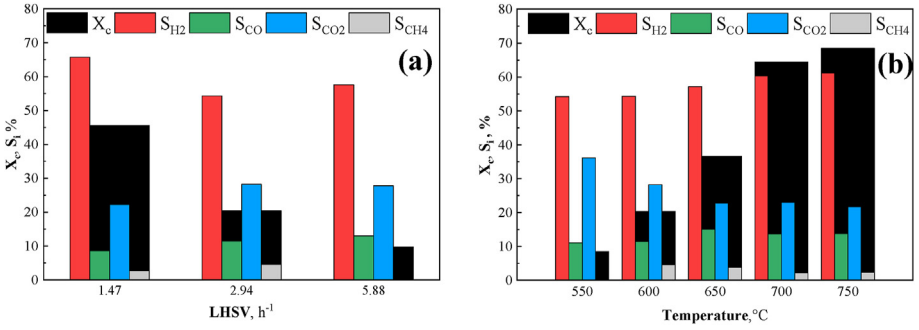

Fig. 9 – Results in terms of carbon conversion and products selectivity obtained during the steam reforming of distilled pyrolysis oil: at constant temperature (600 °C) and different LHSV values (a); and at different temperatures and constant LHSV of 2.94 h^{-1} (b).

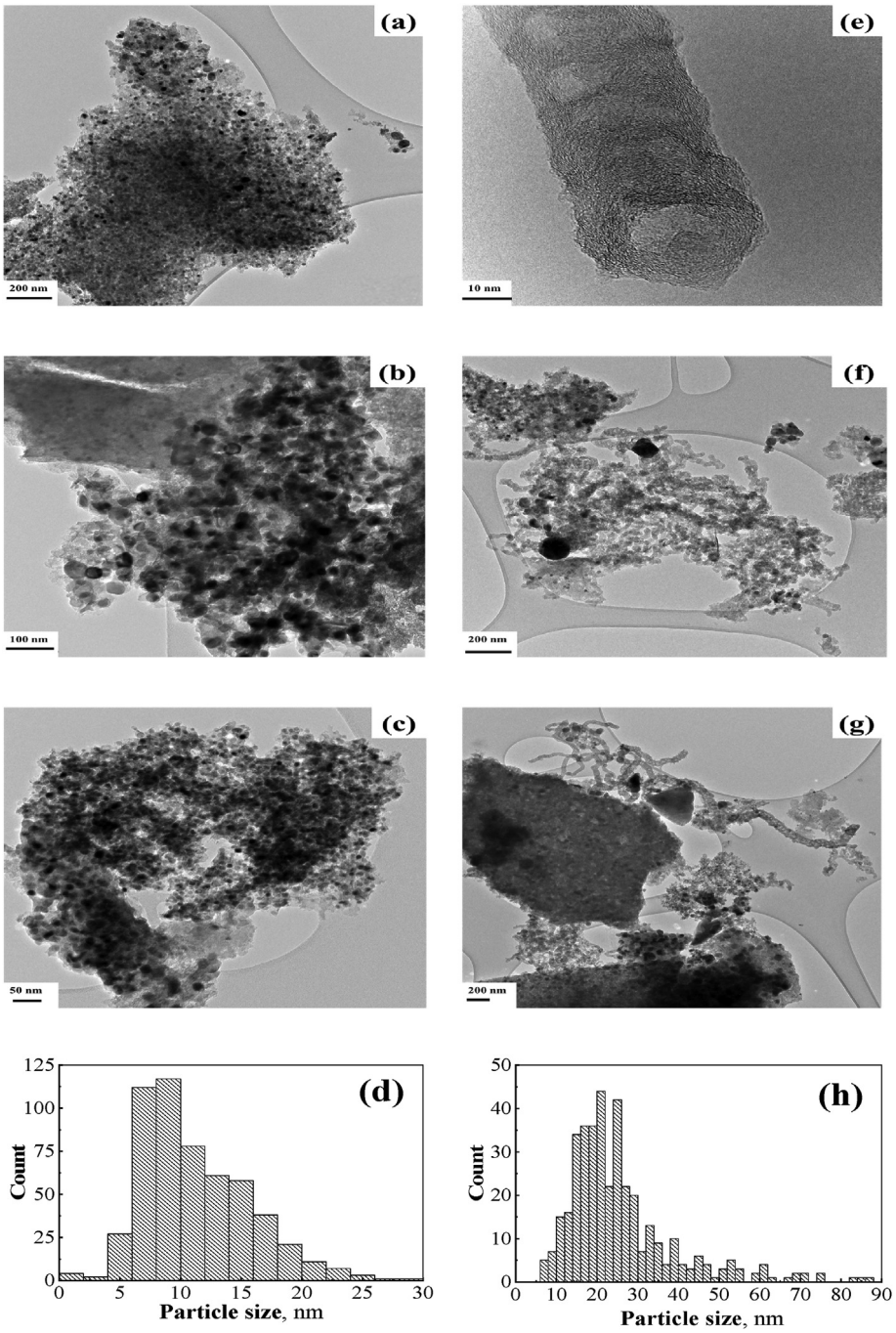

Fig. 11 – TEM images and metal particle size distribution of fresh (a, b, c, d) and spent (e, f, g, h) BCCoNi catalyst used in steam reforming of distilled pyrolysis oil at 700 °C and 1.47 h^{-1}.

Once the reactor reached the setpoint, the distilled oil was then fed into the system. As can be seen in Fig. 10, and similarly to that observed for the model mixture, the conversion reached a transient peak (84%) and then rapidly decreased to an almost constant value (65%). The thermal treatment under nitrogen slightly regenerated the catalyst, confirming the presence of heavier compounds adsorbed on the solid surface. As observed for the steam reforming of both the acetic acid and model mixture, the pressure drop remained reasonably constant, suggesting that the possible coke deposition did not lead to a deactivation of the catalyst. The yields of gaseous species remained almost constant during the whole experiment. The main difference between the results shown in Figs. 6a and 10 was that, in the first case, the conversion did not stabilize to a constant value; however, in the case of pyrolysis oil, a stable value (plateau) was achieved after 150 min. Such value remained constant even after the thermal regeneration of the catalyst.

Fig. 11 shows the TEM images of both the fresh and spent BCCoNi catalyst. From Fig. 11d and h, it can be seen that the size of metal nanoparticles was larger for the spent catalyst. This could be explained by sintering phenomena, leading to

the formation of larger clusters (black agglomerates in Fig. 11f). Nevertheless, the observed sintering of the activate phase did not result in an evident loss of catalytic activity. Furthermore, carbon nanotubes with an internal diameter of ca. 20 nm (see Fig. 11e) were observed on the surface of the spent catalyst [88,89]. Their presence could be attributed to the decomposition of guaiacols and furfurals, which, due to their aromatic structure, could promote the formation of this kind of carbon nanostructures [90,91].

Conclusions

In view of the results reported in the present study, the following conclusions can be drawn:

1. Physically activated (at mild temperature and moderate pressure) wheat straw-derived biochar appears as a promising support material for heterogeneous metal-based catalysts. Among the five metallic active phases tested for the steam reforming of acetic acid, nickel resulted to be the best choice. In particular, a Ni loading of 10 wt % showed a good tradeoff between acetic acid conversion and resistance to deactivation. Furthermore, the addition of a second metallic phase (i.e., 7 wt % of cobalt) greatly improved the catalyst activity and stability.
2. The bimetallic Co–Ni-based catalyst was also tested for steam reforming of a pyrolysis oil model mixture containing water, acetone, ethanol, acetic acid, and eugenol. Results showed a severe catalyst deactivation after a few minutes of run time, where conversion decreased from 50% to a steady value of 30%. This could be attributed to catalyst poisoning caused by the adsorption of relatively heavy compounds derived from the decomposition of eugenol.
3. Due to the presence of sugar-derived compounds, which led to a rapid deactivation of the catalyst, the real slow pyrolysis was distilled in order to be tested in steam reforming experiments. For this liquid feed, it was possible to obtain a total carbon conversion of 65% and a selectivity toward hydrogen of 55% by properly setting the operating conditions (temperature and liquid space velocity). A 2-step long-time stability test revealed that, despite the presence of heavier organic compounds adsorbed on the catalyst, both the conversion and hydrogen yield remained reasonably constant over time, indicating good stability of the catalyst. Further investigations will be required to further fine-tuning the operating conditions and evaluate the performance of the catalysts for even longer periods of time.

Declaration of competing interest

The authors declare that they have no known competing financial interests or personal relationships that could have appeared to influence the work reported in this paper.

Acknowledgments

This project received funding from the European Union's Horizon 2020 research and innovation programme under the Marie Skłodowska-Curie grant agreement No 721991. The authors also acknowledge the funding from the Aragón Government (Ref. T22_20R), co-funded by FEDER 2014–2020 "Construyendo Europa desde Aragón". The authors gratefully thank José Antonio Manso and Olga Marín for their help in the preparation and characterization of the samples. Authors would like to acknowledge the use of Servicio General de Apoyo a la Investigación-SAI, Universidad de Zaragoza.

Nomenclature

d_p	Pore diameter (nm)
F_c	Carbon molar flow rate (mol min^{-1})
F_i	Products molar flow rate (mol min^{-1})
F_{iEq}	Products molar flow rate at equilibrium conditions (mol min^{-1})
Q_{mix}	Volume flow rate of the liquid blend (mL h^{-1})
S/C	Steam to carbon molar ratio
S_i	Product selectivity (%)
S_L	Langmuir surface area (m^2 g^{-1})
V_{cat}	Catalyst volume (mL)
V_{meso}	Volume of mesopores (cm^3 g^{-1})
V_{micro}	Volume of micropores (cm^3 g^{-1})
V_{tot}	Total pore volume (cm^3 g^{-1})
X_{AcOH}	Acetic acid conversion in acetic acid steam reforming (%)
X_c	Carbon conversion (%)
Y_{Ac*}	Acetone yield in acetic acid steam reforming (%)
Y_{H2*}	Hydrogen yield in acetic acid steam reforming (%)
Y_i	Product yield (%)

Acronyms

AcOH	Acetic Acid
CHN	Ultimate analysis
CO_2-TPD	CO_2 temperature programmed desorption
DRIFT	Diffuse reflectance *infrared* fourier transform spectroscopy
LHSV	Liquid hourly space velocity; LHSV = Q_{mix} V_{cat}^{-1}
NLDFT	Non-local density functional theory
PSD	Pore size distribution
TCD	Thermal conductivity detector
TEM	Transmission electron microscopy
TPR	Temperature programmed reduction
XRF	X-ray fluorescence spectroscopy
μ-GC	Micro gas chromatograph

Appendix A. Supplementary data

Supplementary data to this article can be found online at https://doi.org/10.1016/j.ijhydene.2021.05.193.

REFERENCES

[1] Gentile G, Debiagi PEA, Cuoci A, Frassoldati A, Ranzi E, Faravelli T. A computational framework for the pyrolysis of anisotropic biomass particles. Chem Eng J 2017;321:458–73. https://doi.org/10.1016/j.cej.2017.03.113.

[2] Debiagi P, Gentile G, Cuoci A, Frassoldati A, Ranzi E, Faravelli T. A predictive model of biochar formation and characterization. J Anal Appl Pyrolysis 2018;134:326–35. https://doi.org/10.1016/j.jaap.2018.06.022.

[3] Anca-Couce A, Scharler R. Modelling heat of reaction in biomass pyrolysis with detailed reaction schemes. Fuel 2017;206:572–9. https://doi.org/10.1016/j.fuel.2017.06.011.

[4] Xiu S, Shahbazi A. Bio-oil production and upgrading research: a review. Renew Sustain Energy Rev 2012;16:4406–14. https://doi.org/10.1016/j.rser.2012.04.028.

[5] Santamaria L, Lopez G, Arregi A, Amutio M, Artetxe M, Bilbao J, et al. Influence of the support on Ni catalysts performance in the in-line steam reforming of biomass fast pyrolysis derived volatiles. Appl Catal B Environ 2018;229:105–13. https://doi.org/10.1016/j.apcatb.2018.02.003.

[6] Phongprueksathat N, Meeyoo V, Rirksomboon T. Steam reforming of acetic acid for hydrogenproduction : catalytic performances of Ni and Co supported on Ce0·75Zr0·25O2 catalysts. Int J Hydrogen Energy 2019;44:9359–67. https://doi.org/10.1016/j.ijhydene.2019.02.085.

[7] Sueyasu T, Oike T, Mori A, Kudo S, Norinaga K, Hayashi JI. Simultaneous steam reforming of tar and steam gasification of char from the pyrolysis of potassium-loaded woody biomass. Energy Fuels 2012;26:199–208. https://doi.org/10.1021/ef201166a.

[8] Hu X, Lu G. Investigation of the steam reforming of a series of model compounds derived from bio-oil for hydrogen production. Appl Catal B Environ 2009;88:376–85. https://doi.org/10.1016/j.apcatb.2008.10.021.

[9] Trane-Restrup R, Jensen AD. Steam reforming of cyclic model compounds of bio-oil over Ni-based catalysts: product distribution and carbon formation. Appl Catal B Environ 2015;165:117–27. https://doi.org/10.1016/j.apcatb.2014.09.026.

[10] Augusto BL, Ribeiro MC, Aires FJCS, da Silva VT, Noronha FB. Hydrogen production by the steam reforming of ethanol over cobalt catalysts supported on different carbon nanostructures. Catal Today 2020;344:66–74. https://doi.org/10.1016/j.cattod.2018.10.029.

[11] Vagia EC, Lemonidou AA. Hydrogen production via steam reforming of bio-oil components over calcium aluminate supported nickel and noble metal catalysts. Appl Catal Gen 2008;351:111–21. https://doi.org/10.1016/j.apcata.2008.09.007.

[12] Shen Y, Zhao P, Shao Q, Takahashi F, Yoshikawa K. In situ catalytic conversion of tar using rice husk char/ash supported nickel-iron catalysts for biomass pyrolytic gasification combined with the mixing-simulation in fluidized-bed gasifier. Appl Energy 2015;160:808–19. https://doi.org/10.1016/j.apenergy.2014.10.074.

[13] Song H, Zhang L, Watson RB, Braden D, Ozkan US. Investigation of bio-ethanol steam reforming over cobalt-based catalysts. Catal Today 2007;129:346–54. https://doi.org/10.1016/j.cattod.2006.11.028.

[14] Lin SSY, Kim DH, Ha SY. Metallic phases of cobalt-based catalysts in ethanol steam reforming: the effect of cerium oxide. Appl Catal Gen 2009;355:69–77. https://doi.org/10.1016/j.apcata.2008.11.032.

[15] Zhang Z, Hu X, Zhang L, Yang Y, Li Q, Fan H, et al. Steam reforming of guaiacol over Ni/Al2O3 and Ni/SBA-15: impacts of support on catalytic behaviors of nickel and properties of coke. Fuel Process Technol 2019;191:138–51. https://doi.org/10.1016/j.fuproc.2019.04.001.

[16] An L, Dong C, Yang Y, Zhang J, He L. The influence of Ni loading on coke formation in steam reforming of acetic acid. Renew Energy 2011;36:930–5. https://doi.org/10.1016/j.renene.2010.08.029.

[17] Coll R, Salvadó J, Farriol X, Montané D. Steam reforming model compounds of biomass gasification tars: conversion at different operating conditions and tendency towards coke formation. Fuel Process Technol 2001;74:19–31. https://doi.org/10.1016/S0378-3820(01)00214-4.

[18] Chen J, Sun J, Wang Y. Catalysts for steam reforming of bio-oil: a review. Ind Eng Chem Res 2017;56:4627–37. https://doi.org/10.1021/acs.iecr.7b00600.

[19] Xiong X, Yu IKM, Cao L, Tsang DCW, Zhang S, Ok YS. A review of biochar-based catalysts for chemical synthesis, biofuel production, and pollution control. Bioresour Technol 2017;246:254–70. https://doi.org/10.1016/j.biortech.2017.06.163.

[20] Qian K, Kumar A, Zhang H, Bellmer D, Huhnke R. Recent advances in utilization of biochar. Renew Sustain Energy Rev 2015;42:1055–64. https://doi.org/10.1016/j.rser.2014.10.074.

[21] Lee J, Kim KH, Kwon EE. Biochar as a catalyst. Renew Sustain Energy Rev 2017;77:70–9. https://doi.org/10.1016/j.rser.2017.04.002.

[22] Dufour A, Celzard A, Fierro V, Martin E, Broust F, Zoulalian A. Catalytic decomposition of methane over a wood char concurrently activated by a pyrolysis gas. Appl Catal Gen 2008;346:164–73. https://doi.org/10.1016/j.apcata.2008.05.023.

[23] Shen Y. Chars as carbonaceous adsorbents/catalysts for tar elimination during biomass pyrolysis or gasification. Renew Sustain Energy Rev 2015;43:281–95. https://doi.org/10.1016/j.rser.2014.11.061.

[24] Manyà JJ, Azuara M, Manso JA. Biochar production through slow pyrolysis of different biomass materials: seeking the best operating conditions. Biomass Bioenergy 2018;117:115–23. https://doi.org/10.1016/j.biombioe.2018.07.019.

[25] Shan R, Han J, Gu J, Yuan H, Luo B, Chen Y. A review of recent developments in catalytic applications of biochar-based materials. Resour Conserv Recycl 2020;162:105036. https://doi.org/10.1016/j.resconrec.2020.105036.

[26] Di Stasi C, Alvira D, Greco G, González B, Manyà JJ. Physically activated wheat straw-derived biochar for biomass pyrolysis vapors upgrading with high resistance against coke deactivation. Fuel 2019;255:115807. https://doi.org/10.1016/j.fuel.2019.115807.

[27] Liu WJ, Jiang H, Yu HQ. Development of biochar-based functional materials: toward a sustainable platform carbon. Material. Chem Rev 2015;115:12251–85. https://doi.org/10.1021/acs.chemrev.5b00195.

[28] Di Stasi C, Greco G, Canevesi RLS, Izquierdo MT, Fierro V, Celzard A, et al. Influence of activation conditions on textural properties and performance of activated biochars for pyrolysis vapors upgrading. Fuel 2020:119759. https://doi.org/10.1016/j.fuel.2020.119759.

[29] Lee J, Kim KH, Kwon EE. Biochar as a catalyst. Renew Sustain Energy Rev 2017;77:70–9. https://doi.org/10.1016/j.rser.2017.04.002.

[30] Buentello-Montoya D, Zhang X, Li J, Ranade V, Marques S, Geron M. Performance of biochar as a catalyst for tar steam reforming: effect of the porous structure. Appl Energy 2020;259:114176. https://doi.org/10.1016/j.apenergy.2019.114176.

[31] Quan C, Wang H, Gao N. Development of activated biochar supported Ni catalyst for enhancing toluene steam reforming. Int J Energy Res 2020;44:5749–64. https://doi.org/10.1002/er.5335.

[32] Wang Y, Zhang Z, Zhang S, Wang Y, Hu S, Xiang J, et al. Steam reforming of acetic acid over Ni/biochar catalyst treated with HNO3: impacts of the treatment on surface properties and catalytic behaviors. Fuel 2020;278:118341. https://doi.org/10.1016/j.fuel.2020.118341.
[33] Greco G, Di Stasi C, Rego F, González B, Manyà JJ. Effects of slow-pyrolysis conditions on the products yields and properties and on exergy efficiency: a comprehensive assessment for wheat straw. Appl Energy 2020;279:115842. https://doi.org/10.1016/j.apenergy.2020.115842.
[34] Greco G, Videgain M, Di Stasi C, González B, Manyà JJ. Evolution of the mass-loss rate during atmospheric and pressurized slow pyrolysis of wheat straw in a bench-scale reactor. J Anal Appl Pyrolysis 2018;136:18–26. https://doi.org/10.1016/j.jaap.2018.11.007.
[35] Song X, Li K, Wang C, Sun X, Ning P, Tang L. Regeneration performance and mechanism of modified walnut shell biochar catalyst for low temperature catalytic hydrolysis of organic sulfur. Chem Eng J 2017;330:727–35. https://doi.org/10.1016/j.cej.2017.08.016.
[36] Wan HJ, Wu BS, Zhang CH, Xiang HW, Li YW, Xu BF, et al. Study on Fe-Al2O3 interaction over precipitated iron catalyst for Fischer-Tropsch synthesis. Catal Commun 2007;8:1538–45. https://doi.org/10.1016/j.catcom.2007.01.002.
[37] Paasikallio V, Kihlman J, Sánchez CA, Simell P, Solantausta Y, Lehtonen J. Steam reforming of pyrolysis oil aqueous fraction obtained by one-step fractional condensation. Int J Hydrogen Energy 2015;40:3149–57. https://doi.org/10.1016/j.ijhydene.2015.01.025.
[38] Cakiryilmaz N, Arbag H, Oktar N, Dogu G, Dogu T. Catalytic performances of Ni and Cu impregnated MCM-41 and Zr-MCM-41 for hydrogen production through steam reforming of acetic acid. Catal Today 2019;323:191–9. https://doi.org/10.1016/j.cattod.2018.06.004.
[39] Fu P, Zhang A, Luo S, Yi W, Hu S, Zhang Y. Catalytic steam reforming of biomass-derived acetic acid over two supported Ni catalysts for hydrogen-rich syngas production. ACS Omega 2019;4:13585–93. https://doi.org/10.1021/acsomega.9b01985.
[40] Lozano P, Simón A, García L, Ruiz J, Oliva M, Arauzo J. Influence of the Ni-Co/Al-Mg catalyst loading in the continuous aqueous phase reforming of the bio-oil aqueous fraction. Processes 2021;9:81. https://doi.org/10.3390/pr9010081.
[41] Zhang Z, Zhang X, Zhang L, Wang Y, Li X, Zhang S, et al. Steam reforming of guaiacol over Ni/SiO2 catalyst modified with basic oxides: impacts of alkalinity on properties of coke. Energy Convers Manag 2020;205:112301. https://doi.org/10.1016/j.enconman.2019.112301.
[42] Ma Z, Xiao R, Zhang H. Catalytic steam reforming of bio-oil model compounds for hydrogen-rich gas production using bio-char as catalyst. Int J Hydrogen Energy 2017;42:3579–85. https://doi.org/10.1016/j.ijhydene.2016.11.107.
[43] Jiang L, Hu S, Wang Y, Su S, Sun L, Xu B, et al. Catalytic effects of inherent alkali and alkaline earth metallic species on steam gasification of biomass. Int J Hydrogen Energy 2015;40:15460–9. https://doi.org/10.1016/j.ijhydene.2015.08.111.
[44] Wang Y, Zhang Z, Zhang S, Wang Y, Hu S, Xiang J, et al. Steam reforming of acetic acid over Ni/biochar catalyst treated with HNO3: impacts of the treatment on surface properties and catalytic behaviors. Fuel 2020;278:118341. https://doi.org/10.1016/j.fuel.2020.118341.
[45] Ji Y, Zhao Z, Duan A, Jiang G, Liu J. Comparative study on the formation and reduction of bulk and Al 2O3-supported cobalt oxides by H2-TPR technique. J Phys Chem C 2009;113:7186–99. https://doi.org/10.1021/jp8107057.
[46] Melnikov P, Nascimento VA, Arkhangelsky IV, Zanoni Consolo LZ, De Oliveira LCS. Thermal decomposition mechanism of iron(III) nitrate and characterization of intermediate products by the technique of computerized modeling. J Therm Anal Calorim 2014;115:145–51. https://doi.org/10.1007/s10973-013-3339-1.
[47] Brockner W, Ehrhardt C, Gjikaj M. Thermal decomposition of nickel nitrate hexahydrate, Ni(NO3)2·6H2O, in comparison to Co(NO3)2·6H2O and Ca(NO3)2·4H2O. Thermochim Acta 2007;456:64–8. https://doi.org/10.1016/j.tca.2007.01.031.
[48] Li D, Zhao L, Cao X, Xiao Z, Nan H, Qiu H. Nickel-catalyzed formation of mesoporous carbon structure promoted capacitive performance of exhausted biochar. Chem Eng J 2021;406:126856. https://doi.org/10.1016/j.cej.2020.126856.
[49] Chen J, Wang M, Wang S, Li X. Hydrogen production via steam reforming of acetic acid over biochar-supported nickel catalysts. Int J Hydrogen Energy 2018;43:18160–8. https://doi.org/10.1016/j.ijhydene.2018.08.048.
[50] Nguyen HKD, Pham VV, Do HT. Preparation of Ni/biochar catalyst for hydrotreating of bio-oil from microalgae biomass. Catal Lett 2016;146:2381–91. https://doi.org/10.1007/s10562-016-1873-8.
[51] Martínez R, Romero E, Guimon C, Bilbao R. CO2 reforming of methane over coprecipitated Ni-Al catalysts modified with lanthanum. Appl Catal Gen 2004;274:139–49. https://doi.org/10.1016/j.apcata.2004.06.017.
[52] Taghavi S, Tavasoli A, Asghari A, Signoretto M. Loading and promoter effects on the performance of nitrogen functionalized graphene nanosheets supported cobalt Fischer-Tropsch synthesis catalysts. Int J Hydrogen Energy 2019;44:10604–15. https://doi.org/10.1016/j.ijhydene.2019.03.015.
[53] de Barros Dias Moreira J, Bastos de Rezende D, Márcia Duarte Pasa V. Deoxygenation of Macauba acid oil over Co-based catalyst supported on activated biochar from Macauba endocarp: a potential and sustainable route for green diesel and biokerosene production. Fuel 2020;269:117253. https://doi.org/10.1016/j.fuel.2020.117253.
[54] Chew LM, Kangvansura P, Ruland H, Schulte HJ, Somsen C, Xia W, et al. Effect of nitrogen doping on the reducibility, activity and selectivity of carbon nanotube-supported iron catalysts applied in CO2 hydrogenation. Appl Catal Gen 2014;482:163–70. https://doi.org/10.1016/j.apcata.2014.05.037.
[55] Tavasoli A, Barati M, Karimi A. Conversion of sugarcane bagasse to gaseous and liquid fuels in near-critical water media using K2O promoted Cu/γ-Al2O3-MgO nanocatalysts. Biomass Bioenergy 2015;80:63–72. https://doi.org/10.1016/j.biombioe.2015.04.031.
[56] Alipour Z, Meshkani F, Rezaei M. Effect of K2O on the catalytic performance of Ni catalysts supported on nanocrystalline Al 2O3 in CO2 reforming of methane. Iran J Hydrog Fuel Cell 2015;4:215–26.
[57] Yang M, Lingjun Z, Xiaonan Z, Prasert R, Shurong W. CO2 methanation over nickel-based catalysts supported on MCM-41 with in situ doping of zirconium. J CO2 Util 2020;42:101304. https://doi.org/10.1016/j.jcou.2020.101304.
[58] Liu X, Sun L, Deng WQ. Theoretical investigation of CO2 adsorption and dissociation on low index surfaces of transition metals. J Phys Chem C 2018;122:8306–14. https://doi.org/10.1021/acs.jpcc.7b12660.
[61] Nabgan W, Tuan Abdullah TA, Mat R, Nabgan B, Gambo Y, Triwahyono S. Influence of Ni to Co ratio supported on ZrO2 catalysts in phenol steam reforming for hydrogen production. Int J Hydrogen Energy 2016;41:22922–31. https://doi.org/10.1016/j.ijhydene.2016.10.055.
[62] Turap Y, Wang I, Fu T, Wu Y, Wang Y, Wang W. Co–Ni alloy supported on CeO2 as a bimetallic catalyst for dry reforming

of methane. Int J Hydrogen Energy 2020;45:6538–48. https://doi.org/10.1016/j.ijhydene.2019.12.223.
[63] Ochoa A, Bilbao J, Gayubo AG, Castaño P. Coke formation and deactivation during catalytic reforming of biomass and waste pyrolysis products: a review. Renew Sustain Energy Rev 2020;119:109600. https://doi.org/10.1016/j.rser.2019.109600.
[64] Navarro RM, Guil-Lopez R, Ismail AA, Al-Sayari SA, Fierro JLG. Ni- and PtNi-catalysts supported on Al2O3 for acetone steam reforming: effect of the modification of support with Ce, La and Mg. Catal Today 2015;242:60–70. https://doi.org/10.1016/j.cattod.2014.07.036.
[65] Zhang Z, Hu X, Li J, Gao G, Dong D, Westerhof R, et al. Steam reforming of acetic acid over Ni/Al2O3 catalysts: correlation of nickel loading with properties and catalytic behaviors of the catalysts. Fuel 2018;217:389–403. https://doi.org/10.1016/j.fuel.2017.12.114.
[66] Wang Z, Wang C, Chen S, Liu Y. Co-Ni bimetal catalyst supported on perovskite-type oxide for steam reforming of ethanol to produce hydrogen. Int J Hydrogen Energy 2014;39:5644–52. https://doi.org/10.1016/j.ijhydene.2014.01.151.
[67] Megía PJ, Cortese M, Ruocco C, Vizcaíno AJ, Calles JA, Carrero A, et al. Catalytic behavior of co-based catalysts in the kinetic study of acetic acid steam reforming. Ind Eng Chem Res 2020;59:19531–8. https://doi.org/10.1021/acs.iecr.0c03599.
[68] Kumar A, Sinha ASK. Hydrogen production from acetic acid steam reforming over nickel-based catalyst synthesized via MOF process. Int J Hydrogen Energy 2020;45:24397–411. https://doi.org/10.1016/j.ijhydene.2020.06.040.
[69] Fu M, Qi W, Xu Q, Zhang S, Yan Y. Hydrogen production from bio-oil model compounds dry (CO2) reforming over Ni/Al2O3 catalyst. Int J Hydrogen Energy 2016;41:1494–501. https://doi.org/10.1016/j.ijhydene.2015.11.104.
[70] Vizcaíno AJ, Carrero A, Calles JA. Hydrogen production by ethanol steam reforming over Cu-Ni supported catalysts. Int J Hydrogen Energy 2007;32:1450–61. https://doi.org/10.1016/j.ijhydene.2006.10.024.
[71] Afolabi ATF, Kechagiopoulos PN, Liu Y, Li CZ. Kinetic features of ethanol steam reforming and decomposition using a biochar-supported Ni catalyst. Fuel Process Technol 2021;212:106622. https://doi.org/10.1016/j.fuproc.2020.106622.
[72] Comas J, Marino F, Laborde M, Amadeo N. Bio-ethanol steam reforming on Ni/Al2O3 catalyst. Chem Eng J 2004;98:61–8. https://doi.org/10.1016/S1385-8947(03)00186-4.
[73] Lahijani P, Zainal ZA, Mohammadi M, Mohamed AR. Conversion of the greenhouse gas CO2 to the fuel gas CO via the Boudouard reaction: a review. Renew Sustain Energy Rev 2015;41:615–32. https://doi.org/10.1016/j.rser.2014.08.034.
[74] Ledesma EB, Campos C, Cranmer DJ, Foytik BL, Ton MN, Dixon EA, et al. Vapor-phase cracking of eugenol: distribution of tar products as functions of temperature and residence time. Energy Fuels 2013;27:868–78. https://doi.org/10.1021/ef3018332.
[75] Lu P, Qian X, Huang Q, Chi Y, Yan J. Catalytic cracking of toluene as a tar model compound using sewage-sludge-derived char. Energy Fuels 2016;30:8327–34. https://doi.org/10.1021/acs.energyfuels.6b01832.
[76] Li J, Mei X, Zhang L, Yu Z, Liu Q, Wei T, et al. A comparative study of catalytic behaviors of Mn, Fe, Co, Ni, Cu and Zn–Based catalysts in steam reforming of methanol, acetic acid and acetone. Int J Hydrogen Energy 2020;45:3815–32. https://doi.org/10.1016/j.ijhydene.2019.03.269.
[77] Hu X, Dong D, Shao X, Zhang L, Lu G. Steam reforming of acetic acid over cobalt catalysts: effects of Zr, Mg and K addition. Int J Hydrogen Energy 2017;42:4793–803. https://doi.org/10.1016/j.ijhydene.2016.12.033.
[78] Wu Y, Pang Y, Chen Y, Zhai M, Zheng M. Study on the steam gasification reaction of biomass char under the synergistic effect of Ca-Fe: analysis of kinetic characteristics. Int J Energy Res 2021:1–15. https://doi.org/10.1002/er.6366.
[79] Wanke SE, Flynn PC. The sintering of supported metal catalysts. Catal Rev 1975;12:93–135. https://doi.org/10.1080/01614947508067523.
[80] Kumar A, Sinha ASK. Hydrogen production from acetic acid steam reforming over nickel-based catalyst synthesized via MOF process. Int J Hydrogen Energy 2020;45:24397–411. https://doi.org/10.1016/j.ijhydene.2020.06.040.
[81] Mahamulkar S, Yin K, Agrawal PK, Davis RJ, Jones CW, Malek A, et al. Formation and oxidation/gasification of carbonaceous deposits: a review. Ind Eng Chem Res 2016;55:9760–818. https://doi.org/10.1021/acs.iecr.6b02220.
[82] Santamaria L, Artetxe M, Lopez G, Cortazar M, Amutio M, Bilbao J, et al. Effect of CeO2 and MgO promoters on the performance of a Ni/Al2O3 catalyst in the steam reforming of biomass pyrolysis volatiles. Fuel Process Technol 2020;198:106223. https://doi.org/10.1016/j.fuproc.2019.106223.
[83] Hervy M, Weiss-Hortala E, Pham Minh D, Dib H, Villot A, Gérente C, et al. Reactivity and deactivation mechanisms of pyrolysis chars from bio-waste during catalytic cracking of tar. Appl Energy 2019;237:487–99. https://doi.org/10.1016/j.apenergy.2019.01.021.
[84] Chen J, Wang M, Wang S, Li X. Hydrogen production via steam reforming of acetic acid over biochar-supported nickel catalysts. Int J Hydrogen Energy 2018;43:18160–8. https://doi.org/10.1016/j.ijhydene.2018.08.048.
[85] Da Silva ALM, Den Breejen JP, Mattos LV, Bitter JH, De Jong KP, Noronha FB. Cobalt particle size effects on catalytic performance for ethanol steam reforming - smaller is better. J Catal 2014;318:67–74. https://doi.org/10.1016/j.jcat.2014.07.020.
[86] Chang JR, Chang SL, Lin TB. γ-Alumina-supported Pt catalysts for aromatics reduction: a structural investigation of sulfur poisoning catalyst deactivation. J Catal 1997;169:338–46. https://doi.org/10.1006/jcat.1997.1709.
[87] Marquevich M, Czernik S, Chornet E, Montané D. Hydrogen from biomass: steam reforming of model compounds of fast-pyrolysis oil. Energy Fuels 1999;13:1160–6. https://doi.org/10.1021/ef990034w.
[88] Belin T, Epron F. Characterization methods of carbon nanotubes: a review. Mater Sci Eng B 2005;119:105–18. https://doi.org/10.1016/j.mseb.2005.02.046.
[89] Liu W, Chai S, Mohamed AR, Hashim U. Synthesis and characterization of graphene and carbon nanotubes: a review on the past and recent developments. J Ind Eng Chem 2014;20:1171–85. https://doi.org/10.1016/j.jiec.2013.08.028.
[90] Hu X, Wang Y, Mourant D, Gunawan R, Lievens C, Chaiwat W, et al. Polymerization on heating up of bio-oil: a model compound study. AIChE J 2013;59:888–900. https://doi.org/10.1002/aic.13857.
[91] Zhang L, Yu Z, Li J, Zhang S, Hu S, Xiang J, et al. Steam reforming of typical small organics derived from bio-oil: correlation of their reaction behaviors with molecular structures. Fuel 2020;259:116214. https://doi.org/10.1016/j.fuel.2019.116214.

Appendix A: supplementary material

Optimization of the operating conditions for steam reforming of slow pyrolysis oil over an activated biochar-supported Ni-Co catalyst

Christian Di Stasi[1*], *Marta Cortese*[2], *Gianluca Greco*[1], *Simona Renda*[2], *Belén González*[1], *Vincenzo Palma*[2], *Joan J. Manyà*[1]

[1] Aragón Institute of Engineering Research (I3A), Thermochemical Processes Group, University of Zaragoza, Escuela Politécnica Superior, Crta. Cuarte s/n, 22071 Huesca, Spain

[2] University of Salerno, Department of Industrial Engineering, Via Giovanni Paolo II 132, 84084, Fisciano (SA), Italy

[*] Corresponding author at: *Aragón Institute of Engineering Research (I3A), Thermochemical Processes Group, University of Zaragoza, Technological College of Huesca, Crta. Cuarte s/n, 22071 Huesca, Spain*

E-mail address: christiandistasi@unizar.es.

CO_2-TPD analysis

From the comparison between the desorption profiles obtained for the activated biochar (BC) and the monometallic catalysts, one can distinguish between the adsorption sites of the BC support itself and those observed for each active specie. As shown in Fig. A.1, BC presents mainly weak and strong basic adsorption sites, and only a modest amount of medium basic sites (which could also be ascribable to the shoulder of the weak adsorption sites). The addition of either Ni or Co to BC resulted in a remarkable increase in the weak basic sites and the formation of a large number of medium basic sites. For their part, the number of strong basic sites was reduced, especially when Ni was used as metal active phase. This could indicate that such sites are the ones involved in the direct bond between the support and the metallic phases. With regard to the addition of Ce, Fe and K, Fig. A.1 also shows a decrease in the number of strong basic sites; however, the creation of new medium basic sites was not as marked as in the case of Ni or Co.

Concerning the bimetallic formulations, their CO_2 desorption profiles were almost comparable to that of the BC in terms of signal intensity. Since the bimetallic BC-supported catalysts were prepared via two impregnation steps (with Ni always added through the second impregnation), it seems that Ni arrangement onto the surface was different in bimetallic formulations, leading to just a slight increase in weak and medium basic sites (see Fig. A.5). For the specific case of the BCCoNi catalyst, several CO_2 desorption peaks were observed, suggesting that different types of active sites are present in the catalyst.

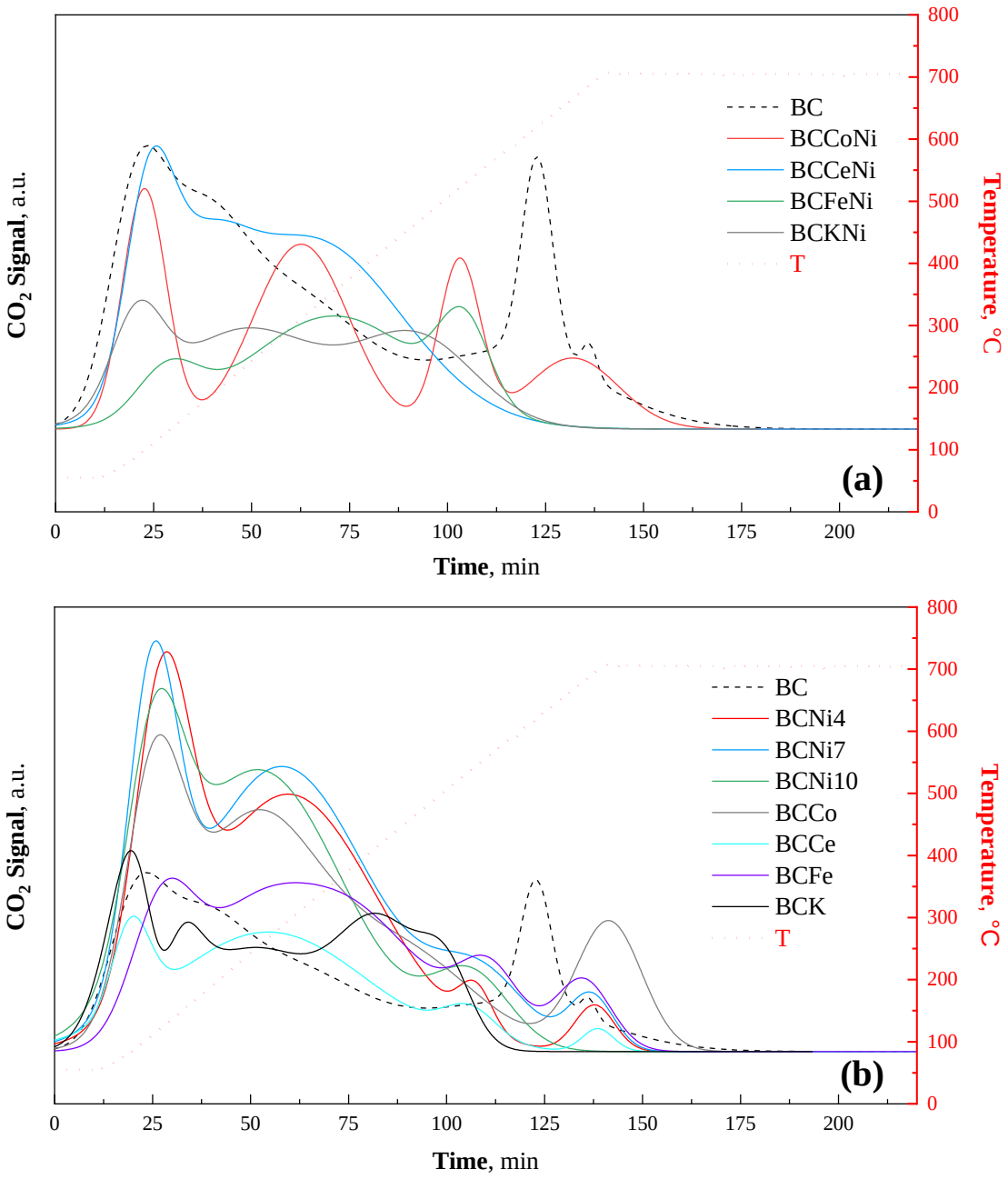

Fig. A.1. Temperature programmed CO_2 desorption results obtained: bimetallic (a), and monometallic (b) catalysts.

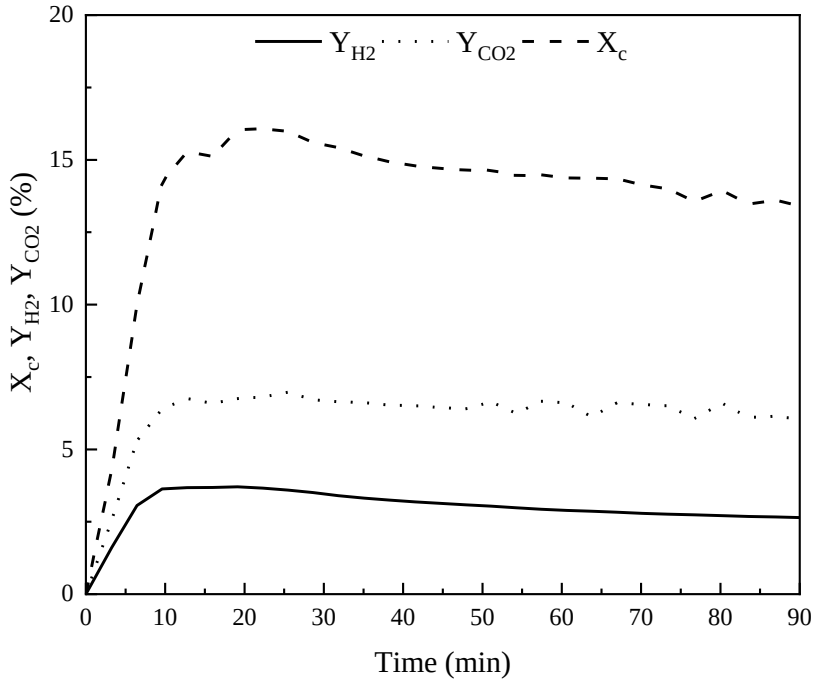

Fig. A.2. Results obtained during the steam reforming of the model mixture at 600 °C and at a LHSV of 2.94 h^{-1} over activated biochar (BC).

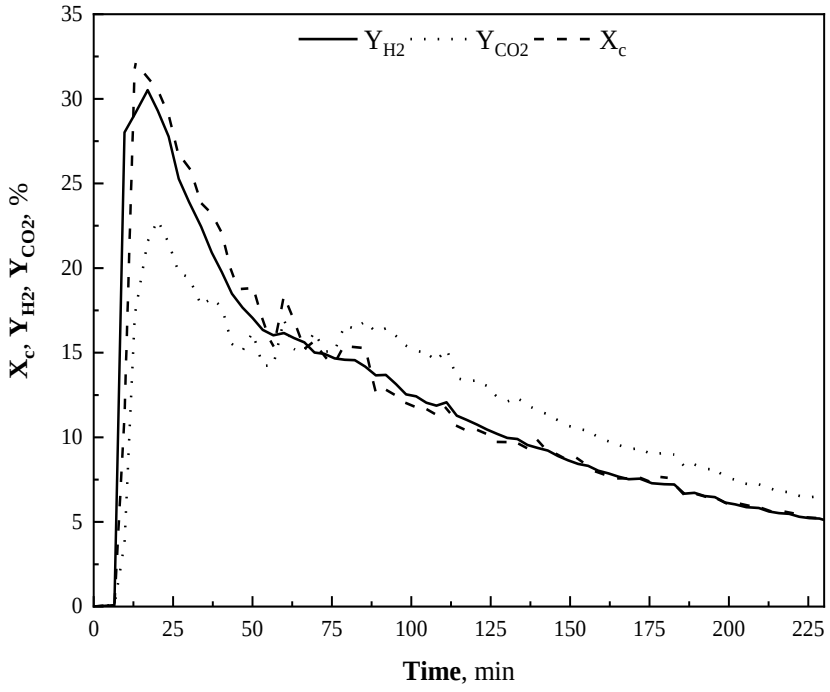

Fig. A.3. Catalytic behavior of the BCCoNi catalyst during a steam reforming experiment of the model mixture at 600°C, 2.94 h^{-1} (LHSV) and using a relatively high flow rate of carrier gas (N_2).

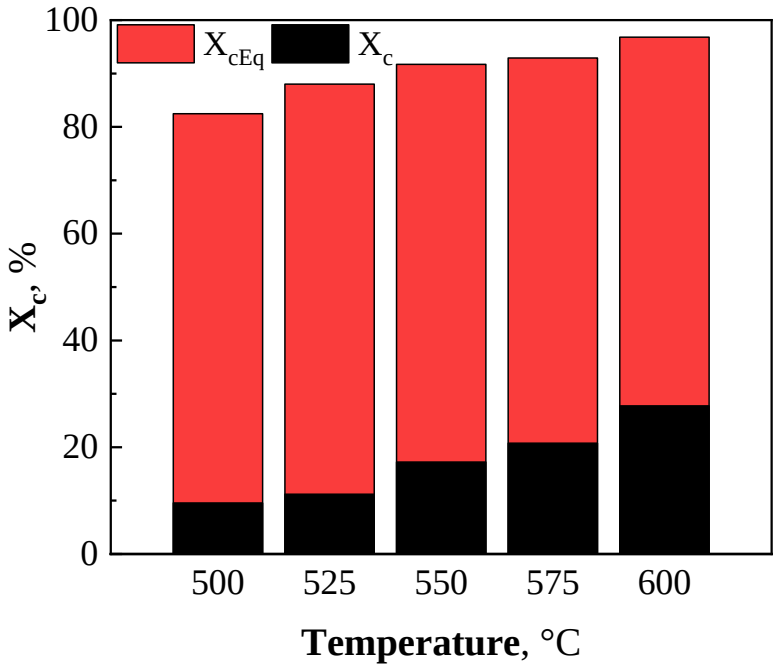

Fig. A.4. Experimental (X_c) and maximum (X_{cEq}) conversion values obtained during the for steam reforming tests of the model mixture over the BCCoNi catalyst at 2.94 h^{-1} and different temperatures in the range of 500−600 °C.

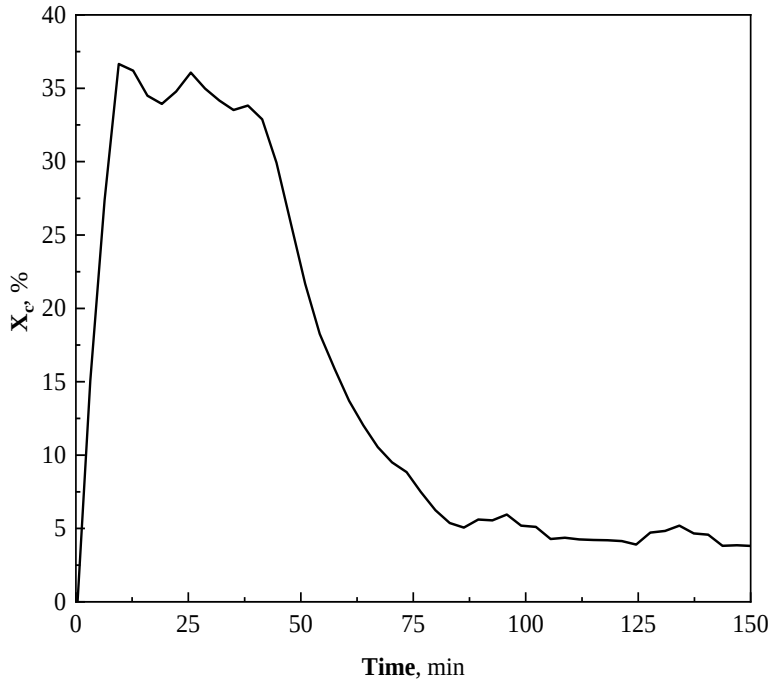

Fig. A.5. Carbon conversion obtained during the steam reforming (at 600°C and a LHSV of 2.94 h^{-1}) of real pyrolysis oil over BCCoNi catalyst.

6.4. Ni-based catalyst supported on activated biochar and ceria for CO_2 methanation

Once assessed the feasibility of using biochar as catalytic support, its implementation in CCU processes was investigated (objective IV). To this aim, ceria and urea-doped activated biochars were used as support of Ni-based catalysts for CO_2 methanation purposes. Several samples were prepared and tested to identify the optimal contents of CeO_2 and Ni. After several CO_2 methanation experiments carried out at 0.35–1.0 MPa and 300–500 °C, it was found that the most suitable catalyst was a wheat straw-derived activated biochar loaded with 30 wt. % of CeO_2 and 20 wt. % of Ni. Using this catalyst, a CO_2 conversion of 65% with a CH_4 selectivity of 95% was reached at 1.0 MPa, 400 °C, and 13200 h^{-1}. From the study of the influence of the GHSV, it was deduced that the most likely reaction mechanism was reverse water-gas shift reaction followed by CO hydrogenation. A comparison with other catalysts reported in the literature showed that the activated biochar doped with CeO_2 could be considered as a valid alternative to the commonly used supports.

N-doping of the carbon support as an alternative to the use of ceria was also investigated. Even though using urea as a dopant resulted in the introduction of nitrogenated functionalities in the surface of BC, the improvement of the catalytic activity of the resulting catalyst was modest in comparison to that attained when ceria was used as dopant.

In conclusion, the outcomes of this work indicate that biochar could also be employed as a renewable biomass-derived support for the catalytic conversion of CO_2 to methane. This result could expand the possible application fields of biochar and, consequently, its intrinsic value.

sustainability

MDPI

Article

Wheat-Straw-Derived Activated Biochar as a Renewable Support of Ni-CeO_2 Catalysts for CO_2 Methanation

Christian Di Stasi [1,*], Simona Renda [2], Gianluca Greco [1], Belén González [1], Vincenzo Palma [2] and Joan J. Manyà [1]

[1] Aragón Institute of Engineering Research (I3A), Thermochemical Processes Group, Escuela Politécnica Superior-University of Zaragoza, Crta. Cuarte s/n, 22071 Huesca, Spain; greco@unizar.es (G.G.); belenglez@unizar.es (B.G.); joanjoma@unizar.es (J.J.M.)

[2] Department of Industrial Engineering, University of Salerno, Via Giovanni Paolo II 132, 84084 Fisciano, SA, Italy; srenda@unisa.it (S.R.); vpalma@unisa.it (V.P.)

* Correspondence: christiandistasi@unizar.es

Abstract: Ceria- and urea-doped activated biochars were used as support for Ni-based catalysts for CO_2 methanation purposes. Different materials were prepared and tested to find the best catalytic formulation. After several CO_2 methanation experiments—carried out at 0.35–1.0 MPa and 300–500 °C—it was found that the most suitable catalyst was a wheat-straw-derived activated biochar loaded with 30 wt.% of CeO_2 and 20 wt.% of Ni. Using this catalyst, a CO_2 conversion of 65% with a CH_4 selectivity of 95% was reached at 1.0 MPa, 400 °C, and 13,200 h^{-1}. From the study of the influence of the gas hourly space velocity, it was deduced that the most likely reaction mechanism was a reverse water–gas shift reaction, followed by CO hydrogenation. N-doping of the carbon support as an alternative to the use of ceria was also investigated. However, both CO_2 conversion and selectivity toward CH_4 values were clearly lower than those obtained for the ceria-containing catalyst cited above. The outcomes of this work indicate that a renewable biomass-derived support can be effectively employed in the catalytic conversion of CO_2 to methane.

Keywords: CO_2 methanation; Sabatier reaction; biochar; urea; ceria

Citation: Di Stasi, C.; Renda, S.; Greco, G.; González, B.; Palma, V.; Manyà, J.J. Wheat-Straw-Derived Activated Biochar as a Renewable Support of Ni-CeO_2 Catalysts for CO_2 Methanation. *Sustainability* **2021**, *13*, 8939. https://doi.org/10.3390/su13168939

Academic Editors: Matthew Jones and Changhyun Roh

Received: 30 June 2021
Accepted: 6 August 2021
Published: 10 August 2021

1. Introduction

Since the second industrial revolution, human civilization started to be highly dependent on fossil fuels. Their continuous exploitation resulted in the increase in the atmospheric CO_2 content, which is associated with several environmental issues [1–3]. In recent years, different strategies have been postulated to substantially reduce CO_2 emissions. Among them, coupling carbon capture utilization (CCU) with power-to-gas (PtG) schemes could represent a very promising option [4,5]. Through this approach, the electric energy produced from renewable sources is used to produce hydrogen via water electrolysis. The resulting hydrogen and the CO_2 sequestered from power plants or industrial processes are then employed as reactants for the Sabatier reaction (Equation (1)) to produce methane, which—unlike hydrogen—could easily be injected into the national grid.

$$CO_2 + 4\,H_2 \rightleftharpoons CH_4 + 2\,H_2O;\ \Delta H_{298K} = -165\ \text{KJ mol}^{-1} \quad (1)$$

The reaction is highly exothermic and generally carried out in the temperature range of 200−500 °C. However, CO_2 conversion toward CH_4 involves high activation energies, which make the reaction less likely at relatively low temperatures [6]. Therefore, the use of an appropriate catalyst is mandatory. Noble metals-based catalysts—such as Ru [7], Rh [8], and Pt [9]—have been reported to be active and selective for methanation purposes. However, their high cost and limited availability encouraged research into cheaper alternatives, such as transition metal-based catalysts. Among the latter, Ni-based catalysts appear as a

promising option due to their low cost and remarkable catalytic performance [10–12]. Since the main role of nickel is to dissociate H_2 molecules [13], a catalyst support that is able to adsorb and activate a large amount of CO_2 is essential for a successful catalytic formulation. To this end, reducible metal oxides, such as ZrO_2 [14] and CeO_2 [15], have been extensively used due to the presence of surface oxygen vacancies at the interface between the active metal and support. In the case of Ni/Ceria catalyst, Renda et al. [9] obtained outstanding performances in terms of methane yield (75%) and CO_2 conversion (73%) at 0.1 MPa and 350 °C. Meanwhile, Alarcón et al. [16] achieved, with an $Ni/CeO_2/\gamma\text{-}Al_2O_3$, a stable CO_2 conversion of 90% for at least 120 h.

Carbon-based supports like activated carbon and carbon nanotubes [17–22] are gaining attention because of their chemical stability and surface chemistry tunability. However, the main problem related to these materials is that their production is usually highly energy consuming. Another drawback is that their highly microporous structure could result in diffusional limitations of both reactants and products. Moreover, in the absence of certain surface functional groups, the interaction between the metallic active phase and the support is poor, leading to metal sintering phenomena [20]. To improve the properties of carbonaceous supports, the introduction of N-containing functional groups appears as a very promising approach. In addition to the enhanced electronic interaction, nitrogen doping could also lead to the incorporation of basic sites within the carbon framework, resulting in an enhanced CO_2 adsorption [23,24].

From a sustainability point of view, renewable carbon materials are excellent candidates to be used as catalyst supports. For instance, biochar—an aromatic carbon-rich solid produced via slow pyrolysis of biomass [25]—is currently receiving growing interest as a potential starting material for advanced catalytic applications, owing to its low cost and versatility [26]. The addition of this biomass-derived material to the most effective catalytic formulations (e.g., Ni/Ceria) could notably decrease the overall catalyst cost; also, at its end-life stage, the carbon support could be burnt to recover energy and active phases [27]. However, there are still very few studies in literature describing the performance of biochar-based metal catalysts in CO_2 methanation. Among them, Wang and co-workers produced and tested Ni- and Ru-based catalysts supported on ceria- [28] and urea-doped biochar [23]. Their results showed very good CO_2 conversion, even at low temperatures. Nevertheless, ceria and urea were added to the raw biomass, instead of biochar. To strengthen the value chain of biochar systems, it seems more interesting to produce engineered biochar-derived materials as value-added products, which can generate important revenues for large-scale biochar production systems.

In this work, a wheat-straw-derived activated biochar was produced and then doped with CeO_2 to produce Ni-based catalysts, which were then tested for CO_2 methanation. Several catalytic experiments were carried out at different temperatures, pressures, and gas space velocities to find the optimal catalytic formulation and operating conditions. Furthermore, urea-doped activated biochars were also synthesized and used as catalyst supports to assess the influence of the surface N-containing functional groups on the catalytic performance.

2. Materials and Methods

2.1. Materials

Wheat straw pellets were pyrolyzed under N_2 atmosphere at 500 °C and atmospheric pressure. Details concerning the pyrolysis device and procedure can be found in a previous article [29]. The resulting raw biochar was crushed and sieved to obtain particle sizes within the range of 0.212–1.41 mm. Then, biochar was physically activated with CO_2 at 700 °C and 1.0 MPa for 2 h in a fixed-bed reactor (made of alloy UNS N06600, 28.1 mm ID, and 600 mm long). These operating conditions were proven to be effective to obtain a material with a more hierarchical pore size distribution [30].

The catalysts tested in this work were prepared via wet impregnation of the above-mentioned activated biochar using $Ce(NO_3)_3{\cdot}6H_2O$ or $CO(NH_2)_2$ (urea) as dopant agents.

The aqueous solutions were stirred at 80 °C until complete water evaporation and then dried overnight at 110 °C. The resulting dried mixtures were finally calcined at 550 °C for 3 h under inert atmosphere (N_2) using the above-mentioned reactor. The doped activated biochars were then impregnated with an aqueous solution of $Ni(NO_3)_2 \cdot 6H_2O$, which was used as source of the catalytic active phase, following the same procedure as that used for the dopant agents. The Ni loading percentage was calculated considering the mass of the calcined doped support. The nomenclature employed for the produced catalysts is the following: BCCe*X*Ni*Y* or BCN*X*Ni*Y*, where *X* is the loading (wt.%) of ceria (Ce) or urea (N) and *Y* corresponds to the loading of nickel (Ni). Table S1 (in Supplementary Materials) summarizes all the produced materials and their nomenclatures.

2.2. Catalytic Experiments

Methanation tests were carried out in a tubular fixed-bed reactor (made of alloy UNS N10276), where around 1 g of catalyst was placed. The reactor was then filled with an inert material (Kaowool™ fiber) to avoid reactions outside of the catalytic bed. A K-type thermocouple was placed in the center of the catalytic bed to monitor the temperature evolution during the tests. Before each catalytic test, the bed was exposed to a reducing atmosphere (N_2/H_2, 90/10 vol.%) at 550 °C for 2.5 h to ensure the complete reduction of the nickel oxide. Once the preliminary reduction step was concluded, the reactor was cooled down to 300 °C under inert atmosphere and pressurized to the desired pressure value. Then, a mixture of $N_2/H_2/CO_2$ (50/40/10 vol.%) was fed to the reactor. Starting from 300 °C, the bed temperature was increased in steps of 50 °C and maintained constant for the time needed to obtain an almost constant product concentration. The composition of the outlet gaseous stream (CO, CO_2, CH_4, H_2, and light hydrocarbons such as C_2H_4, C_2H_6, and C_2H_2) was measured, using N_2 as internal standard, by means of a dual-channel micro-gas chromatograph (μ-GC 490 from Agilent, USA). A schematic representation of the experimental system is shown in Figure S1.

The catalytic activity of the tested samples was evaluated in terms of CO_2 conversion (X_{CO2}) and selectivity toward CO and CH_4 (S_{CO}, S_{CH4}), as defined in Equations (2)–(4). In these equations, F_i is the molar flow rate of the "*i*" species. The thermodynamic equilibrium values of X_{CO2}, S_{CO}, and S_{CH4} were calculated using the process simulation software Aspen Plus v_{10} (Gibbs free energy model).

$$X_{CO2} = (F_{CO2,\,in} - F_{CO2,\,out})\, F_{CO2,\,in}{}^{-1} \cdot 100 \quad (2)$$

$$S_{CH4} = F_{CH4,\,out}\, (F_{CO,\,out} + F_{CH4,\,out} + F_{C2H2,\,out} + F_{C2H6,\,out} + F_{C2H4,\,out})^{-1} \cdot 100 \quad (3)$$

$$S_{CO} = F_{CO,\,out}\, (F_{CO,\,out} + F_{CH4,\,out} + F_{C2H2,\,out} + F_{C2H6,\,out} + F_{C2H4,\,out})^{-1} \cdot 100 \quad (4)$$

2.3. Characterization of Carbon Materials

The textural characterization of the activated biochar (BC) and produced catalysts was performed from the N_2 adsorption/desorption isotherms at −196 °C, which were obtained using an ASAP 2020 automatic adsorption analyzer (Micromeritics, USA). Approximately 120 mg of sample was degassed under vacuum at 150 °C. The Langmuir model was adopted to evaluate the specific surface area (S_L). The total pore volume (V_{tot}) was calculated from the amount of N_2 adsorbed at high relative pressure (0.99). The specific volumes of micropores (V_{mic}), as well as the micro and mesopore surface area (S_{tmicro} and S_{tmeso}), were calculated using the *t*-plot method, whereas a non-local density functional theory (NLDFT) model assuming slit-pore geometry was used to evaluate the pore size distribution, from which the mesopore volume (V_{meso}) was estimated by subtracting the cumulative volume of micropores ($d_p < 2$ nm) from the total volume ($d_p < 50$ nm). The software MicroActive from Micromeritics was used for all the above-mentioned calculations.

The activated biochar (BC) was also characterized in terms of proximate analysis (in quadruplicate according to ASTM standards), ultimate analysis (using an analyzer

CHN628 from Leco Corporation, USA), and inorganic species (using an ADVANT'XP+XRF spectrometer from Thermo ARL, Switzerland).

The morphology features of both fresh and spent selected catalysts were observed by transmission electron microscopy (TEM) using a Tecnai F_{20} microscope (FEI, USA). Samples were previously sonicated for 5 min in an aqueous solution of ethanol. Furthermore, and in order to obtain information about the functional groups available in the surface, X-ray photoelectron spectroscopy (XPS) analyses were carried out using an XPS Spectrometer AXIS Supra (Kratos, UK) equipped with a mono Al Kα X-Ray source (120 W, 8 mA, 15 kV).

Temperature-programmed reduction (TPR) experiments were also conducted to evaluate the reducibility properties of the prepared catalysts. For these experiments, 0.5 g of each sample was loaded into the reactor used for the methanation tests and heated under a reducing stream (5% H_2 in Ar, at a flow rate of 0.5 NL min^{-1}) at a heating rate of 15 °C min^{-1} from 50 to 600 °C. The outlet hydrogen concentration was monitored online by means of a Hiden QGA analytical mass spectrometer.

3. Results

3.1. Effect of Ceria Loading

In the first stage, research was aimed at assessing the effect of the addition of ceria at different loadings (i.e., 10, 30, and 50 wt.%) on the performance of a Ni-based catalyst supported on the activated biochar. Nickel percentage in the catalyst formulation was kept constant at 40 wt.%, which was a commonly value reported in earlier studies [31,32]. As a preliminary step, the catalytic performance of the wheat straw activated biochar (BC) and the Ni-based catalyst (BCNi40) was tested. The obtained outcomes showed no catalytic activity in the case of BC, confirming that the carbonaceous support was completely inert under reaction conditions (data are not shown here). In the case of BCNi40, a maximum CO_2 conversion of 11% was reached at $_{1.0}$ MPa and 500 °C (i.e., relative severe conditions) with almost null selectivity to CH_4 (see Figure S2).

Figure 1 summarizes the results obtained from catalytic tests conducted at a specific gas volumetric flow rate of 15 NL g^{-1} h^{-1}, at three absolute pressure values (0.35, 0.60, and 1.0 MPa), and temperatures in the range of 300–500 °C. As shown in Figure 1a, at 1.0 MPa the BCCe10Ni40 catalyst started to be active at 400 °C. However, and despite the increase in CO_2 conversion with the increase in temperature (with a maximum value of 40% at 500 °C), the observed high selectivity toward CO seems to confirm the dominant role of the reverse water gas shift (rWGS) reaction. Furthermore, as shown in Figure 1b,c, the BCCe10Ni40 catalyst was completely inactive at lower operating pressures.

The catalysts with higher amounts of ceria (30 and 50 wt.%) started to be active at 350 °C. In this case, the rWGS reaction was also the dominant reaction at relatively low temperatures, at which the CH_4 selectivity was very low (especially at 0.60 and 0.35 MPa). At 1.0 MPa, both the CO_2 conversion and selectivity toward CH_4 markedly increased with temperature in the range of 350–450 °C. At higher temperatures, a quasi-plateau was achieved for both variables.

In summary, we can conclude that, among the three tested catalysts, the BCCe30Ni40 showed the best catalytic activity for CO_2 methanation. In fact, at 1.0 MPa and 400 °C it was possible to reach 60% CO_2 conversion along with a selectivity toward methane of 90%. Therefore, it seems evident that ceria had a positive effect on the catalytic process, probably as a consequence of the introduced oxygen vacancies, which have a certain affinity for oxygen atoms present in CO_2 [33]. Furthermore, the introduction of CeO_2 leads to the formation of basic sites, which are essential for CH_4 production due to the enhancement of CO_2 adsorption [15]. Another positive effect of ceria is its ability to stabilize and better disperse the nickel species, leading to a stronger interaction between the catalytic active phase and its support [34]. However, excessive loadings of ceria (i.e., 50 wt.%) could result in a massive encapsulation of the support due to the formation of a ceria shell, which can lead to a significant loss in specific surface area and poorer dispersion of nickel species [16]. By contrast, low ceria loadings (i.e., 10 wt.%) could not be sufficient to ensure good extents

of CO_2 conversions toward methane, as proven by the high selectivity toward CO observed for both BCCe10Ni40 and BCNi40 catalysts.

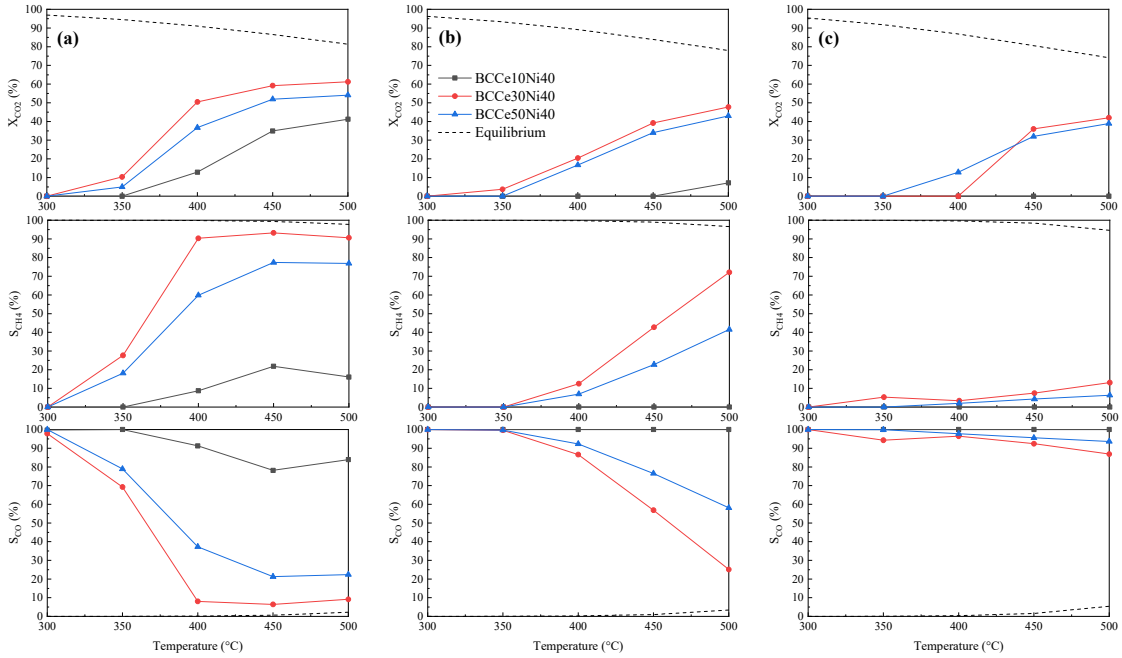

Figure 1. Results obtained using BCCeXNi40 at different ceria loadings during CO_2 methanation experiments, carried out at 15 NL g^{-1} h^{-1}, in the temperature range of 300–500 °C and at (**a**) 1.0 MPa, (**b**) 0.60 MPa, and (**c**) 0.35 MPa.

3.2. Effect of Nickel Loading

Once the optimal ceria loading was identified, Ni-CeO_2/BC catalysts with different Ni loadings (i.e., 10, 20, 30, and 40 wt.%) were tested under the same operating conditions used in the previous section. Results from the catalytic tests are displayed in Figure 2.

The decrease in Ni loading from 40 to 30 wt.% did not show a marked variation in the catalytic activity. CO_2 conversion gradually increased with the increase in temperature, reaching its maximum value at 500 °C. At this temperature and 1.0 MPa, the outlet stream was mainly composed of methane with a selectivity close to that at equilibrium. Interestingly, a further decrease in Ni loading (i.e., 10 and 20 wt.%) significantly enhanced the catalytic performance, especially at relatively lower temperatures. In fact, a selectivity toward CH_4 of almost 100% was observed for the BCCe30Ni20 catalyst at 350 °C and 1.0 MPa. This finding could be related to the fact that a high metal content could lead to particle agglomeration [35]. To further explore the effect of Ni loading, an additional catalytic test was carried out using the BCNi20 catalyst (without ceria doping) at 1.0 MPa. From Figure S2 (in which the catalytic performance of both BCNi20 and BCNi40 catalysts is shown), it can be deduced that an excessive Ni loading could lead to a critical decline in the catalytic activity due to the poorer dispersion of Ni within the carbon matrix. Furthermore, the synergistic role of ceria should also be highlighted, which significantly improved the catalytic performance of the BCNi20 catalyst (see Figure 2a and Figure S2 for comparative purposes).

On the other hand, a decrease in the absolute pressure resulted in an expected decrease in the catalytic activity (see Figure 2b,c). At lower pressures, CO_2 started to be reactive at higher temperatures. It was observed that the performance of the four tested catalysts showed a similar dependence on temperature, reaching the highest CO_2 conversion of ≈55% and ≈40% at 0.60 and 0.35 MPa, respectively. However, the selectivity toward CH_4 was strongly dependent on the Ni loading of the catalyst. In this sense, and in line with the remarks made above, the BCCe30Ni20 catalysts clearly exhibited the best catalytic

performance. The best Ni loading of 20 wt.% is in agreement with the results reported in previous studies for Ni-based catalysts supported on different materials [6,15].

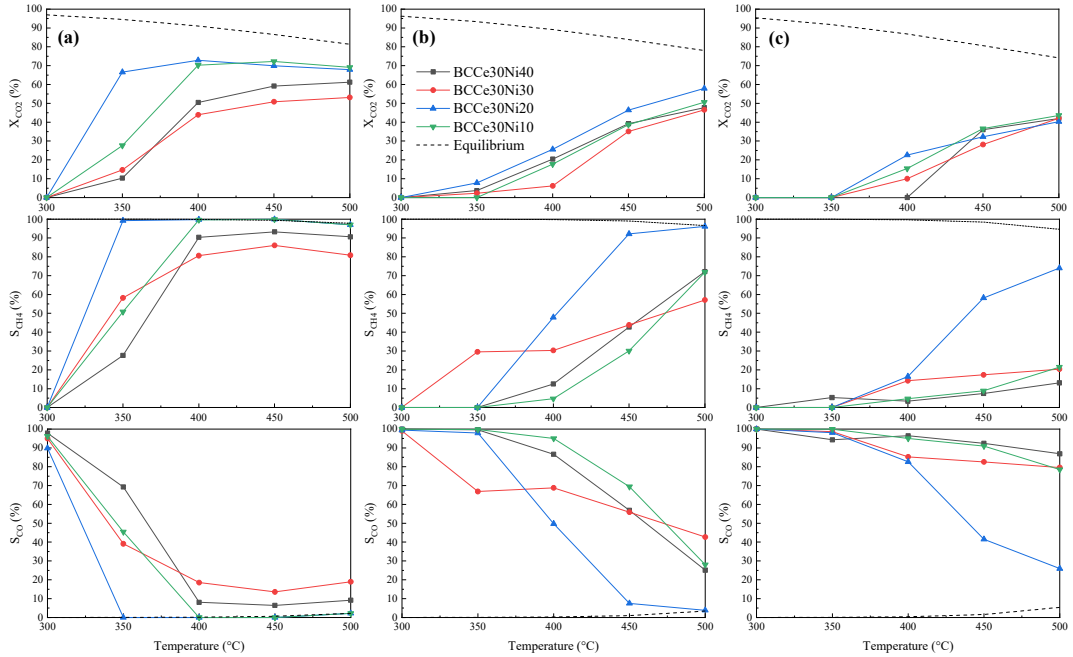

Figure 2. Results obtained during the study about the influence of Ni loadings on BCCe30 catalysts employed in CO_2 methanation experiments, which were carried out at 15 NL g^{-1} h^{-1}, in the temperature range of 300–500 °C and at (**a**) 1.0 MPa, (**b**) 0.60 MPa, and (**c**) 0.35 MPa.

3.3. Influence of Gas Space Velocity

Since CO_2 methanation is a highly exothermic process, a relatively high gas hourly space velocity (GHSV), usually greater than 10,000 h^{-1}, is required in order to avoid large temperature rises, which can affect both conversion and selectivity and also lead to a fast deactivation of the catalyst through metal phase sintering and/or encapsulation of active sites [20]. To explore the effect of GHSV, three different sets of experiments were carried out using the best catalyst (BCCe30Ni20) at the following gas volumetric flow rates: 15, 30, and 60 NL g^{-1} h^{-1}; which corresponded to 6600, 13,200, and 26,400 h^{-1}, respectively (apparent density of the catalyst = 440 kg m^{-3}). Results obtained from these experiments are summarized in Figure 3.

From the results obtained at 1.0 MPa (see Figure 3a), it was evident that the maximum carbon dioxide conversion was attained at 6600 h^{-1}, as expected. At this pressure and at temperatures higher than 400 °C, the catalytic performances, in terms of conversion and selectivity toward CH_4, at 15 and 30 NL g^{-1} h^{-1} were quite similar. The main difference lay in the catalyst activity at low temperatures (<400 °C), at which the lowest space velocity resulted in the highest CO_2 conversion. However, at lower operating pressures (see Figure 3b,c), an increase in GHSV dramatically affected the distribution of the products, leading to a marked increase in the selectivity toward CO at the expense of that toward methane.

Despite the fact that the CO_2 methanation reaction over Ni-based catalysts has been extensively investigated, there still are controversial views on the reaction mechanism. Two possible reaction pathways have been proposed so far: the formate route and the CO route. The first route involves the direct activation of the adsorbed CO_2 and subsequent formation of carbonates, which react with the dissociated hydrogen to produce formate species and, finally, methane [36]. The second possible mechanism firstly implies the conversion of CO_2 via rWGS to produce CO, which remains adsorbed on the active sites and is gradually hydrogenated to CH_4 [37]. The occurrence of one or another mechanism

could strictly be related to the properties of the catalyst support [33]. Ye et al. [38] studied the CO_2 methanation reaction mechanism over a Ni/CeO_2 catalyst and concluded that CO_2 was firstly adsorbed on the catalyst and then transformed into carbonate, bicarbonate, formate, and, finally, methane. However, and in light of the outcomes shown in Figure 3 (especially in terms of selectivity toward CO and CH_4), one can hypothesize that methane was produced through the CO route (rWGS and subsequent CO hydrogenation). The observed higher yields of CO at higher GHSV values could be explained by the fact that the gas residence time was not long enough to achieve complete hydrogenation of CO.

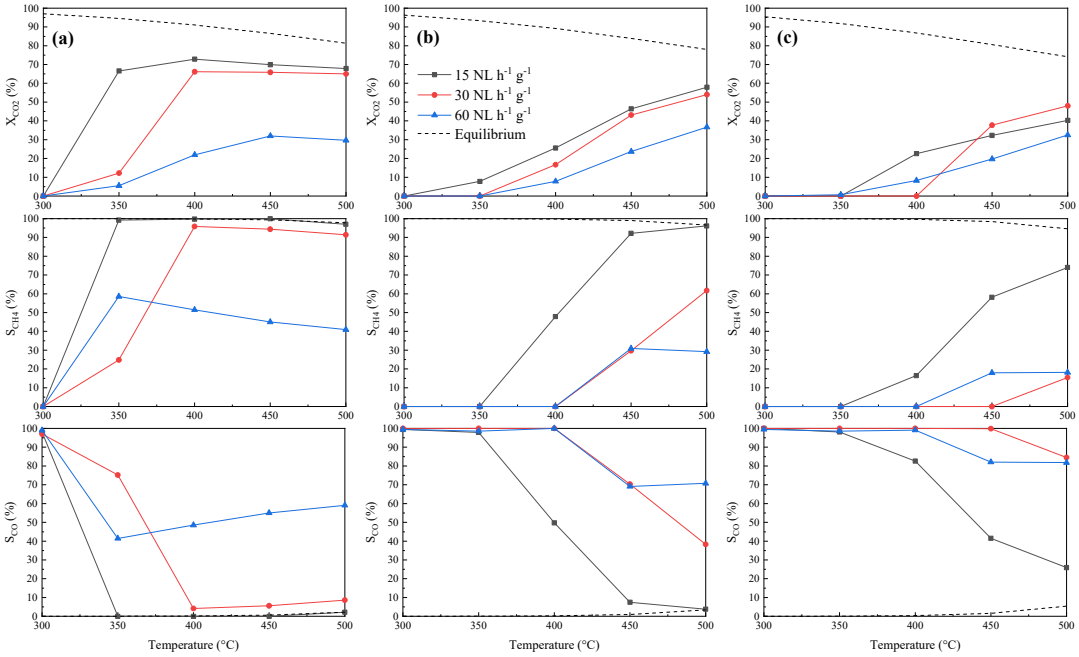

Figure 3. Study of the influence of gas space velocity on the catalytic performance of the BCCe30Ni20 catalyst. CO_2 methanation tests were conducted at 15, 30, and 60 NL g^{-1} h^{-1} (GHSV values of 6600, 13,200, and 26,400 h^{-1}, respectively), in the temperature range of 300–500 °C and at (**a**) 1.0 MPa, (**b**) 0.60 MPa, and (**c**) 0.35 MPa.

Since the catalytic performance of the BCCe30Ni20 catalyst at 1.0 MPa and temperatures starting from 400 °C was similar regardless of the gas space velocity tested (6600 or 13,200 h^{-1}), a specific gas volumetric flow rate of 30 NL g^{-1} h^{-1}, instead of 15 NL g^{-1} h^{-1}, is preferred from a practical point of view (13,200 h^{-1} is above the recommended threshold of 10,000 h^{-1}). Under this set of operating conditions, the BCCe30Ni20 catalyst exhibited a reasonably good activity, leading to conversion and selectivity values within the range reported in previous studies (see Table 1). The relatively low value of X_{CO2} observed for the catalyst developed in the present study could be related to the relatively high GHSV value used herein.

Table 1. CO_2 conversion and CH_4 selectivity values reported in some previous studies for catalytic CO_2 methanation.

Catalyst	Loading (wt.%)	Support	Pressure (MPa) and Temperature (°C)	Specific Gas Volumetric Flow Rate (NL g^{-1} h^{-1})	XCO_2 and SCH_4 (%)	Ref.
$Ni/\gamma\text{-}Al_2O_3$	12 (Ni)	Alumina	2, 210	-	80, 99.5	[39]
$35Ni_5Fe\_AX$	35(Ni)/5(Fe)	Xerogel	1, 220	9.6	63, 99.5	[40]
Fe/N-CNT	9.5 (Fe)	CNT	2.5, 350	50	25, 40	[41]
Ni/SiO_2	10 (Ni)	SiO_2	2, 310	20	77, 100	[42]
$Ni\text{-}15En/ZrO_2\text{-}1.5$	15 (Ni)	ZrO_2	0.5, 360	15	94, 97	[43]
Co/ZrO_2	2 (Co)	ZrO_2	3, 400	7.2	65, 99	[44]
Ni/Ce-ABC	15 (Ni)/15 (CeO_2)	Activated biochar	1, 400	6	87, 92	[28]
Ru/N-ABC	2 (Ru)	Activated biochar	1, 380	6	94, 100	[23]
BCCe30Ni20	20 (Ni)/30 (CeO_2)	Activated biochar	1, 400	30	65, 95	This work

3.4. N-Doping of the Carbonaceous Support

As an alternative to the use of CeO_2 as a dopant to improve the catalytic performance, the catalyst support (BC) was doped with urea. This kind of N-doping has been extensively assessed to improve the CO_2 uptake of activated carbon-based adsorbents [45]. Thermal decomposition of urea under an inert atmosphere leaves N atoms in the carbon lattice [46], which can stabilize Ni precursors in the support, enhancing the active phase dispersion (i.e., reducing the metallic particle size). Furthermore, N-doping could also increase the basicity of the support, which favors strong CO_2 adsorption [6]. To this end, the BCNi20 catalyst was doped with urea at three different loadings (i.e., 50, 67, and 75 wt.%), calcined at 500 °C under N_2, and then tested for CO_2 methanation at 1.0 MPa and 30 NL g^{-1} h^{-1}.

The results obtained at this stage are graphically summarized in Figure 4. As it can be deduced from the figure, the catalytic performance was progressively improved by increasing the loading of urea. By comparing the performances of the N-doped catalysts with that of the BCNi20 material, the beneficial effect of the urea addition was evident. Specifically, the higher the urea loading, the better the CO_2 conversion and methane selectivity. Even though the reactant conversions followed the same trend with the increase in temperature for all the tested samples, the production of methane became significant using a support:urea loading ratio greater than 1:0.5. The best results were obtained for the BCN75Ni20 catalyst at 500 °C, at which both the CO_2 conversion and selectivity toward CH_4 were equal to 45%. However, the catalytic performance of the best N-doped catalyst was clearly lower than that measured for the best ceria-doped catalyst (BCCe30Ni20), suggesting that using urea as dopant instead of ceria is not a recommended practice.

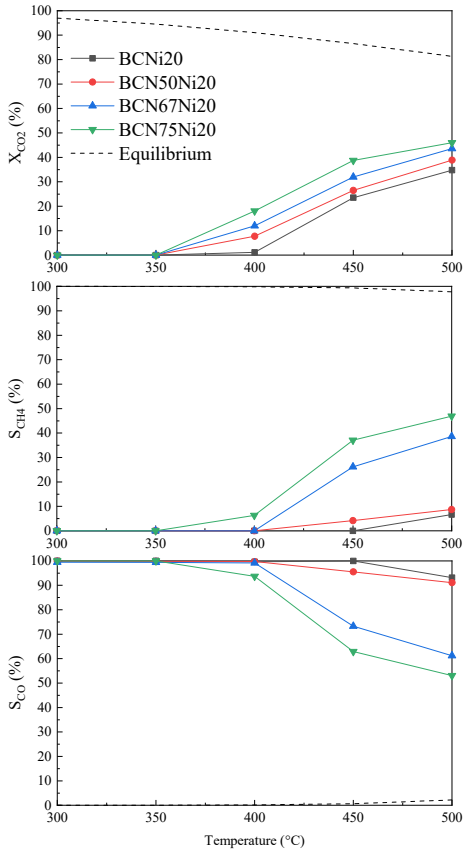

Figure 4. Catalytic performance of N-doped BCNi20 catalysts for CO_2 methanation experiments carried out at 30 NL g^{-1} h^{-1}, in the temperature range of 300–500 °C, and at 1.0 MPa.

3.5. Properties of Activated Biochar (BC) and Best-Performing Catalysts

In this section, the results from the characterization studies, which were mostly conducted for BC, BCCe30Ni20, and BCN75Ni20 materials, are presented.

For the wheat-straw-derived activated biochar used as support (BC), results from proximate, ultimate, and XRF analyses are reported in Table S2. As expected, the physical activation of pristine biochar resulted in a marked increase in the specific content of ashes. The composition of the inorganic matter revealed a high percentage of potassium, which can provide extra basic sites for CO_2 adsorption and activation.

Table S3 summarizes the textural properties of the three assessed materials. As can be seen, BC exhibited a highly microporous structure with a small volume of mesopores. For their part, both catalysts showed a remarkable decrease in specific surface area (compared to that of support) due to the impregnation and calcination steps. In addition, the observed decrease in the micropore volume was accompanied by an increase in the mesopore volume, probably caused by a certain collapse of the porous structure [47]. In this sense, a more hierarchical pore size distribution (with more mesopores) could be beneficial to enhance the diffusion of both reactants and products.

TPR analysis was performed on selected samples to evaluate the effect of CeO_2- and N-doping on the reduction of both the Ni-containing species and the support. From Figure S3, it can be seen that BC exhibited a reduction peak at relatively high temperatures (550 °C). Wang et al. [28] attributed this hydrogen consumption to the reduction of certain functional groups in the surface of carbonaceous support. Both the BCN75 and BCCe30 catalysts underwent reduction to some extent. For the BCCe30 material, the hydrogen consumption at 500 °C was mainly due to partial CeO_2 reduction at the surface, which was somewhat unexpected at such a low temperature [16]. This finding can probably be ascribed to the reductive properties of the carbon support [48]. On the other hand, hydrogen consumption in the range of 450–550 °C was observed for the BCN75 catalyst, although the mass spectrometer detected the presence of ammonia and the absence of water in the outlet stream. This result suggests that the calcination temperature was high enough to ensure the complete decomposition of the urea loaded; therefore, the surface of BC was mainly functionalized with C-N bonds. Some of these N-groups can undergo hydrogenation during TPR, leading to the observed release of NH_3.

Concerning the BCNi20 catalyst, the observed reduction of Ni-containing species at 400–550 °C is in agreement with previous studies [49]. As shown in Figure S3, two separated reduction peaks can be distinguished (α-peak at low temperature and β-peak at high temperature), which represents the portion of nickel bonded with the support through weak or strong interactions, respectively.

For both BCN75Ni20 and BCCe30Ni20 samples, Ni reduction can be observed at approximately 300 °C, which is an unusually low reduction temperature. This suggests that both ceria and urea doping strategies resulted in an improved reduction of NiO, which usually occurs at 500 °C for carbon-based supports [28]. It seems that Ni-Ce interactions increased the reducibility of NiO, generating more Ni sites that were accessible for the reactants to perform methanation [16]. Lower reduction temperatures usually indicate weaker metal–support interactions, which are not beneficial for the catalytic activity. However, for the specific case of the CO_2 methanation reaction, weak interactions are the factor main responsible for the reactant conversion [50,51]. Therefore, the high catalytic activity of the BCCe30Ni20 could be ascribed to the high reducibility of nickel oxide [17].

Figure 5 and Figure S4 show the TEM images for both BCCe30Ni20 and BCN75Ni20 catalysts before and after their employment in CO_2 methanation experiments at 30 NL g^{-1} h^{-1}, 400 °C, and 1.0 MPa. From Figure 5a,b (fresh BCCe30Ni20), it could be observed that a relatively good dispersion of Ni nanoparticles (NPs) was achieved for this catalyst. Nevertheless, the relatively high Ni loading resulted in some agglomerates, which are particularly visible in Figure 5b. The presence of metal NPs agglomerates was evident for the spent BCCe30Ni20 catalyst (see Figure 5c,d), which could be the main cause of catalyst deactivation [52]. Some earlier works ascribed the metal agglomeration to the formation of mobile species, which tend to migrate, causing Ni sintering and, consequently, catalyst deactivation [53]. Furthermore, Bartholomew et al. [54] stated that the water produced by methanation could accelerate the sintering process. On the other hand, Figure S4a,b shows that the N-doped BC support was

not as efficient as ceria in ensuring a good dispersion of Ni NPs. In this case, the spent sample also showed evident sintering phenomena (see Figure S4c,d). By comparing the TEM images of BCCe30Ni20 and BCN75Ni20 catalysts, it is possible to state that the improved nickel dispersion obtained after ceria introduction could be the main reason explaining the different catalytic outcomes observed for both materials.

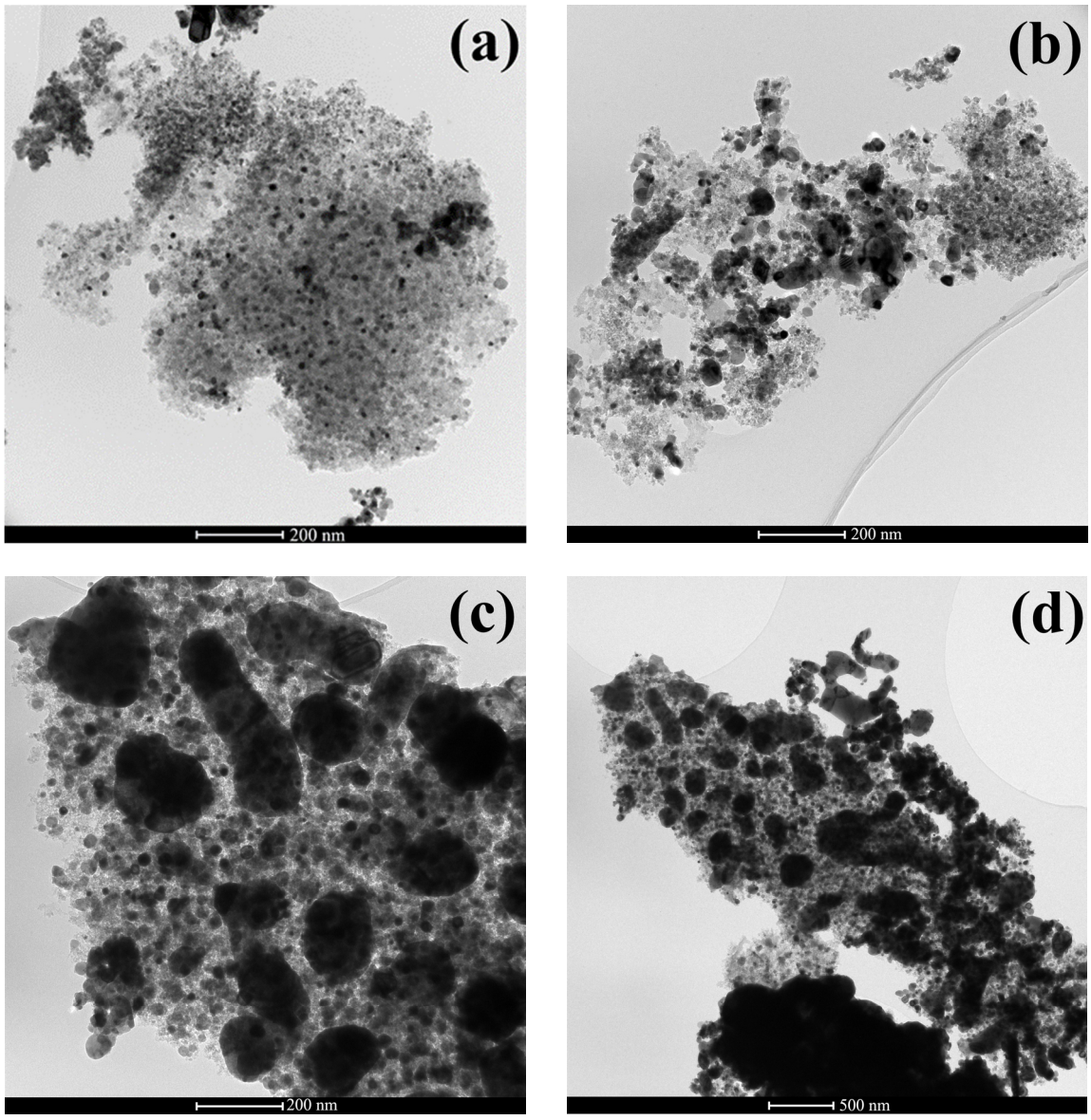

Figure 5. TEM images of BCCe30Ni20 catalyst: (**a**,**b**) fresh and (**c**,**d**) spent after CO_2 methanation at 30 NL g^{-1} h^{-1}, 400 °C and 1.0 MPa.

The full XPS spectra of the support (BC), as well as the fresh and spent BCN75Ni20 catalysts, are displayed in Figure S5. The elemental compositions calculated from the XPS analyses, which are listed in Table S4, indicate that N-doping was successfully implemented (higher atomic N:C ratios for N-doped materials). Furthermore, the huge decrease in Ni content in the spent catalyst could be ascribed to a certain encapsulation of the metal NPs inside carbon deposits, which resulted in a decrease in the metal fraction measured via XPS. The high-resolution spectra of the N1s binding energy region for the above-mentioned materials are shown in Figure S6. The spectra were deconvoluted into two peaks: pyridinic-N (398 eV) [23] and pyrrolic-N (400.8 eV) [55]. Figure S6 clearly shows that BC contained a certain number of N-containing functional groups, which originated

from the biomass precursor, as already confirmed by the ultimate analysis (see Table S2). Urea doping resulted in higher pyridinic-N content, with respect to the undoped support. As can deduced from Figure S6, the contents of both pyridinic- and pyrrolic-N remained almost constant after the catalytic test, suggesting the relative stability of these functional groups under the tested operating conditions.

4. Conclusions

Using wheat straw activated biochar loaded with 30 wt.% of ceria and 20 wt.% of nickel, it was possible to obtain a CO_2 conversion of 65% and a selectivity toward CH_4 of 95% at 1.0 MPa, 400 °C, and 13,200 h^{-1}. The rWGS-CO hydrogenation route was proposed as a reaction mechanism. Despite the fact that using urea as a dopant resulted in the introduction of nitrogenated functionalities in the surface of BC, the improvement of the catalytic activity of the resulting catalyst was modest in comparison to that attained when ceria was used as dopant.

Supplementary Materials: The following are available online at https://www.mdpi.com/article/10.3390/su13168939/s1, Table S1: Summary of all the catalysts synthesized and tested in this work; Table S2: Proximate, ultimate, and inorganic matter analysis; Table S3: Textural characterization; Table S4: Surface composition measured by XPS; Figure S1: Schematic overview of the experimental device; Figure S2: Results obtained during methanation experiments using the BCNi20 and BCNi40; Figure S3: Hydrogen uptake profiles from TPR for different materials; Figure S4: TEM images of BCN75Ni20; Figure S5: Full XPS spectra; Figure S6: XPS high-resolution spectra; Nomenclature.

Author Contributions: Conceptualization, C.D.S., J.J.M. and S.R.; methodology, C.D.S., G.G. and S.R.; validation, J.J.M., B.G. and V.P.; formal analysis, C.D.S.; data curation, C.D.S., S.R., J.J.M. and V.P.; writing—original draft preparation, C.D.S. and J.J.M.; writing—review and editing, G.G., S.R., J.J.M., B.G. and V.P.; supervision, J.J.M.; project administration, J.J.M.; funding acquisition, J.J.M. All authors have read and agreed to the published version of the manuscript.

Funding: This project received funding from the European Union's Horizon 2020 research and innovation program under the Marie Skłodowska-Curie grant agreement No 721991. The authors also acknowledge the funding from the Aragón Government (Ref. T22_20R), co-funded by FEDER 2014–2020 "Construyendo Europa desde Aragón".

Acknowledgments: The authors gratefully thank José Antonio Manso, Olga Marín, and Miguel González for their help in the preparation and characterization of the samples. Authors would like to acknowledge the use of Servicio General de Apoyo a la Investigación-SAI, Universidad de Zaragoza.

Conflicts of Interest: The authors declare no conflict of interest.

References

1. Butenschön, M.; Lovato, T.; Masina, S.; Caserini, S.; Grosso, M. Alkalinization Scenarios in the Mediterranean Sea for Efficient Removal of Atmospheric CO_2 and the Mitigation of Ocean Acidification. *Front. Clim.* **2021**, *3*, 1–11. [CrossRef]
2. de Souza Mendonça, A.K.; de Silva, S.A.; Pereira, L.Z.; Bornia, A.C.; de Andrade, D.F. An Overview of Environmental Policies for Mitigation and Adaptation to Climate Change and Application of Multilevel Regression Analysis to Investigate the CO_2 Emissions over the Years of 1970 to 2018 in All Brazilian States. *Sustainability* **2020**, *12*, 9175. [CrossRef]
3. Huang, W.-J.; Kao, K.-J.; Liu, L.-L.; Liao, C.-W.; Han, Y.-L. An Assessment of Direct Dissolved Inorganic Carbon Injection to the Coastal Region: A Model Result. *Sustainability* **2018**, *10*, 1174. [CrossRef]
4. Baena-Moreno, F.M.; Rodríguez-Galán, M.; Vega, F.; Alonso-Fariñas, B.; Vilches Arenas, L.F.; Navarrete, B. Carbon capture and utilization technologies: A literature review and recent advances. *Energy Sources Part A Recover. Util. Environ. Eff.* **2019**, *41*, 1403–1433. [CrossRef]
5. Thema, M.; Bauer, F.; Sterner, M. Power-to-Gas: Electrolysis and methanation status review. *Renew. Sustain. Energy Rev.* **2019**, *112*, 775–787. [CrossRef]
6. Gonçalves, L.P.L.; Sousa, J.P.S.; Soares, O.S.G.P.; Bondarchuk, O.; Lebedev, O.I.; Kolen'Ko, Y.V.; Pereira, M.F. The role of surface properties in CO_2 methanation over carbon-supported Ni catalysts and their promotion by Fe. *Catal. Sci. Technol.* **2020**, *10*, 7217–7225. [CrossRef]
7. Petersen, E.M.; Rao, R.G.; Vance, B.C.; Tessonnier, J.-P. SiO_2/SiC supports with tailored thermal conductivity to reveal the effect of surface temperature on Ru-catalyzed CO_2 methanation. *Appl. Catal. B Environ.* **2021**, *286*, 119904. [CrossRef]

8. Younas, M.; Sethupathi, S.; Kong, L.L.; Mohamed, A.R.; Muhammad, Y. CO_2 methanation over Ni and Rh based catalysts: Process optimization at moderate temperature. *Int. J. Energy Res.* **2018**, *42*, 3289–3302. [CrossRef]
9. Renda, S.; Ricca, A.; Palma, V. Study of the effect of noble metal promotion in Ni-based catalyst for the Sabatier reaction. *Int. J. Hydrog. Energy* **2021**, *46*, 12117–12127. [CrossRef]
10. Garbarino, G.; Kowalik, P.; Riani, P.; Antoniak-Jurak, K.; Pieta, P.; Lewalska-Graczyk, A.; Lisowski, W.; Nowakowski, R.; Busca, G.; Pieta, I.S. Improvement of Ni/Al_2O_3 Catalysts for Low-Temperature CO_2 Methanation by Vanadium and Calcium Oxide Addition. *Ind. Eng. Chem. Res.* **2021**, *60*, 6554–6564. [CrossRef]
11. Agnelli, M.; Swaan, H.; Marquez-Alvarez, C.; Martin, G.; Mirodatos, C. CO Hydrogenation on a Nickel Catalyst: II. A Mechanistic Study by Transient Kinetics and Infrared Spectroscopy. *J. Catal.* **1998**, *175*, 117–128. [CrossRef]
12. Zhang, Z.; Tian, Y.; Zhang, L.; Hu, S.; Xiang, J.; Wang, Y.; Xu, L.; Liu, Q.; Zhang, S.; Hu, X. Impacts of nickel loading on properties, catalytic behaviors of Ni/γ–Al_2O_3 catalysts and the reaction intermediates formed in methanation of CO. *Int. J. Hydrog. Energy* **2019**, *44*, 9291–9306. [CrossRef]
13. Wolf, M.; Wong, L.H.; Schüler, C.; Hinrichsen, O. CO_2 methanation on transition-metal-promoted Ni-Al catalysts: Sulfur poisoning and the role of CO_2 adsorption capacity for catalyst activity. *J. CO2 Util.* **2020**, *36*, 276–287. [CrossRef]
14. Li, W.; Nie, X.; Jiang, X.; Zhang, A.; Ding, F.; Liu, M.; Liu, Z.; Guo, X.; Song, C. ZrO_2 support imparts superior activity and stability of Co catalysts for CO_2 methanation. *Appl. Catal. B Environ.* **2018**, *220*, 397–408. [CrossRef]
15. Hu, F.; Tong, S.; Lu, K.; Chen, C.-M.; Su, F.-Y.; Zhou, J.; Lu, Z.-H.; Wang, X.; Feng, G.; Zhang, R. Reduced graphene oxide supported Ni-Ce catalysts for CO_2 methanation: The support and ceria promotion effects. *J. CO2 Util.* **2019**, *34*, 676–687. [CrossRef]
16. Alarcón, A.; Guilera, J.; Díaz-López, J.A.; Andreu, T. Optimization of nickel and ceria catalyst content for synthetic natural gas production through CO_2 methanation. *Fuel Process. Technol.* **2019**, *193*, 114–122. [CrossRef]
17. Cam, L.M.; Ha, N.T.T.; Van Khu, L.; Brown, T.C.; Ha, N.N. Carbon Dioxide Methanation Over Nickel Catalysts Supported on Activated Carbon at Low Temperature. *Aust. J. Chem.* **2019**, *72*, 969. [CrossRef]
18. Feng, Y.; Yang, W.; Chu, W. Effect of Ca modification on the catalytic performance of Ni/AC for CO_2 methanation. *Integr. Ferroelectr.* **2016**, *172*, 40–48. [CrossRef]
19. Wang, W.; Chu, W.; Wang, N.; Yang, W.; Jiang, C. Mesoporous nickel catalyst supported on multi-walled carbon nanotubes for carbon dioxide methanation. *Int. J. Hydrog. Energy* **2016**, *41*, 967–975. [CrossRef]
20. Wang, W.; Duong-Viet, C.; Ba, H.; Baaziz, W.; Tuci, G.; Caporali, S.; Nguyen-Dinh, L.; Ersen, O.; Giambastiani, G.; Pham-Huu, C. Nickel Nanoparticles Decorated Nitrogen-Doped Carbon Nanotubes (Ni/N-CNT); a Robust Catalyst for the Efficient and Selective CO_2 Methanation. *ACS Appl. Energy Mater.* **2018**, *2*, 1111–1120. [CrossRef]
21. Antoniak-Jurak, K.; Kowalik, P.; Konkol, M.; Próchniak, W.; Bicki, R.; Raróg-Pilecka, W.; Kuśtrowski, P.; Ryczkowski, J. Sulfur tolerant Co–Mo–K catalysts supported on carbon materials for sour gas shift process—Effect of support modification. *Fuel Process. Technol.* **2016**, *144*, 305–311. [CrossRef]
22. Antoniak-Jurak, K.; Kowalik, P.; Próchniak, W.; Raróg-Pilecka, W.; Kuśtrowski, P.; Ryczkowski, J. Sour gas shift process over sulfided Co–Mo–K catalysts supported on carbon material—Support characterization and catalytic activity of catalysts. *Fuel Process. Technol.* **2015**, *138*, 305–313. [CrossRef]
23. Wang, X.; Liu, Y.; Zhu, L.; Li, Y.; Wang, K.; Qiu, K.; Tippayawong, N.; Aggarangsi, P.; Reubroycharoen, P.; Wang, S. Biomass derived N-doped biochar as efficient catalyst supports for CO_2 methanation. *J. CO2 Util.* **2019**, *34*, 733–741. [CrossRef]
24. Ashok, J.; Pati, S.; Hongmanorom, P.; Tianxi, Z.; Junmei, C.; Kawi, S. A review of recent catalyst advances in CO_2 methanation processes. *Catal. Today* **2020**, *356*, 471–489. [CrossRef]
25. Manyà, J.J. Pyrolysis for Biochar Purposes: A Review to Establish Current Knowledge Gaps and Research Needs. *Environ. Sci. Technol.* **2012**, *46*, 7939–7954. [CrossRef] [PubMed]
26. Wang, S.; Wang, H.; Yin, Q.; Zhu, L.; Yin, S. Methanation of bio-syngas over a biochar supported catalyst. *New J. Chem.* **2014**, *38*, 4471–4477. [CrossRef]
27. Dufour, A.; Celzard, A.; Fierro, V.; Martin, E.; Broust, F.; Zoulalian, A. Catalytic decomposition of methane over a wood char concurrently activated by a pyrolysis gas. *Appl. Catal. A Gen.* **2008**, *346*, 164–173. [CrossRef]
28. Wang, X.; Yang, M.; Zhu, X.; Zhu, L.; Wang, S. Experimental study and life cycle assessment of CO_2 methanation over biochar supported catalysts. *Appl. Energy* **2020**, *280*, 115919. [CrossRef]
29. Greco, G.; Di Stasi, C.; Rego, F.; González, B.; Manyà, J.J. Effects of slow-pyrolysis conditions on the products yields and properties and on exergy efficiency: A comprehensive assessment for wheat straw. *Appl. Energy* **2020**, *279*, 115842. [CrossRef]
30. Di Stasi, C.; Greco, G.; Canevesi, R.L.S.; Izquierdo, M.T.; Fierro, V.; Celzard, A.; González, B.; Manyà, J.J. Influence of activation conditions on textural properties and performance of activated biochars for pyrolysis vapors upgrading. *Fuel* **2021**, *289*, 119759. [CrossRef]
31. Gnanakumar, E.S.; Chandran, N.; Kozhevnikov, I.V.; Grau-Atienza, A.; Ramos-Fernandez, E.V.; Sepulveda-Escribano, A.; Shiju, N.R. Highly efficient nickel-niobia composite catalysts for hydrogenation of CO_2 to methane. *Chem. Eng. Sci.* **2019**, *194*, 2–9. [CrossRef]
32. Hwang, S.; Lee, J.; Hong, U.G.; Gil Seo, J.; Jung, J.C.; Koh, D.J.; Lim, H.; Byun, C.; Song, I.K. Methane production from carbon monoxide and hydrogen over nickel–alumina xerogel catalyst: Effect of nickel content. *J. Ind. Eng. Chem.* **2011**, *17*, 154–157. [CrossRef]

33. Shen, L.; Xu, J.; Zhu, M.; Han, Y.-F. Essential Role of the Support for Nickel-Based CO_2 Methanation Catalysts. *ACS Catal.* **2020**, *10*, 14581–14591. [CrossRef]
34. Le, M.C.; Van, K.L.; Nguyen, T.H.T.; Nguyen, N.H. The Impact of Ce-Zr Addition on Nickel Dispersion and Catalytic Behavior for CO_2 Methanation of Ni/AC Catalyst at Low Temperature. *J. Chem.* **2017**, *2017*, 1–11. [CrossRef]
35. Gödde, J.; Merko, M.; Xia, W.; Muhler, M. Nickel nanoparticles supported on nitrogen–doped carbon nanotubes are a highly active, selective and stable CO_2 methanation catalyst. *J. Energy Chem.* **2021**, *54*, 323–331. [CrossRef]
36. Fatah, N.; Jalil, A.; Salleh, N.; Hamid, M.; Hassan, Z.; Nawawi, M.G.M. Elucidation of cobalt disturbance on Ni/Al_2O_3 in dissociating hydrogen towards improved CO_2 methanation and optimization by response surface methodology (RSM). *Int. J. Hydrog. Energy* **2020**, *45*, 18562–18573. [CrossRef]
37. Yan, B.; Zhao, B.; Kattel, S.; Wu, Q.; Yao, S.; Su, D.; Chen, J.G. Tuning CO_2 hydrogenation selectivity via metal-oxide interfacial sites. *J. Catal.* **2019**, *374*, 60–71. [CrossRef]
38. Ye, R.-P.; Li, Q.; Gong, W.; Wang, T.; Razink, J.J.; Lin, L.; Qin, Y.-Y.; Zhou, Z.; Adidharma, H.; Tang, J.; et al. High-performance of nanostructured Ni/CeO_2 catalyst on CO_2 methanation. *Appl. Catal. B Environ.* **2020**, *268*, 118474. [CrossRef]
39. Lim, J.Y.; McGregor, J.; Sederman, A.; Dennis, J. Kinetic studies of CO 2 methanation over a Ni/γ-Al_2O_3 catalyst using a batch reactor. *Chem. Eng. Sci.* **2016**, *141*, 28–45. [CrossRef]
40. Hwang, S.; Hong, U.G.; Lee, J.; Baik, J.H.; Koh, D.J.; Lim, H.; Song, I.K. Methanation of Carbon Dioxide Over Mesoporous Nickel–M–Alumina (M = Fe, Zr, Ni, Y, and Mg) Xerogel Catalysts: Effect of Second Metal. *Catal. Lett.* **2012**, *142*, 860–868. [CrossRef]
41. Chew, L.M.; Kangvansura, P.; Ruland, H.; Schulte, H.J.; Somsen, C.; Xia, W.; Eggeler, G.; Worayingyong, A.; Muhler, M. Effect of nitrogen doping on the reducibility, activity and selectivity of carbon nanotube-supported iron catalysts applied in CO_2 hydrogenation. *Appl. Catal. A Gen.* **2014**, *482*, 163–170. [CrossRef]
42. Ye, R.-P.; Liao, L.; Reina, T.R.; Liu, J.; Chevella, D.; Jin, Y.; Fan, M.; Liu, J. Engineering Ni/SiO_2 catalysts for enhanced CO_2 methanation. *Fuel* **2021**, *285*, 119151. [CrossRef]
43. Quan, Y.; Zhang, N.; Zhang, Z.; Han, Y.; Zhao, J.; Ren, J. Enhanced performance of Ni catalysts supported on ZrO_2 nanosheets for CO_2 methanation: Effects of support morphology and chelating ligands. *Int. J. Hydrog. Energy* **2021**, *46*, 14395–14406. [CrossRef]
44. Li, W.; Liu, Y.; Mu, M.; Ding, F.; Liu, Z.; Guo, X.; Song, C. Organic acid-assisted preparation of highly dispersed Co/ZrO2 catalysts with superior activity for CO_2 methanation. *Appl. Catal. B Environ.* **2019**, *254*, 531–540. [CrossRef]
45. Sivadas, D.L.; Vijayan, S.; Rajeev, R.; Ninan, K.; Prabhakaran, K. Nitrogen-enriched microporous carbon derived from sucrose and urea with superior CO_2 capture performance. *Carbon* **2016**, *109*, 7–18. [CrossRef]
46. Lin, Z.; Waller, G.; Liu, Y.; Liu, M.; Wong, C.-P. Facile Synthesis of Nitrogen-Doped Graphene via Pyrolysis of Graphene Oxide and Urea, and its Electrocatalytic Activity toward the Oxygen-Reduction Reaction. *Adv. Energy Mater.* **2012**, *2*, 884–888. [CrossRef]
47. Kumar, A.; Sinha, A. Hydrogen production from acetic acid steam reforming over nickel-based catalyst synthesized via MOF process. *Int. J. Hydrog. Energy* **2020**, *45*, 24397–24411. [CrossRef]
48. Quan, C.; Wang, H.; Gao, N. Development of activated biochar supported Ni catalyst for enhancing toluene steam reforming. *Int. J. Energy Res.* **2020**, *44*, 5749–5764. [CrossRef]
49. Chen, J.; Wang, M.; Wang, S.; Li, X. Hydrogen production via steam reforming of acetic acid over biochar-supported nickel catalysts. *Int. J. Hydrog. Energy* **2018**, *43*, 18160–18168. [CrossRef]
50. Li, M.; Amari, H.; van Veen, A.C. Metal-oxide interaction enhanced CO_2 activation in methanation over ceria supported nickel nanocrystallites. *Appl. Catal. B: Environ.* **2018**, *239*, 27–35. [CrossRef]
51. Zhu, M.; Tian, P.; Kurtz, R.; Lunkenbein, T.; Xu, J.; Schlögl, R.; Wachs, I.E.; Han, Y. Strong Metal–Support Interactions between Copper and Iron Oxide during the High-Temperature Water-Gas Shift Reaction. *Angew. Chem. Int. Ed.* **2019**, *58*, 9083–9087. [CrossRef] [PubMed]
52. Coll, R.; Salvadó, J.; Farriol, X.; Montané, D. Steam reforming model compounds of biomass gasification tars: Conversion at different operating conditions and tendency towards coke formation. *Fuel Process. Technol.* **2001**, *74*, 19–31. [CrossRef]
53. Miao, B.; Ma, S.S.K.; Wang, X.; Su, H.; Chan, S.H. Catalysis mechanisms of CO_2 and CO methanation. *Catal. Sci. Technol.* **2016**, *6*, 4048–4058. [CrossRef]
54. Bartholomew, C. Sintering of alumina-supported nickel and nickel bimetallic methanation catalysts in H_2/H_2O atmospheres. *J. Catal.* **1983**, *79*, 34–46. [CrossRef]
55. Li, K.; Chen, W.; Yang, H.; Chen, Y.; Xia, S.; Xia, M.; Tu, X.; Chen, H. Mechanism of biomass activation and ammonia modification for nitrogen-doped porous carbon materials. *Bioresour. Technol.* **2019**, *280*, 260–268. [CrossRef]

Supplementary materials

Wheat straw-derived activated biochar as a renewable support of Ni-CeO_2 catalysts for CO_2 methanation

Christian Di Stasi [a,*], Simona Renda [b], Gianluca Greco [a], Belén González [a], Vincenzo Palma [b], Joan J. Manyà [a]

[a] *Aragón Institute of Engineering Research (I3A), Thermochemical Processes Group, University of Zaragoza, Escuela Politécnica Superior, Crta. Cuarte s/n, 22071 Huesca, Spain*

[b] *University of Salerno, Department of Industrial Engineering, Via Giovanni Paolo II 132, 84084, Fisciano (SA), Italy*

[*] Corresponding authors

E-mail addresses: christiandistasi@unizar.es (Christian Di Stasi)

Table S1. Summary of all the catalysts synthesized and tested in this work.

Sample ID	CeO_2, wt. %	Ni, wt. %	$CO(NH_2)_2$, wt. %
BC	/	/	/
BCCe10Ni40	10	40	/
BCCe30Ni40	30	40	/
BCCe50Ni40	50	40	/
BCCe30Ni10	30	10	/
BCCe30Ni20	30	20	/
BCCe30Ni30	30	30	/
BCCe30Ni40	30	40	/
BCN50Ni20	/	20	50
BCN67Ni20	/	20	67
BCN75Ni20	/	20	75

Table S2. Proximate, ultimate, and inorganic matter analysis of the physically activated biochar (BC) employed as catalyst support.

Ultimate analysis (wt. %)	
Carbon	67.38
Hydrogen	1.12
Nitrogen	1.94
Oxygen [a]	29.56
Proximate analysis (wt. %)	
Moisture	N.D.
Volatiles	8.27
Ashes	41.92
Fixed Carbon[a]	50.72
Inorganic matter (wt. % in ash)	
SiO_2	17.52
K_2O	16.68
CaO	7.40
P_2O_5	2.45
MgO	1.51
Al_2O_3	1.11
Fe_2O_3	1.05
S	0.716
Cl	0.702
Na_2O	0.216

[a] Values calculated by difference.

Table S3. Specific surface area (Langmuir, S_L) and pore volumes (V_{tot}, V_{micro} and V_{meso}) of BC, BCN75Ni20, and BCCe30Ni20 materials.

Sample	S_L	S_{tmicro} ($m^2\ g^{-1}$)	S_{tmeso}	V_{tot}	V_{micro} ($cm^3\ g^{-1}$)	V_{meso}
BC	600	579	21.5	0.224	0.200	0.020
BCCe30Ni20	241	186	55.4	0.138	0.056	0.080
BCN75Ni20	310	278	31.7	0.135	0.090	0.040

Table S4. Surface composition measured by XPS and peak contributions of C1s, N1s, O1s and Ni2p for fresh and spent BCN75Ni20 catalyst —methanation experiment at 30 NL g^{-1} h^{-1}, 400 °C and 1.00 MPa.

Sample	Surface concentration (at. %)			
	C1s	N1s	O1s	Ni2p
BC	81.1	2.0	16.9	–
BCN75Ni20	41.6	2.3	41.3	14.8
BCN75Ni20-spent	43.2	1.8	45.9	9.1

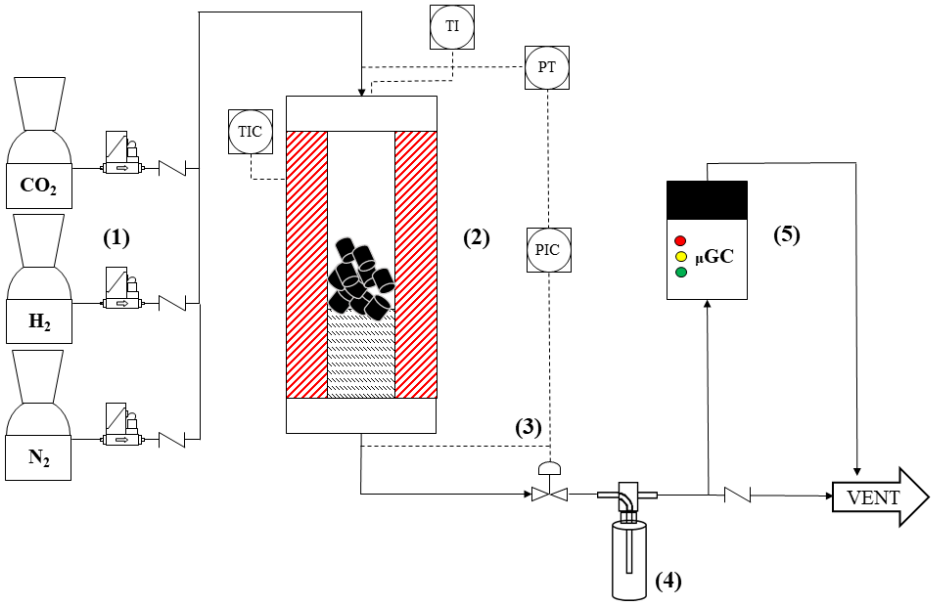

Figure S1. Schematic overview of the experimental device used in this work: feeding system (1); fixed-bed reactor and furnace (2); servo-controlled valve (3); water trap with $CaCl_2$ (4); and µ-GC analyzer (5).

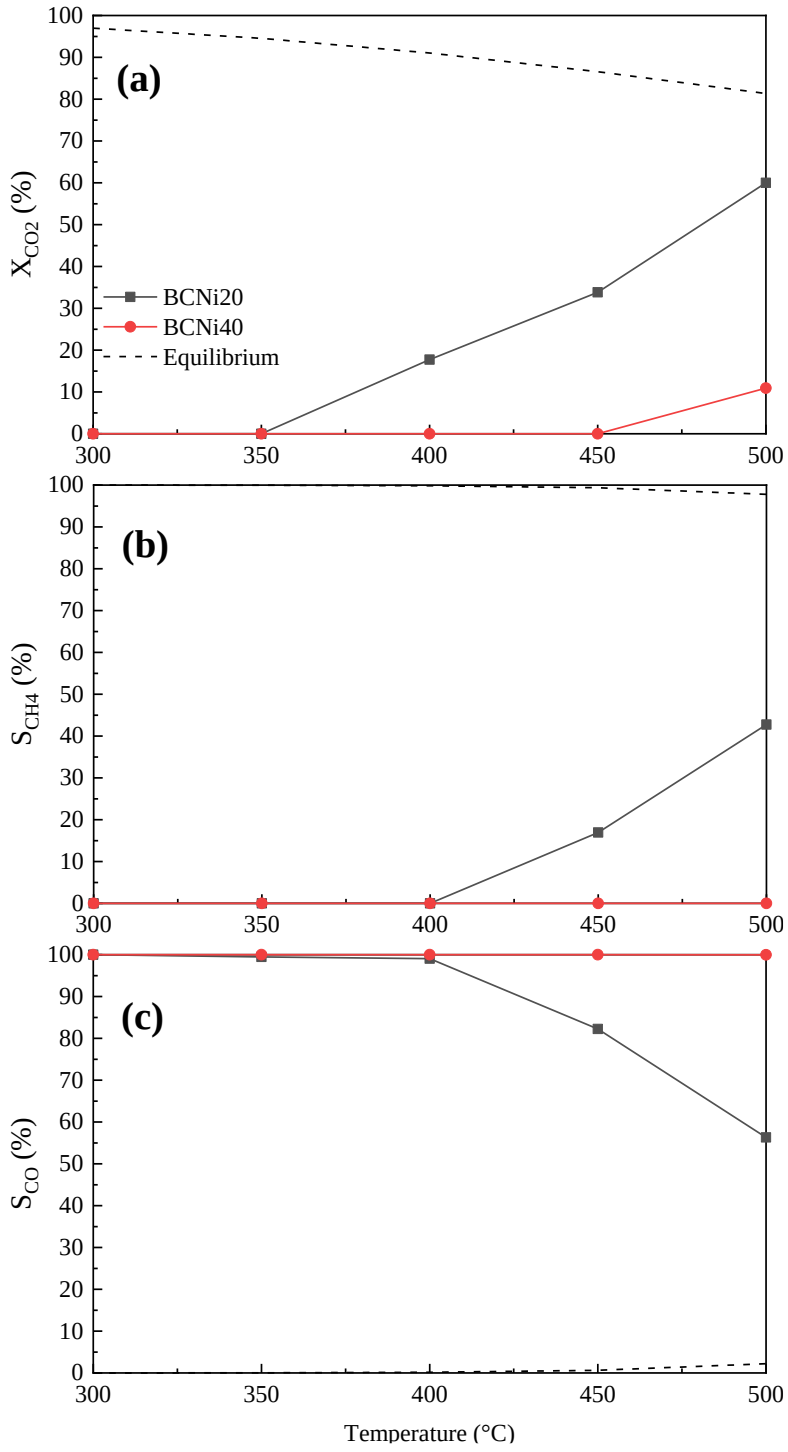

Figure S2. Results obtained during methanation experiments using the BCNi20 and BCNi40 catalysts at 1.0 MPa and 15 NL g^{-1} h^{-1}.

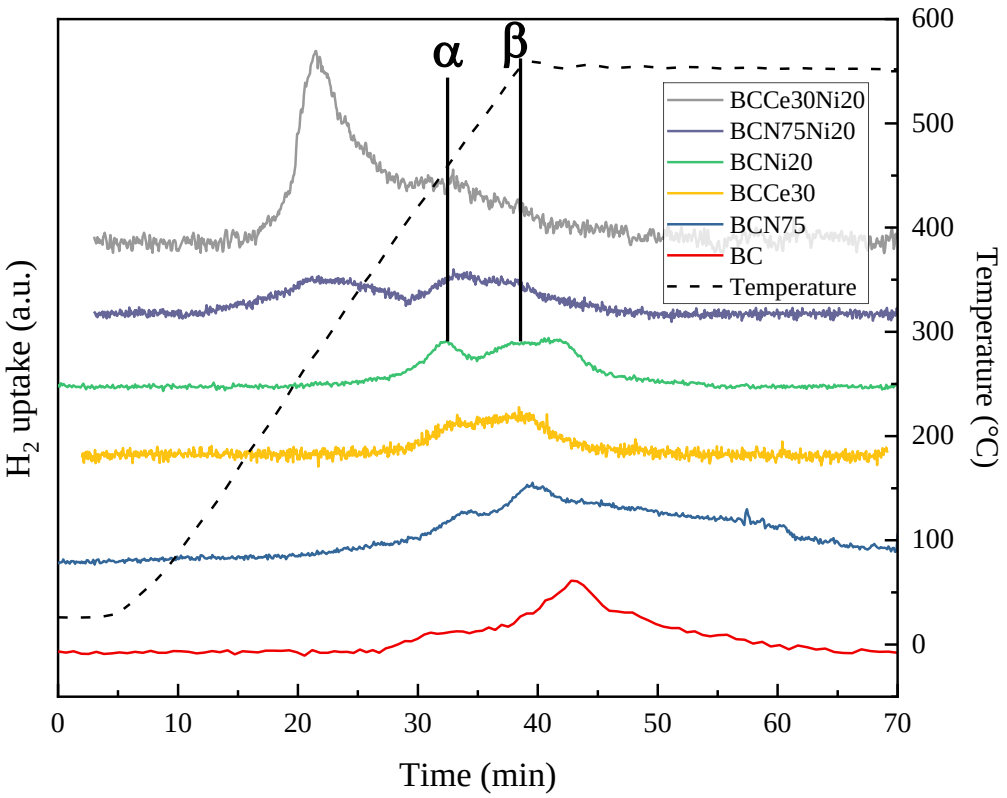

Figure S3. Hydrogen uptake profiles from TPR for different materials.

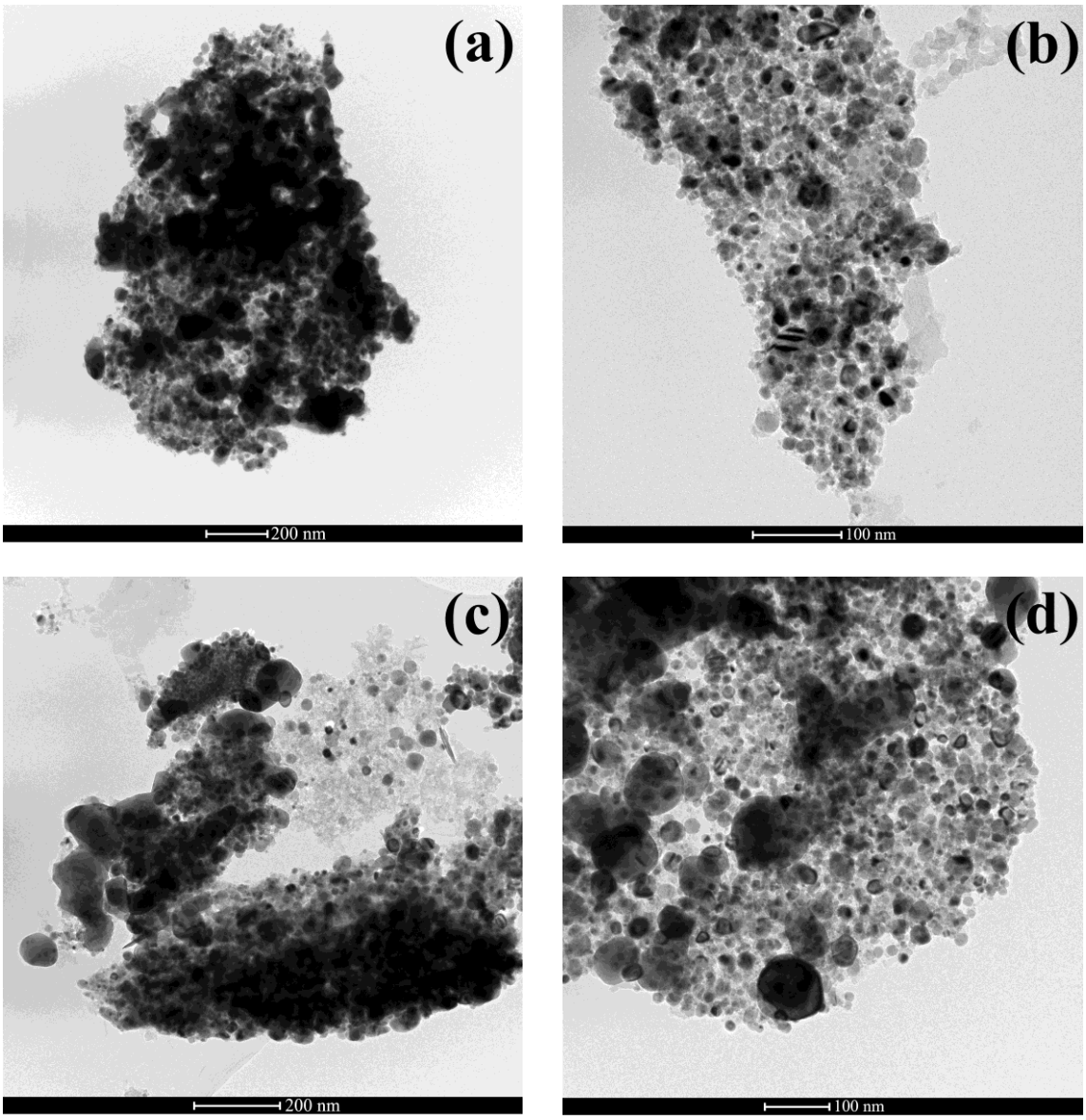

Figure S4. TEM images of BCN75Ni20 catalyst: fresh (a, b) and spent (c, d) after CO_2 methanation at 30 NL g^{-1} h^{-1}, 400 °C and 1.0 MPa.

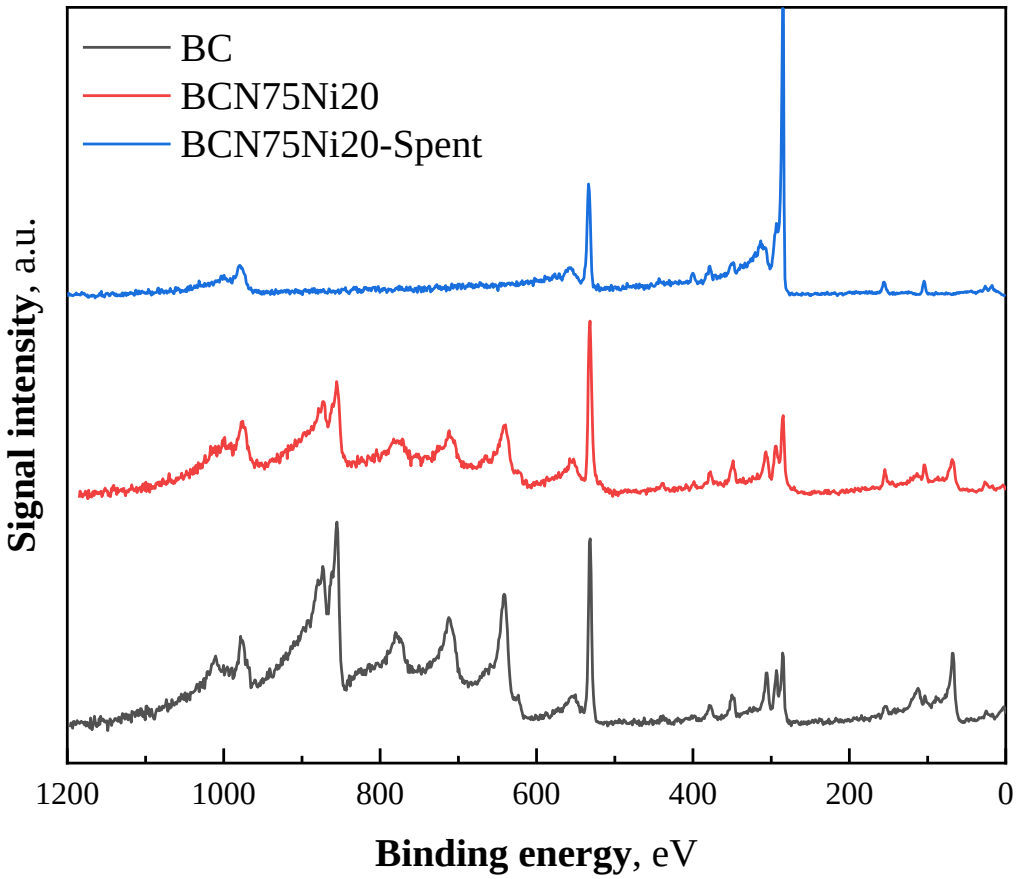

7

Figure S5. Full XPS spectra of BC, fresh BCN150Ni20, and spent BCN150Ni20 after CO_2 methanation at 30 NL g^{-1} h^{-1}, 400 °C and 1.0 MPa.

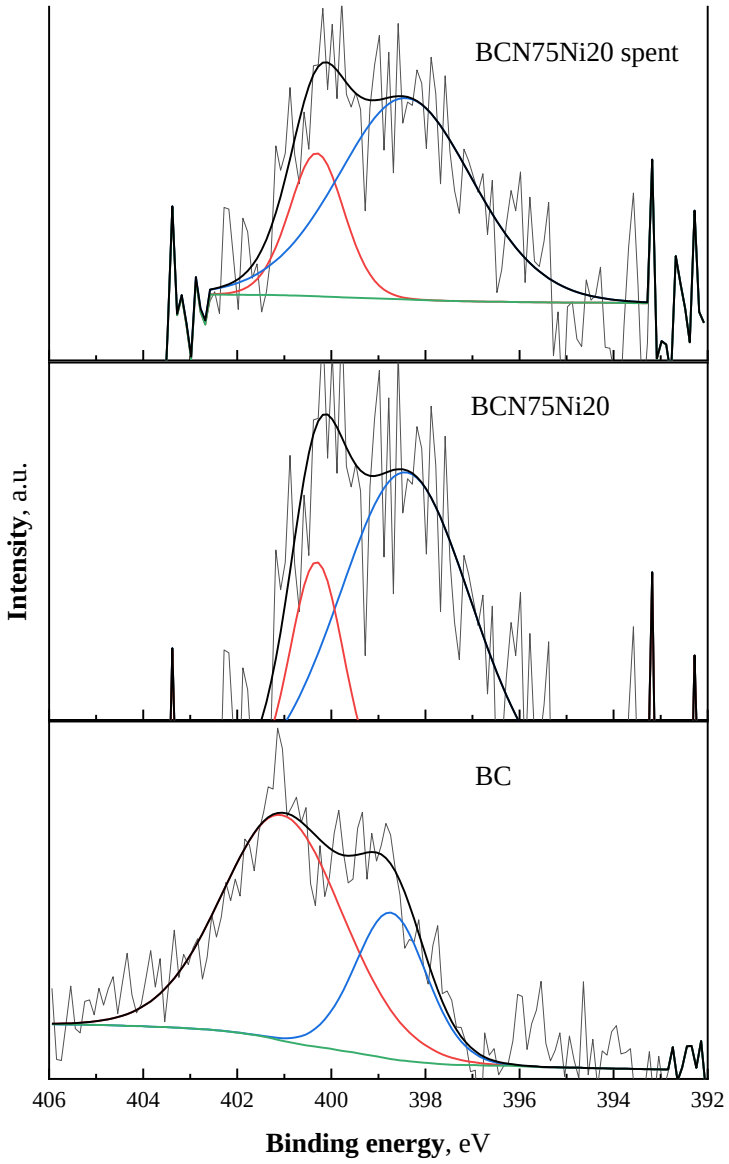

Figure S6. XPS high resolution spectra of N 1s of activated biochar (support), as well as fresh and spent BCN150Ni20 catalyst (CO_2 methanation at 30 NL g^{-1} h^{-1}, 400 °C and 1.0 MPa).

Nomenclature

d_p Pore diameter (nm)

F_i Molar flow rate (mol min^{-1})

S_i Product selectivity (%)

S_L Langmuir surface area (m^2 g^{-1})

S_{tmeso} Mesopores t-plot surface area (m^2 g^{-1})

S_{tmicro} Micropores t-plot surface area (m^2 g^{-1})

V_{meso} Volume of mesopores (cm^3 g^{-1})

V_{micro} Volume of micropores (cm^3 g^{-1})

V_{tot} Total pore volume (cm^3 g^{-1})

X_{CO2} Carbon dioxide conversion (%)

Acronyms

CHN Ultimate analysis

GSV Gas space velocity

GHSV Gas hourly space velocity

NL Fluid volume in liter evaluated at standard conditions according to IUPAC

NLDFT Non-local density functional theory

NPs Nanoparticles

PSD Pore size distribution

PtG Power-to-Gas

rWGS Reverse water gas shift

TCD Thermal conductivity detector

TEM *Transmission electron microscopy*

TPR Temperature programmed reduction

XPS X-ray photoelectron spectroscopy

XRF X-ray fluorescence spectroscopy

μ-GC Micro gas chromatograph

7. Conclusions / Conclusiones

Considering the initial objectives and the results obtained in this work, the following conclusions can be drawn:

- The effects that the activating conditions have on the textural properties of the resulting activated biochar have been assessed properly. The most remarkable finding was that the pressure positively affects the activation process even at relatively low temperatures (650 °C).
- Activated biochar can effectively be employed as catalytic support in slow pyrolysis vapors upgrading applications. Its significant ash content could play an active role in avoiding catalytic deactivation. In particular, the potassium-containing species are capable to catalyze the gasification of coke deposits produced during the process, freeing the surface of the carbonaceous support. This was also demonstrated by the superior catalytic activity showed by unwashed chemically activated biochar (i.e., with residual K_2CO_3).
- Despite the good catalytic performance of the chemically activated biochar, the high specific surface area and more hierarchical pore size distribution make the physically activated biochar the most appropriate material to be used as catalytic support.
- The investigation of several mono and bimetallic catalysts supported on activated biochar led to the identification of the best catalytic formulation to be employed in pyrolysis oil steam reforming. In fact, a physically activated biochar loaded with 7 wt. % cobalt and 10 wt. % nickel showed no deactivation after the first 14 h of reaction with a constant carbon conversion of 65 %.
- Finally, ceria-doped activated biochar was successfully employed as catalytic support for the CO_2 methanation process, paving the way to a possible integration of biochar to numerous catalytic applications. Even though the results in terms of CH_4 selectivity and CO_2 conversions were promising, the studied formulation must be improved in order to enhance the stability of the catalyst.

In light of the above-mentioned results, it is possible to state that the main objectives initially set (in line with the goals of the GreenCarbon European Training Network) have been accomplished.

In my opinion, the most remarkable achievements obtained in this PhD project are: (i) the determination of the role that the activating pressure has on the textural properties of the resulting activated biochar and (ii) the production of a relatively stable activated biochar-based catalyst for the upgrading of pyrolysis vapors.

Teniendo en cuenta los objetivos iniciales y los resultados obtenidos en este trabajo, se pueden deducir las conclusiones siguientes:

- Se han identificado los efectos de las condiciones de activación sobre las propiedades texturales del biochar activado resultante. El hallazgo más importante ha sido el efecto positivo que un aumento de la presión (durante la activación con CO_2) ha tenido sobre las propiedades texturales, en términos de área superficial especifica y de distribución de tamaño de poros (más jerarquizada), incluso a una temperatura relativamente baja (650 °C).

- Un biochar activado es apropiado como soporte catalítico en los procesos de mejora de vapores de pirólisis. El alto contenido de cenizas puede jugar un papel clave a la hora de evitar la desactivación del catalizador. En concreto, el potasio es capaz de catalizar el proceso de gasificación del coque, liberando la superficie del soporte.

- A pesar de las buena actividades catalíticas mostrada por los biochars activados químicamente, su área específica más alta y su distribución de tamaño de poros más jerarquizada hacen que el biochar activado físicamente sea el material más prometedor para la producción de soportes catalíticos.

- El estudio sobre diferentes catalizadores mono y bimetallicos soportados en biochar activado ha permitido identificar la mejor formulación catalítica para el reformado húmedo de aceite de pirólisis. En concreto, mediante el uso de un catalizador con un 7 % de níquel y un 10 % de cobalto (en peso) —soportados en biochar activado físicamente— fue posible obtener una conversión de carbono del 65 %, sin signos de desactivación tras 14 horas de operación.

- Finalmente, el biochar dopado con certia ha sido usado como soporte catalítico para el proceso de metanación del CO_2. Aunque los resultados obtenidos en términos de selectividad de CH_4 y conversión de CO_2 son prometedores, sería necesario llevar a cabo una mejora de la formulación catalítica con vistas a mejorar la estabilidad del catalizador a largo plazo.

A la vista de los resultados obtenidos en el presente trabajo, se puede afirmar que los objetivos inicialmente planteados (y en el marco del proyecto GreenCarbon) se han alcanzado satisfactoriamente.

En mi opinión, los logros más destacables de este trabajo han sido: (i) la determinación del efecto que la presión ejerce sobre las propiedades texturales del biochar durante su activación física con CO_2, y (ii) la producción de un catalizador soportado por biochar relativamente estable para el reformado húmedo de aceite de pirólisis.

8. Future perspectives

The potential utilization of biochar has been highlighted throughout this research project. However, there are several aspects that should be investigated more deeply to allow the deployment at large scale of this versatile material in the studied fields of applications:

- Chemical activation with K_2CO_3 should be more investigated. In particular, it may be interesting to disclose the effects that the activating temperature has on the resulting activated biochar properties.
- In this PhD thesis it was also carried out a combined activation process (physical activation with CO_2 of a biochar impregnated with K_2CO_3). However, more efforts should be focused on this activation strategy, which could be an innovative route to produce a highly porous material characterized by a high potassium content, useful to gasify the coke deposit produced during the steam reforming of pyrolysis oil.
- Although the Ni-Co biochar catalyst showed strong stability in steam reforming of distilled pyrolysis oil, the formulation must be improved to enhance the catalytic stability during the upgrading of raw pyrolysis oil. Furthermore, it would be interesting to study the upgrading process in an atmosphere rich in CO_2 to simulate a real pyrolysis vapor composition.
- Even though the application of biochar-based catalysts in CO_2 methanation is encouraging, giving promising results in terms of CH_4 selectivity and CO_2 conversion, the studied formulation must be improved to enhance the stability of the catalyst.

9. References

Afolabi, A.T.F., Kechagiopoulos, P.N., Liu, Y., Li, C.Z., 2021. Kinetic features of ethanol steam reforming and decomposition using a biochar-supported Ni catalyst. Fuel Process. Technol. 212, 106622. https://doi.org/10.1016/j.fuproc.2020.106622

Agnelli, M., Swaan, H.M., Marquez-Alvarez, C., Martin, G.A., Mirodatos, C., 1998. CO hydrogenation on a nickel catalyst: II. A mechanistic study by transient kinetics and infrared spectroscopy. J. Catal. 175, 117–128. https://doi.org/10.1006/jcat.1998.1978

Alarcón, A., Guilera, J., Díaz, J.A., Andreu, T., 2019. Optimization of nickel and ceria catalyst content for synthetic natural gas production through CO2 methanation. Fuel Process. Technol. 193, 114–122. https://doi.org/10.1016/j.fuproc.2019.05.008

Aller, M.F., 2016. Biochar properties: Transport, fate, and impact. Crit. Rev. Environ. Sci. Technol. 46, 1183–1296. https://doi.org/10.1080/10643389.2016.1212368

Angin, D., Altintig, E., Köse, T.E., 2013. Influence of process parameters on the surface and chemical properties of activated carbon obtained from biochar by chemical activation. Bioresour. Technol. 148, 542–549. https://doi.org/10.1016/j.biortech.2013.08.164

Antal, M.J., Allen, S.G., Dai, X., Shimizu, B., Tam, M.S., Grønli, M., 2000. Attainment of the theoretical yield of carbon from biomass. Ind. Eng. Chem. Res. 39, 4024–4031. https://doi.org/10.1021/ie000511u

Antal, M.J., Grønli, M., 2003. The art, science, and technology of charcoal production. Ind. Eng. Chem. Res. https://doi.org/10.1021/ie0207919

Arif, M., Ilyas, M., Riaz, M., Ali, K., Shah, K., Ul Haq, I., Fahad, S., 2017. Biochar improves phosphorus use efficiency of organic-inorganic fertilizers, maize-wheat productivity and soil quality in a low fertility alkaline soil. F. Crop. Res. 214, 25–37. https://doi.org/10.1016/j.fcr.2017.08.018

Arrhenius, S., 1896. On the influence of carbonic acid in the air upon the temperature of the ground. London, Edinburgh, Dublin Philos. Mag. J. Sci. 41, 237–276. https://doi.org/10.1080/14786449608620846

Azuara, M., Sáiz, E., Manso, J.A., García-Ramos, F.J., Manyà, J.J., 2017. Study on the effects of using a carbon dioxide atmosphere on the properties of vine shoots-derived biochar. J. Anal. Appl. Pyrolysis 124, 719–725. https://doi.org/10.1016/j.jaap.2016.11.022

Babu, B. V., 2008. Biomass pyrolysis: A state-of-the-art review. Biofuels, Bioprod. Biorefining. https://doi.org/10.1002/bbb.92

Baena-Moreno, F.M., Rodríguez-Galán, M., Vega, F., Alonso-Fariñas, B., Vilches Arenas, L.F., Navarrete, B., 2019. Carbon capture and utilization technologies: a literature review and recent advances. Energy Sources, Part A Recover. Util. Environ. Eff. 41, 1403–1433. https://doi.org/10.1080/15567036.2018.1548518

Banks, S.W., Nowakowski, D.J., Bridgwater, A. V., 2016. Impact of Potassium and Phosphorus in Biomass on the Properties of Fast Pyrolysis Bio-oil. Energy and Fuels 30, 8009–8018. https://doi.org/10.1021/acs.energyfuels.6b01044

Belete, Y.Z., Mau, V., Yahav Spitzer, R., Posmanik, R., Jassby, D., Iddya, A., Kassem, N.,

Tester, J.W., Gross, A., 2021. Hydrothermal carbonization of anaerobic digestate and manure from a dairy farm on energy recovery and the fate of nutrients. Bioresour. Technol. 333, 125164. https://doi.org/10.1016/j.biortech.2021.125164

Blanco, P.H., Wu, C., Onwudili, J.A., Williams, P.T., 2012. Characterization of tar from the pyrolysis/gasification of refuse derived fuel: Influence of process parameters and catalysis. Energy and Fuels 26, 2107–2115. https://doi.org/10.1021/ef300031j

Bruhn, T., Naims, H., Olfe-Kräutlein, B., 2016. Separating the debate on CO2 utilisation from carbon capture and storage. Environ. Sci. Policy 60, 38–43. https://doi.org/10.1016/j.envsci.2016.03.001

Buentello-Montoya, D., Zhang, X., Li, J., Ranade, V., Marques, S., Geron, M., 2020. Performance of biochar as a catalyst for tar steam reforming: Effect of the porous structure. Appl. Energy 259, 114176. https://doi.org/10.1016/j.apenergy.2019.114176

Cha, J.S., Park, S.H., Jung, S.C., Ryu, C., Jeon, J.K., Shin, M.C., Park, Y.K., 2016. Production and utilization of biochar: A review. J. Ind. Eng. Chem. 40, 1–15. https://doi.org/10.1016/j.jiec.2016.06.002

Chatterjee, R., Sajjadi, B., Mattern, D.L., Chen, W.Y., Zubatiuk, T., Leszczynska, D., Leszczynski, J., Egiebor, N.O., Hammer, N., 2018. Ultrasound cavitation intensified amine functionalization: A feasible strategy for enhancing CO2 capture capacity of biochar. Fuel 225, 287–298. https://doi.org/10.1016/j.fuel.2018.03.145

Chen, H., Tang, Z., Liu, B., Chen, W., Hu, J., Chen, Y., Yang, H., 2021. The new insight about mechanism of the influence of K2CO3 on cellulose pyrolysis. Fuel 295, 120617. https://doi.org/10.1016/j.fuel.2021.120617

Chen, J., Wang, M., Wang, S., Li, X., 2018. Hydrogen production via steam reforming of acetic acid over biochar-supported nickel catalysts. Int. J. Hydrogen Energy 43, 18160–18168. https://doi.org/10.1016/j.ijhydene.2018.08.048

Cheng, N., Wang, B., Wu, P., Lee, X., Xing, Y., Chen, M., Gao, B., 2021. Adsorption of emerging contaminants from water and wastewater by modified biochar: A review. Environ. Pollut. 273, 116448. https://doi.org/10.1016/j.envpol.2021.116448

Chew, L.M., Kangvansura, P., Ruland, H., Schulte, H.J., Somsen, C., Xia, W., Eggeler, G., Worayingyong, A., Muhler, M., 2014. Effect of nitrogen doping on the reducibility, activity and selectivity of carbon nanotube-supported iron catalysts applied in CO2 hydrogenation. Appl. Catal. A Gen. 482, 163–170. https://doi.org/10.1016/j.apcata.2014.05.037

Collard, F.X., Blin, J., 2014. A review on pyrolysis of biomass constituents: Mechanisms and composition of the products obtained from the conversion of cellulose, hemicelluloses and lignin. Renew. Sustain. Energy Rev. 38, 594–608. https://doi.org/10.1016/j.rser.2014.06.013

Czernik, S., Bridgwater, A. V., 2004. Overview of applications of biomass fast pyrolysis oil. Energy and Fuels 18, 590–598. https://doi.org/10.1021/ef034067u

de Miguel Mercader, F., Groeneveld, M.J., Kersten, S.R.A., Venderbosch, R.H., Hogendoorn, J.A., 2010. Pyrolysis oil upgrading by high pressure thermal treatment. Fuel 89, 2829–2837. https://doi.org/10.1016/j.fuel.2010.01.026

Dehkhoda, A.M., Gyenge, E., Ellis, N., 2016. A novel method to tailor the porous structure

of KOH-activated biochar and its application in capacitive deionization and energy storage. Biomass and Bioenergy 87, 107–121. https://doi.org/10.1016/j.biombioe.2016.02.023

Demirbas, A., 2004. Effects of temperature and particle size on bio-char yield from pyrolysis of agricultural residues. J. Anal. Appl. Pyrolysis 72, 243–248. https://doi.org/10.1016/J.JAAP.2004.07.003

Dhyani, V., Bhaskar, T., 2018. A comprehensive review on the pyrolysis of lignocellulosic biomass. Renew. Energy 129, 695–716. https://doi.org/10.1016/j.renene.2017.04.035

Di Blasi, C., Signorelli, G., Di Russo, C., Rea, G., 1999. Product Distribution from Pyrolysis of Wood and Agricultural Residues. Ind. Eng. Chem. Res. 38, 2216–2224. https://doi.org/10.1021/IE980711U

Dong, Q., Li, H., Niu, M., Luo, C., Zhang, J., Qi, B., Li, X., Zhong, W., 2018. Microwave pyrolysis of moso bamboo for syngas production and bio-oil upgrading over bamboo-based biochar catalyst. Bioresour. Technol. 266, 284–290. https://doi.org/10.1016/J.BIORTECH.2018.06.104

Dou, X., Hasa, I., Saurel, D., Vaalma, C., Wu, L., Buchholz, D., Bresser, D., Komaba, S., Passerini, S., 2019. Hard carbons for sodium-ion batteries: Structure, analysis, sustainability, and electrochemistry. Mater. Today 23, 87–104. https://doi.org/10.1016/j.mattod.2018.12.040

Du, Z.-Y., Zhang, Z.-H., Xu, C., Wang, X.-B., Li, W.-Y., 2019. Low-Temperature Steam Reforming of Toluene and Biomass Tar over Biochar-Supported Ni Nanoparticles. ACS Sustain. Chem. Eng. 7, 3111–3119. https://doi.org/10.1021/ACSSUSCHEMENG.8B04872

Ducousso, M., Weiss-Hortala, E., Lyczko, N., Nzihou, A., Castaldi, M.J., 2019. 110th Anniversary: Syngas Production Enhancement Using Calcium- And Potassium-Impregnated Chars. Ind. Eng. Chem. Res. 58, 15134–15141. https://doi.org/10.1021/acs.iecr.9b02238

Dufour, A., Celzard, A., Fierro, V., Martin, E., Broust, F., Zoulalian, A., 2008. Catalytic decomposition of methane over a wood char concurrently activated by a pyrolysis gas. Appl. Catal. A Gen. 346, 164–173. https://doi.org/10.1016/j.apcata.2008.05.023

Durán, I., Álvarez-Gutiérrez, N., Rubiera, F., Pevida, C., 2018. Biogas purification by means of adsorption on pine sawdust-based activated carbon: Impact of water vapor. Chem. Eng. J. 353, 197–207. https://doi.org/10.1016/j.cej.2018.07.100

Elsevier, 2021. Scopus.

Enders, A., Hanley, K., Whitman, T., Joseph, S., Lehmann, J., 2012. Characterization of biochars to evaluate recalcitrance and agronomic performance. Bioresour. Technol. 114, 644–653. https://doi.org/10.1016/j.biortech.2012.03.022

Ergun, S., 1956. Kinetics of the Reaction of Carbon with Carbon Dioxide. J. Phys. Chem. 60, 480–485. https://doi.org/10.1021/J150538A022

Escudero-Curiel, S., Acevedo-García, V., Sanromán, M.Á., Pazos, M., 2021. Eco-approach for pharmaceutical removal: Thermochemical waste valorisation, biochar adsorption and electro-assisted regeneration. Electrochim. Acta 389, 138694. https://doi.org/10.1016/j.electacta.2021.138694

European Commission, 2019. European Green Deal [WWW Document]. URL https://ec.europa.eu/info/strategy/priorities-2019-2024/european-green-deal_en

Feng, D., Zhang, Y., Zhao, Y., Sun, S., Wu, J., Tan, H., 2020. Mechanism of in-situ dynamic catalysis and selective deactivation of H2O-activated biochar for biomass tar reforming. Fuel 279, 118450. https://doi.org/10.1016/j.fuel.2020.118450

Fotouhi Tehrani, N., Aznar, J.S., Kiros, Y., 2015. Coffee extract residue for production of ethanol and activated carbons. J. Clean. Prod. 91, 64–70. https://doi.org/10.1016/j.jclepro.2014.12.031

Freddo, A., Cai, C., Reid, B.J., 2012. Environmental contextualisation of potential toxic elements and polycyclic aromatic hydrocarbons in biochar. Environ. Pollut. 171, 18–24. https://doi.org/10.1016/J.ENVPOL.2012.07.009

Fu, D., Chen, Z., Xia, D., Shen, L., Wang, Y., Li, Q., 2017. A novel solid digestate-derived biochar-Cu NP composite activating H2O2 system for simultaneous adsorption and degradation of tetracycline. Environ. Pollut. 221, 301–310. https://doi.org/10.1016/j.envpol.2016.11.078

Fu, K., Yue, Q., Gao, B., Sun, Y., Zhu, L., 2013. Preparation, characterization and application of lignin-based activated carbon from black liquor lignin by steam activation. Chem. Eng. J. 228, 1074–1082. https://doi.org/10.1016/j.cej.2013.05.028

Fu, P., Zhang, A., Luo, S., Yi, W., Hu, S., Zhang, Y., 2019. Catalytic Steam Reforming of Biomass-Derived Acetic Acid over Two Supported Ni Catalysts for Hydrogen-Rich Syngas Production. ACS Omega 4, 13585–13593. https://doi.org/10.1021/acsomega.9b01985

Garbarino, G., Kowalik, P., Riani, P., Antoniak-Jurak, K., Pieta, P., Lewalska-Graczyk, A., Lisowski, W., Nowakowski, R., Busca, G., Pieta, I.S., 2021. Improvement of Ni/Al2O3catalysts for low-temperature CO2methanation by vanadium and calcium oxide addition. Ind. Eng. Chem. Res. 60, 6554–6564. https://doi.org/10.1021/acs.iecr.0c05556

George W. Huber, Sara Iborra, A., Corma*, A., 2006. Synthesis of Transportation Fuels from Biomass: Chemistry, Catalysts, and Engineering. Chem. Rev. 106, 4044–4098. https://doi.org/10.1021/CR068360D

Georgieva, V.G., Gonsalvesh, L., Tavlieva, M.P., 2020. Thermodynamics and kinetics of the removal of nickel (II) ions from aqueous solutions by biochar adsorbent made from agro-waste walnut shells. J. Mol. Liq. 312, 112788. https://doi.org/10.1016/j.molliq.2020.112788

Gonçalves, L.P.L., Sousa, J.P.S., Soares, O.S.G.P., Bondarchuk, O., Lebedev, O.I., Kolen'ko, Y. V., Pereira, M.F.R., 2020. The role of surface properties in CO2methanation over carbon-supported Ni catalysts and their promotion by Fe. Catal. Sci. Technol. 10, 7217–7225. https://doi.org/10.1039/d0cy01254h

Greco, G., Di Stasi, C., Rego, F., González, B., Manyà, J.J., 2020. Effects of slow-pyrolysis conditions on the products yields and properties and on exergy efficiency: A comprehensive assessment for wheat straw. Appl. Energy 279, 115842. https://doi.org/10.1016/j.apenergy.2020.115842

Greco, G., Videgain, M., Di Stasi, C., González, B., Manyà, J.J., 2018. Evolution of the

mass-loss rate during atmospheric and pressurized slow pyrolysis of wheat straw in a bench-scale reactor. J. Anal. Appl. Pyrolysis 136, 18–26. https://doi.org/10.1016/j.jaap.2018.11.007

Guizani, C., Escudero Sanz, F.J., Salvador, S., 2013. The gasification reactivity of high-heating-rate chars in single and mixed atmospheres of H2O and CO2. Fuel 108, 812–823. https://doi.org/10.1016/j.fuel.2013.02.027

Guo, F., Jia, X., Liang, S., Zhou, N., Chen, P., Ruan, R., 2020. Development of biochar-based nanocatalysts for tar cracking/reforming during biomass pyrolysis and gasification. Bioresour. Technol. 298, 122263. https://doi.org/10.1016/j.biortech.2019.122263

Guo, J., Lua, A.C., 1998. Characterization of chars pyrolyzed from oil palm stones for the preparation of activated carbons. J. Anal. Appl. Pyrolysis 46, 113–125. https://doi.org/10.1016/S0165-2370(98)00074-6

Guo, S., Peng, J., Li, W., Yang, K., Zhang, L., Zhang, S., Xia, H., 2009. Effects of CO2 activation on porous structures of coconut shell-based activated carbons. Appl. Surf. Sci. 255, 8443–8449. https://doi.org/10.1016/J.APSUSC.2009.05.150

Gupta, S., Mondal, P., Borugadda, V.B., Dalai, A.K., 2021. Advances in upgradation of pyrolysis bio-oil and biochar towards improvement in bio-refinery economics: A comprehensive review. Environ. Technol. Innov. 21, 101276. https://doi.org/10.1016/j.eti.2020.101276

Habibollahzade, A., Ahmadi, P., Rosen, M.A., 2021. Biomass gasification using various gasification agents: Optimum feedstock selection, detailed numerical analyses and tri-objective grey wolf optimization. J. Clean. Prod. 284, 124718. https://doi.org/10.1016/j.jclepro.2020.124718

Hayashi, J., Horikawa, T., Takeda, I., Muroyama, K., Nasir Ani, F., 2002. Preparing activated carbon from various nutshells by chemical activation with K2CO3. Carbon N. Y. 40, 2381–2386. https://doi.org/10.1016/S0008-6223(02)00118-5

Hervy, M., Weiss-Hortala, E., Pham Minh, D., Dib, H., Villot, A., Gérente, C., Berhanu, S., Chesnaud, A., Thorel, A., Le Coq, L., Nzihou, A., 2019. Reactivity and deactivation mechanisms of pyrolysis chars from bio-waste during catalytic cracking of tar. Appl. Energy 237, 487–499. https://doi.org/10.1016/j.apenergy.2019.01.021

Hu, F., Tong, S., Lu, K., Chen, C.M., Su, F.Y., Zhou, J., Lu, Z.H., Wang, X., Feng, G., Zhang, R., 2019. Reduced graphene oxide supported Ni-Ce catalysts for CO2 methanation: The support and ceria promotion effects. J. CO2 Util. 34, 676–687. https://doi.org/10.1016/j.jcou.2019.08.020

Hu, X., Lu, G., 2009. Investigation of the steam reforming of a series of model compounds derived from bio-oil for hydrogen production. Appl. Catal. B Environ. 88, 376–385. https://doi.org/10.1016/j.apcatb.2008.10.021

Hwang, S., Hong, U.G., Lee, J., Baik, J.H., Koh, D.J., Lim, H., Song, I.K., 2012. Methanation of carbon dioxide over mesoporous nickel-m-alumina (M 5 Fe, Zr, Ni, Y, and Mg) xerogel catalysts: Effect of second metal. Catal. Letters 142, 860–868. https://doi.org/10.1007/s10562-012-0842-0

Inyang, M.I., Gao, B., Yao, Y., Xue, Y., Zimmerman, A., Mosa, A., Pullammanappallil, P.,

Ok, Y.S., Cao, X., 2016. A review of biochar as a low-cost adsorbent for aqueous heavy metal removal. Crit. Rev. Environ. Sci. Technol. 46, 406–433. https://doi.org/10.1080/10643389.2015.1096880

Iojoiu, E.E., Domine, M.E., Davidian, T., Guilhaume, N., Mirodatos, C., 2007. Hydrogen production by sequential cracking of biomass-derived pyrolysis oil over noble metal catalysts supported on ceria-zirconia. Appl. Catal. A Gen. 323, 147–161. https://doi.org/10.1016/j.apcata.2007.02.018

Jagiello, J., Kenvin, J., Celzard, A., Fierro, V., 2019. Enhanced resolution of ultra micropore size determination of biochars and activated carbons by dual gas analysis using N2 and CO2 with 2D-NLDFT adsorption models. Carbon N. Y. 144, 206–215. https://doi.org/10.1016/j.carbon.2018.12.028

Jawad, A.H., Abdulhameed, A.S., Hanafiah, M.A.K.M., ALOthman, Z.A., Khan, M.R., Surip, S.N., 2021. Numerical desirability function for adsorption of methylene blue dye by sulfonated pomegranate peel biochar: Modeling, kinetic, isotherm, thermodynamic, and mechanism study. Korean J. Chem. Eng. 38, 1499–1509. https://doi.org/10.1007/s11814-021-0801-9

Jedynak, K., Charmas, B., 2021. Preparation and Characterization of Physicochemical Properties of Spruce Cone Biochars Activated by CO2. Materials (Basel). 14, 3859.

Jing, X., Wang, Z., Yu, Z., Zhang, Q., Li, C., Fang, Y., 2013. Experimental and Kinetic Investigations of CO2 Gasification of Fine Chars Separated from a Pilot-Scale Fluidized-Bed Gasifier. Energy and Fuels 27, 2422–2430. https://doi.org/10.1021/EF4002296

Jung, S.H., Kim, J.S., 2014. Production of biochars by intermediate pyrolysis and activated carbons from oak by three activation methods using CO2. J. Anal. Appl. Pyrolysis 107, 116–122. https://doi.org/10.1016/j.jaap.2014.02.011

Kang, K., Qiu, L., Zhu, M., Sun, G., Wang, Y., Sun, R., 2018. Codensification of Agroforestry Residue with Bio-Oil for Improved Fuel Pellets. Energy and Fuels 32, 598–606. https://doi.org/10.1021/acs.energyfuels.7b03482

Kannan, M.P., Richards, G.N., 1990. Gasification of biomass chars in carbon dioxide: dependence of gasification rate on the indigenous metal content. Fuel 69, 747–753. https://doi.org/10.1016/0016-2361(90)90041-N

Kaya, N., Uzun, Z.Y., 2021. Investigation of effectiveness of pine cone biochar activated with KOH for methyl orange adsorption and CO2 capture. Biomass Convers. Biorefinery 11, 1067–1083. https://doi.org/10.1007/s13399-020-01063-8

Kenney, K.L., Smith, W.A., Gresham, G.L., Westover, T.L., 2013. Understanding biomass feedstock variability. Biofuels 4, 111–127. https://doi.org/10.4155/bfs.12.83

Kim, J., Lee, G., Park, J., Kim, S., 2021. Limitation of K2CO3 as a Chemical Agent for Upgrading Activated Carbon. Processes 9, 1000

Kim, K.C., Yoon, T.U., Bae, Y.S., 2016. Applicability of using CO2 adsorption isotherms to determine BET surface areas of microporous materials. Microporous Mesoporous Mater. 224, 294–301. https://doi.org/10.1016/j.micromeso.2016.01.003

Kolb, S.E., Fermanich, K.J., Dornbush, M.E., 2009. Effect of Charcoal Quantity on Microbial Biomass and Activity in Temperate Soils. Soil Sci. Soc. Am. J. 73, 1173–

1181. https://doi.org/10.2136/sssaj2008.0232

Kwiatkowski, M., Fierro, V., Celzard, A., 2019. Confrontation of various adsorption models for assessing the porous structure of activated carbons. Adsorption 25, 1673–1682. https://doi.org/10.1007/s10450-019-00129-y

Lahijani, P., Zainal, Z.A., Mohamed, A.R., Mohammadi, M., 2013. CO2 gasification reactivity of biomass char: Catalytic influence of alkali, alkaline earth and transition metal salts. Bioresour. Technol. 144, 288–295. https://doi.org/10.1016/j.biortech.2013.06.059

Lahijani, P., Zainal, Z.A., Mohammadi, M., Mohamed, A.R., 2015. Conversion of the greenhouse gas CO2 to the fuel gas CO via the Boudouard reaction: A review. Renew. Sustain. Energy Rev. 41, 615–632. https://doi.org/10.1016/j.rser.2014.08.034

Le, M.C., Van, K. Le, Nguyen, T.H.T., Nguyen, N.H., 2017. The Impact of Ce-Zr Addition on Nickel Dispersion and Catalytic Behavior for CO_2 Methanation of Ni/AC Catalyst at Low Temperature. J. Chem. 2017, 4361056. https://doi.org/10.1155/2017/4361056

Ledesma, E.B., Hoang, J.N., Nguyen, Q., Hernandez, V., Nguyen, M.P., Batamo, S., Fortune, C.K., 2013. Unimolecular decomposition pathway for the vapor-phase cracking of eugenol, a biomass tar compound. Energy and Fuels 27, 6839–6846. https://doi.org/10.1021/ef401760c

Lee, J., Kim, K.H., Kwon, E.E., 2017. Biochar as a Catalyst. Renew. Sustain. Energy Rev. 77, 70–79. https://doi.org/10.1016/j.rser.2017.04.002

Lee, J.H., Heo, Y.J., Park, S.J., 2018. Effect of silica removal and steam activation on extra-porous activated carbons from rice husks for methane storage. Int. J. Hydrogen Energy 43, 22377–22384. https://doi.org/10.1016/j.ijhydene.2018.10.039

Lehmann, J., Joseph, S., 2015. Biochar for environmental management, 2nd ed, Biochar for Environmental Management. Routledge. https://doi.org/10.4324/9780203762264-8

Lehmann, J., Kern, D.C., Glaser, B., Woods, W.I., 2004. Amazonian Dark Earths: Origin, Properties, Management, Springer Netherlands. https://doi.org/10.1002/9781118941065.ch33

Lehmann, J., Stephen, J., 2015. Biochar for Environmental Management: Science, Technology and Implementation, Science And Technology.

Leng, L., Xiong, Q., Yang, L., Li, Hui, Zhou, Y., Zhang, W., Jiang, S., Li, Hailong, Huang, H., 2021. An overview on engineering the surface area and porosity of biochar. Sci. Total Environ. 763, 144204. https://doi.org/10.1016/j.scitotenv.2020.144204

Li, J., Chen, Y., Yang, H., Zhu, D., Chen, X., Wang, X., Chen, H., 2017. Correlation of Feedstock and Bio-oil Compound Distribution. Energy and Fuels 31, 7093–7100. https://doi.org/10.1021/acs.energyfuels.7b00545

Li, J., Mei, X., Zhang, L., Yu, Z., Liu, Q., Wei, T., Wu, W., Dong, D., Xu, L., Hu, X., 2020. A comparative study of catalytic behaviors of Mn, Fe, Co, Ni, Cu and Zn–Based catalysts in steam reforming of methanol, acetic acid and acetone. Int. J. Hydrogen Energy 45, 3815–3832. https://doi.org/10.1016/j.ijhydene.2019.03.269

Li, W., Liu, Y., Mu, M., Ding, F., Liu, Z., Guo, X., Song, C., 2019. Organic acid-assisted preparation of highly dispersed Co/ZrO2 catalysts with superior activity for CO2 methanation. Appl. Catal. B Environ. 254, 531–540. https://doi.org/10.1016/j.apcatb.2019.05.028

Li, W., Nie, X., Jiang, X., Zhang, A., Ding, F., Liu, M., Liu, Z., Guo, X., Song, C., 2018. ZrO2 support imparts superior activity and stability of Co catalysts for CO2 methanation. Appl. Catal. B Environ. 220, 397–408. https://doi.org/10.1016/j.apcatb.2017.08.048

Li, X., Zhang, Z., Zhang, L., Fan, H., Li, Xueli, Liu, Q., Wang, S., Hu, X., 2020. Investigation of coking behaviors of model compounds in bio-oil during steam reforming. Fuel 265, 116961. https://doi.org/10.1016/j.fuel.2019.116961

Li, Y., Chen, M., Liu, B., Zhang, Y., Liang, X., Xia, X., 2020. Heteroatom Doping: An Effective Way to Boost Sodium Ion Storage. Adv. Energy Mater. 10. https://doi.org/10.1002/aenm.202000927

Liu, Junhong, Huang, Z., Chen, Z., Sun, J., Gao, Y., Wu, E., 2020. Resource utilization of swine sludge to prepare modified biochar adsorbent for the efficient removal of Pb(II) from water. J. Clean. Prod. 257, 120322. https://doi.org/10.1016/j.jclepro.2020.120322

Liu, Jiwei, Jiang, J., Meng, Y., Aihemaiti, A., Xu, Y., Xiang, H., Gao, Y., Chen, X., 2020. Preparation, environmental application and prospect of biochar-supported metal nanoparticles: A review. J. Hazard. Mater. 388, 122026. https://doi.org/10.1016/j.jhazmat.2020.122026

Liu, S., Wu, G., Gao, Y., Li, B., Feng, Y., Zhou, J., Hu, X., Huang, Y., Zhang, S., Zhang, H., 2021. Understanding the catalytic upgrading of bio-oil from pine pyrolysis over CO2-activated biochar. Renew. Energy 174, 538–546. https://doi.org/10.1016/j.renene.2021.04.085

Liu, W.J., Jiang, H., Yu, H.Q., 2015. Development of Biochar-Based Functional Materials: Toward a Sustainable Platform Carbon Material. Chem. Rev. https://doi.org/10.1021/acs.chemrev.5b00195

Liu, Y., Paskevicius, M., Sofianos, M.V., Parkinson, G., Wang, S., Li, C.Z., 2021a. A SAXS study of the pore structure evolution in biochar during gasification in H2O, CO2 and H2O/CO2. Fuel 292, 120384. https://doi.org/10.1016/j.fuel.2021.120384

Liu, Y., Paskevicius, M., Wang, H., Fushimi, C., Parkinson, G., Li, C.Z., 2020. Difference in tar reforming activities between biochar catalysts activated in H2O and CO2. Fuel 271, 117636. https://doi.org/10.1016/j.fuel.2020.117636

Liu, Y., Paskevicius, M., Wang, H., Parkinson, G., Wei, J., Asif Akhtar, M., Li, C.Z., 2021b. Insights into the mechanism of tar reforming using biochar as a catalyst. Fuel 296, 120672. https://doi.org/10.1016/j.fuel.2021.120672

Lopes, G.K.P., Zanella, H.G., Spessato, L., Ronix, A., Viero, P., Fonseca, J.M., Yokoyama, J.T.C., Cazetta, A.L., Almeida, V.C., 2021. Steam-activated carbon from malt bagasse: Optimization of preparation conditions and adsorption studies of sunset yellow food dye. Arab. J. Chem. 14, 103001. https://doi.org/10.1016/j.arabjc.2021.103001

Lozano-Castelló, D., Calo, J.M., Cazorla-Amorós, D., Linares-Solano, A., 2007. Carbon activation with KOH as explored by temperature programmed techniques, and the effects of hydrogen. Carbon N. Y. 45, 2529–2536. https://doi.org/10.1016/j.carbon.2007.08.021

Lozano, P., Simón, A., García, L., Ruiz, J., Oliva, M., Arauzo, J., 2021. Influence of the Ni-Co/Al-Mg Catalyst Loading in the Continuous Aqueous Phase Reforming of the Bio-Oil Aqueous Fraction. Processes 9, 81. https://doi.org/10.3390/pr9010081

Lu, H.R., El Hanandeh, A., 2019. Life cycle perspective of bio-oil and biochar production from hardwood biomass; what is the optimum mix and what to do with it? J. Clean. Prod. 212, 173–189. https://doi.org/10.1016/j.jclepro.2018.12.025

Lu, Q., Yang, X.C., Dong, C.Q., Zhang, Z.F., Zhang, X.M., Zhu, X.F., 2011. Influence of pyrolysis temperature and time on the cellulose fast pyrolysis products: Analytical Py-GC/MS study. J. Anal. Appl. Pyrolysis 92, 430–438. https://doi.org/10.1016/j.jaap.2011.08.006

Lu, X., Ma, X., Chen, X., 2021. Co-hydrothermal carbonization of sewage sludge and lignocellulosic biomass: Fuel properties and heavy metal transformation behaviour of hydrochars. Energy 221, 119896. https://doi.org/10.1016/j.energy.2021.119896

Lu, Z., Zhang, H., Shahab, A., Zhang, K., Zeng, H., Bacha, A.U.R., Nabi, I., Ullah, H., 2021. Comparative study on characterization and adsorption properties of phosphoric acid activated biochar and nitrogen-containing modified biochar employing Eucalyptus as a precursor. J. Clean. Prod. 303, 127046. https://doi.org/10.1016/j.jclepro.2021.127046

Ma, Q., Chen, W., Jin, Z., Chen, L., Zhou, Q., Jiang, X., 2021. One-step synthesis of microporous nitrogen-doped biochar for efficient removal of CO2 and H2S. Fuel 289, 119932. https://doi.org/10.1016/J.FUEL.2020.119932

Ma, Y., Liu, W.J., Zhang, N., Li, Y.S., Jiang, H., Sheng, G.P., 2014. Polyethylenimine modified biochar adsorbent for hexavalent chromium removal from the aqueous solution. Bioresour. Technol. 169, 403–408. https://doi.org/10.1016/j.biortech.2014.07.014

Ma, Z., Xiao, R., Zhang, H., 2017. Catalytic steam reforming of bio-oil model compounds for hydrogen-rich gas production using bio-char as catalyst. Int. J. Hydrogen Energy 42, 3579–3585. https://doi.org/10.1016/j.ijhydene.2016.11.107

Mai, T.T., Vu, D.L., Huynh, D.C., Wu, N.L., Le, A.T., 2019. Cost-effective porous carbon materials synthesized by carbonizing rice husk and K2CO3 activation and their application for lithium-sulfur batteries. J. Sci. Adv. Mater. Devices 4, 223–229. https://doi.org/10.1016/j.jsamd.2019.04.009

Manyà, J.J., 2019. Advanced Carbon Materials from Biomass: an Overview. Zenodo. https://doi.org/10.5281/ZENODO.3233733

Manyà, J.J., 2012. Pyrolysis for biochar purposes: A review to establish current knowledge gaps and research needs. Environ. Sci. Technol. 46, 7939–7954. https://doi.org/10.1021/es301029g

Manyà, J.J., Azuara, M., Manso, J.A., 2018a. Biochar production through slow pyrolysis of different biomass materials: Seeking the best operating conditions. Biomass and

Bioenergy 117, 115–123. https://doi.org/10.1016/j.biombioe.2018.07.019

Manyà, J.J., García-Morcate, D., González, B., 2020. Adsorption performance of physically activated biochars for postcombustion CO2 capture from dry and humid flue gas. Appl. Sci. 10, 1–17. https://doi.org/10.3390/app10010376

Manyà, J.J., González, B., Azuara, M., Arner, G., 2018b. Ultra-microporous adsorbents prepared from vine shoots-derived biochar with high CO2 uptake and CO2/N2 selectivity. Chem. Eng. J. 345, 631–639. https://doi.org/10.1016/j.cej.2018.01.092

Manyà, J.J., Laguarta, S., Ortigosa, M.A., Manso, J.A., 2014a. Biochar from slow pyrolysis of two-phase olive mill waste: Effect of pressure and peak temperature on its potential stability. Energy and Fuels 28, 3271–3280. https://doi.org/10.1021/ef500654t

Manyà, J.J., Ortigosa, M.A., Laguarta, S., Manso, J.A., 2014b. Experimental study on the effect of pyrolysis pressure, peak temperature, and particle size on the potential stability of vine shoots-derived biochar. Fuel 133, 163–172. https://doi.org/10.1016/j.fuel.2014.05.019

Matos, J., Labady, M., Albornoz, A., Laine, J., Brito, J.L., 2005. Catalytic effect of KOH on textural changes of carbon macro-networks by physical activation. J. Mol. Catal. A Chem. 228, 189–194. https://doi.org/10.1016/j.molcata.2004.09.039

Mcbeath, A. V, Smernik, R.J., Krull, E.S., Lehmann, J., 2014. The influence of feedstock and production temperature on biochar carbon chemistry: A solid-state 13 C NMR study. Biomass and Bioenergy 60, 121–129. https://doi.org/10.1016/j.biombioe.2013.11.002

McGrath, T.E., Geoffrey Chan, W., Hajaligol, M.R., 2003. Low temperature mechanism for the formation of polycyclic aromatic hydrocarbons from the pyrolysis of cellulose, in: Journal of Analytical and Applied Pyrolysis. Elsevier, pp. 51–70. https://doi.org/10.1016/S0165-2370(02)00105-5

Merckel, R.D., Heydenrych, M.D., Sithole, B.B., 2021. Pyrolysis oil composition and catalytic activity estimated by cumulative mass analysis using Py-GC/MS EGA-MS. Energy 219, 119428. https://doi.org/10.1016/J.ENERGY.2020.119428

Midilli, A., Kucuk, H., Topal, M.E., Akbulut, U., Dincer, I., 2021. A comprehensive review on hydrogen production from coal gasification: Challenges and Opportunities. Int. J. Hydrogen Energy 46, 25385–25412. https://doi.org/10.1016/j.ijhydene.2021.05.088

Mielenz, J.R., 2009. Biofuels, Methods in molecular biology (Clifton, N.J.). Humana Press, Totowa, NJ. https://doi.org/10.1007/978-1-60761-214-8_11

Min, F., Zhang, M., Zhang, Y., Cao, Y., Pan, W.P., 2011. An experimental investigation into the gasification reactivity and structure of agricultural waste chars. J. Anal. Appl. Pyrolysis 92, 250–257. https://doi.org/10.1016/J.JAAP.2011.06.005

Mishra, S., Kumar Upadhyay, R., 2021. Review on Biomass Gasification: Gasifiers, Gasifying mediums, and Operational parameters. Mater. Sci. Energy Technol. 4, 329–340. https://doi.org/10.1016/j.mset.2021.08.009

Mullen, C.A., Boateng, A.A., 2011. Characterization of water insoluble solids isolated from various biomass fast pyrolysis oils. J. Anal. Appl. Pyrolysis 90, 197–203.

https://doi.org/10.1016/j.jaap.2010.12.004

Ning, S.K., Hung, M.C., Chang, Y.H., Wan, H.P., Lee, H.T., Shih, R.F., 2013. Benefit assessment of cost, energy, and environment for biomass pyrolysis oil. J. Clean. Prod. 59, 141–149. https://doi.org/10.1016/j.jclepro.2013.06.042

Noichi, H., Uddin, A., Sasaoka, E., 2010. Steam reforming of naphthalene as model biomass tar over iron–aluminum and iron–zirconium oxide catalyst catalysts. Fuel Process. Technol. 91, 1609–1616. https://doi.org/10.1016/J.FUPROC.2010.06.009

Paasikallio, V., Kihlman, J., Sánchez, C.A., Simell, P., Solantausta, Y., Lehtonen, J., 2015. Steam reforming of pyrolysis oil aqueous fraction obtained by one-step fractional condensation. Int. J. Hydrogen Energy 40, 3149–3157. https://doi.org/10.1016/j.ijhydene.2015.01.025

Park, H.J., Park, S.H., Sohn, J.M., Park, J., Jeon, J.K., Kim, S.S., Park, Y.K., 2010. Steam reforming of biomass gasification tar using benzene as a model compound over various Ni supported metal oxide catalysts. Bioresour. Technol. 101, S101–S103. https://doi.org/10.1016/j.biortech.2009.03.036

Pastorova, I., Botto, R.E., Arisz, P.W., Boon, J.J., 1994. Cellulose char structure: a combined analytical Py-GC-MS, FTIR, and NMR study. Carbohydr. Res. 262, 27–47. https://doi.org/10.1016/0008-6215(94)84003-2

Patra, B.R., Mukherjee, A., Nanda, S., Dalai, A.K., 2021. Biochar production, activation and adsorptive applications: a review. Environ. Chem. Lett. 19, 2237–2259. https://doi.org/10.1007/s10311-020-01165-9

Paz-Ferreiro, J., Méndez, A., Gascó, G., 2015. Application of Biochar for Soil Biological Improvement, in: Guo, M., He, Z., Uchimiya, S.. (Eds.), Agricultural and Environmental Applications of Biochar: Advances and Barriers. Soil ScienceSociety of America, pp. 145–174. https://doi.org/10.2136/SSSASPECPUB63.2014.0041.5

Petersen, E.M., Rao, R.G., Vance, B.C., Tessonnier, J.P., 2021. SiO2/SiC supports with tailored thermal conductivity to reveal the effect of surface temperature on Ru-catalyzed CO2 methanation. Appl. Catal. B Environ. 286, 119904. https://doi.org/10.1016/j.apcatb.2021.119904

Phongprueksathat, N., Meeyoo, V., Rirksomboon, T., 2019. Steam reforming of acetic acid for hydrogenproduction : Catalytic performances of Ni and Co supported on Ce0·75Zr0·25O2 catalysts. Int. J. Hydrogen Energy 44, 9359–9367. https://doi.org/10.1016/j.ijhydene.2019.02.085

Pratt, K., Moran, D., 2010. Evaluating the cost-effectiveness of global biochar mitigation potential. Biomass and Bioenergy 34, 1149–1158. https://doi.org/10.1016/j.biombioe.2010.03.004

Puig-Gamero, M., Esteban-Arranz, A., Sanchez-Silva, L., Sanchez, P., 2021. Obtaining activated biochar from olive stone using a bench scale high-pressure thermobalance. J. Environ. Chem. Eng. 9, 105374. https://doi.org/10.1016/j.jece.2021.105374

Qian, K., Kumar, A., Zhang, H., Bellmer, D., Huhnke, R., 2015. Recent advances in utilization of biochar. Renew. Sustain. Energy Rev. 42, 1055–1064. https://doi.org/10.1016/j.rser.2014.10.074

Quan, Y., Zhang, N., Zhang, Z., Han, Y., Zhao, J., Ren, J., 2021. Enhanced performance of

Ni catalysts supported on ZrO2 nanosheets for CO2 methanation: Effects of support morphology and chelating ligands. Int. J. Hydrogen Energy 46, 14395–14406. https://doi.org/10.1016/j.ijhydene.2021.01.236

Querejeta, N., Rubiera, F., Pevida, C., 2019. Enhanced capacity to CO2 sorption in humid conditions with a K-doped biocarbon. J. Energy Chem. 34, 208–219. https://doi.org/10.1016/j.jechem.2018.09.023

Rathnayake, D., Creber, H., Van Poucke, R., Sohi, S., Meers, E., Mašek, O., Ronsse, F., 2021a. Biochar from sawmill residues: characterization and evaluation for its potential use in the horticultural growing media. Biochar 3, 201–212. https://doi.org/10.1007/s42773-021-00092-4

Rathnayake, D., Ehidiamhen, P.O., Egene, C.E., Stevens, C. V., Meers, E., Mašek, O., Ronsse, F., 2021b. Investigation of biomass and agricultural plastic co-pyrolysis: Effect on biochar yield and properties. J. Anal. Appl. Pyrolysis 155, 105029. https://doi.org/10.1016/j.jaap.2021.105029

Renda, S., Ricca, A., Palma, V., 2021. Study of the effect of noble metal promotion in Ni-based catalyst for the Sabatier reaction. Int. J. Hydrogen Energy 46, 12117–12127. https://doi.org/10.1016/j.ijhydene.2020.05.093

Rioche, C., Kulkarni, S., Meunier, F.C., Breen, J.P., Burch, R., 2005. Steam reforming of model compounds and fast pyrolysis bio-oil on supported noble metal catalysts. Appl. Catal. B Environ. 61, 130–139. https://doi.org/10.1016/j.apcatb.2005.04.015

Rodríguez-Reinoso, F., López-González, J. de D., Berenguer, C., 1984. Activated carbons from almond shells—II: Characterization of the pore structure. Carbon 22, 13–18. https://doi.org/10.1016/0008-6223(84)90128-3

Ronsse, F., van Hecke, S., Dickinson, D., Prins, W., 2013. Production and characterization of slow pyrolysis biochar: Influence of feedstock type and pyrolysis conditions. GCB Bioenergy 5, 104–115. https://doi.org/10.1111/gcbb.12018

Sajjadi, B., Chen, W.-Y., Egiebor, N.O., 2019. A comprehensive review on physical activation of biochar for energy and environmental applications. Rev. Chem. Eng. 35, 735–776. https://doi.org/10.1515/REVCE-2017-0113

Sayğılı, H., Akkaya Sayğılı, G., 2019. Optimized preparation for bimodal porous carbon from lentil processing waste by microwave-assisted K2 CO3 activation : Spectroscopic characterization and dye decolorization activity. J. Clean. Prod. 226, 968–976. https://doi.org/10.1016/j.jclepro.2019.04.121

Scheirs, J., Camino, G., Tumiatti, W., 2001. Overview of water evolution during the thermal degradation of cellulose. Eur. Polym. J. 37, 933–942. https://doi.org/10.1016/S0014-3057(00)00211-1

Schmidt, H.P., Wilson, K., 2014. The 55 uses of biochar. Biochar J.

Schneider, C., Zeller, M., Böhm, D., Kolb, T., 2021. Influence of pressure on the gasification kinetics of two high-temperature beech wood chars with CO2, H2O and its mixture. Fuel 299, 120523. https://doi.org/10.1016/j.fuel.2021.120523

Senneca, O., 2007. Kinetics of pyrolysis, combustion and gasification of three biomass fuels. Fuel Process. Technol. 88, 87–97. https://doi.org/10.1016/j.fuproc.2006.09.002

Shen, J., Wang, X.S., Garcia-Perez, M., Mourant, D., Rhodes, M.J., Li, C.Z., 2009. Effects of particle size on the fast pyrolysis of oil mallee woody biomass. Fuel 88, 1810–1817. https://doi.org/10.1016/j.fuel.2009.05.001

Shen, Y., 2015. Chars as carbonaceous adsorbents/catalysts for tar elimination during biomass pyrolysis or gasification. Renew. Sustain. Energy Rev. 43, 281–295. https://doi.org/10.1016/j.rser.2014.11.061

Shen, Y., Zhao, P., Shao, Q., 2014. Porous silica and carbon derived materials from rice husk pyrolysis char. Microporous Mesoporous Mater. 188, 46–76. https://doi.org/10.1016/j.micromeso.2014.01.005

Smith, P., 2016. Soil carbon sequestration and biochar as negative emission technologies. Glob. Chang. Biol. 22, 1315–1324. https://doi.org/10.1111/gcb.13178

Sohi, S., Lopez-Capel, E., Krull, E., Bol, R., 2009. Biochar's roles in soil and climate change: A review of research needs. CSIRO L. Water Sci. Rep. Ser. 5, 64.

Song, X., Li, K., Wang, C., Sun, X., Ning, P., Tang, L., 2017. Regeneration performance and mechanism of modified walnut shell biochar catalyst for low temperature catalytic hydrolysis of organic sulfur. Chem. Eng. J. 330, 727–735. https://doi.org/10.1016/j.cej.2017.08.016

Stephens, J.C., 2014. Time to stop investing in carbon capture and storage and reduce government subsidies of fossil-fuels. Wiley Interdiscip. Rev. Clim. Chang. 5, 169–173. https://doi.org/10.1002/wcc.266

Sueyasu, T., Oike, T., Mori, A., Kudo, S., Norinaga, K., Hayashi, J.I., 2012. Simultaneous steam reforming of tar and steam gasification of char from the pyrolysis of potassium-loaded woody biomass. Energy and Fuels 26, 199–208. https://doi.org/10.1021/ef201166a

Takanabe, K., Aika, K.I., Seshan, K., Lefferts, L., 2004. Sustainable hydrogen from bio-oil—Steam reforming of acetic acid as a model oxygenate. J. Catal. 227, 101–108. https://doi.org/10.1016/J.JCAT.2004.07.002

Tancredi, N., Cordero, T., Rodríguez-Mirasol, J., Rodríguez, J.J., 1996. CO2 gasification of eucalyptus wood chars. Fuel 75, 1505–1508. https://doi.org/10.1016/0016-2361(96)82641-X

Thema, M., Bauer, F., Sterner, M., 2019. Power-to-Gas: Electrolysis and methanation status review. Renew. Sustain. Energy Rev. 112, 775–787. https://doi.org/10.1016/j.rser.2019.06.030

Tian, H., Hu, Q., Wang, J., Chen, D., Yang, Y., Bridgwater, A. V., 2021. Kinetic study on the CO2 gasification of biochar derived from Miscanthus at different processing conditions. Energy 217, 119341. https://doi.org/10.1016/j.energy.2020.119341

Tomczyk, A., Sokołowska, Z., Boguta, P., 2020. Biochar physicochemical properties: pyrolysis temperature and feedstock kind effects. Rev. Environ. Sci. Biotechnol. 19, 191–215. https://doi.org/10.1007/s11157-020-09523-3

Tsai, W.T., Chang, C.Y., Wang, S.Y., Chang, C.F., Chien, S.F., Sun, H.F., 2001. Preparation of activated carbons from corn cob catalyzed by potassium salts and subsequent gasification with CO2. Bioresour. Technol. 78, 203–208. https://doi.org/10.1016/S0960-8524(00)00111-5

UNFCCC, 2005. Clarifications of definition of biomass and consideration of changes in carbon pools due to a CDM project activity.

Vagia, E.C., Lemonidou, A.A., 2008. Hydrogen production via steam reforming of bio-oil components over calcium aluminate supported nickel and noble metal catalysts. Appl. Catal. A Gen. 351, 111–121. https://doi.org/10.1016/j.apcata.2008.09.007

Videgain-Marco, M., Marco-Montori, P., Martí-Dalmau, C., Jaizme-Vega, M. del C., Manyà-Cervelló, J.J., García-Ramos, F.J., 2020. Effects of Biochar Application in a Sorghum Crop under Greenhouse Conditions: Growth Parameters and Physicochemical Fertility. Agronomy 10, 104. https://doi.org/10.3390/agronomy10010104

Vochozka, M., Maroušková, A., Váchal, J., Straková, J., 2016. Biochar pricing hampers biochar farming. Clean Technol. Environ. Policy 18, 1225–1231. https://doi.org/10.1007/s10098-016-1113-3

Walton, K.S., Snurr, R.Q., 2007. Applicability of the BET method for determining surface areas of microporous metal-organic frameworks. J. Am. Chem. Soc. 129, 8552–8556. https://doi.org/10.1021/ja071174k

Wan, H.J., Wu, B.S., Zhang, C.H., Xiang, H.W., Li, Y.W., Xu, B.F., Yi, F., 2007. Study on Fe-Al2O3 interaction over precipitated iron catalyst for Fischer-Tropsch synthesis. Catal. Commun. 8, 1538–1545. https://doi.org/10.1016/j.catcom.2007.01.002

Wang, L., Sun, F., Hao, F., Qu, Z., Gao, J., Liu, M., Wang, K., 2020. A green trace K2CO3 induced catalytic activation strategy for developing coal-converted activated carbon as advanced candidate for CO2 adsorption and supercapacitors. Chem. Eng. J. 383, 123205. https://doi.org/10.1016/j.cej.2019.123205

Wang, N., Chen, D., Arena, U., He, P., 2017. Hot char-catalytic reforming of volatiles from MSW pyrolysis. Appl. Energy 191, 111–124. https://doi.org/10.1016/j.apenergy.2017.01.051

Wang, W., Duong-Viet, C., Ba, H., Baaziz, W., Tuci, G., Caporali, S., Nguyen-Dinh, L., Ersen, O., Giambastiani, G., Pham-Huu, C., 2019. Nickel Nanoparticles Decorated Nitrogen-Doped Carbon Nanotubes (Ni/N-CNT); A Robust Catalyst for the Efficient and Selective CO2 Methanation. ACS Appl. Energy Mater. 2, 1111–1120. https://doi.org/10.1021/acsaem.8b01681

Wang, X., Liu, Y., Zhu, L., Li, Y., Wang, K., Qiu, K., Tippayawong, N., Aggarangsi, P., Reubroycharoen, P., Wang, S., 2019. Biomass derived N-doped biochar as efficient catalyst supports for CO2 methanation. J. CO2 Util. 34, 733–741. https://doi.org/10.1016/j.jcou.2019.09.003

Wang, X., Yang, M., Zhu, X., Zhu, L., Wang, S., 2020. Experimental study and life cycle assessment of CO2 methanation over biochar supported catalysts. Appl. Energy 280, 115919. https://doi.org/10.1016/j.apenergy.2020.115919

Wang, Y., Zhang, Z., Zhang, S., Wang, Yi, Hu, S., Xiang, J., Hu, X., 2020. Steam reforming of acetic acid over Ni/biochar catalyst treated with HNO3: Impacts of the treatment on surface properties and catalytic behaviors. Fuel 278, 118341. https://doi.org/10.1016/j.fuel.2020.118341

Wolf, M., Wong, L.H., Schüler, C., Hinrichsen, O., 2020. CO2 methanation on transition-

metal-promoted Ni-Al catalysts: Sulfur poisoning and the role of CO2 adsorption capacity for catalyst activity. J. CO2 Util. 36, 276–287. https://doi.org/10.1016/j.jcou.2019.10.014

Xiong, J., Xu, J., Zhou, M., Zhao, W., Chen, C., Wang, M., Tan, W., Koopal, L., 2021. Quantitative Characterization of the Site Density and the Charged State of Functional Groups on Biochar. ACS Sustain. Chem. Eng. 9, 2600–2608. https://doi.org/10.1021/acssuschemeng.0c09051

Xu, B., Argyle, M.D., Shi, X., Goroncy, A.K., Rony, A.H., Tan, G., Fan, M., 2020. Effects of mixture of CO2 /CH4 as pyrolysis atmosphere on pine wood pyrolysis products. Renew. Energy 162, 1243–1254. https://doi.org/10.1016/J.RENENE.2020.08.069

Yan, Q., Wan, C., Liu, J., Gao, J., Yu, F., Zhang, J., Cai, Z., 2013. Iron nanoparticles in situ encapsulated in biochar-based carbon as an effective catalyst for the conversion of biomass-derived syngas to liquid hydrocarbons. Green Chem. 15, 1631–1640. https://doi.org/10.1039/C3GC37107G

Yang, H., Chen, Z., Chen, W., Chen, Y., Wang, X., Chen, H., 2020. Role of porous structure and active O-containing groups of activated biochar catalyst during biomass catalytic pyrolysis. Energy 210, 118646. https://doi.org/10.1016/j.energy.2020.118646

Yang Lim, J., McGregor, J., Sederman, A.J., Dennis, J.S., 2016. Kinetic studies of CO2 methanation over a Ni/γ-Al2O3 catalyst using a batch reactor. Chem. Eng. Sci. 141, 28–45. https://doi.org/10.1016/j.ces.2015.10.026

Yang, Q., Zhou, H., Bartocci, P., Fantozzi, F., Mašek, O., Agblevor, F.A., Wei, Z., Yang, H., Chen, H., Lu, X., Chen, G., Zheng, C., Nielsen, C.P., McElroy, M.B., 2021. Prospective contributions of biomass pyrolysis to China's 2050 carbon reduction and renewable energy goals. Nat. Commun. 12, 1–12. https://doi.org/10.1038/s41467-021-21868-z

Yang, Z., Kumar, A., Huhnke, R.L., Buser, M., Capareda, S., 2016. Pyrolysis of eastern redcedar: Distribution and characteristics of fast and slow pyrolysis products. Fuel 166, 157–165. https://doi.org/10.1016/j.fuel.2015.10.101

Ye, R.P., Liao, L., Reina, T.R., Liu, Jiaxu, Chevella, D., Jin, Y., Fan, M., Liu, Jian, 2021. Engineering Ni/SiO2 catalysts for enhanced CO2 methanation. Fuel 285, 119151. https://doi.org/10.1016/j.fuel.2020.119151

Yorgun, S., Vural, N., Demiral, H., 2009. Microporous and Mesoporous Materials Preparation of high-surface area activated carbons from Paulownia wood by ZnCl 2 activation. Microporous Mesoporous Mater. 122, 189–194. https://doi.org/10.1016/j.micromeso.2009.02.032

Younas, M., Sethupathi, S., Kong, L.L., Mohamed, A.R., 2018. CO2 methanation over Ni and Rh based catalysts: Process optimization at moderate temperature. Int. J. Energy Res. 42, 3289–3302. https://doi.org/10.1002/er.4082

Yu, P., Tang, W., Wu, F.F., Zhang, C., Luo, H.Y., Liu, H., Wang, Z.G., 2020. Recent progress in plant-derived hard carbon anode materials for sodium-ion batteries: a review. Rare Met. 39, 1019–1033. https://doi.org/10.1007/s12598-020-01443-z

Yuan, J.H., Xu, R.K., Zhang, H., 2011. The forms of alkalis in the biochar produced from

crop residues at different temperatures. Bioresour. Technol. 102, 3488–3497. https://doi.org/10.1016/j.biortech.2010.11.018

Zhang, Q., Chang, J., Wang, T., Xu, Y., 2007. Review of biomass pyrolysis oil properties and upgrading research. Energy Convers. Manag. 48, 87–92. https://doi.org/10.1016/j.enconman.2006.05.010

Zhang, X., Zheng, H., Li, G., Gu, J., Shao, J., Zhang, S., Yang, H., Chen, H., 2021. Ammoniated and activated microporous biochar for enhancement of SO2 adsorption. J. Anal. Appl. Pyrolysis 156, 105119. https://doi.org/10.1016/j.jaap.2021.105119

Zhang, Y., Wang, J., Feng, Y., 2021. The effects of biochar addition on soil physicochemical properties: A review. Catena 202, 105284. https://doi.org/10.1016/j.catena.2021.105284

Zhang, Z., Tian, Y., Zhang, L., Hu, S., Xiang, J., Wang, Y., Xu, L., Liu, Q., Zhang, S., Hu, X., 2019. Impacts of nickel loading on properties, catalytic behaviors of Ni/Al2O3 catalysts and the reaction intermediates formed in methanation of CO2. Int. J. Hydrogen Energy 44, 9291–9306. https://doi.org/10.1016/j.ijhydene.2019.02.129

Zhang, Z., Zhang, X., Zhang, L., Wang, Y., Li, X., Zhang, S., Liu, Q., Wei, T., Gao, G., Hu, X., 2020. Steam reforming of guaiacol over Ni/SiO2 catalyst modified with basic oxides: Impacts of alkalinity on properties of coke. Energy Convers. Manag. 205, 112301. https://doi.org/10.1016/j.enconman.2019.112301

Zhao, B., O'Connor, D., Zhang, J., Peng, T., Shen, Z., Tsang, D.C.W., Hou, D., 2018. Effect of pyrolysis temperature, heating rate, and residence time on rapeseed stem derived biochar. J. Clean. Prod. 174, 977–987. https://doi.org/10.1016/J.JCLEPRO.2017.11.013

Zhao, L.F., Hu, Z., Lai, W.H., Tao, Y., Peng, J., Miao, Z.C., Wang, Y.X., Chou, S.L., Liu, H.K., Dou, S.X., 2021. Hard Carbon Anodes: Fundamental Understanding and Commercial Perspectives for Na-Ion Batteries beyond Li-Ion and K-Ion Counterparts. Adv. Energy Mater. 11, 1–28. https://doi.org/10.1002/aenm.202002704

Zhu, X., Li, C., Li, J., Xie, B., Lü, J., Li, Y., 2018. Thermal treatment of biochar in the air/nitrogen atmosphere for developed mesoporosity and enhanced adsorption to tetracycline. Bioresour. Technol. 263, 475–482. https://doi.org/10.1016/j.biortech.2018.05.041

Zimmerman, A.R., 2010. Abiotic and microbial oxidation of laboratory-produced black carbon (biochar). Environ. Sci. Technol. 44, 1295–1301. https://doi.org/10.1021/es903140c